Sol-gel photopolymerization of inorganic precursors and application for mesoporous silica films elaboration

Heloise de Paz-Simon

UNIVERSITÉ DE HAUTE-ALSACE

Année 2013 N° d'ordre:

THÈSE

Pour l'obtention du titre de

DOCTEUR en Chimie des Matériaux

Présentée par :

Héloïse De Paz-Simon

SOL-GEL PHOTOPOLYMERIZATION OF INORGANIC PRECURSORS AND APPLICATION FOR MESOPOROUS SILICA FILMS ELABORATION

ETUDE DE LA PHOTOPOLYMERISATION SOL-GEL DE PRECURSEURS INORGANIQUES ET APPLICATION POUR L'ELABORATION DE FILMS DE SILICE MESOPOREUSE

Soutenue le 21 octobre 2013 devant la commission d'examen :

M. J.-L. BLIN	Rapporteur
M. C. BOISSIÈRE	Examinateur
M. A. CHEMTOB	Co-directeur de thèse
Mme C. CROUTXÉ-BARGHORN	Directrice de thèse
Mme B. LEBEAU	Examinatrice
Mme S. THERIAS	Rapporteur

A ma mère, pour tous les sacrifices que tu as faits pour nous.

A ma fille, tu écourtes mes nuits, tu compliques mes jours mais un seul de tes sourires me suffit pour tout oublier. J'espère que dans quelques années tu seras fière de ta maman.

SUMMARY

REMERCIEMENTS

Dans un premier temps, je souhaiterais remercier le Prof. Xavier Allonas de m'avoir accueillie et permis de faire une thèse au sein de son laboratoire. Cette thèse n'aurait jamais pu être possible sans mes deux directeurs de thèse : le Prof. Céline Croutxé-Barghorn et le Dr. Abraham Chemtob. Je vous remercie tous les deux chaleureusement pour tout ce que vous m'avez enseigné et apporté pendant ces 3 années de thèse. Céline, ta vision industrielle du projet, ton dynamisme, ta convivialité et tes encouragements constants m'ont permis de m'épanouir dans ce projet. Abraham, j'ai pu énormément apprendre de ta rigueur scientifique, de ta créativité et de ton acharnement au travail. La qualité de l'encadrement reçue me permettra, je l'espère, de bien débuter ma vie de chercheur. Merci encore à vous, ces 3 années ont été un réel plaisir malgré une période de rédaction difficile.

Je tiens aussi à remercier monsieur Fleury et la fondation de l'école de chimie pour avoir financé ma thèse.

La seconde partie de cette thèse a été réalisée en collaboration avec l'équipe de matériaux à porosité contrôlée de l'institut des Matériaux de Mulhouse (IS2M). Je remercie le Dr. Bénédicte Lebeau de nous avoir fait confiance pour ce projet, et de nous avoir laissé libre accès à son laboratoire. De manière plus générale je tiens à remercier toute l'équipe : le Dr. Severinne Rigolet pour le temps passé sur les résultats de RMN solide, Laure Michelin pour les analyses DRX et les précieux conseils, le Dr. Loïc Vidal pour les analyses MEB et MET, le Dr. Habiba Nouali pour les conseils en manométrie d'adsorption et le Dr. Didier LeNouën pour la RMN liquide.

Ma gratitude va aussi pour mes examinateurs et rapporteurs de thèse, le Prof. Jean-Luc Blin, les Drs Sandrine Therias, Bénédicte Lebeau et Cédric Boissière. Merci de m'avoir fait l'honneur d'examiner et de rapporter ma thèse et merci pour votre présence et vos conseils lors de la soutenance de thèse.

Cette thèse n'aurait jamais pu être aussi agréable sans mes collègues et le personnel du laboratoire. Merci à Jacqueline Marchioro, Julie Buguet et Marjolaine Bessière pour tout le travail qu'elles font au quotidien. Merci à mes acolytes de bureau David et Miléna dans un premier temps puis Florent, quelques parties de « basket de bureau » rien de mieux pour décompresser en période de rédaction. Merci Rémy pour tous ces supers gâteaux que tu nous as fait gouter. Merci aussi à Hanène, Haja et Bandar la « team 2010 ». Merci aux anciens et aux nouveaux, Vanessa, Nadia, Lingli, Emeline, Feyza… Je voulais remercier aussi les collègues du MPC qui m'ont souvent aidée sur les manips dans leur laboratoire, Taissire, Gaëtan, Atika…. Ma reconnaissance va aussi pour les étudiants que j'ai encadrés et qui ont contribué à une partie des

résultats présentés ici : Florian Crest, Mathilde Sibeaud, Quentin Miesch et Jérémy Ramos. J'espère vous avoir donné goût à la recherche.

Au cours de mes 3 ans de thèse j'ai aussi eu l'occasion de travailler sur un second projet qui n'a pas été présenté dans ce manuscrit, je tenais à remercier chaleureusement l'Institut Charles Sadron (ICS), le Prof. Christian Gauthier, les Drs Vincent Lehouérou et Léandro Jacomine pour tout ce que ils m'ont enseigné et pour le temps qu'ils m'ont consacré. Merci aussi au Collège de France et au Dr. Cédric Boissière de m'avoir accueillie pour une série de manips dans leur laboratoire à Paris, malgré des résultats non concluants je garde un bon souvenir de mon passage chez vous.

Enfin si j'ai pu autant apprécier cette thèse, c'est aussi grâce à ma famille qui m'a toujours soutenue et encouragée dans mes projets. Merci à mes parents pour votre amour, votre éducation et votre confiance. Merci à mes sœurs et à mon frère même si ils ont toujours rien compris à ce que je fais, ils sont fiers de moi. Merci aux petits weekends à Nice qui permettaient de faire des coupures dans le froid Alsacien. Un grand merci aussi à mes beaux-parents de nous avoir accueillis à Strasbourg presque tous les week-ends, ce qui nous a permis de ne jamais nous tracasser sur ce que nous allions manger pour le week-end.

En anglais on dirait « last but not least », ici je dirais le meilleur pour la fin, un très grand merci à mon mari qui est merveilleux et a fait preuve d'une grande patience avec moi lorsque je rentrais fatiguée et stressée d'une très longue journée de rédaction bien souvent peu productive. Merci de m'avoir soutenue et encouragée tout au long de ces 3 années de thèses. Merci de m'avoir suivie à Mulhouse, la ville la plus glamour de France. Promis, la prochaine destination sera au soleil. Et, enfin, merci pour cette magnifique petite famille que nous formons et qui me comble de bonheur.

GENERAL INTRODUCTION

The Laboratory of Photochemistry and Macromolecular Engineering (LPIM) has been working for more than a decade on the preparation of hybrid organic-inorganic films via photoinitiated polymerizations. As a recent achievement, simultaneous organic-inorganic (sol-gel) polymerization triggered by UV irradiation has been described[1-5]. While organic photopolymerizations (radical, cationic) are well-established in the literature[6-8], the concept and principle of a photoinduced sol-gel process have been scarcely investigated. Its key feature is the photogeneration of acid or basic species acting as catalysts for the hydrolysis and condensation reactions of alkoxysilane-based films. Another peculiarity is the absence of solvent and water in the initial formulation including only the silicon source and a photoacid, PAG (or photobase, PBG) generator. In principle, water necessary for hydrolysis is continuously supplied by the atmospheric moisture, thus giving a crucial role to the relative humidity (RH). Figure 1 highlights the major differences between a conventional sol-gel process and its photoinduced homologue. As other advantages, this UV-driven process permits a temporal and spatial control of the reactions, as well as high polycondensation rates in seconds or minutes typically. In addition, highly crosslinked films that do not require post treatment step are prepared. This new process active at ambient temperature is fully compliant with the recent environmental regulations limiting the energetic expense, the use of toxic products and solvent emission.

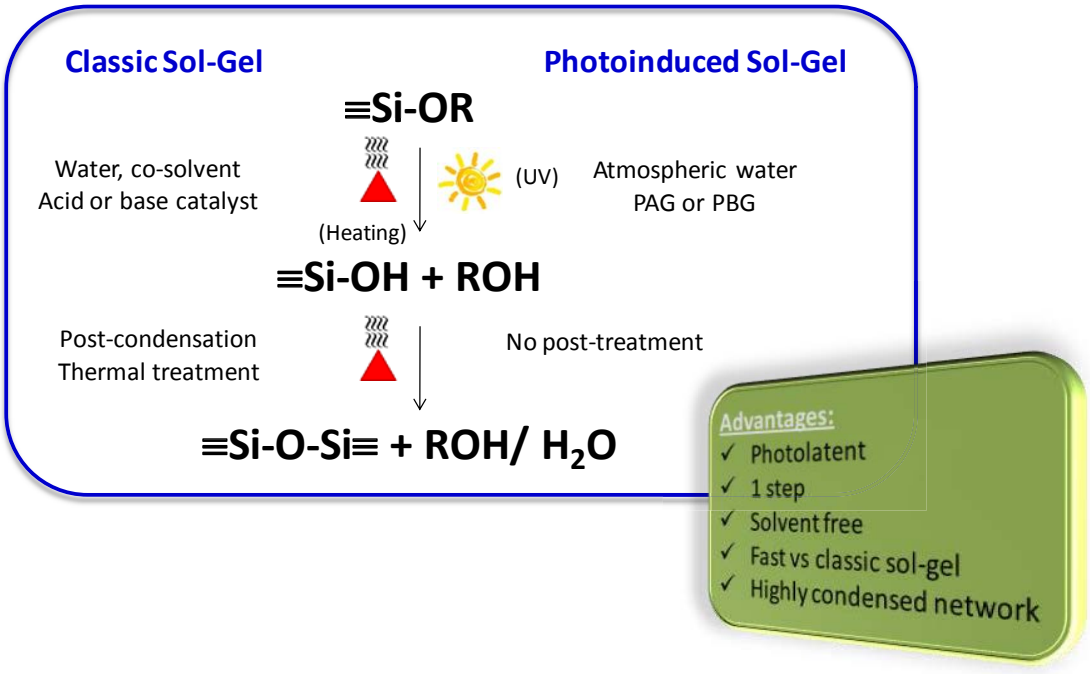

Figure 1: Comparison between conventional and photoinduced sol-gel pathway

Since the first patent of Fox *et al.*[9] in the 1970s, only very few studies have addressed the sol-gel photopolymerization. The implementation of hybrid organosilane precursors having specific properties and a wide application scope has attracted the largest interest[1,3-5,10]. Yet, it is both useful and relevant to investigate the behavior of inorganic alkoxy precursors in a photoinduced sol-gel process in order to have a better understanding of this emerging process. In the literature, numerous studies deal with the sol-gel process[11,12] as well as the impact of various parameters: catalyst nature and its concentration[13,14], precursor steric hindrance and inductive effect[15,16] , water concentration[13,17], etc. However, there is no equivalent study in a photoinduced process.

In a first part of this PhD manuscript, we have attempted to provide an exhaustive and rational description of the photosol-gel process. We start by providing basic knowledge in sol-gel chemistry. In particular, the interest of this "soft chemistry" process for the elaboration of hybrid and inorganic films has been emphasized. In addition, the potential of an alternative photosol-gel process has been underlined, with a number of examples of the literature concerning mainly the synthesis of hybrid films. Then, our experimental results on the photopolymerization process of alkoxysilane precursors have been extensively discussed. For this, non-volatile oligomeric inorganic precursors polydimethoxysiloxane (PDMOS) or polydiethoxysiloxane (PDEOS) films have been photopolymerized in presence of diphenyliodonium salt as PAG, as shown in Figure 2.

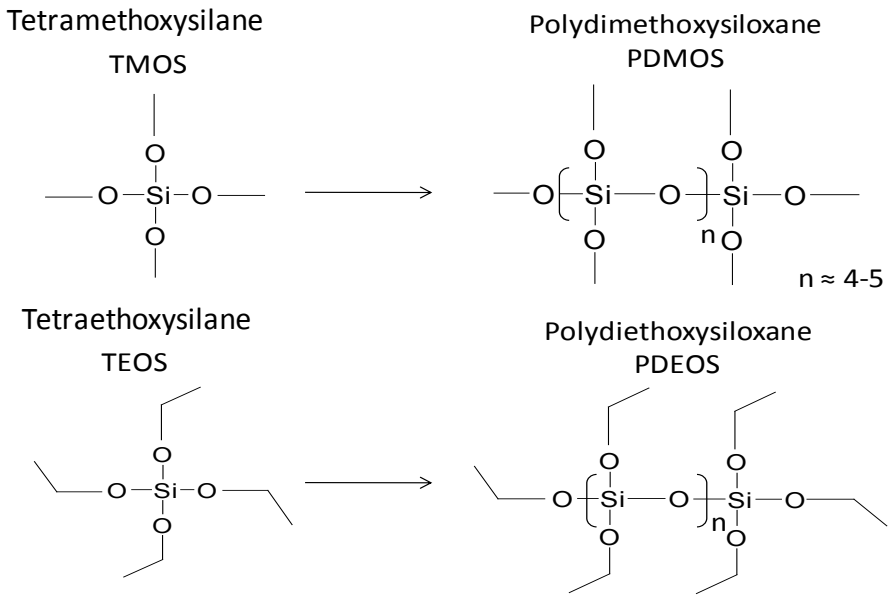

Figure 2: Example of pure inorganic precursors in their monomeric and their oligomeric form

To study this fast and complex photopolymerization process, an important part of our investigation relies on real-time Fourier transform infrared spectroscopy (RT-FTIR), which is a

powerful *in situ* tool. In addition, ^{29}Si solid state NMR brings complementary data on the siloxane network. A kinetic and mechanistic study of the photoacid-catalyzed sol-gel reactions, based on the effect of numerous experimental parameters is proposed. Furthermore, an equivalent photobase-catalyzed sol-gel process based on photogenerated tertiary amine has been also studied thoroughly, which is very rare in the literature[18-20]. A systematic comparison between photoacid and photobase-catalyzed process was proposed in order to highlight their differences as regards to reactivity and final film properties. Our goal is to review all the key parameters affecting the course of this reaction. The summary of this first part is schematically represented in Figure 3.

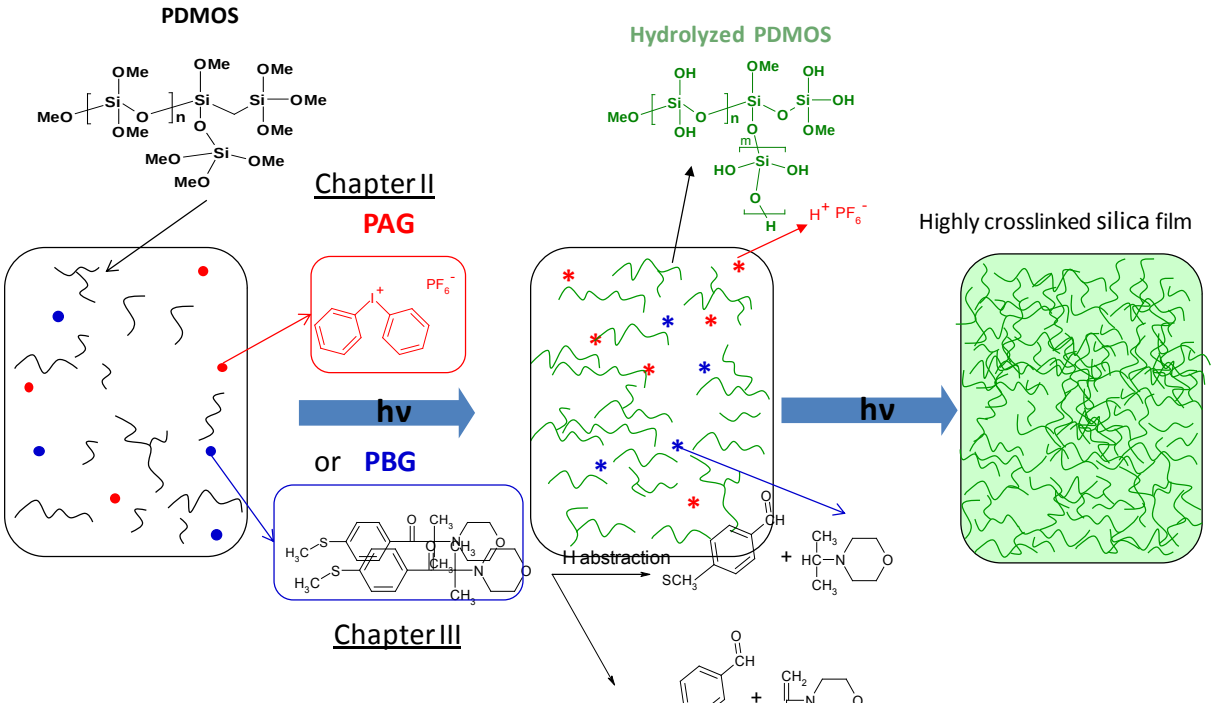

Figure 3: Two photochemical routes to silica films through photoacid or photobase catalysis

Once an exhaustive picture of this inorganic photopolymerization has been given, the second part of the manuscript covers aspects related to the use of this photoprocess for the preparation of mesoporous silica films. Since their discovery in 1992 by the Mobil Oil Company[21-23], mesoporous material aroused a lot of interest both in academic and industrial field. Currently, their synthesis as thin well-shaped films is highly desired and of interest for practical applications. Mesoporous silica or hybrid films[24,25] are frequently used as low *k* dielectric coatings in microelectronic devices and sensors. Understanding the surfactant self-assembly mechanism, controlling the pores size and structure as well as developing innovative process are crucial challenges for chemists in this research field.

The conventional synthesis procedure starts from a silica source in presence of surfactant, and hybrid mesoporous structures are prepared subsequently via a sol-gel process by condensation

of an inorganic phase around organic surfactant lyotropic phases. This organic template is then eliminated by calcination to liberate the porosity and create a perforated and ordered material at the mesoscopic level. Ideally, the resultant mesoporous material displays an important specific surface, a perfectly controlled porosity and well defined pore diameters from 2 to 50 nm. The most widely studied method to synthesize mesoporous silica films is the Evaporation Induced Self-Assembly (EISA) process[26-28]. Self-Assembly of the surfactant and inorganic network condensation are triggered by solvent evaporation. In a typical process, the inorganic precursor and surfactant are mixed in a large excess of solvent (ethanol) in presence of water and after deposition as thin film the solvent evaporation drives the self-assembly and the inorganic condensation. However, this method is sensitive and multi-variable; in addition a large excess of solvent is required as well as a post-treatment step in order to ensure a good condensation of the inorganic wall.

We begin this second part of the manuscript with a chapter dedicated to mesoporous materials with an emphasis on film formation. Then, we propose to extend our photoinduced sol-gel process for the elaboration of mesoporous silica film. We expect that water- and solvent-free conditions will allow film preparation to be less sensitive to evaporation and process conditions. Use of PAG have been rarely handled for the preparation of mesoporous silica film[29]. First, we have focused on the feasibility of such photoprocess. This second part has been conducted with the helpful collaboration of the team “Matériaux à Porosité Contrôlée” from the Institut de Science des Matériaux de Mulhouse (Dr. Bénédicte LEBEAU, Laure MICHELIN and Dr. Séverinne RIGOLET). Wormlike silica mesostructures are first described. Different parameters affecting the film mesostructuration have been systematically screened. Additionally RT-FTIR and solid state NMR are used to shed light on kinetics and self-assembly of the UV induced mesostructuration process. Finally, we have been interested in optimizing the process to obtain periodically ordered films. In a last part, a 100% UV process for the single-step elaboration of mesoporous silica films has been devised. The summary of this second part is sketched in Figure 4.

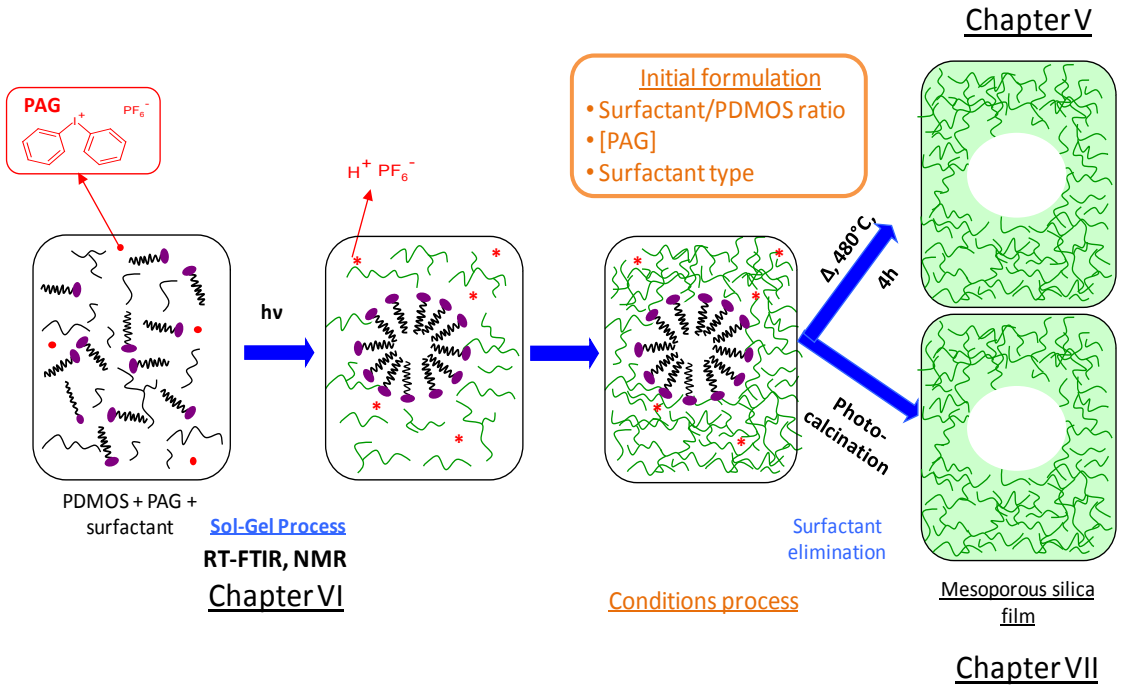

Figure 4: Summary of the different studies described in the second part of this manuscript

REFERENCE GENERAL INTRODUCTION

(1) Chemtob, A.; Versace, D.-L.; Belon, C.; Croutxe-Barghorn, C.; Rigolet, S. *Macromolecules* **2008**, 41, 7390.
(2) Versace, D.-L.; Chemtob, A.; Croutxé-Barghorn, C.; Rigolet, S. *Macromol. Mater. Eng.* **2010**, 295, 355.
(3) Belon, C.; Chemtob, A.; Croutxé-Barghorn, C.; Rigolet, S.; Schmitt, M.; Bistac, S.; Le Houérou, V.; Gauthier, C. *Polym. Int.* **2010**, 59, 1175.
(4) Belon, C.; Chemtob, A.; Croutxé-Barghorn, C.; Rigolet, S.; Le Houérou, V.; Gauthier, C. *J. Polym. Sci. Part A*, **2010**, 48, 4150.
(5) Chemtob, A.; Belon, C.; Croutxé-Barghorn, C.; Rigolet, S.; Vidal, L.; Brendlé, J.; Mandel, J.; Blanchard, N. *Polym. Eng. Sci.* **2011**, 51, 1466.
(6) Fouassier, J.-P.; Rabek, J. F. *Radiation Curing in Polymer Science and Technology*; Elsevier Science ed., **1993**; Vol. 1 à 4.
(7) Fouassier, J.-P. *Photoinitiation, Photopolymerization, and Photocuring: Fundamentals and Applications*; Hanser ed., **1995.**
(8) Schwalm, R. *UV Coatings: Basics, Recent Developments and New Applications*; Elsevier Science, **2006**.
(9) Fox, F. J.; Noren, R. W.; Krankkala, G. E.; US Patent No. 4101513, **1978**.
(10) Chemtob, A.; Belon, C.; Croutxe-Barghorn, C.; Brendle, J.; Soulard, M.; Rigolet, S.; Le Houerou, V.; Gauthier, C. *New J. Chem.* **2010**, 34, 1068.
(11) Brinker, C.; Scherer, G. *Sol-Gel Science: The Physics and Chemistry of Sol Gel Processing*; Academic Press Inc: San Diego, **1990**.
(12) Brinker, C.; Hurd, A. J.; Schunk, P. R.; Frye, G. C.; Ashley, C. S. *J. Non-Cryst. Solids* **1992**, 147-148, 424.
(13) Aelion, R.; Loebel, A.; Eirich, F. *J. Am. Chem. Soc.* **1950**, 72, 5705.
(14) Pope, E. J. A.; Mackenzie, J. D. *J. Non-Cryst. Solids* **1986**, 87, 185.
(15) Osterholtz, F. D.; Pohl, E. R. *J. Adhes. Sci.Technol.* **1992**, 6, 127.
(16) Loy, D. A.; Baugher, B. M.; Baugher, C. R.; Schneider, D. A.; Rahimian, K. *Chem. Mater.* **2000**, 12, 3624.

(17) Assink, R. A.; Kay, B. D. *J. Non-Cryst. Solids* **1988**, 99, 359.
(18) Harkness, B. R.; Takeuchi, K.; Tachikawa, M. *Macromolecules* **1998**, 31, 4798.
(19) Harkness, B. R.; Takeuchi, K.; Tachikawa, M. *Polym. Advan. Technol.* **1999**, 10, 669.
(20) Uraoka, Y.; Tadanaga, K.; Tatsumisago, M. *Chem. Mater.* **2010**, 22, 6125.
(21) Beck, J. S.; Vartuli, J. C.; Roth, W. J.; Leonowicz, M. E.; Kresge, C. T.; Schmitt, K. D.; Chu, C. T. W.; Olson, D. H.; Sheppard, E. W. *J. Am. Chem. Soc.* **1992**, 114, 10834.
(22) Kresge, C. T.; Leonowicz, M. E.; Roth, W. J.; Vartuli, J. C.; Beck, J. S. *Nature* 1992, 359, 710.
(23) Yoshida, E.; Kuwayama, S. *Polymers* **2010**, 2, 623.
(24) Nicole, L.; Boissiere, C.; Grosso, D.; Quach, A.; Sanchez, C. *J. Mater. Chem.* **2005**, 15, 3598.
(25) Sanchez, C.; Boissière, C.; Grosso, D.; Laberty, C.; Nicole, L. *Chem. Mater.* **2008**, 20, 682.
(26) Brinker, C. J.; Lu, Y.; Sellinger, A.; Fan, H. *Adv. Mater.* **1999**, 11, 579.
(27) Yang, H.; Kuperman, A.; Coombs, N.; Mamiche-Afara, S.; Ozin, G. A. *Nature* **1996**, 379, 703.
(28) Grosso, D.; Cagnol, F.; Soler-Illia, G. J. d. A. A.; Crepaldi, E. L.; Amenitsch, H.; Brunet-Bruneau, A.; Bourgeois, A.; Sanchez, C. *Adv. Funct. Mater.* **2004**, 14, 309.
(29) Doshi D. A.; Huesing N. K.; Lu M.; Fan H.; Lu Y.; Simmons-Potter K.; Potter B. G.; Hurd A. J.; Brinker, C. J. *Science* **2000**, 290, 107.

INTRODUCTION GENERALE

Le Laboratoire de Photochimie et d'Ingénierie Macromoléculaires (LPIM) travaille depuis plusieurs dizaines d'années à la préparation de films hybrides organique-inorganique par polymérisation photoinduite. Récemment, le laboratoire a montré la faisabilité d'une polymérisation concomitante de réseau organique et inorganique (sol-gel) déclenchée par rayonnement UV[1-5]. Alors que la photopolymérisation organique (radicalaire et cationique) est bien connue en littérature,[6-8] le procédé sol-gel photoinduit a été très peu étudié. Le principe repose sur la photogénération d'espèces acides et basiques capables de catalyser les réactions d'hydrolyse et de condensation des films à base d'alkoxysilane. Un second point important est l'absence d'eau et de solvant dans la formulation de départ ; cette dernière contient seulement la source de silice et le photogénérateur d'acide (PGA) ou de base (PGB). De plus, l'eau est approvisionnée en continue par l'humidité atmosphérique ce qui donne un rôle essentiel au taux d'humidité relative (HR). La Figure 1 ci-dessous souligne les principales différences entre le procédé sol-gel conventionnel et son alternative photoinduite. Entre autres avantages, ce procédé UV permet un contrôle spatio-temporel des réactions ainsi que des vitesses de polycondensation de l'ordre de quelques secondes à quelques minutes. Aucune étape de post-traitement n'est nécessaire pour obtenir des films fortement réticulés. Ce nouveau procédé actif à température ambiante est en complète adéquation avec les nouvelles régulations environnementales qui limitent les dépenses énergétiques, l'utilisation de produits toxiques et l'émission de solvant.

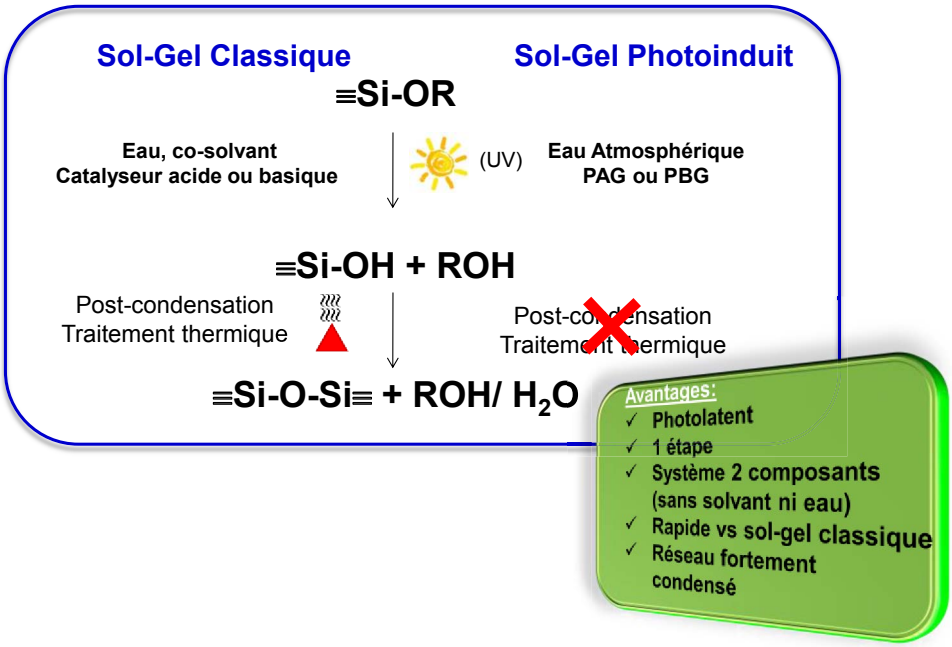

Figure 1: Comparaison entre le procédé sol-gel conventionnel et photoinduit

Depuis le premier brevet déposé par Fox *et al.*[9] dans les années 1970, peu d'études ont été menées sur la photopolymérisation sol-gel. Un intérêt plus marqué s'est porté sur les précurseurs hybrides de type organosilanes qui ont des propriétés spécifiques et un plus large champ d'applications[1,3-5,10]. Néanmoins, l'étude de précurseurs alkoxysilane purement inorganique permet d'analyser leur comportement et de mieux comprendre le procédé sol-gel photoinduit. Dans la littérature, de nombreuses études décrivent le procédé sol-gel[11,12], telles que l'influence de différents paramètres : la nature et concentration du catalyseur[13,14], l'encombrement stérique du précurseurs, l'effet inductif des substituants[15,16], la concentration en eau,[13,17] etc… Cependant, il n'existe pas d'étude équivalente pour le procédé photoinduit.

Dans la première partie de ce manuscrit, nous avons tenté d'apporter une description approfondie et rationnelle du procédé photosol-gel. Nous commençons par rappeler les connaissances de base de la chimie sol-gel. En particulier, l'intérêt de la « chimie douce » pour l'élaboration de films inorganique et hybride est mis en avant. De plus, le potentiel de cette alternative photochimique est souligné avec de nombreux exemples de la littérature concernant notamment la synthèse de films hybrides. Puis, les résultats expérimentaux obtenus lors de la photopolymérisation de précurseurs alkoxysilanes sont amplement discutés. Pour cela, des films à partir de précurseurs inorganiques, oligomériques et non volatils tel que le polydimethoxysiloxane (PDMOS) ou le polydiethoxysiloxane (PDEOS) (Figure 2) ont été photopolymerisés en présence d'un sel de diphenyliodonium comme PGA.

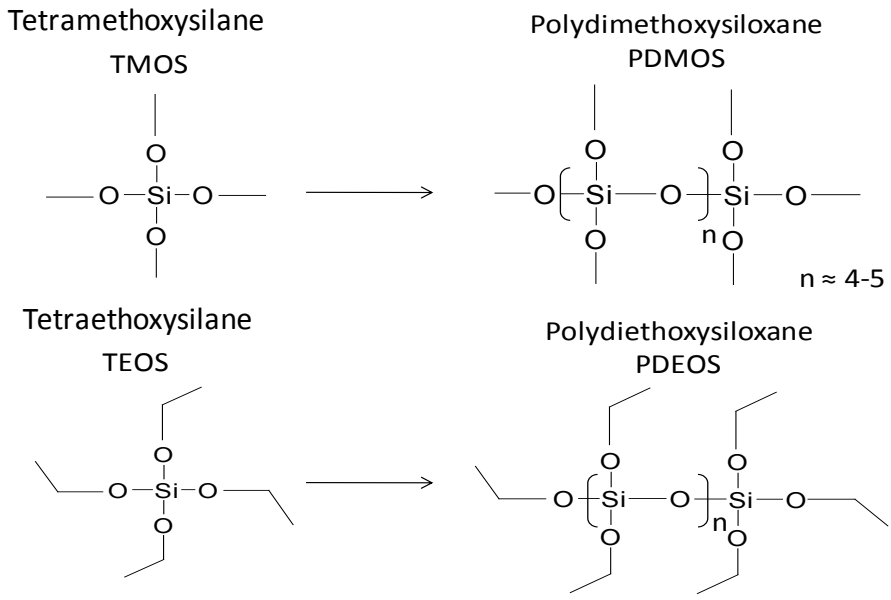

Figure 2: Exemple des précurseurs inorganiques dans leur forme monomérique et oligomérique.

Pour l'étude de ce procédé rapide et complexe, une partie importante de nos recherches se sont appuyées sur la spectroscopie infrarouge à transformée de Fourier résolue dans le temps (RT-

FTIR). De plus, la RMN du ^{29}Si à l'état solide a apporté des informations complémentaires sur le réseau silicaté formé. A partir de l'analyse de nombreux paramètres expérimentaux, nous avons réalisé une étude cinétique et mécanistique des réactions sol-gel catalysées par des photoacides. En outre, une étude équivalente en catalyse basique basée sur des amines tertiaires photogénérées a aussi été menée ce qui est extrêmement rare en littérature[18-20]. Une comparaison systématique entre le procédé catalysé par des photoacides et des photobases est proposée afin de souligner les différences de réactivité et les propriétés finales des films. Notre but est de passer en revue les paramètres clés qui vont influencer les réactions. Le résumé de la première partie est représenté schématiquement à la Figure 3.

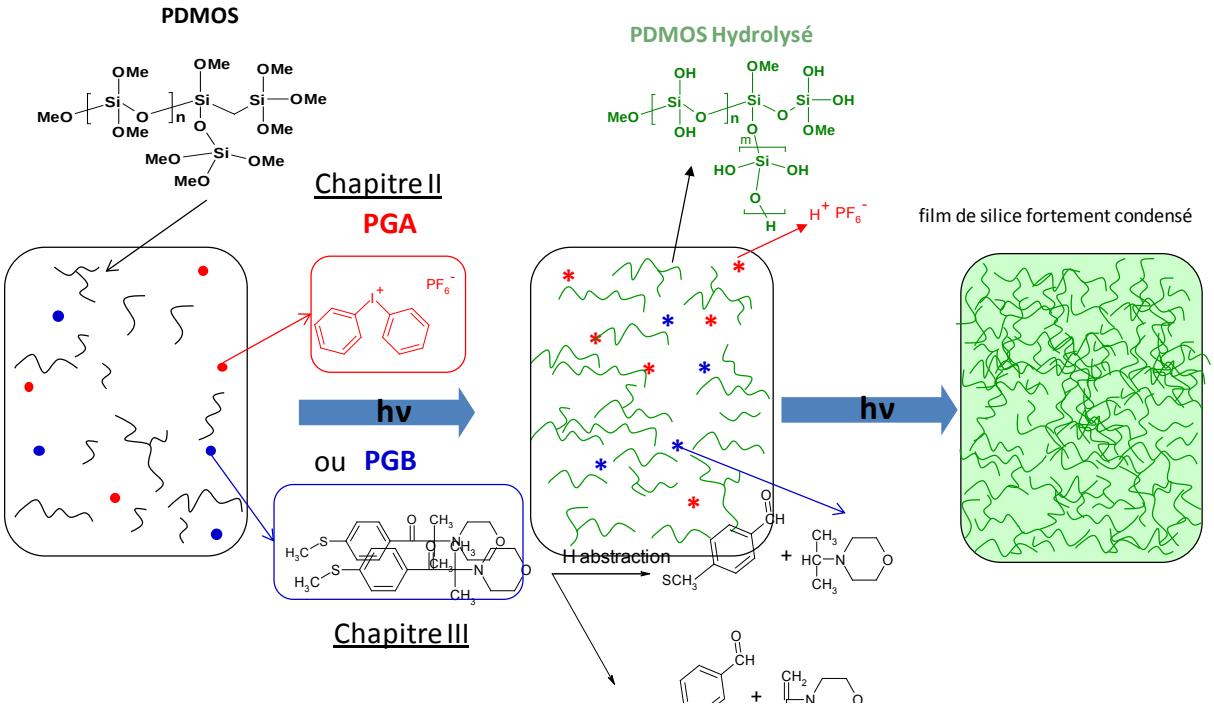

Figure 3:Procédés photochimiques pour la préparation de films de silice en catalyse acide et basique

La seconde partie de ce manuscrit propose l'utilisation du procédé photoinduit pour la préparation de films de silice mésoporeuse. Depuis leur découverte en 1992 par la compagnie Mobil Oil, les matériaux mésoporeux ont éveillé un intérêt aussi bien académique qu'industriel. Actuellement, la synthèse de film mince bien défini est particulièrement intéressante pour des applications pratiques. Les films mésoporeux silicatés ou hybrides[24,25]avec des constantes diélectriques (k) très faibles sont fréquemment utilisés comme membranes pour des systèmes en microélectronique ou dans le domaine des capteurs. La compréhension du mécanisme d'auto-assemblage du tensioactif, le contrôle de la structure et de la taille des pores ainsi que le développement de nouveaux procédés innovants sont des challenges primordiaux pour les chercheurs en chimie.

La procédure de synthèse conventionnelle nécessite une source de silice en présence d'un agent structurant ; la structure hybride mésostructurée est préparée par la suite *via* un procédé sol-gel impliquant la condensation d'une phase inorganique autour d'une phase organique lyotropique de tensioactif. L'agent structurant organique est ensuite éliminé par calcination pour libérer la porosité et créer un matériau « perforé » et organisé à l'échelle mésoscopique. Idéalement, le matériau ainsi formé présente une importante surface spécifique, une porosité parfaitement contrôlée et un diamètre de pore allant de 2 à 50 nm. La méthode la plus répandue pour la synthèse de ce type de matériau est basée sur l'évaporation de solvant (Evaporation Induced Self-Assembly)[26-28]. Dans un procédé type, le précurseur inorganique et le tensioactif sont mélangés dans une importante quantité de solvant (éthanol) en présence d'eau, après déposition de la formulation sous forme de couche mince l'évaporation du solvant va induire l'auto-assemblage du tensioactif et la condensation du réseau inorganique. Néanmoins cette méthode est sensible et multi-variable. De plus une importante quantité de solvant est nécessaire ainsi qu'une étape de post-traitement thermique pour assurer la bonne condensation des parois inorganiques.

Dans la seconde partie de ce manuscrit, nous commençons par un chapitre dédié aux matériaux mésoporeux et plus particulièrement aux films. Puis, nous proposons d'appliquer le procédé photosol-gel pour préparer des films de silice mésoporeuse. Nous nous attendons à ce que les conditions initiales sans eau ni solvant permettent la préparation de films moins sensibles aux conditions de dépôt et d'évaporation. L'utilisation de PGA a été rarement utilisée pour préparer de tels matériaux[29]. Dans un premier temps, nous nous sommes focalisés sur la faisabilité d'un tel procédé. Cette seconde partie a été réalisée en collaboration avec l'équipe de « Matériaux à Porosité Contrôlée » de l'Institut de Science des Matériaux de Mulhouse IS2M (Dr. Bénédicte LEBEAU, Laure MICHELIN and Dr. Séverinne RIGOLET). Des structures silicatées vermiculaires sont d'abord décrites. Différents paramètres pouvant affecter la mésostructuration du film ont été systématiquement passés en revue. De plus, la RT-FTIR et la RMN du silicium à l'état solide ont été employées pour faire la lumière sur la cinétique et l'auto-assemblage de ce procédé dans lequel la mésostructuration est induite par l'UV. Finalement nous nous sommes intéressés à l'optimisation de la méthode pour obtenir des films organisés. Dans un dernier point, un procédé 100% UV a été mis en place afin de réaliser des films mésoporeux en une seule étape. Le résumé de cette seconde partie est représenté schématiquement dans la Figure 4.

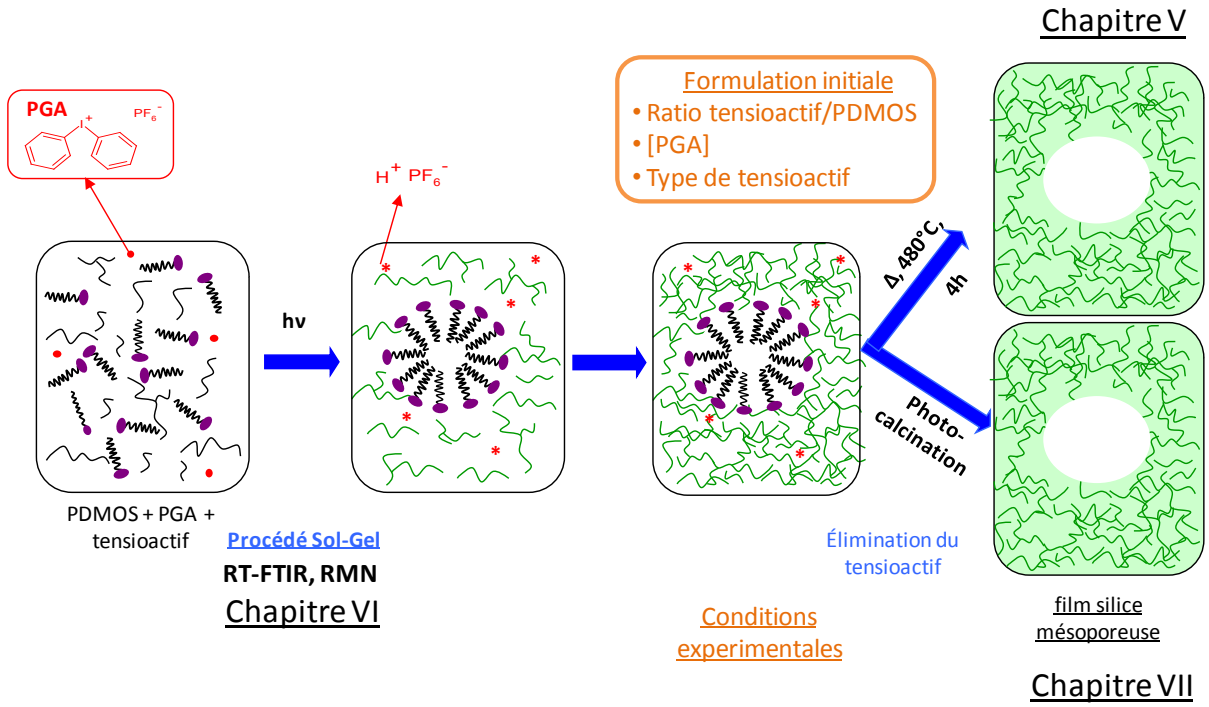

Figure 4: Résumé des différentes études décrites dans la seconde partie du manuscrit

REFERENCES

(1) Chemtob, A.; Versace, D.-L.; Belon, C.; Croutxe-Barghorn, C.; Rigolet, S. *Macromolecules* **2008**, 41, 7390.
(2) Versace, D.-L.; Chemtob, A.; Croutxé-Barghorn, C.; Rigolet, S. *Macromol. Mater. Eng.***2010**, 295, 355.
(3) Belon, C.; Chemtob, A.; Croutxé-Barghorn, C.; Rigolet, S.; Schmitt, M.; Bistac, S.; Le Houérou, V.; Gauthier, C. *Polym. Int.* **2010**, 59, 1175.
(4) Belon, C.; Chemtob, A.; Croutxé-Barghorn, C.; Rigolet, S.; Le Houérou, V.; Gauthier, C. *J. Polym. Sci. Part A*, **2010**, 48, 4150.
(5) Chemtob, A.; Belon, C.; Croutxé-Barghorn, C.; Rigolet, S.; Vidal, L.; Brendlé, J.; Mandel, J.; Blanchard, N. *Polym. Eng. Sci.* **2011**, 51, 1466.
(6) Fouassier, J.-P.; Rabek, J. F. *Radiation Curing in Polymer Science and Technology*; Elsevier Science ed., **1993**; Vol. 1 à 4.
(7) Fouassier, J.-P. *Photoinitiation, Photopolymerization, and Photocuring: Fundamentals and Applications*; Hanser ed., **1995.**
(8) Schwalm, R. *UV Coatings: Basics, Recent Developments and New Applications*; Elsevier Science, **2006**.
(9) Fox, F. J.; Noren, R. W.; Krankkala, G. E.; US Patent No. 4101513, **1978**.
(10) Chemtob, A.; Belon, C.; Croutxe-Barghorn, C.; Brendle, J.; Soulard, M.; Rigolet, S.; Le Houerou, V.; Gauthier, C. *New J. Chem.***2010**, 34, 1068.
(11) Brinker, C.; Scherer, G. *Sol-Gel Science: The Physics and Chemistry of Sol Gel Processing*; Academic Press Inc: San Diego, **1990**.
(12) Brinker, C.; Hurd, A. J.; Schunk, P. R.; Frye, G. C.; Ashley, C. S. *J. Non-Cryst. Solids***1992**, 147-148, 424.
(13) Aelion, R.; Loebel, A.; Eirich, F. *J. Am. Chem. Soc.***1950**, 72, 5705.
(14) Pope, E. J. A.; Mackenzie, J. D. *J. Non-Cryst. Solids***1986**, 87, 185.
(15) Osterholtz, F. D.; Pohl, E. R. *J. Adhes. Sci.Technol.***1992**, 6, 127.
(16) Loy, D. A.; Baugher, B. M.; Baugher, C. R.; Schneider, D. A.; Rahimian, K. *Chem. Mater.***2000**, 12, 3624.
(17) Assink, R. A.; Kay, B. D. *J. Non-Cryst. Solids***1988**, 99, 359.
(18) Harkness, B. R.; Takeuchi, K.; Tachikawa, M. *Macromolecules* **1998**, 31, 4798.
(19) Harkness, B. R.; Takeuchi, K.; Tachikawa, M. *Polym. Advan. Technol.***1999**, 10, 669.
(20) Uraoka, Y.; Tadanaga, K.; Tatsumisago, M. *Chem. Mater.***2010**, 22, 6125.

(21) Beck, J. S.; Vartuli, J. C.; Roth, W. J.; Leonowicz, M. E.; Kresge, C. T.; Schmitt, K. D.; Chu, C. T. W.; Olson, D. H.; Sheppard, E. W. *J. Am. Chem. Soc.***1992**, 114, 10834.
(22) Kresge, C. T.; Leonowicz, M. E.; Roth, W. J.; Vartuli, J. C.; Beck, J. S. *Nature* 1992, 359, 710.
(23) Yoshida, E.; Kuwayama, S. *Polymers***2010**, 2, 623.
(24) Nicole, L.; Boissiere, C.; Grosso, D.; Quach, A.; Sanchez, C. *J. Mater. Chem.***2005**, 15, 3598.
(25) Sanchez, C.; Boissière, C.; Grosso, D.; Laberty, C.; Nicole, L. *Chem. Mater.***2008**, 20, 682.
(26) Brinker, C. J.; Lu, Y.; Sellinger, A.; Fan, H. *Adv. Mater.***1999**, 11, 579.
(27) Yang, H.; Kuperman, A.; Coombs, N.; Mamiche-Afara, S.; Ozin, G. A. *Nature***1996**, 379, 703.
(28) Grosso, D.; Cagnol, F.; Soler-Illia, G. J. d. A. A.; Crepaldi, E. L.; Amenitsch, H.; Brunet-Bruneau, A.; Bourgeois, A.; Sanchez, C. *Adv. Funct. Mater.***2004**, 14, 309.
(29) Doshi D. A.; Huesing N. K.; Lu M.; Fan H.; Lu Y.; Simmons-Potter K.; Potter B. G.; Hurd A. J.; Brinker, C. J. *Science***2000**, 290, 107.

CHAPTER I: FROM A CONVENTIONAL TO A PHOTOINDUCED PROCESS: SOL-GEL CHEMISTRY

ABBREVIATIONS (PART I)

AFM	Atomic force microscopy
BP	Benzophenone
CD	Condensation degree
CP-MAS	Cross polarization magic angle spinning
DMA	Dynamic mechanical analysis
DSC	Differential scanning calorimetry
EISA	Evaporation induced self-assembly
GPTMS	3-glycidoxypropyltrimethoxysilane
LO	Longitudinal optic
NMR	Nuclear magnetic resonance
PAG	Photoacid generator
PBG	Photobase generator
PDEOS	Polydiethoxysiloxane
PDMOS	Polydimethoxysiloxane
PDMS	Polydimethylysiloxane
PI	Photoinitiator
RH	Relative humidity
RT-FTIR	Real-time Fourier transform infrared
SAM	Self-assembled monolayer
SEM	Scanning electron microscopy
SPE-MAS	Single pulse excitation magic angle spinning
TEM	Transmission electronic microscopy
TEOS	Tetraethoxysilane
TMOS	tetramethoxysilane
TO	Transversal optic
TPP	triphenylphosphine
XRD	X-ray diffraction

INTRODUCTION

The aim of the first part of this work is an extensive study of the photosol-gel process in acid and basic conditions. Nevertheless, before this, it is necessary to review some basics of conventional sol-gel chemistry and to outline the interest of a photoinduced process.

In the first point, our goal is to cover some basic aspects of sol-gel chemistry. Principle and interest as well as scientific aspect of this process are reviewed. Reactive mechanisms for hydrolysis and condensation reactions in acid or basic conditions and the influence of various parameters are detailed. We also highlight the major structural differences occurring in the material depending on the conditions processes. In a second point, we emphasize the interest of sol-gel chemistry for the preparation of hybrid films. We distinguish two families of materials, the one where organic and inorganic parts are homogeneously linked together and materials where organic and inorganic parts undergo a phase controlled separation. To finish, in a third point, we present the interest of a photoinduced sol-gel process to produce inorganic and hybrid films. We start by describing the basics of photochemistry and its application in organic polymerization via a radical or cationic way. Then, we demonstrate how this photoinduced process can extend to inorganic polymerization leading to a photosol-gel process. We also present the photoacid-catalyzed pathway and its use for the preparation of inorganic and hybrid films. Finally, the photobase-catalyzed route is as well depicted.

I. BASICS OF SOL-GEL CHEMISTRY

I.1. PRINCIPLE AND INTEREST

The first sol gel polymerization was carried out by Ebelmen in 1845; he reported the conversion of silicic acid into solid glass in the presence of humidity[1,2]. Such process exists in the nature for millions years. Indeed, some unicellular algae (like diatoms) are able to create fine glass structures from the silica dissolved in the ocean without any fusion step (Figure I.1)[3]. This bio-mineralization process implies chemical reactions known as “sol-gel polymerization”.

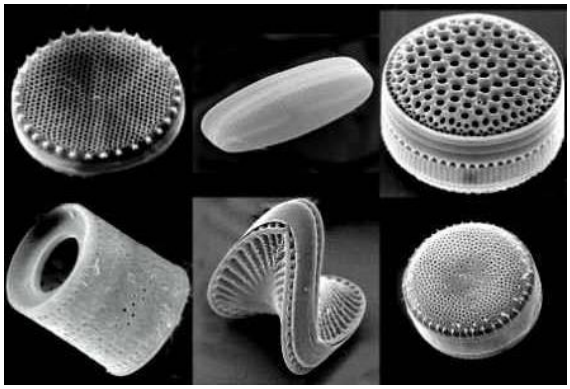

Figure I.1: Examples of diatoms silica structures

However, it was necessary to wait until 1930s for further development in sol-gel chemistry with the German company Schott who used this technique to produce covering industrial glass; then the first patent was deposited in 1939 by Schott-Glaswerke for the preparation of rear view mirror[4]. Nevertheless, for most people the beginning of sol-gel is associated to the first international conference on glass and ceramics in 1981[5]. Nowadays and since the end of eighties, sol-gel polymerization is commonly used in industry in the field of materials science and ceramic engineering.

The sol-gel process relies on the formation of an inorganic condensed network starting from liquid precursors by a succession of hydrolysis and hetero- or homo-condensation reactions at moderate temperature (20 to 150°C). Hydrolysis activates the polymerization while condensation ensures the chain growth of the network. Precursors used are inorganic salts ($SiCl_4$, metal halides) or more frequently metal alkoxide like $M(OR)_x$ where M= Si, Sn, Ti, Zr, Al, Mo, V etc. and R is an alkoxide moieties[6]. Nevertheless, most works on sol-gel chemistry concerns silica species. The reaction can proceed along a hydrolytic or non-hydrolytic pathway depending on the initial precursors and the use of water or not. However, hydrolytic pathway is by far the most widespread[7] and only this later will be discussed here.

Equation for hydrolysis (1) and condensation (2a and b) reactions are represented in Scheme I.1.[6,8]. As water and alkoxides are generally immiscible, a mutual solvent such as an alcohol is generally utilized. With the presence of this homogenizing agent, hydrolysis is facilitated due to the miscibility of the alkoxide and water[9].

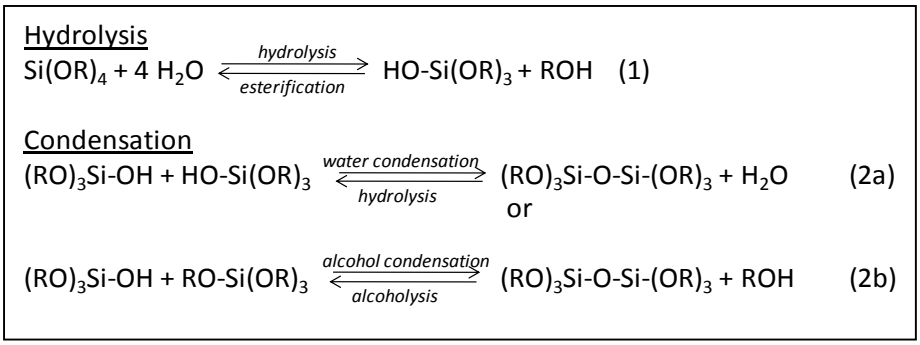

Scheme I.1: General equations for hydrolysis/condensation reactions in neutral media

The first step consists in the formation of colloids containing oligomers, polymers and cyclic species defining the sol structure. Afterwards the solid particle presents in the sol undergo crosslinking reactions and forms the gel. Sol-gel process corresponds to the transition between a stable dispersion of colloidal oligomers and partially hydrolyzed monomer (liquid) to a tridimensional network of an infinite viscosity where the oxide are swelled by solvent called "gel"[8]. Transition from sol to gel is usually expressed by the gel point. Finally, a drying step under atmospheric or supercritical conditions leads respectively to the formation of vitreous and dense material (xerogel) or open and macroporous structure (aerogel). This step is very delicate as strong capillary forces occur and shrinkage, collapse or complete destruction (i. e. formation of powder) of the material is often observed. Figure I.2 below summarizes the transition from a liquid sol to a solid dense or porous material.

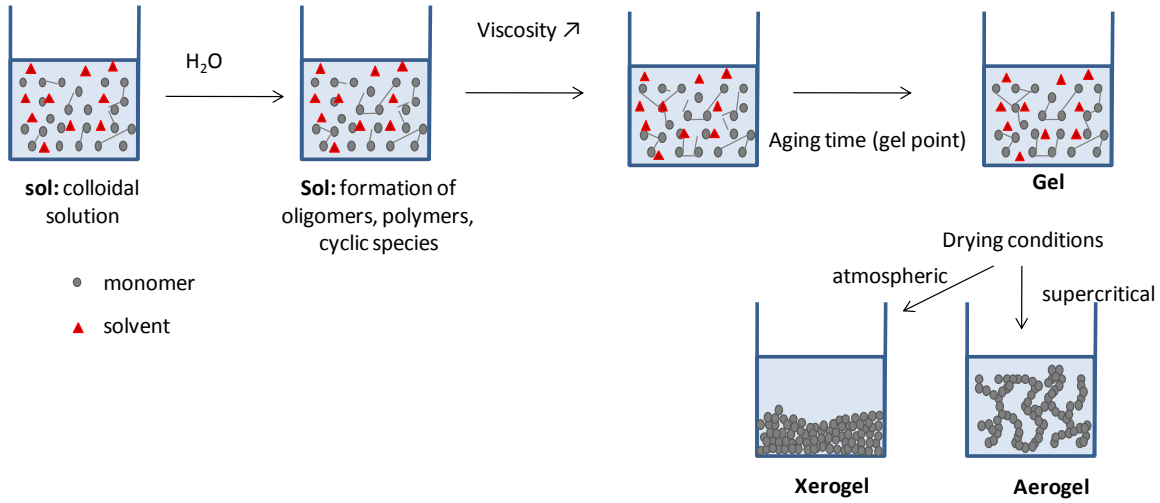

Figure I.2: Schematic representation of the sol-gel transition

The silicon based sol gel process has been highly investigated; therefore the fundamental reactions are discussed here. Silicon chemistry takes an important part of sol-gel science and lot of works are dedicated to this chemistry as silica is the first component for the fabrication of ceramics, glass and glass derivatives; sol-gel process is frequently used instead of fusion method

for their preparation. Indeed, due to its mild conditions of preparation, sol-gel process is frequently called "soft" chemistry as it implies temperatures much less important than the very high ones (1200-1500°C) traditionally required for the preparation of glass and ceramics by fusion[5]. In addition with this process, ceramics or glass with high purity and a better homogeneity are formed. However, compared to other transition metals, silica is less electropositive making it less susceptible to nucleophilic attack. Slower hydrolysis and condensation kinetics are expected and a catalyst is in most case needed to ensure the sol-gel polymerization. Acid (i. e. HCl, HF, H_2SO_4 or HNO_3), basic (i. e. NH_4OH, NaOH) or nucleophilic (i. e. KF, NH_4F) catalysts can be used leading to very different materials. Hydrolysis and condensation rates as well as final structure obtained are strongly influenced by the pH.

In brief, sol-gel process possesses various advantages:

- the soft chemistry conditions that allow incorporations of dyes or organic species to prepare a large variety of hybrid materials having various applications[10-12]
- the large diversity of alkoxide precursors presenting various properties
- the possibility to prepare an important range of materials which can be implemented under various forms (i.e.. powders, fibers, monoliths, particles and films) depending on the synthesis and drying conditions (Figure I.3).

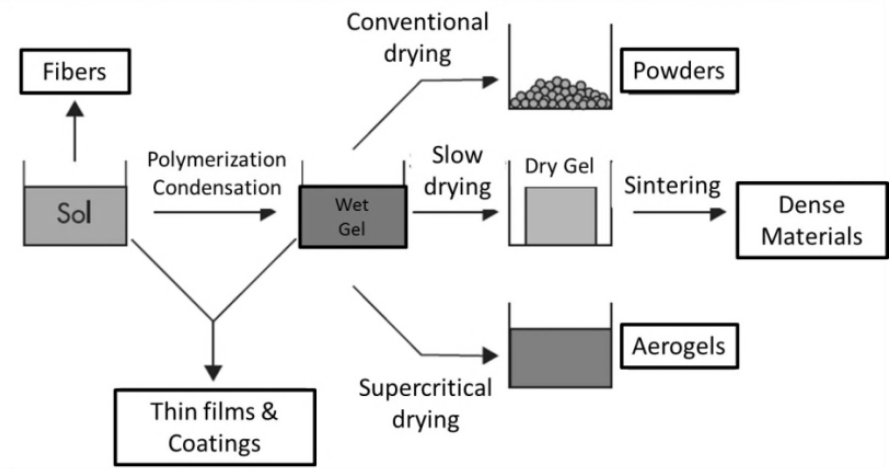

Figure I.3: Various shapes of sol-gel materials depending on the synthesis and drying conditions

Among these numerous materials, preparation of thin films and coatings is by far the most important use. Prior to gelation, the sol is cast by spin, dip or spray coating into a thin film, then solvent evaporation and capillary force lead to a dense film. Sol-gel derived glass and ceramic materials have been developed as coatings, especially for dielectric and electronic thin film devices[13], (anti)reflective or protective coatings[14-17] and so on.

I.2. SCIENTIFIC ASPECT OF THE SOL-GEL PROCESS

In the case of the hydrolytic pathway, the sol gel process takes place in two steps, first hydrolysis of the alkoxide precursor followed by condensation reaction. In order to have acceptable reactions rates it is necessary to add acid or basic catalysts. Nucleophilic catalyst can also be employed but will not be discussed here. Depending on the type of catalyst (i.e. acid or basic) different mechanisms are involved and material with different properties and morphologies are prepared. In the following paragraphs, our goal is to review the reactive mechanisms in acid and basic conditions as well as the different parameters that will influence these reactions:

- Nature and concentration of catalyst
- Nature of substituent: steric and inductive effect
- Water concentration
- Solvent presence

Finally, the polymerization reaction influenced by the acid or basic conditions is also reviewed and relied to the difference of morphologies of the final material.

I.2.1. Reactive mechanisms

Hydrolysis

Hydrolysis occurs by reaction between a water molecule and an alkoxide to form a silanol bond and liberate an alcohol. In acid catalysis, the protonation of the alkoxide is favored[6,18]. By consequence, the electronic density on the Si central atom is decreasing and this later becomes more electrophile and will be more susceptible to water attack as represented in Scheme I.2A. The oxygen of the water molecule will undergo a nucleophilic attack (SN_2) on the silicon atom. A silanol bond is formed and thus, facilitates the departure of the protonated alkoxide moieties as well as the regeneration of the catalyst. In the literature different catalytic processes have been proposed: Pohl and Osterholz[18,19] have suggested a tetrahedral inversion representative of a SN_2 nucleophilic substitution. However, mechanisms implying flank side attack[20] or siliconium ion intermediate[21,22] have also been proposed. However, several authors argue against this later mechanism[23].

Under neutral or basic conditions (Scheme I.2B), water is replaced by OH^- ions that are strongly attired by the electropositive metal Si. The hydroxyl anion directly attacks the silicon atom by a SN_2 mechanism. A silanol bond is thus formed and an alcoolate is released. This later reacts with water molecule to form the corresponding alcohol and regenerate the catalyst. In the literature, Iler[24] and Keefer[20] have suggested a tetrahedral inversion representative of a SN_2 nucleophilic

substitution similar to the acid catalysis. Pohl and Osterholtz[18] also proposed a mechanism implying a stable penta-coordinated intermediate.

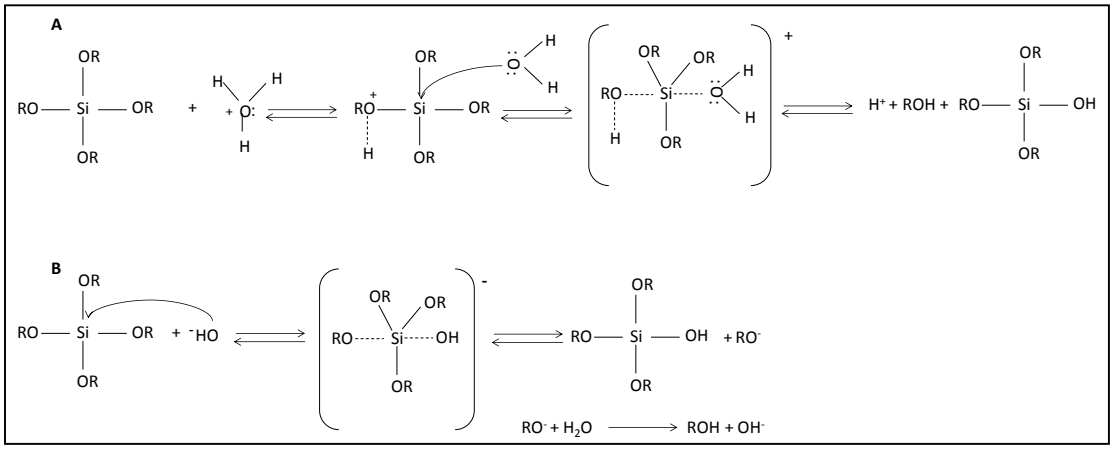

Scheme I.2: Hydrolysis mechanism in acid (A) and basic (B) catalysis

Condensation

Condensation reactions occur between two partially hydrolyzed alkoxy precursors and proceed also through a SN_2 mechanism. Condensation can only take place since few alkoxide moieties have been hydrolyzed but in general, condensation starts before hydrolysis is complete. Two competitive mechanisms are involved: water- and alcohol-condensation corresponding respectively to homo- and hetero-condensation (Scheme I.1).

At pH < 2, acid catalyzed condensation involved protonated silanols and may take place preferentially between neutral species and protonated silanols situated on monomers, end groups of chains whereas under basic conditions deprotonated silanols react on a neutral silanol. In both cases, condensation reaction occurs via a nucleophilic attack and implies a penta- or hexa-coordinated silicon intermediate (Scheme I.3A and B).

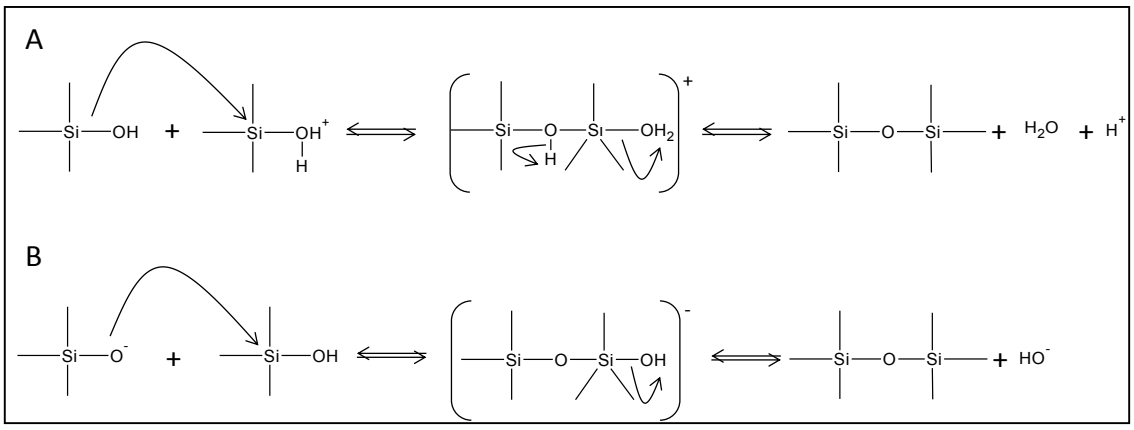

Scheme I.3: Condensation mechanism in acid (A) and basic (B) catalysis

I.2.2. Influence of various parameters

Nature and concentration of catalyst

Sol gel process is likely to occur without catalyst; however addition of acid or basic catalyst clearly leads to more rapid and complete reactions. As already detailed in the previous paragraph, the type of catalyst will greatly influences hydrolysis and condensation rates as well as the gel formation[6,25,26]. According to Aelion[23], the rate and extent of the hydrolysis reaction is most influenced by the strength and concentration of the acid- or base catalyst. Aelion and Pope[25] showed that strong acids behave similarly and have a better catalytic activity compared to weaker acid. However under basic conditions, with weaker bases such as, ammonium hydroxide and pyridine, larger concentrations are required to have acceptable reaction time. Condensation reactions are as well acid and base specific. In brief, strongly acid media favors hydrolysis step and decrease the condensation one whereas the opposite is observed in more neutral and basic pH.

Nature of substituents: steric and inductive effect

In acidic and basic media, both steric and inductive effects play an important role. However, acid catalysis is more sensitive to steric hindrance whereas basic catalysis is greatly influenced by the inductive effect. Inductive effects (electron providing or electron withdrawing) have an important role in hydrolysis and condensation reactions. Electronic density depending on the nature of the substituent on the silica atom decreases as follow: R > OR > OH > OSi. Intermediate states positively charged as in acid catalysis are stabilized by electron providing substituent whereas negatively charged ones (base catalysis) are favored by electron withdrawing substituent. Nevertheless, the main difference between acid and basic catalysis is that in acid conditions, the intermediate is positively charged so as hydrolysis goes along OR moieties are replaced by OH functions decreasing the intermediary stability and thus decreasing the hydrolysis rate. In contrary, under basic conditions, the intermediate is negatively charged, replacing OR moieties by OH ones favors the intermediary stability and increase the reaction rate. The inductive effects of Si substituent in acid and basic catalysis are summarized in Figure I.4.

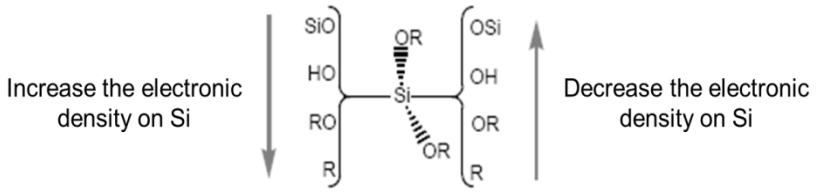

Figure I.4: Inductive effects of Si substituent in acid and basic catalysis

A study of Pohl and Osterholtz[19] and Loy[27] showed that, in acid conditions the steric effect is much more important than the inductive one. More voluminous R moieties tend to decrease the reactivity on the Si atom due to steric hindrance. End chains are less impeded leading to linear, weakly branched structure. Condensation reaction rate are also influenced by steric and inductive effect. According to Voronkov *et al.*[28] longer alkyl chains or aromatic substituent tends to decrease the reaction in acid condition. In the case of basic conditions, similar tends is observed for steric hindrance however as steric and inductive effect are going in opposite sense, the effect is much less important.

Water concentration

The presence of water can be defined as a H_2O: Si molar ratio defined as r; depending on the desired end product it can be varied from less than 1 up to over 50. An increased value of r is expected to promote the hydrolysis reaction. The acid catalysis is more influenced by the presence of water and solvent than the basic one. Indeed, Aelion *et al.* found the acid-catalyzed hydrolysis of TEOS to be first-order in water concentration; however, they observed an apparent zero-order dependence of the water concentration under basic conditions. Differing extents of precursor hydrolysis should affect the relative rates of the alcohol- or water-producing condensation reactions. Generally, under stoichiometric additions of water ($r << 2$), the alcohol producing-condensation mechanism is favored, whereas, the water-forming condensation reaction is favored when $r > 2$[29]. A low water concentration (r = 1-2) favors a linear structure[30], good conditions for the formation of fibers. Intermediate value of r leads to sphere or disk shaped particles whereas important amount of water in the initial formulation (r = 20 – 50) supports a monodispere spherical particles. However, since water is the by-product of the condensation reaction, large values of R promote siloxane bond hydrolysis (reverse reaction) and a too large excess of water is damaging for the condensation rate and can lead to phase separation.

Solvent presence

Solvent, mostly alcohol is often added to ensure miscibility between the inorganic precursor and water. The presence and the type of solvent also influence the reactivity. Artaki *et al.*[31] divide solvent in three classes: protic polar, aprotic polar and aprotic apolar solvents. According to them, in acid conditions protic polar solvents (methanol, formamide) tend to form H bonds and stabilize the intermediate. In opposition under basic conditions, aprotic polar solvent are more likely to stabilize the intermediate In addition, protic solvent as it has labile protons can also be involved in reverse reaction: (esterification, hydrolysis and alcoholysis). Finally, Artaki *et al.* report that polar solvent leads to linear structure in opposition to an apolar solvent giving mostly spherical and dense one[6,32].

I.2.3. Sol-gel transition

Sol-gel transition and final structure of the material depend mostly on pH and on the H_2O: Si ratio, r. At pH < 2, hydrolysis and condensation reactions occur via a SN_2 mechanism between protonated alkoxide groups. Hydrolysis rate is more important than condensation one. Depolymerization is negligible and condensation irreversible. At high r (r > 4) hydrolysis is complete at an early stage and condensation occurs between hydrolyzed species by a reaction limited cluster-cluster aggregation. Condensation is favored between species at end chains and tends to form weakly branched structure. At low r, condensation starts before hydrolysis is complete and favors alcohol condensation leading to a cluster-cluster aggregation mechanism and even more weakly branched structure.

At pH > 7, hydrolysis and condensation involve OH^- and SiO^- species. At high r value, hydrolysis and alcoholysis (reverse reactions) are favored and provide a source of monomers. Growth occurs via a monomer – cluster aggregation by addition of monomer on the more highly condensed particles. Spherical particles are formed and repulsion between them takes place and prevents gelification. Compact structures are formed. At low r value, unhydrolyzed site are incorporated in the growing cluster and porous material are formed.

In brief, under acid-catalyzed conditions, linear or randomly branched polymers which entangle and form additional branches are formed resulting in gelation and leading to condensation of small clusters afterwards. On the other hand, under base-catalyzed conditions, more highly branched clusters which do not interpenetrate prior to gelation are formed and highly crosslinked sol particles are formed (Figure I.5).

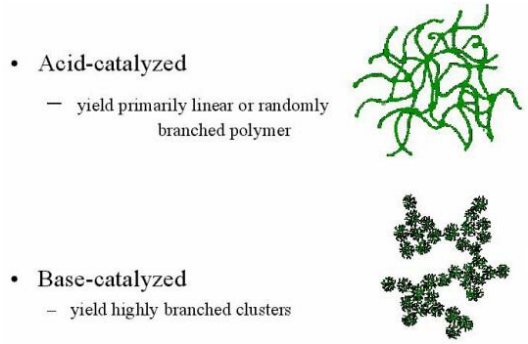

Figure I.5: Summary of acid or basic sol-gel transition

II. HYBRID MATERIAL BY THE SOL-GEL PROCESS

II.1. PRINCIPLE AND INTEREST

The main interest in sol gel chemistry relies on the soft inorganic chemistry conditions allowing incorporation of dyes or organic components. New hybrid materials whose synthesis was not possible by the fusion method are now available. The development of hybrid organic-inorganic material exploded in the eighties with the expansion of sol-gel process. The broad field of inorganic-organic hybrid materials is largely dominated by the silicon based sol-gel process. This success is due notably to his good processability and the stability of Si-C bond during the formation of silica network allowing the production of organic modified inorganic network in one step[33].

Hybrid material is an expanding field in material chemistry due to the formation of novel functional material and the possibility to create unique material by an infinite combination of organic and inorganic material. Such materials are interesting not only to design new materials for academics research but also for the development of innovative industrial applications. It is now possible to combine organic and inorganic properties in one material and create multifunctional materials. When no phase separation occurs, homogeneous materials at molecular and nanoscale are created whereas when a controlled phase separation between the inorganic and organic phases happens, structured material can be formed.

II.2. CLASSIFICATION OF MATERIAL

Hybrid material is defined at two moieties blended at molecular scale where one is organic and the other inorganic. It includes a large variety of versatile materials. A major point in the formation of hybrid material is to avoid or to control the phase segregation between the organic and inorganic parts. Nature of interactions between the organic and inorganic group is of crucial

importance. Sanchez *et al.*[34,35] proposed a classification of material based on the different interactions. Class I material implies only weak interactions such as Van der Waals, hydrogen bonding or electrostatic interactions between the two phases whereas in class II material strong chemical interactions (i.e. covalent or coordinative bonds) link together organic and inorganic components. Bond's strength and the various possible bonds are summarized in Figure I.6.

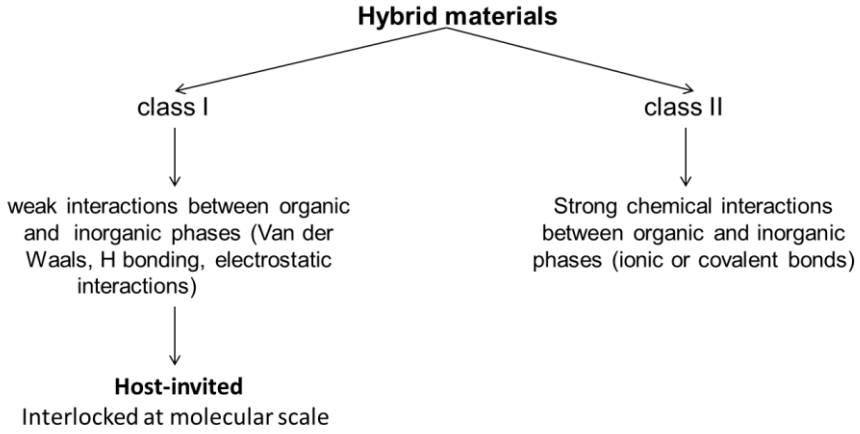

Figure I.6: Classification of hybrid materials

Class I materials are often characterized as host-invited materials as the organic and inorganic part are interlocked at molecular scale without strong interactions. It is also possible to distinguish various hybrid materials by their structural properties.

- Organic molecules (such as molecules, biomolecules, enzymes, cells…) are physically entrapped in the inorganic network formed upon gelation. Such system requires finding a suitable solvent where molecules or macromolecules are soluble and compatible with gelification. However during solvent evaporation step, this system often shows phase separation issues due to difference in polarity or leaching of the molecule. In that, concentration of organic molecules entrapped is thus limited. This process is particularly used for optic dyes[36] or enzymes[37] at low concentration.
- Organic molecules or polymers (surfactants, block copolymers…) are introduced in the sol-gel material and will undergo a controlled phase separation. Gelification of the inorganic part occurs simultaneously "around" stabilized mesophases leading to mesostructured materials. After elimination of the organic part, highly ordered porous materials are generally obtained.

In opposition in class II hybrid materials, covalent bonds between organic and inorganic part exist giving no or low phase separation and more homogeneous final material. In the field of coatings, class II materials allow the formation of thicker and more flexible films and avoid films

shrinkage frequently observed in inorganic films during evaporation[38]. In this case, it is necessary to use combined precursors containing organic function(s) (R') and hydrolyzable alkoxide moieties (OR) in the form $R'_{(x)}SiOR_{(4-x)}$[39]. Depending on x value, x = 0, 1, or 2 respectively Q, T or D units are formed as summarized in Figure I.7. Replacement of an alkoxysilane moiety by an organic group tends to decrease the reactivity as well as crosslinking degree of the final material.

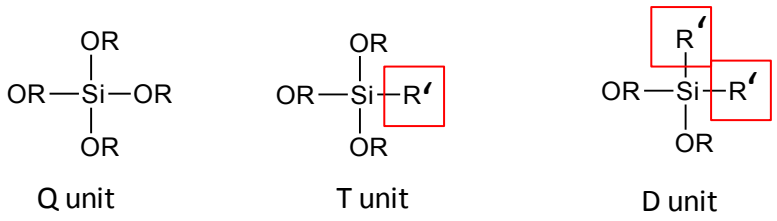

Figure I.7: Structures of inorganic or hybrid materials

However, the introduction of an organic moiety R' confers also various physical properties (mechanical, hydrophobic, electrochemical, optical…) to the final polymer. As covalent bonds link the inorganic and organic parts, this later can only be eliminated by heating at high temperature and avoid leaching problem.

We generally distinguish different types of organic functionalization engendering characteristic structural properties.

- Network modifier: in the final structure the inorganic network is only modified by the organic group R'. R' is a nonfunctional and non hydrolyzable organic group such as alkyl or fluoride atoms conferring new properties to the material (Figure I.8).
- Network functionalizer or builder: R' is a reactive (NH_2, NCO…) or polymerizable (acrylate, vinyl, epoxyde…) organic group. In this case the process takes place in 2 steps: firstly the gelification of the inorganic functionalized precursor followed by an organic polymerization or photopolymerization of the R' moieties (Figure I.8).

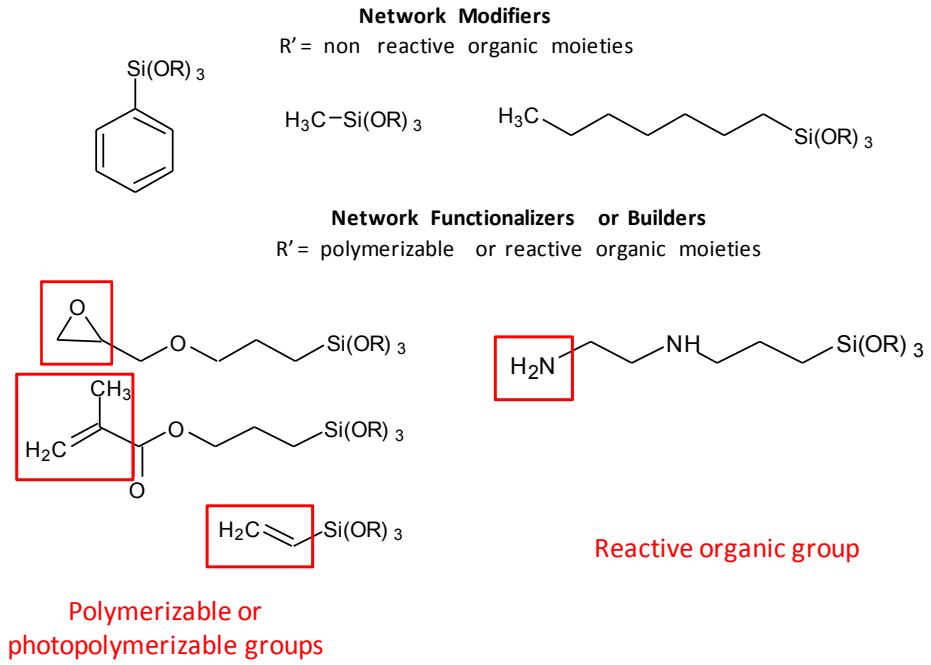

Figure I.8: Example of network modifiers, functionalizers or builders

Combination of organic and inorganic matrix is of particular interest because it allows access to specific properties arising from individual and synergic contribution of both parts. Indeed, the phase morphology and the interfacial region provide interesting new properties.

III. TOWARD A PHOTOINDUCED PROCESS

III.1. LIMITS OF THE CLASSIC SOL GEL PATHWAY

As detailed previously, sol-gel process is associated to an inorganic polymerization, with a succession of hydrolysis and condensation reactions. Despite the apparently simple method, the process can quickly become more complex and undergo competition between hydrolysis and condensation reactions as well as reverse reactions.

A conventional sol-gel pathway presents several limits:

- Necessity to add solvents to ensure miscibility with water. Since the alcohols widely used in sol-gel chemistry are volatile and inflammable, this is an important drawback for industrial used.
- No control of hydrolysis and condensation reactions is possible when starting with a precursor/water/solvent/catalyst initial formulation. A multi-step preparation method is implemented. Although it is well established in the literature, a number of technical problems arise due to the instability and limited pot life of the alkoxide-derived sols.

- Depending on experimental conditions, sol-gel reactions can take few hours or few days to achieve well condensed material.
- Thermal post-treatments are often performed to complete the densification and polycondensation as well as enhance mechanical and chemical stability[6,40]. In addition, presence of solvent favours material shrinkage due to evaporation during the drying step.

Alternative process implying photogenerated catalyst has been proposed. This method requires atmospheric water diffusion for the hydrolysis step and is mostly implemented for film preparation. As early as 1978, a patent from Fox *et al.*[41] reported a photoacid-catalyzed sol-gel alternative to produce silica-based films in a single step and without the need for solvent. The idea relies on three majors points:

- The replacement of conventional acid catalysts (i. e. acetic acid, HCl, HF, HNO_3) in the formulation by photoacid generators (PAG). The PAG is introduced in the formulation in it non-active form and Brönsted superacids will be liberated through UV exposure. Such catalysts have already been used in cationic organic photopolymerization. They are very efficient catalysts for epoxy ring opening and vinyl ether polymerization. The initial formulation is thus photolatent.
- The combination of fast PAG decomposition rate and superacidity induces a rapid solidification of the liquid precursor film, without apparent transition from a sol to a gel. Highly condensed films can potentially be achieved through appropriate choice and concentration of PAG, thus alleviating the constraint of thermal post-treatment and making such photoprocess suitable to thermally sensitive substrates.
- Atmospheric water naturally present in the atmosphere is used for the hydrolysis step. This obviates the addition of water in the initial formulation. By consequence, no solvent is required to ensure miscibility between the alkoxysilane precursor and water. The process starts from water- and solvent free formulation.

In order to better understand, the photoinduced pathway it is necessary to review some basics of photochemistry. In the next paragraphs, we will explain photopolymerization process for organic polymerization via a radical or cationic pathway and then extrapolated to inorganic polymerization (i. e. photosol-gel). In a last point, we will present the state of the art on the use of photoacid and photobase catalyzed sol-gel process for the preparation of inorganic and hybrid films.

III.2. INTRODUCTION TO PHOTOCHEMISTRY

Photochemistry can be defined as "radiation curing" system. Radiation makes a reference to light excitation by Ultraviolet (UV), visible or near IR photons (Table I.1) while curing is defined by RadTech North America association as "*the use of radiation as an energy source to induce the rapid conversion of specially formulated 100% reactive liquids to solids*". In another word, photochemistry is the trigger of chemical reactions by light in order to yield solid material[42-44]. The domain of the electromagnetic spectrum depends on the energy of the photons. Here, we will only focus on UV curing from 200 to 400 nm.

Table I.1

Domain of the electromagnetic spectrum	**λ wavelength (nm)**
UV	200-400 nm
Visible light	400 -700 nm
Near IR	700 – 1000 nm

Since the beginning of UV curing in the late 1970s, this technology has known a rapid development for industrial scale. Predominantly, photochemistry is adapted for material shaped as thin films. This technology is of particular interest for application in domains such as varnishes, paints, coatings (for wood, plastic, walls, metal, optical fibers…) as well as a large scale of applications in the printing industry, microelectronics, optics, stereolithography and so on[43]. This technology is also frequently referred as "green" as it implies rapid cure, low energy, room temperature reactions, non-polluting reactive, solvent-free formulation and it is low cost.

The initial formulation consists of liquid compounds which can be monomers, oligomers or prepolymers deposited as thin film or coating. After exposure to UV, two kinds of reaction occur: photocrosslinking or photopolymerization depending on if it implies respectively the formation of a crosslinks between macromolecular chains or the creation of a polymer through a chain reaction. Most of the time the initial monomers do not produce initiating species upon light exposure, they are not directly photoactive. The addition of a photoinitiator (PI) (low molecular weight organic molecule) is required in order to initiate the chemical reaction. A photosensitizer which is able to absorb light and transfer it to another molecule or a coinitiator that does not absorb light but participate in the production of reactive species is also sometime required[42].

III.3. ORGANIC PHOTOPOLYMERIZATION

In the organic photopolymerization reaction, the formation of the polymer network occurred in 3 steps: the initiation implying the generation of the reactive species, then the propagation step where the polymer network form and extend and the termination step which stop the reaction (Scheme I.4). The propagation step goes through the growth of polymeric chains. The reaction is very fast at the beginning and progressively slows down due to monomer concentration decrease and increase of the film viscosity. Finally, termination step is reached by lack of mobility of the radical species, by bimolecular reactions (recombination or dismutation) or by reaction with impurities. If the monomer contains only one reactive function a linear polymer is formed whereas if it has more than one reactive function a tridimensional crosslinked polymer network is formed. Organic photopolymerization implies mostly two categories of reactions: radical or cationic photopolymerization therefore different type of PIs will be used.

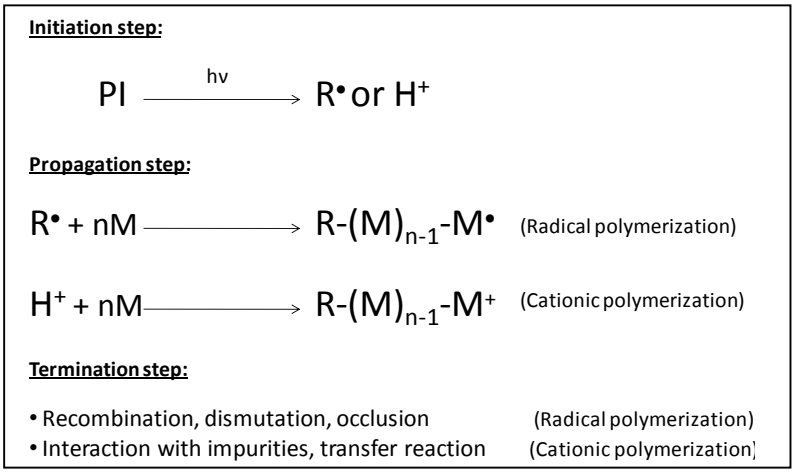

Scheme I.4: Summary of the organic polymerization steps

III.3.1. Radical photopolymerization

Radical photopolymerization have lot of applications[44] in the coating domains (varnish and paints), graphical art, microelectronic adhesives and so on…

In radical pathway, the polymerization initiation step is achieved by addition of active radical species (issue from photolysis of radical PI) on the unsaturated carbon bonds (C=C) of various monomers. The main monomers polymerizing via a radical mechanism are: unsaturated Polyester/styrene, acrylate/methacrylate or thiol/ene monomers. In most case, radical PIs are issued from the photolysis of aromatic carbonyl compounds. Aromatic ketones (hydroxyalkylphenone, aminoalkylphenone) are well known to undergo a homolytic cleavage (Norrish type I) under UV exposition leading to the formation of alkyl or benzoyl radicals[45].

Other aromatic ketones like benzophenone or thioxanthone are more likely to proceed via a photoreduction process by hydrogen abstraction or electron transfer. The different mechanisms for PIs formation are presented in Scheme I.5.

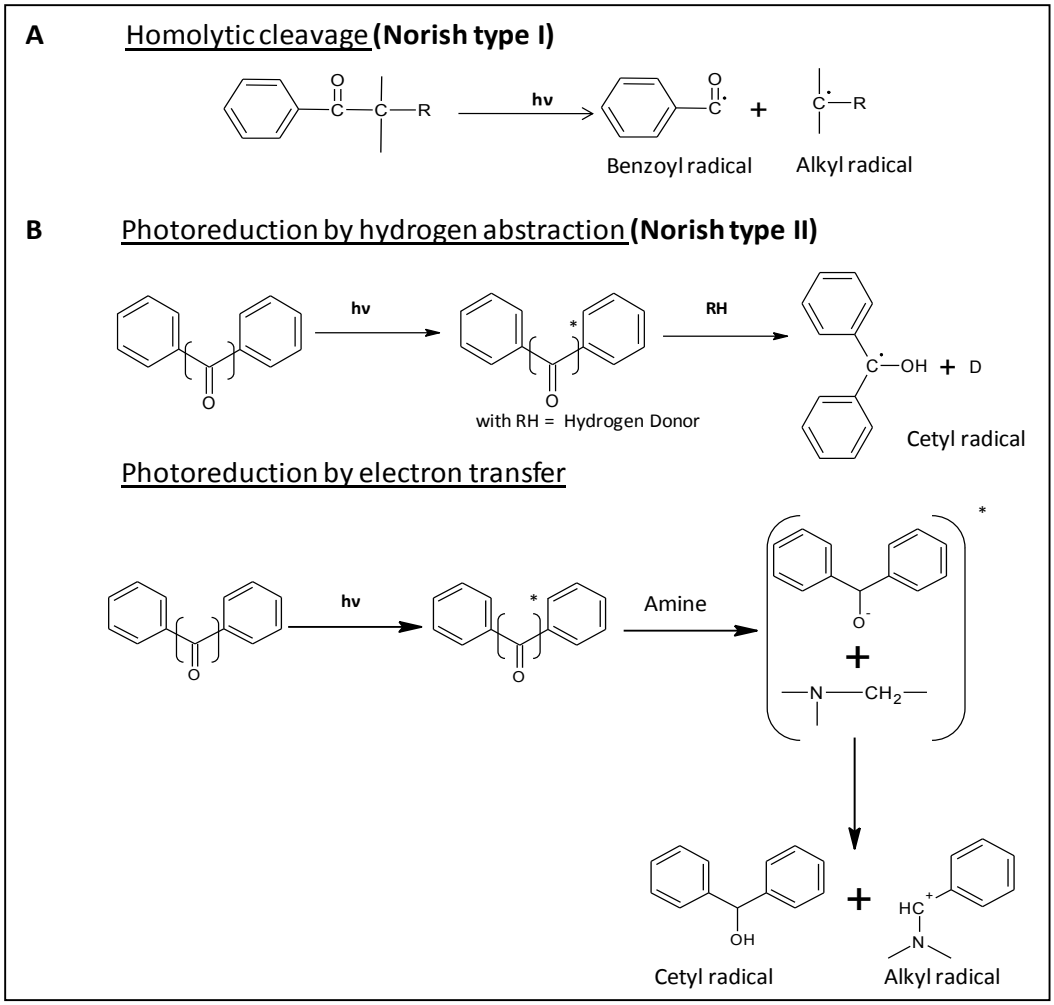

Scheme I.5: Mechanisms of type I and II radical photoinitiator photolysis

An important point in radical photopolymerization concerns secondary reactions and more particularly oxygen inhibition. When using a radical PI, this later can be deactivated at its singlet or triplet state or it can react with oxygen to form peroxide radicals which are no longer able to activate polymerization. This secondary undesired reactions lead to inhibition time and decrease of polymerization rate and final conversion. Ways to overcome oxygen inhibition are thoroughly studied in radical photopolymerization[46-48]. Among them increase of the light intensity or the PI concentration in order to create more radicals are frequently proposed. Working with more viscous monomers or thicker films to decrease the oxygen diffusion is also a possibility. Finally it can be introduced in the formulation oxygen scavengers that will

preferentially react with oxygen. Typical oxygen scavengers are hydrogen donor compounds (amine or thiol[49]) or phosphorous compounds[47].

III.3.2. Cationic photopolymerization

Despite it insensitivity toward oxygen inhibition, the cationic pathway is less developed than the radical one. Major's applications are in the field of protective or decorative coatings, inks, adhesives, photoresist for microelectronic and stereolithography[42].

Three classes of PIs for cationic polymerization are in general reported in the literature: diazonium salt, organometallic derivatives or onium salt. The two first liberate Lewis acids during photolysis whereas onium salt liberates Brönsted acids able of initiating the polymerization. Onium salts are the most often used cationic PI and will be the only one detailed here. They are very efficient for photoinitiation as a source of cationic radicals or Brönsted acids. The general structure of onium salt is represented in Scheme I.6.

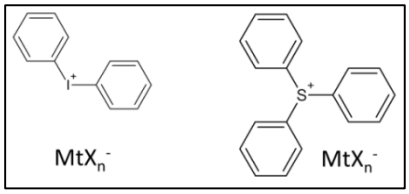

Scheme I.6: Example of diaryliodonium and triarylsulfonium salt. MtX_n^- represents BF_4^-, PF_6^-, AsF_6^-, SbF_6^-…

Onium salts (Scheme I.6) have been proposed as efficient cationic PIs based on their general structure and the combination of the cationic and anionic part. The aromatic organic moiety ensures both an absorption in the range of 200 to 320 nm and solubility with the precursor to form a low-viscous and stable solution in absence of UV light. And in parallel, the character of the anion will greatly influence the acid strength. Voluminous and thus low nucleophilic anions induce higher propagation and polymerization rate. General trends for MtX_n^- counter ions reactivity is as follow[50]: $BF_4^- < PF_6^- < AsF_6^- < SbF_6^-$.

Brönsted superacids are generated via the direct photolysis of onium salt under UV exposure. The UV irradiation causes a cascade of homolytic and heterolytic cleavages (Scheme I.7) yielding protonic Brönsted superacids ($H^+MtX_n^-$). The strongly delocalized charge on the anions (low electron pair donor ability) imparts a high catalytic reactivity to these protonic acids. Both heterolytic (1) and homolytic (2) reactions involving proton donors (RH) are responsible for the formation of superacids ($H^+MtX_n^-$).

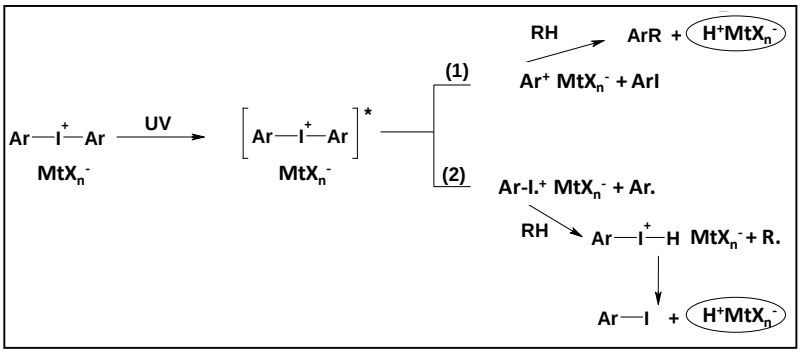

Scheme I.7: Mechanism of UV-induced photolysis of a diaryliodonium salt.

In the case of cationic photopolymerization, the propagation is quite different from radical polymerization; oxonium ions are produced and chains reactions propagate leading to polyether network formation. For epoxide moieties, it goes through an epoxy ring opening. As recombination between two cationic species is not possible termination step occurs through reaction with nucleophilic species presents in the media such as bases, hydroxylated molecules or counter ions. Contrary to radical photopolymerization, no oxygen inhibition takes place in this kind of polymerization. In addition the mechanism is also less susceptible to secondary reactions.

III.4. INORGANIC PHOTOPOLYMERIZATION

III.4.1. Photoacid catalysis

Photosol-gel process

Catalysis of organic polymerization by strong photogenerated acids as described before has been extended to inorganic polymerization. Despite this relatively simple concept, the use of photogenerated catalysts for the sol-gel polymerization has been rarely reported and described in the literature and only few patents exist. Here, we distinguish different types of precursors crosslinking via a photosol-gel process:

- inorganic precursors having or not a non reactive R group
- bridged alkoxysilane precursors

As already discussed, the first work on photoacid-catalyzed sol-gel alternative was reported by Fox *et al.*[41] in 1978. They report for the first time the use of onium salt as efficient catalyst for condensation polymerization of silane (R_xSiX_{4-x}) where R is a hydrocarbyl and X is a labile hydrolysable group (halogen, hydrogen or OR). These new types of catalyst (onium salt) are activated by incident radiation in the presence of catalytic amount of moisture (atmospheric water). Under these conditions, inorganic polymers with excellent properties were obtained.

They reported that only a weak amount of photocatalyst (typically 0.5 to 5 wt. % within the hydrolysable silane) was needed. In addition, the initial formulation is stable when stored in anhydrous media. Furthermore, another important point reported was the possibility to add dyes, plasticizers, fillers or radiation absorbers in the formulation in order to expand the film properties.

After Fox patent, no more paper refers to this photochemical pathway. It was only, 20 years later that the same idea was developed in the literature by Brinker *et al.*[51]. They report the use of photogenerated acid to promote siloxane condensation. Starting with tetraethoxysilane (TEOS) precursor in presence of a surfactant and a PAG, they prepare by a conventional sol-gel process weakly condensed mesophased photosensitive thin film. Then, the PAG was only used under selective UV exposure to prepare patterned regions with more or less highly condensed silica network. According to their work the photogeneration of acid encourages siloxane condensation. Then, in 2001, Sekiguchi *et al.*[52] reported the general preparation of photocurable composition including organosilane compounds (R_xSiX_{4-x}) where R is a non reactive moiety . They discussed the various advantages such as rapid photocurable rate, excellent storage stability, heat and scratch resistance as well as the possibility to coat a large range of substrate. Few years later, 2 patents[53-55] described the use of such precursors for the fabrication of inks, adhesives or coatings. They report a large variety of organosilane precursors and photoacids generators.

The second point concerns bridged precursors having two alkoxysilane moieties separated by an organic group. The first photosol-gel synthesis implying bridged trialkoxysilane was realized by Kowaleska *et al.*[56] in 2005. Synthesis was performed without addition of water or solvent, and atmospheric humidity was sufficient to promote hydrolysis reaction. In this study, they investigated the influence of the PAG nature; they work with diaryliodonium salt and changed the nature of the anion. By titration, they measured the Brönsted acid generation rate. Finally ^{29}Si NMR (Nuclear Magnetic Resonance) was useful to evidence the high condensation degree of silica network formed. Few years later in 2009, Moreau *et al.*[57] proposed the spatially controlled irradiation of bis triethoxysilane precursor having a fluorescent organic function in presence of PAGs. They characterize for the first time hydrolysis and condensation reactions by FTIR (Fourier transform infrared) spectroscopy. Finally, recently in our laboratory[58], we work on bridged polysilsesquioxane films crosslinked via a conventional or photoinduced sol-gel pathway. We used a series of three precursors with different organic moiety structures. Advantages of the photoinduced method (i.e. few seconds' synthesis compared to hours, higher condensation degrees, no addition of water and solvent) were highlighted (Figure I.9).

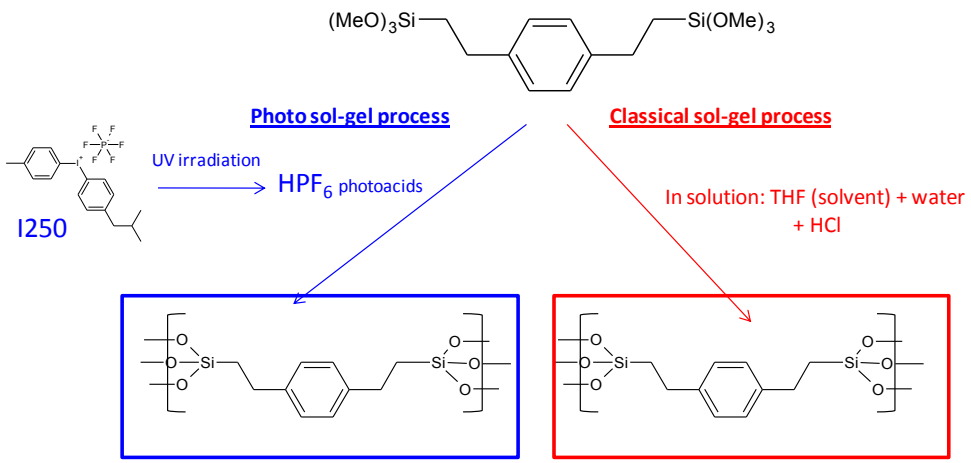

Figure I.9: Bridged polysilsesquioxane films crosslinked via a classical or a photosol-gel process[58]

As can be seen, only few works about inorganic sol-gel photopolymerization have been reported so far in the literature. No systematical investigation on the hydrolysis and condensation reactions triggered by UV has been realized. A fundamental study on the various parameters influencing theses reactions lacks as well as a comparison with the "conventional" sol-gel pathway. In the second chapter of this manuscript, we propose an extensive study of completely inorganic precursors.

Combination of organic photopolymerization and photosol-gel process

In the literature most work about photoinduced sol-gel process concerns the preparation of hybrid materials by combination of organic and inorganic photopolymerization. The concept of UV curable hybrid-material is quite well documented. However, in the large majority of the paper, the organic resin is indeed photocured with cationic or radical PI whereas the inorganic part is crosslinked via a classic sol-gel pathway not involving photoprocess[59-62]. Among works referring to hybrid organic/inorganic UV curable coating, an important part is published as patents highlighting the large interest for industrial applications. In this paragraph, our main goal is to review works where both organic and sol-gel reactions are triggered by UV. Most works using such process have been realized within our laboratory. Here, we distinguish two classes of materials, the one that are homogeneously linked together and the one that undergo a phase separation leading to macroporous or mesostructured films.

Organic and inorganic networks homogeneously linked together

Crivello *et al.* in 1995 were the first to report the combination of organic and inorganic photopolymerization. Working with an epoxytrialkoxysilane precursor in presence of a triarylsulfonium salt, the authors relate the concomitant formation of a polyethylene oxide and

siloxane networks[63]. Brönsted photoacids liberated under UV exposure were able to catalyze simultaneously the organic and sol-gel reactions. Atmospheric moisture was sufficient to promote hydrolysis and condensation reactions without additional water.

Since 2008, in our laboratory, we revisit this novel one-step methodology for preparing hybrid sol-gel coatings by UV irradiation of simple and commercial bifunctional hybrid precursors $R'Si(OR)_3$ where R = alkoxysilane moieties and R' = organic epoxy function[64] (Figure I.10) or vinylether function[65]. Another interesting point is the addition of hybrid precursor to organic resins such as organic epoxy functionalized resin[66]. In each case, the onium salt was able to simultaneously catalyze the organic polymerization of epoxy or vinyl ether functions and liberated Brönsted superacids were very efficient for hydrolysis/condensation catalysis.

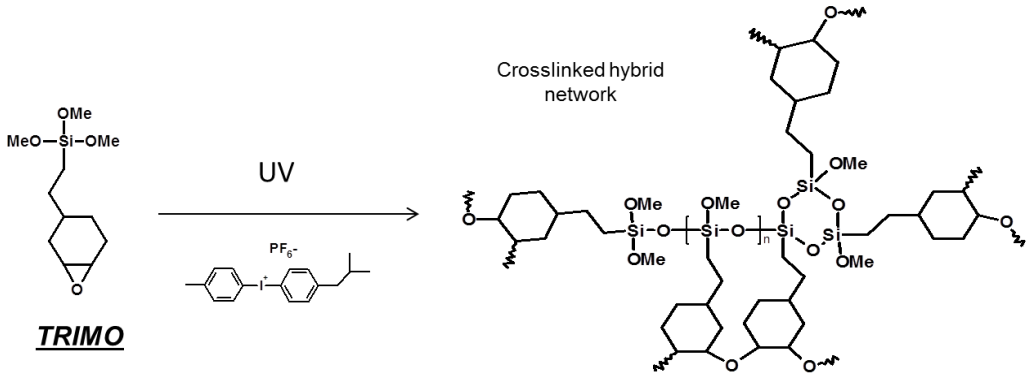

Figure I.10: Concomitant Organic-Inorganic UV-Curing Catalyzed by Photoacids[64]

This new methodology presents various advantages such as stable, solvent free, one pot formulation and reactions occurring at room temperature in presence of catalytic amount of water. Competition between organic and inorganic polymerization rates was studied by *in situ* real-time Fourier transform infrared spectroscopy (RT-FTIR), a complete study of the resultant hybrid film were realized by ^{29}Si and ^{13}C NMR solid state and XRD (X-ray diffraction). The formation of homogeneous molecular hybrid organic-inorganic with local organization was reported. Influence of various parameters such as nature of the hybrid monomer, film thickness, type of substrate, laminated condition and so on was also investigated. Finally, films were also mechanically and thermally studied by Dynamic Mechanical Analysis (DMA), Differential Scanning Calorimetry (DSC), tribological and scratch tests. Hybrid organic-inorganic films are a powerful tool for tailoring mechanical properties.

Within our laboratory, we also report a tandem photoacid-catalyzed polymerization of n-alkyltrimethoxysilane precursors and a diglycidyl ether organic monomer[67]. Organosilane precursor exhibiting different structures and chain lengths (n-butyl, n-octyl, n-dodecyl, n-

hexadecyl, isobutyl and isooctyl) were systematically investigated to afford a range of transparent alkylsiloxane-polyether hybrids. Competitive organic–inorganic reactions kinetics were investigated using RT-FTIR. A main emphasis has been on discussing the effect of the alkyl substituent structure on the photoinduced polymerization kinetics and the silicate networks characterized by ^{29}Si solid-state NMR. To avoid phase separation, the rate of formation of the two phases was tailored to favor concomitancy upon modulating several experimental parameters: film thickness, alkyl structure, PAG concentration. Finally, the viscoelastic and surface properties were also assessed by DMA and water contact angle measurements, respectively.

Beside these academic works, various patents were published by companies

- Versteeg *et al.*[68] in 2009 reported the use of cationic photoinitiator (onium salt) as catalyst for both organic polymerization of cyclic ether and photosol-gel catalysis of at least one hydrolyzable group of silane resin. They proposed to use cationic polymerization in order to overcome oxygen inhibition currently occurring with radical photoinitiator. They found various advantages such as solvent free formulation, fast curing and very homogeneous resulting coating.
- Another patent[69] in 2010 related the preparation of ORMOSILs by a hybrid sol-gel process with metal alkoxide precursors and introduction of organic moieties in minority in order to overcome thickness limit of completely inorganic films. These types of coating are an intermediary between silicon rubber and silica glass leading to transparent glass-like products.
- Finally, Spyrou *et al.*[70] in 2011 reported UV cured hybrid formulations of alkoxysilane components with a PAG introduced in radiation curable crosslinkable formulations (epoxy/acrylate, polyester/acrylate and polyether /acrylate). Such materials showed good properties for adhesion and corrosion control on metal substrate.
- In our laboratory we also develop, UV cured hybrid sol-gel coatings for corrosion protection of aluminum alloy (ANR project Mhyrcea ANR 08-03). Applications for aeronautical industry were targeted.

A second step in the work of hybrid organic-inorganic sol-gel photopolymerization developed in our laboratory, consisted in the combination of two photoinitiators: a PAG (onium salt) able to catalyze inorganic polymerization and a radical PI (hydroxyphenylketone) that will be efficient for radical polymerization. Process is quite similar to the previous one, and starts from hybrid precursor $R'Si(OR)_3$ where R = alkoxysilane moieties and R’ = acrylate or methacrylate moieties.

Polymerization occurs in one step and atmospheric water is sufficient to initiate hydrolysis reaction. Reactions kinetics (RT-FTIR), film microstructure (NMR, XRD) and mechanical characterization (DSC, DMA, scratch resistance, nanoindentation) were studied[71]. Hybrid precursor copolymerized with organic acrylate or methacrylate resins were also analyzed[72]. Works are summarized in Figure I.11 below.

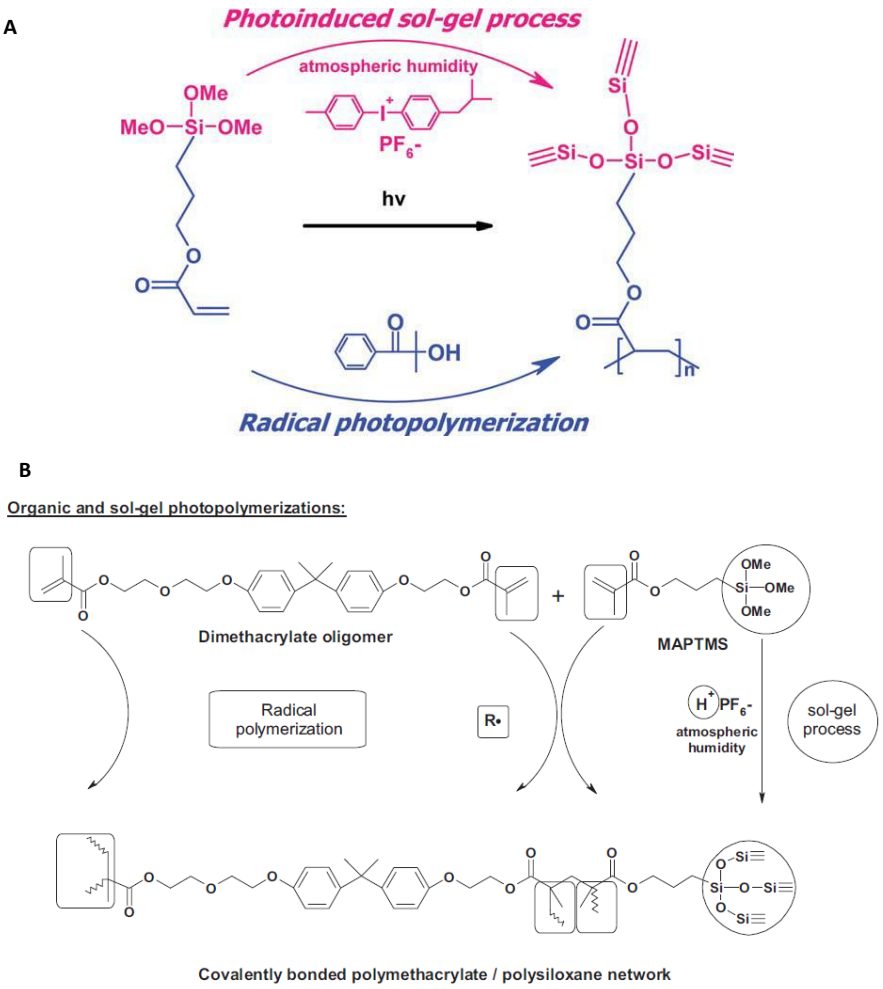

Figure I.11: One-step organic–inorganic photopolymerization of acrylate trimethoxysilane hybrid precursor (A)[71]. Dual organic/inorganic UV-initiated reaction (B)[72].

In brief, hybrid organic-inorganic materials have been prepared simultaneously in one step thanks to an UV process. Depending on the type of organic photopolymerization (i. e. cationic or radical) a PAG or combination of a PI and a PAG was required. Homogeneous and transparent films with a local organization were obtained. The combination of organic and inorganic parts leads to improved mechanical properties.

Organic and inorganic networks undergoing a controlled phase separation

This section will focus on materials in which a phase separation is photogenerated in hybrid material. The following approaches were also developed in our laboratory.

Macroporous silica films are prepared by a photoinduced phase separation avoiding the intervention of a template. The mixture of 3-(glycidyloxypropyl)trimethoxysilane (GPTMS), and poly(diethoxysiloxane) (PDEOS), without any add of solvent and water was submitted to UV illumination in the presence of a diaryl iodonium salt to afford macroporous hybrid films[73]. The formation of macropores was found to be strongly dependent on the concentration of PDEOS. Recently, further development concerned functionalized macroporous hybrid films using GPTMS and long hydrophobic alkyl chain precursors[74]. No template or additives were required. The 3D network formed as well as the homogeneously dispersed micro or nano patterns were assessed by a variety of microscope techniques (Scanning Electron Microscopy (SEM), optical microscope, Atomic Force Microscopy (AFM)). By using spatially-resolved confocal Raman spectroscopy, we showed a preferential localization of the condensed n-alkylsiloxane species at the surface of the pores to form conformationally ordered monolayers.

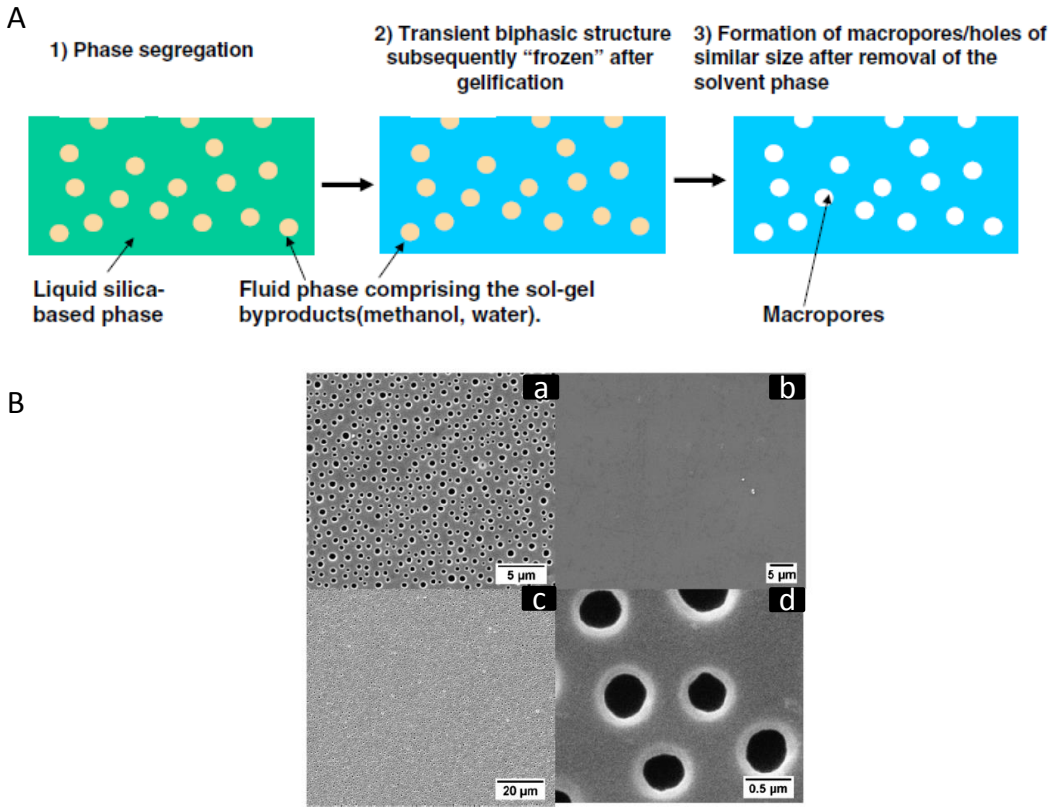

Figure I.12: Representation of the macropore formation mechanism (A). SEM pictures (a, c, d) of the hybrid macroporous films based on GPTMS and C_{12}TMS (0.5 M) under different magnifications showing well-ordered nanoperforations. For comparison, a flat hybrid film composed of GPTMS only is displayed in picture b (B)[74].

Long range ordered lamellar mesostructures can also be achieved by UV process. Starting from inorganic precursor of type $R'Si(Cl)_3$[75] or $R'Si(OR)_3$[76-78] where R = alkoxysilane moieties and R' = long alkyl chain, it was possible to prepare long range order lamellar mesostructured films. Self-assembly occurs due to hydrophobic Van der Waals interactions between the alkyl chains and the inorganic network (Si-O-Si) formed by sol-gel process in presence of Brönsted superacids photogenerated. Films were studied by ^{29}Si and ^{13}C solid state NMR, XRD and (Transmission Electron Microscopy (TEM) microscopy whereas hydrolysis kinetics and conformational behavior of the alkyl chains during UV irradiation were assessed by RT-FTIR. The effect of the alkyl chain length on the level of ordering (short or long range order), the alkyl chain packing arrangement (bilayered or interdigitated) and conformational order (gauche or trans) were also studied[76]. Surface photopatterning of organosilane self-assembled monolayers (SAM) was as well realized. The essential chemistry relies on a spatially controlled photoacid-catalyzed hydrolysis and polycondensation of n-alkyltrimethoxysilane precursors. Amphiphilic siloxane species are photogenerated locally and are able to self-assemble spontaneously into a long-range-ordered lamellar mesostructure[77].

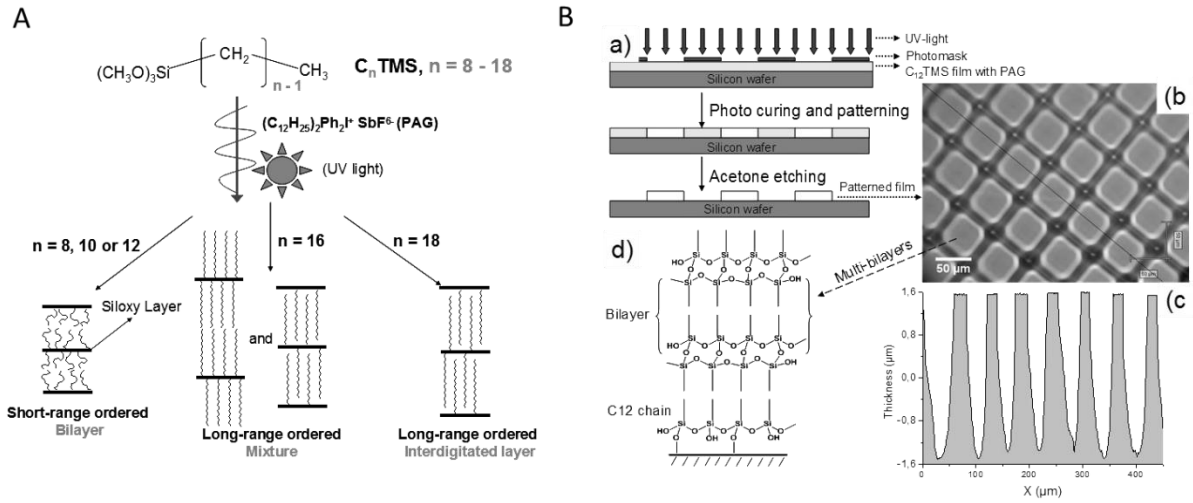

<u>Figure I.13:</u> (A) Schematic representation of the alkyl chain length dependence on lamellar phase structure and ordering[76]. (B) (a) Schematic of the preparation process for photopatterned long-range organized hybrid films based on C_{12}TMS; (b) optical microscope image of the patterned film, (c) the cross-section determined by optical profilometry measurement, (d) simplified representation of the stacked bilayer crystalline phase of the patterned area[77].

In brief, from hybrid precursors $R'SiOR_3$, films with a controlled phase separation were prepared in absence of surfactant or template. In the first case, entrapment of by product of the sol-gel reaction (water and alcohol) and their subsequent elimination lead to macroporous films and in the second case, Van der Waals interactions between the alkyl chains favour lamellar mesostructure. Kinetics parameters play a crucial role in the self organization of films.

Figure I.14 below summarizes the different works done in the literature concerning photoacid catalyzed sol-gel polymerization. In this manuscript, we will first focus on sol-gel photopolymerization of completely inorganic precursors $Si(OR)_4$ and in a second part we will investigate preparation of films with a phase controlled separation in presence of a template. As far as we are aware, no such study has been realized so far. We think that using a photoinduced process could confer several advantages for preparation of these materials.

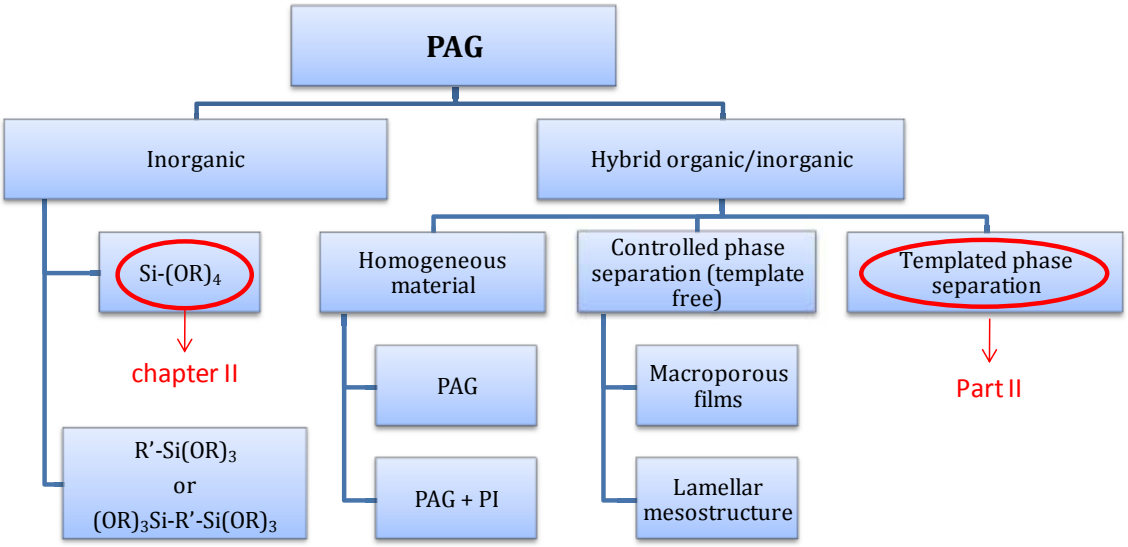

Figure I.14: Summary of the different works done in the literature concerning photoacid catalyzed sol-gel polymerization. Emphasize on future works presented in this manuscript.

III.4.2. Photobase catalysis

Compared to radical or photoacid catalysis, photobase catalysis has been much less developed in the literature. However, efficient conventional base catalyzed organic and inorganic polymerizations are reported in the literature.

According to Dietliker et al. in 2007, many organic cross-linked materials of excellent quality could be achieved with conventional base catalysts[79]. Among these organic polymerization reactions, we notice epoxy anionic polymerization, and step growth polymerizations based on multiple nucleophilic additions (*e.g.* epoxy with amine, thiol or carboxylic acid) or Michael additions (*e.g.* malonate or aceto-acetate with acrylates). In parallel, use of amine as catalyst for inorganic polymerization is also very accessible. Sol-gel process represents an excellent example of reaction in which amines have already proved their catalytic utility[80]. For instance, ammonia is known for decades as an efficient catalyst for hydrolysis and condensation of alkoxysilanes in aqueous solutions. Tertiary amines such as dimethylamino pyridine and *N*-methyl imidazole are among the most efficient sol-gel catalysts[81]. Mono- and polyamines have been also reported in

biomimetic sol-gel approaches to mimic the role of protein amino groups in biogenic silica production[82]. The key feature is that the effectiveness of an amine as a sol-gel catalyst appears to be less dependent on strong nucleophilicity and basicity, which is in sharp contrast with most base-catalyzed organic reactions[83]. pKa value defining the degree of protonation, PBG and water concentration are clearly more important for sol-gel reaction efficiency.

Transposition into photolatent composition would be highly desirable as a way to afford novel one-part systems, reactive on demand and at ambient temperature[84]. However, photobase-catalyzed organic reactions mainly focused on photogenerated amines but they have shown a limited potential for growth since their discovery in the late 1980s[85-89]. The problem is the lack of suitable photolatent amines[90]. To be effective without heat activation, most of these organic reactions require photolatent molecules releasing strongly basic tertiary amines, exhibiting typically a pKa > 12[91]. To date, only photogenerated amidine- or guanidine-type tertiary amines were successful in reaching such a strong basicity level.[84] However, slow cross-linking reactions (> 10 min) and storage difficulties due to premature gelation were even reported,[92] confirming how challenging the design of new efficient PBG was.
Nevertheless, it seems that photogenerated tertiary amines of weak nucleophilicity could be suitable for use in high speed cross-linking of alkoxy monomers without the need of additional heat treatment. The concept of photobase-catalyzed sol-gel process has been reported in patents[93,94]. However, very few in-depth studies can be found in the academic literature[95-98]. In the following paragraph we draw a state of the art of base-catalyzed photosol-gel process and we extent to hybrid material.

Photosol gel process

Proof for the increasing interest for photobase catalyzed inorganic polymerization is the number of patents that can be found in the literature.

- Pioneer work in 1996 was proposed by Hanson *et al.* starting from TEOS precursor in presence of water/ethanol and a trimethylbenzhydrylammonium salt, the authors showed that it was possible to obtain cross-linked film under UV irradiation followed by heat treatment.
- Then, ten years later, Bachon *et al.*[93] reported hardenable compositions that contain at least one silyl-terminated polymer and at least one photolatent base, the silyl-terminated polymer consisting of a linear or branched polymer that is free of silane groups and which carries terminal silane groups. PBGs are photolatent tertiary amines and amidines

(i. e. diazabicyclo-octane, N-alkylmorpholines, tetramethyl guanidines (TMG), diazabicyclononenes (DBN), diazabicycloundecenes (DBU) and imidazoles.

- Very recently (2012), Yang *et al.*[94] report curable-on-demand polysiloxane coating composition comprising reactive silane functionality and at least one photoactivatable composition that, upon exposure to radiation, generates one base selected from amidines, guanidines, phosphazenes, proazaphosphatranes. Formulations exhibit enhanced storage stability and/or pot life and that can be coated in completely solvent-free form. Upon photoactivation, the curable polysiloxane compositions can cure relatively rapidly even at temperatures as low as ambient, without the need for heat activation, and the photoactivatable compositions can be effective in relatively small amounts

As far as we are aware, we found only three papers reporting the utilization of PBGs as efficient catalysts for sol-gel reactions.

- Harkness *et al*. at the end of the 1990s relate hydrolysis and condensation reactions catalyzed by photogenerated base. They report the photopatterning of hydrogen silsesquioxanes and various silyl hydrides containing organosilicone resins. It was possible to prepare stable photocurable composition by adding photobase generators (PBGs) such as 2-Nitrobenzyl carbamates or N-Methylnifedipines to the initial precursors containing hydrolyzable silyl hydride[95] or a mix of silyl hydride and functional silanol[96]. After UV irradiation active bases are liberated and are efficient to catalyze hydrolysis of the silyl hydride in presence of residual water supplied by atmospheric air. Then subsequent condensation of generated silanol and silyl hydride occurs to yield a thermally stable inorganic network. Irradiation through a photomask allows preparation of patterned surface. Compared to PAG chemistry and classic sol gel chemistry lower film shrinkage was observed.
- Recently, Uraoka *et al.* proposed the formation of porous methylsilsesquioxane thin film prepared by a photosol-gel process[99]. In a first step, the inorganic precursor methyltriethoxysilane is hydrolyzed in acid media in presence of PPG (polypropylene glycol) as template; then in a second time cobalt (III) amine is added as PBG. The photogenerated amine worked as catalyst for the condensation reaction. They noticed that in absence of UV curing (only acid catalysis) they have important film shrinkage, because silica network formation occurs simultaneously with PPG decomposition whereas when the film is irradiated under UV for 10 minutes these two processes are decorrelated leading to limited shrinkage and better defined porosity (Figure I.15).

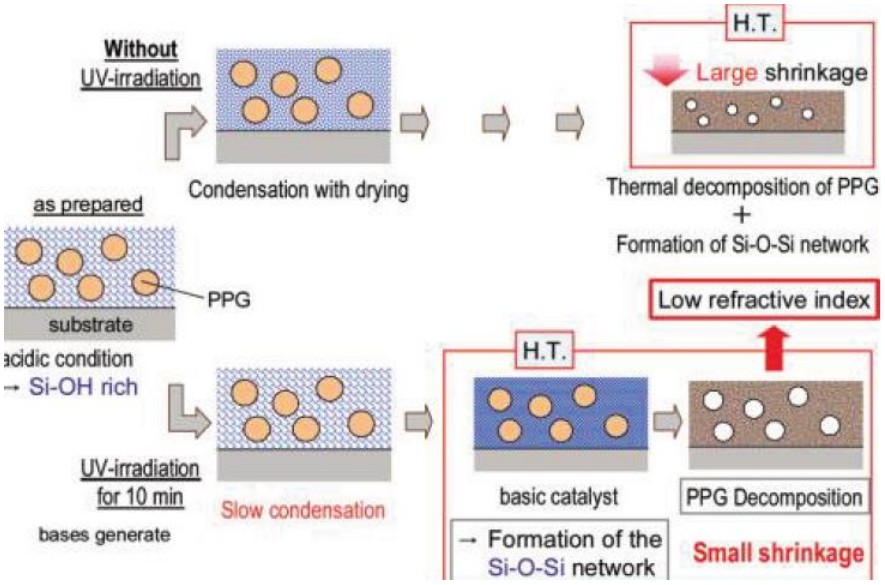

Figure I.15: Schematic showing the preparation of the porous methylsilsesquioxane film with UV irradiation using $[Co(en)_3]Cl_3$ as a PBG[99].

Combination of organic photopolymerization and photosol-gel process

So far, only one paper from our laboratory has reported the elaboration of hybrid films by a sol-gel process catalyzed by photogenerated base[98]. Using α-amino acetophenone PBG, the authors were able to catalyze simultaneously the anionic photopolymerization of epoxy functions and the hydrolysis/condensation of alkoxysilane moieties to achieve a solid cross-linked film. Tandem photopolymerization is known to lead to more homogeneous interpenetrated networks. The two different polymerization reactions are followed by RT-FTIR to bring information on the Si-O-Si network formation and the anionic polymerization. Films were also characterized by ^{29}Si and ^{13}C solid state NMR in order to determine the condensation degree and to confirm the partial ring opening of epoxy moieties.

As we can see, photobase-catalyzed polymerization is only scarcely studied in the literature. Efficiency is limited and an additional heating is required in almost all systems. Much work remains in this area. First point is to find adapted PBG that does not require post treatment step. In the third chapter, we propose a complete study on photobase catalyzed sol gel process. In addition a comparison with an equivalent photoacid catalyzed system is also made. As for PAG, use of PBG can also be extrapolated for the preparation of hybrid organic-inorganic material in one step. Finally, PBG can as well be used as catalysts for various organic reactions.

CONCLUSION

In this first chapter, we have presented the main principle of sol-gel reactions. We have detailed the reactive mechanisms of hydrolysis and condensations reactions that take place in acid and basic conditions. We highlighted how this difference of mechanism leads to different final materials. In addition, we also focus on the major parameters that will influence the kinetics of reaction. Looking at these basic concepts is essential if we want to understand works presented in this manuscript. In a second time, we underline the interest of sol-gel chemistry for the elaboration of hybrid materials. Indeed, soft chemistry favors the preparation of such materials having a sensitive organic part. A multitude of hybrid materials can be prepared by this pathway. The types of bonding (i.e. weak interactions or strong covalent bonds) as well as interfacial interactions (phase segregation) are of high importance for the final structure of the material. Finally, we showed the interest for a photoinduced sol-gel process for preparation of pure or hybrid films. In this last part we draw a state of the art on the work already realized with photoacids and photobases as catalysts. A lack of an extensive study on reactive mechanisms and influence of various key parameters has been noticed. In addition we become aware of the quasi total absence of study on photobases catalyzed system and on systematic comparison with equivalent photoacids catalyzed system.

In the next chapter, an extensive study of the sol-gel photopolymerization is undergone. Hydrolysis, condensation and sol-gel by-products are thoroughly investigated. In addition, the influence of several experimental parameters on hydrolysis is analyzed. Finally, the possibility to use such sol-gel photochemistry to cross-link silicone has been considered.

CHAPTER I REFERENCES

(1) Ebelmen, M. *C. R. Acad. Sci.* **1845**, 21, 502.
(2) Ebelmen, M. *C. R. Acad. Sci.* **1847**, 25, 854.
(3) Glaser, R. H.; Wilkes, G. L. *Polym. Bull.* **1988**, 19, 51.
(4) Geffcken, W.; Berger, H. **1939**; German patent 736411.
(5) Zarzycki, J. *J. Sol-Gel Sci. Techn.* **1997**, 8, 17.
(6) Brinker, C.; Scherer, G. *Sol-Gel Science: The Physics and Chemistry of Sol Gel Processing*; Academic Press Inc: San Diego, **1990**.
(7) Sakka, S. *Handbook of sol-gel science and technology. 1. Sol-gel processin*g; Kluwer Academic Publishers, **2005**.
(8) Fabien, M.; Pierre, A. *Techniques de l'ingénieur Procédés industriels de base en chimie et pétrochimie* **2005**, base documentaire : TIB329DUO.
(9) Prassas, M.; Hench, L. L. In *Ultrastructure processing of ceramics, glasses, and composites*; Hench, L. L., Ulrich, D. R., Eds.; Wiley: **1984**, p 100.
(10) Schottner, G.; Kron, J.; Deichmann, A. *J. Sol-Gel Sci. Techn.* **1998**, 13, 183.

(11) Schottner, G.; Rose, K.; Posset, U. *J. Sol-Gel Sci. Techn.* **2003**, 27, 71.
(12) Amberg-Schwab, S.; Katschorek, H.; Weber, U.; Burger, A.; Hänsel, R.; Steinbrecher, B.; Harzer, D. *J. Sol-Gel Sci. Techn.* **2003**, 26, 699.
(13) Klein, L. *Sol Gel technology for thin films, fibers, preforms, electronic and specialty shapes*; L.C. Klein ed.; Noyes Pub., **1988.**
(14) Zhang, Q.; Shen, J.; Wang, J.; Wu, G.; Chen, L. *Int. J. Inorg. Mater.* **2000**, 2, 319.
(15) Roux, S.; Audebert, P.; Pagetti, J.; Roche, M. *J. Mater. Chem.* **2001**, 11, 3360.
(16) Voevodin, N.; Grebasch, N.; Soto, W.; Arnold, F.; Donley, M. *Surf. Coat. Tech.* **2001**, 140, 24.
(17) Bautista, M. C.; Morales, A. *Solar Ener. Mat. Sol. C.* **2003**, 80, 217.
(18) Pohl, E. R.; Osterholtz, F. D. Molecular *Characterisation of Composites Interfaces*; New York Plenum ed., **1985.**
(19) Osterholtz, F. D.; Pohl, E. R. *J. Adhes. Sci.Technol.* **1992**, 6, 127.
(20) Keefer, K. D. *In Better ceramics through chemistry*; North Holland: **1984**, p 15.
(21) Timms, R. E. *J. Chem. Soc. A* **1971**, 0, 1969.
(22) Jada, S. *J. Am. Ceram. Soc.* **1987**, 70, C.
(23) Swain, C. G.; Esteve, R. M.; Jones, R. H. *J. Amer. Chem. Soc.***1949**, 71, 965.
(24) Iler, R. K. *The Chemistry of Silica: Solubility, Polymerization, Colloid and Surface Properties and Biochemistry of Silica*; Wiley, **1979**.
(25) Pope, E. J. A.; Mackenzie, J. D. *J. Non-Cryst. Solids* **1986**, 87, 185.
(26) Aelion, R.; Loebel, A.; Eirich, F. *J. Am. Chem. Soc.* **1950**, 72, 5705.
(27) Loy, D. A.; Baugher, B. M.; Baugher, C. R.; Schneider, D. A.; Rahimian, K. *Chem. Mater.* **2000**, 12, 3624.
(28) Voronkov, M. G.; Mileshkevich, V. P.; Yuzhelevskii, A. *The Siloxane Bond: Physical Properties and Chemical Transformations*; Consultants Bureau, **1978**.
(29) Assink, R. A.; Kay, B. D. *J. Non-Cryst. Solids* **1988**, 99, 359.
(30) Sakka, S.; Kamiya, K.; Makita, K.; Yamamoto, Y. *J. Non-Cryst. Solids* **1984**, 63, 223.
(31) Artaki, I.; Zerda, T.; Jonas, J. *J. Non-Cryst. Solids* **1986**, 81, 381.
(32) Assink, R. A.; Kay, B. D. *J. Non-Cryst. Solids* **1988**, 99, 359.
(33) Kickelbick, G. In *Hybrid Materials*; Wiley, **2007**, p 1.
(34) Judeinstein, P.; Sanchez, C. *J. Mater. Chem.* **1996,** 6, 511.
(35) C. Sanchez; *Les matériaux hybrides : définition et classification, in Matériaux Hybrides*, **1996**, O. F. d. T. Avancées, Paris, 27-31.
(36) Jerónimo, P. C.; Araújo, A. N.; Conceição BSM Montenegro, M. *Talanta* **2007**, 72, 13.
(37) Avnir, D.; Braun, S.; Lev, O.; Ottolenghi, M. *Chem. Mater*. **1994**, 6, 1605.
(38) Guglielmi, M. *J. Sol-Gel Sci. Techn.* **1997**, 8, 443.
(39) Schmidt, H.; Scholze, H.; Kaiser, A. *J. Non-Cryst. Solids* **1984**, 63, 1.
(40) Brinker, C. J.; Hurd, A. J.; Schunk, P. R.; Frye, G. C.; Ashley, C. S. *J. Non-Cryst. Solids* **1992**, 147-148, 424.
(41) Fox, F. J.; Noren, R. W.; Krankkala, G. E. **1978**; US4101513.
(42) Fouassier, J.-P. *Photoinitiation, Photopolymerization, and Photocuring: Fundamentals and Applications*; Hanser ed., **1995**.
(43) Fouassier, J.-P.; Rabek, J. F. *Radiation Curing in Polymer Science and Technology*; Elsevier Science ed., **1993**; Vol. Vol. 1 à 4.
(44) Schwalm, R. *UV Coatings: Basics, Recent Developments and New Applications*; Elsevier Science, **2006**.
(45) Christian, D. *Techniques de l'ingénieur Plastochimie et analyse physico-chimique* **2000**, base documentaire : TIB139DUO.
(46) Studer, K.; Decker, C.; Beck, E.; Schwalm, R. *Prog. Org. Coat.* **2003**, 48, 92.
(47) Belon, C.; Allonas, X.; Croutxé-barghorn, C.; Lalevée, J. *J. Polym. Sci. Pol. Chem.* **2010**, 48, 2462.
(48) Courtecuisse, F.; Belbakra, A.; Croutxé-Barghorn, C.; Allonas, X.; Dietlin, C. Journal *J. Polym. Sci. Pol. Chem.* **2011**, 49, 5169.
(49) Courtecuisse, F.; Cerezo, J.; Croutxé-Barghorn, C.; Dietlin, C.; Allonas, X. *J. Polym. Sci. Pol. Chem.* **2013**, 51, 635.
(50) Crivello, J. V. *J. Photopolym. Sci. Tec.* **2009**, 22, 575.
(51) Doshi D. A.; Huesing N. K.; Lu M.; Fan H.; Lu Y.; Simmons-Potter K.; Potter B. G.; Hurd A. J.; Brinker, C. J. *Science* **2000**, 290, 107.

(52) Fan, H.; Lu, Y.; Stump, A.; Reed, S. T.; Baer, T.; Schunk, R.; Perez-Luna, V.; Lopez, G. P.; Brinker, C. J. *Nature* **2000**, 405, 56.
(53) Liu, J.; Leir, C. M.; Moore, G. G. I.; Sherman, A. A.; Everaerts, A. I.; Boulos, M. A. **2001**; US6204350
(54) Wu, D.; Liu, J.; Dennison, K. A. **2003**; US20030007050.
(55) Wu, D.; Liu, J.; Dennison, K. A. **2004**; US6719422.
(56) Kowalewska, A. *J. Mater. Chem.* **2005**, 15, 4997.
(57) Sallenave, X.; Dautel, O. J.; Wantz, G.; Valvin, P.; Lère-Porte, J.-P.; Moreau, J. J. E. *Adv. Funct. Mater.* **2009**, 19, 404.
(58) Chemtob, A.; Belon, C.; Croutxe-Barghorn, C.; Brendle, J.; Soulard, M.; Rigolet, S.; Le Houerou, V.; Gauthier, C. *New J. Chem*. **2010**, 34, 1068.
(59) Gilberts, J.; Tinnemans, A. H. A.; Hogerheide, M. P.; Koster, T. P. M. *J. Sol-Gel Sci. Techn.* **1998**, 11, 153.
(60) Soppera, O.; Croutxé-Barghorn, C. *J. Polym. Sci. Pol. Chem.* **2003**, 41, 716.
(61) Amerio, E.; Sangermano, M.; Malucelli, G.; Priola, A.; Voit, B. *Polymer* **2005**, 46, 11241.
(62) Malucelli, G.; Priola, A.; Sangermano, M.; Amerio, E.; Zini, E.; Fabbri, E. *Polymer* **2005**, 46, 2872.
(63) Crivello, J. V.; Bi, D.; Lu, Y. *Macromol. Symp.* **1995**, 95, 79.
(64) Chemtob, A.; Versace, D.-L.; Belon, C.; Croutxe-Barghorn, C.; Rigolet, S. *Macromolecules* **2008**, 41, 7390.
(65) Chemtob, A.; Belon, C.; Croutxé-Barghorn, C.; Rigolet, S.; Vidal, L.; Brendlé, J.; Mandel, J.; Blanchard, N. *Polym. Eng. Sci.* **2011**, 51, 1466.
(66) Belon, C.; Chemtob, A.; Croutxé-Barghorn, C.; Rigolet, S.; Schmitt, M.; Bistac, S.; Le Houérou, V.; Gauthier, C. *Polym. Int.* **2010**, 59, 1175.
(67) Ni, L.; Moreau, N.; Chemtob, A.; Croutxé-Barghorn, C. *J. Sol-Gel Sci. Techn.* **2012**, 64, 500.
(68) Versteeg D. **2009**; US20090318578
(69) Gvishi R. **2010**; WO2010064240
(70) Spyrou E. **2011**; US20110060068
(71) Belon, C.; Chemtob, A.; Croutxé-Barghorn, C.; Rigolet, S.; Le Houérou, V.; Gauthier, C. *J. Polym. Sci. Pol. Chem.* **2010**, 48, 4150.
(72) Belon, C.; Chemtob, A.; Croutxé-Barghorn, C.; Rigolet, S.; Le Houérou, V.; Gauthier, C. *Macromol. Mater. Eng.* **2011**, 296, 506.
(73) Chemtob, A.; Peter, M.; Belon, C.; Dietlin, C.; Croutxe-Barghorn, C.; Vidal, L.; Rigolet, S. *J. Mater. Chem.* **2010**, 20, 9104.
(74) Chemtob, A.; Ni, L.; Dietlin, C.; Croutxé-Barghorn, C.; Kitzmann, P.; Brogly, M.; Vidal, L. *Surf. Coat. Tech.* **2012**, 209, 64.
(75) Chemtob, A.; Ni, L.; Croutxé-Barghorn, C.; Demarest, A.; Brendlé, J.; Vidal, L.; Rigolet, S. *Langmuir* **2011**, 27, 12621.
(76) Ni, L.; Chemtob, A.; Croutxé-Barghorn, C.; Brendlé, J.; Vidal, L.; Rigolet, S. *J. Mater. Chem.* **2012**, 22, 643.
(77) Ni, L.; Chemtob, A.; Croutxé-Barghorn, C. ; Brendlé, J.; Vidal, L.; Rigolet, S. *Langmuir* **2012,** 28, 7129.
(78) Ni, L.; Chemtob, A.; Croutxé-Barghorn, C. ; Brendlé, J.; Vidal, L.; Rigolet, S. *J. Phys. Chem. C* **2012**, 116, 24320.
(79) Dietliker, K.; Husler, R.; Birbaum, J. L.; Ilg, S.; Villeneuve, S.; Studer, K.; Jung, T.; Benkhoff, J.; Kura, H.; Matsumoto, A.; Oka, H. *Prog. Org. Coat.* **2007**, 58, 146.
(80) Brinker, C. J.; Scherer, G. W. *Sol-Gel Science*; Academic Press: San Diego, **1990**.
(81) Corriu, R. J. P.; Guerin, C.; Henner, B. J. L.; Wang, Q. *Organometallics* **1991**, 10, 3200.
(82) Delak, K. M.; Sahai, N. *Chem. Mater*. **2005**, 17, 3221.
(83) Wu, K. H.; Chang, T. C.; Yang, C. C.; Wang, G. P. *Thin Solid Films* **2006**, 513, 84.
(84) Dietliker, K.; Misteli, K.; Studer, K.; Lordelot, C.; Jung, T.; Benkhoff, J.; Sitzmann, E. In RadTech Vienna, **2007**.
(85) Pincock, J. A.; A., J. *Tetrahedron Lett.* **1979**, 20, 1029.
(86) Cameron, J. F.; Frechet, J. M. J. *J. Am. Chem. Soc.* **1991**, 113, 4303.
(87) Ito, K.; Nishimura, M.; Sashio, M.; Tsunooka, M. *Chem. Lett.* **1992**, 1153−1156.
(88) Jensen, K. H.; Hanson, J. E. *Chem. Mater.* **2002**, 14, 918.
(89) Weit, S. K.; Kutal, C.; Allen, R. D. *Chem. Mater.* **1992**, 4, 453−457.
(90) Suyama, K.; Shirai, M. *Prog. Polym. Sci.* **2009**, 34, 194.
(91) Sun, X.; Gao, J. P.; Wang, Z. Y. *J. Am. Chem. Soc.* **2008**, 130, 8130.

(92) Dietliker, K.; Engelbrecht, L.; Jung, T.; Mistelli, K.; Studer, K. **2008**; WO2008119688.
(93) Bachon, T. **2005**; WO2005100482.
(94) Yang, Y.; Semonick, M.; Moore, G.; Boardman, L.; Craton M. **2012;** WO2012003153.
(95) Harkness, B. R.; Takeuchi, K.; Tachikawa, M. *Macromolecules* **1998**, 31, 4798.
(96) Harkness, B. R.; Takeuchi, K.; Tachikawa, M. *Polym. Adv. Technol.* **1999**, 10, 669.
(97) Uraoka, Y.; Tadanaga, K.; Tatsumisago, M. *Chem. Mater*. **2010**, 22, 6125.
(98) Chemtob, A.; Courtecuisse, F.; Croutxe-Barghorn, C.; Rigolet, S. *New J. Chem.* **2011**, 35, 1803.
(99) Uraoka, Y.; Tadanaga, K.; Tatsumisago, M. *Chem. Mater.* **2010**, 22, 6125.

CHAPTER II: SOL-GEL PHOTOPOLYMERIZATION OF INORGANIC ALKOXYSILANE PRECURSORS IN PHOTOACID CATALYSIS

De Paz, H.; Chemtob, A.; Croutxé-Barghorn, C.; Le Nouen, D.; Rigolet, S. *J. Phys. Chem. B***2012**, 116, 5260.

A. Chemtob, H. De Paz-Simon, C. Croutxé-Barghorn, S.Rigolet "UV-Activated Silicone Oligomer Cross-Linking Through Photoacid and Photobase Organocatalysts." Accepted in *J. Appl. Polym. Sci.*

INTRODUCTION

In previous works performed in our laboratory, hybrid films prepared by single-step organic-inorganic photopolymerizations were extensively investigated.[1-4] While organic photopolymerization is well-known and often reported in the literature, the concept of photoinduced or photoacid-catalyzed sol-gel process has been rarely studied. In this chapter, our goal is to discuss exhaustively and for the first time some mechanistic and kinetic aspects of photoinduced sol-gel process involving inorganic alkoxysilane precursors. The first part relates to the understanding of hydrolysis and condensation reactions triggered by UV under acidic conditions as well as the investigation of by-products formed during these reactions. The effect of the hydrolysable function and that of the actinic wavelength on the photoinduced sol-gel process are also studied. The second part deals with fundamental questions as regards to photoacid-catalyzed hydrolysis and condensation in silicate films. We attempt to define what chemical, physical and photochemical parameters determine the precise sequence, kinetics and advancement of these reactions under different processing conditions. Among the numerous parameters studies are the film thickness, the relative humidity (RH), the nature and the concentration of PAG. Finally, the last part focuses on the formation of hybrid films by copolymerization with OH-terminated polydimethylsiloxane (PDMS) oligomers.

An important part of our investigation lies on the *in situ* analysis of the sol-gel kinetics by RT-FTIR spectroscopy. FTIR technique has been known for decades as a powerful routine characterization technique, which provides extensive information about optical, vibrational, chemical and structural properties in sol-gel materials, in particular on films.[5-10] However, the systematic presence of solvent saturating the signal and the weak reactivity inherent in a conventional sol-gel polymerization makes the implementation of a rapid scan time-resolved FTIR either incompatible or useless. In our system, no water is added in solution which is a remarkable feature since its presence would have required the use of co-solvents to ensure miscibility with the inorganic precursor. Despite the absence of water, the reaction mechanism remains definitively hydrolytic. However, the hydrolysis stage is fed by the continuous flux of atmospheric moisture diffusing into the sample. The implementation of a solvent-free and fast photosol-gel process opens new opportunities for RT-FTIR, with the possibility to investigate structural aspects but also reaction kinetics and the formation of by-products, without affecting the course of the polymerization. Furthermore, solid-state NMR spectroscopy is employed as a very sensitive technique for probing the siloxane structure and the degree of condensation.

I. EXPERIMENTAL CONDITIONS

I.1. CHEMICALS

In order to give insight into the mechanistic aspects of a UV-mediated sol-gel process, we start with simple and model inorganic alkoxysilane precursors cast as films. As silicon sources, oligomeric precursors based on PDMOS and polydiethoxysiloxane (PDEOS) are preferred to their monomeric analogues (tetramethoxysilane (TMOS) and tetraethoxysilane (TEOS)) so as to avoid evaporation issues. PDMOS and PDEOS are non-hydrolyzed oligomeric silicate precursors derived respectively from TMOS and TEOS. Their SiO_2 equivalents are 51 and 40 wt. % respectively, which corresponds to an average of five silicon atoms per oligomer. The structure of the different precursors is given in Table II.1.

Actually, PDMOS and PDEOS consist in a mixture of linear, branched and cyclic structures. Liquid state NMR technique was essential to shed light on their precise structures.Although their ^{29}Si liquid-state NMR spectra are quite complex, they were useful for the speciation of the oligomeric silicate condensates. PDMOS and PDEOS spectra contain four signals Q^0, Q^1, Q^2 and Q^3.Q refers to tetrahedral silicon and the superscript is the number of siloxane bonds attached to the central silicon atom(from 0 up to 4). The Q^0 signal was attributed to traces of TMOS or TEOS monomers. The Q^1 species were assigned to dimers, Q^2 resonances showed the contribution from cyclic species and finally Q^3 were attributed to more complex structure. Compared to PDMOS, the ethoxy silicate derivative is characterized by a higher proportion in $Q^0$and Q^3 species. We note also the importance of cyclic siloxane species which are more prominent in PDEOS than in PDMOS (see Appendix I for more details).

Table II.1: Structures of the main compounds

PDMOS Liquid state ^{29}Si NMR			
Species	Structure	Proportion (%)	
Q^0	$(Si-(OR)_4)$	2 %	
Q^1	$(RO)_3$-Si-(OSi)	50 %	
Q^2	$(RO)_2$ -Si-$(OSi)_2$	44%	
Q^3	(RO) -Si-$(OSi)_3$	4 %	
PDEOS Liquid state ^{29}Si NMR			
Species	Structure	Proportion (%)	
Q^0	$(Si-(OR)_4)$	8 %	
Q^1	$(RO)_3$-Si-(OSi)	34 %	
Q^2	$(RO)_2$ -Si-$(OSi)_2$	43 %	
Q^3	(RO) -Si-$(OSi)_3$	16 %	
Diphenyliodonium hexafluorophosphate (φ_2I^+ PF_6^-)			

The PAG is a diphenyliodonium hexafluorophosphate salt (Φ_2I^+ PF_6^-) purchased from Sigma Aldrich and used as received. This PAG was chosen for its good solubility in the inorganic precursors. Despite a low overlapping between its absorption spectrum and the emission spectrum of the UV lamp used (Figure II.1), no sensitizer or co-initiator was required. The cationic part of the PAG ensures light absorption and solubility while the anionic part determines the acid strength. The anion has an important role on the degree of separation of the ion pair. Stronger acids are formed when larger and thus less nucleophilic anions are used.

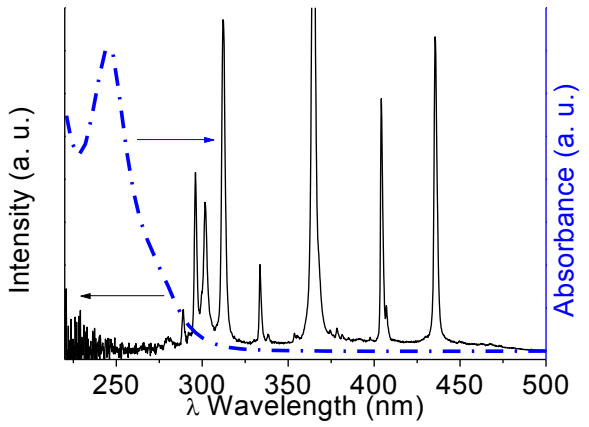

Figure II.1: Overlapping of the PAG absorption spectrum (dash dotted line) in dichloromethane (5. 10-5 M) and the Hg-Xe lamp emission spectrum equipped with a 365 nm reflector (plain line)

I.2. SAMPLES PREPARATION

In a typical procedure, 2% wt. of PAG was dissolved in the inorganic precursors (PDMOS or PDEOS) to form a photolatent solution in absence of UV light. The resultant solution was stable in dark with a pot life exceeding 3 months. Then the resulting formulation was deposited on a BaF_2 pellet using a spin coater to produce a 0.9 ± 0.2 µm and a 2.1 ± 0.5 µm liquid film layer for respectively PDMOS and PDEOS. Irradiation was performed at room temperature using a Hamamatsu Hg-Xe lamp (spectra presented in Figure II.1) fitted with a flexible waveguide. The sample was placed at 3 cm from this later and the light intensity measured was approximately 200 mW/cm^2. Experiments were realized in an environmental cell where the temperature was controlled to be around 22 ± 2°C and the RH was maintained around 30 %.

In addition, a second UV irradiation system was used for samples devoted to ^{29}Si solid state NMR which requires a greater quantity for the analysis. For this, films were prepared onto borosilicate glass substrates and photopolymerized under a UV conveyor with a belt speed of 10 m/min using a microwave lamp (H lamp, Fusion), at a light intensity of 1.46 J/cm^2 per pass. The samples were subjected to 5 successive passes under the conveyor to yield transparent solid film. During UV irradiation, the RH was maintained between 30-35 %. Finally thin films were scratched to collect solid powder of PDMOS or PDEOS.

II. UNDERSTANDING OF THE PHOTOINDUCED SOL-GEL PROCESS USING RT-FTIR

II.1. INTEREST OF THE RT-FTIR TECHNIQUE

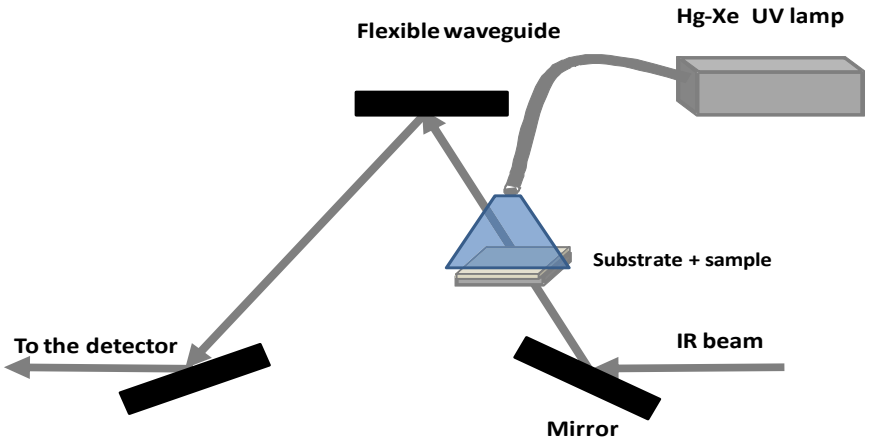

Figure II.2: RT-FTIR experimental device

The kinetic investigation lies on the *in situ* analysis of the sol-gel reaction by RT-FTIR spectroscopy. In our special set-up, the analyzing IR beam is triggered simultaneously with the

polymerizing UV light, as sketched in Figure II.2.The implementation of a solvent-free and fast photo sol-gel process opens new opportunities for RT-FTIR, with the possibility to investigate structural aspects but also reaction kinetics and the formation of by-products, without affecting the course of the polymerization. The diverse reactions that take place in our system are summarized in Scheme II.1. All the sol-gel reactions are presented using $SiOR_4$ (with R = CH_3) as precursor in order to simplify the equations.

Hydrolysis

$Si(OR)_4 + 4H_2O \rightarrow HO\text{-}Si(OR)_3 + ROH$ with R = CH_3 (1)

Condensation

$(RO)_3\,Si\text{-}OR + HO\text{-}Si(OR)_3 \rightarrow (RO)_3\text{-}Si\text{-}O\text{-}Si\text{-}(OR)_3 + ROH$ (2a)

$(RO)_3\,Si\text{-}OH + HO\text{-}Si(OR)_3 \rightarrow (RO)_3\text{-}Si\text{-}O\text{-}Si\text{-}(OR)_3 + H_2O$ (2b)

Scheme II.1: Hydrolysis and condensation reactions occurring in the sol-gel process

To give insight into the sol-gel process, the evolution of various characteristic IR bands is investigated temporally.Figure II.3 provides the 3D *in situ* time-resolved spectra of a PDMOS and PDEOS films containing 2% wt. of PAG under UV irradiation on a timescale of 300 seconds in the 2600–3750 cm^{-1} and the 700-1300 cm^{-1} range. The main IR band assignments of PDMOS and PDEOS are gathered in Table II.2.

Table II.2: Main infrared absorption bands of PDMOS and PDEOS[8,11]

Wavenumber (cm^{-1})	Assignment		Wavenumber (cm^{-1})	Assignment
2977	$\nu_{asym}CH_3$ (stretching)	(PDEOS)	~ 3740	υ OH (free)
2950	$\nu_{asym}CH_3$	(PDMOS)	~ 3400	υ OH (H bended)
2929	ν_{asym} CH_2	(PDEOS)	1640	H_2O (bending)
2890	ν_{sym} CH_3	(PDEOS)	~ 1100	ν_{asym} Si-O-Si
2848	ν_{sym} CH_3	(PDMOS)	930	υ $Si\text{-}O^-$, υ Si-OH
1458	δ_{asym} CH_3	(PDMOS)	800	ν_{sym} Si-O-Si
1196	ρ CH_3 (rocking)	(PDMOS)	460	ρ Si-O-Si (rocking)
1100-1090	ν_{asym} C-O			
960	ρ CH_3	(PDEOS)		
839	ν_{sym}Si-O	(PDMOS)		
793	ν_{sym}Si-O	(PDEOS)		

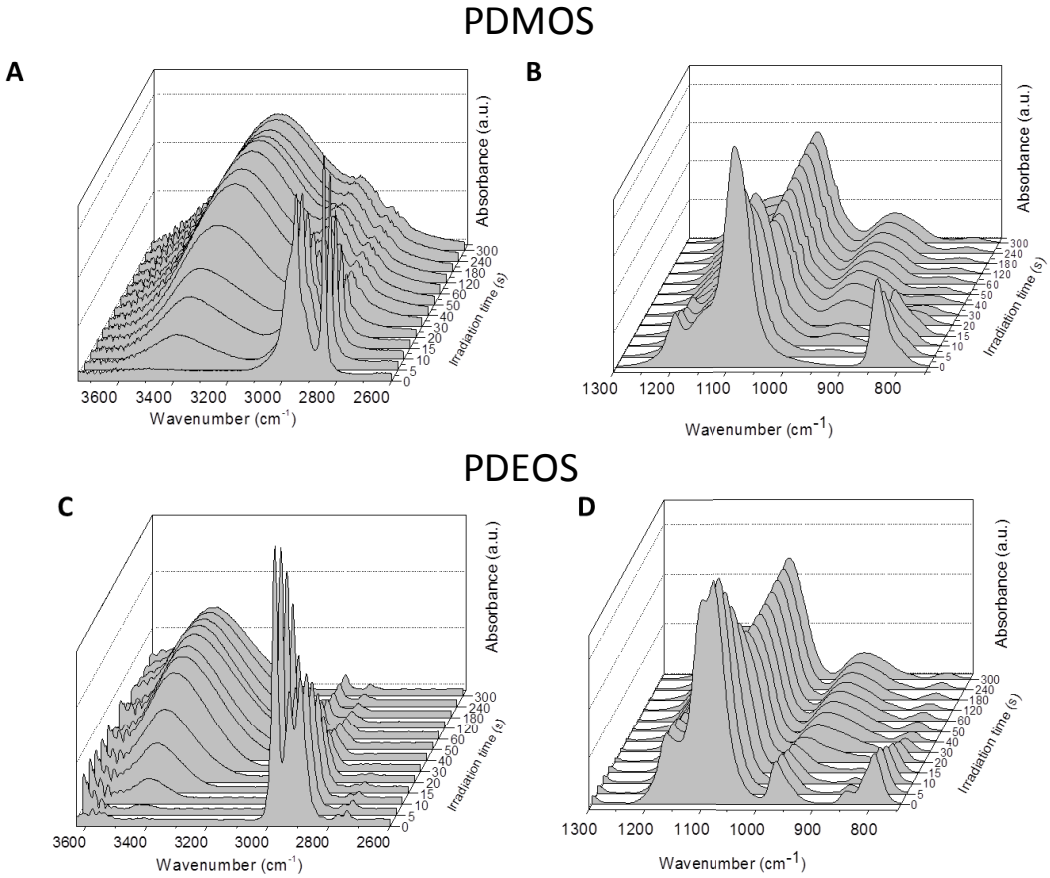

Figure II.3:*In situ* time-resolved FTIR spectra on a timescale of 300 s of a PDMOS (top) and PDEOS (bottom) films containing 2% wt. of PAG under UV irradiation in the range of 3750 - 2600 cm^{-1}(A, C) and 1300 - 700 cm^{-1}(B, D).

The first region (Figure II.3A and 3C) encompasses mainly the OH (3400 cm^{-1}) and alkoxy (~ 2900 cm^{-1}) stretching modes involved in the hydrolysis stage while the second (Figure II.3B and 3D) is more informative of polycondensation reactions through the Si-O-Si (1100 cm^{-1}) and Si-OH (930 cm^{-1}) stretching modes. Before reaction (t = 0 s), we note that a broad band around 1100 cm^{-1} is already visible in PDMOS and PDEOS spectra as expected from their oligomeric structures while the absence of any OH signal confirms the absence of hydrolysed products. In the following sections, three distinct and concomitant processes were investigated: hydrolysis, polycondensation and the development of sol-gel by-products (water, alcohol).

II.2. HYDROLYSIS REACTION

For PDMOS, we choose to study the symmetric CH_3 stretching vibration, $\nu_{sym}(CH_3)$ at 2848 cm^{-1}as it appears as a sharp isolated band, making it well-suited for a temporal analysis of the hydrolysis kinetics. Similarly, the asymmetric CH_3 stretching mode at 2977 cm^{-1} appears as a representative and easy to follow band for PDEOS. Systematic integration of these bands gave a

unique insight into the fast hydrolysis conversion-time curve. In parallel, the silanol formation can be studied by following either the large OH bands between 3200-3600 cm^{-1}or the stretching band Si-OH at 930 cm^{-1}. The large OH band actually encompasses the contribution of all hydroxyl-containing compounds: silanol and possibly methanol and water by-products.The Si-OH band is well resolved for PDMOS but for PDEOS due to overlapping of the ρCH_3 (960 cm^{-1}) and the SiOH band (930 cm^{-1}), the silanol evolution cannot be studied .Figure II.4A and B represents the relative evolution of alkoxy, silanol and OH bands during the irradiation of the PDMOS and PDEOS film respectively.

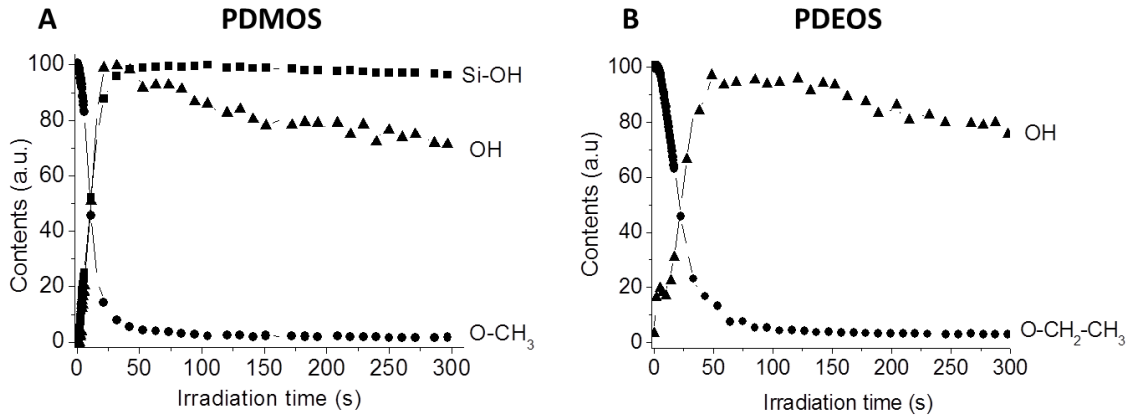

Figure II.4: Area evolution of the FTIR bands: O-CH_3 (•, $\nu_{sym}(CH_3)$, 2848 cm^{-1}), OH (▲, ν(OH), 3400 cm-1) and Si-OH (■, υ(Si-O), 930 cm^{-1}) during the UV irradiation of films based on PDMOS (A) and PDEOS (B).

As represented in Figure II.4A for PDMOS, only 11 s were necessary to consume half the methoxysilyl functions. Secondly, a slowdown happens and 50 s of irradiation were required to reach a full hydrolysis, which is an indirect indication of concomitant condensation reactions affecting the course of the hydrolysis in a more constraint silicate environment. Under most conditions in conventional sol-gel chemistry, condensation is known to start before hydrolysis is complete. Hydrolysis is also manifested by the formation of Si-OH groups, which absorb like the alcohols at 3700-3200 cm^{-1} owing to the stretching of the OH-O bonds (Figure II.3A). Even after 5 s irradiation, the OH stretching band is centered at 3400 cm^{-1}, suggesting the formation of a majority of hydrogen-bonded OH groups, with almost no contribution from free surface silanols (3740 cm^{-1}). As shown in Figure II.4A, a complete correspondence between methoxy moieties disappearance and the OH band growth during the hydrolysis stage is observed, which is in agreement with the direct conversion of Si-OCH_3 into Si-OH. More specific of silanol is a strong band due to Si-O stretching vibrations occurring at 930 cm^{-1}, whose evolution also coincides precisely with that of the alkoxide groups. Substitution of methoxy groups for ethoxy groups does not change the general trend (Figure II.4B). The main difference is that the hydrolysis rate

of PDEOS is significantly lowered, leading to delayed full consumption, as expected from the alkoxy group hindrance effect reported in conventional sol-gel chemistry.[12,13]

II.3. CONDENSATION REACTION

II.3.1. RT-FTIR study

The 1000-1300 cm^{-1} region including the Si-O-Si stretching band massif is representative of the polycondensation reactions. However this difficulty to monitor condensation reactions is twofold:

- First, the Si-O-Si antisymmetric stretching band is not resolved due to the presence of the strong ν_{asym} (Si-)O-C band (1090 cm^{-1}), changing during the hydrolysis.
- Second, the Si-O-Si antisymmetric stretching band needs to be deconvoluted to gain information on the polycondensation reactions,

Nevertheless, the completion of hydrolysis after 50 s makes this region uniquely representative of the silica network, and therefore exploitable to investigate the progress of condensation. We recognize in Figure II.3B, the signature of the IR spectrum of pure silica at the end of hydrolysis with a band centered at 1065 cm^{-1} related to longitudinal optical mode (LO_3) of the antisymmetric stretching accompanied by a clearly visible shoulder at 1140 cm^{-1} associated to the transverse optical mode (TO_3) of the same vibration. Following the assignment proposed by Fidalgo *et al.*,[9] the broad envelope was deconvoluted into four Gaussians (Figure II.5A): two major bands at 1065 (LO_3) and 1140 cm^{-1} (TO_3) with two minor components at 1075 and 1205 cm^{-1}. These latter bands were attributed to equivalent modes, but of different structural units (4-fold ring), and will not be discussed here.

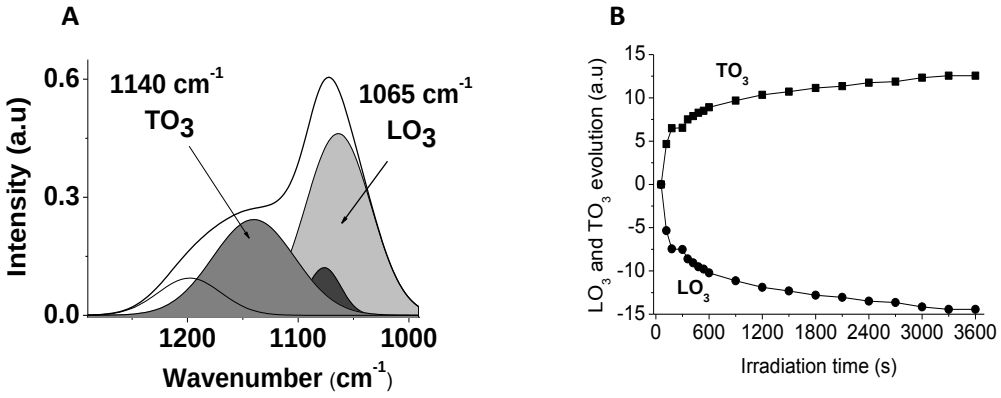

Figure II.5: Deconvolution of the FTIR absorption spectrum of the PDMOS film in the 1000-1300 cm^{-1} interval (A). Relative evolution of TO_3 (■) and LO_3 (●) Si-O-Si asymmetric stretching modes during the irradiation time (B)

The evolution of the relative areas underlying the two dominant bands (LO_3 and TO_3) was estimated throughout a longer irradiation time of 3600 s. As seen graphically in Figure II.5B, a slight increase in area of the TO component was accompanied by a decrease of that of LO. Similar evolution has already been reported by Innocenzi *et al.*[10] upon thermal treatment and interpreted as the sign of the formation of additional siloxane bonds or perhaps siloxane bond orientation. Thus, the general trend supports a condensation occurring not only in a concomitant way with hydrolysis but also subsequently. There are two other signs in line with the previous conclusion of a continued condensation after hydrolysis (t > 50 s): a sharp decrease in the area of the OH band at 3400 $cm^{-1}$and a slight reduction of the Si-OH band at 930 cm^{-1}, both evaluated in Figure II.4A. Similar evolution for the Si-O-Si massif was observed for PDEOS, however no systematic deconvolution and monitoring of the LO_3 and TO_3 bands were performed. In accordance with these results, the photoacid-catalyzed sol-gel mechanism would proceed in two consecutive stages comprising a first part in which fast hydrolysis and condensation reactions take place concurrently (t < 50 s) followed by a single and slow condensation step (t > 50 s).

II.3.2. Solid state ^{29}Si NMR

A better overview of the siloxane network microstructure was also given by solid-state ^{29}Si NMR. The NMR study is the result of a collaboration with Dr Severinne Rigolet from the team of "Matériaux à Porosité Côntrolée" (Institut des Matériaux de Mulhouse, IS2M, University of Haute-Alsace, UHA). This technique is powerful to bring information on the various environments of the silicon atom, as shown in Table II.3.

Table II.3: Structure and shifts of the various substructures observable by ^{29}Si NMR in tetra-alkoxysilane precursors.

	Structure	Shift (δ_{Si}) ppm
Q^0	$Si-(OR)_4$	-78
Q^1	$(RO)_3$-Si-(OSi)	-85
Q^2	$(RO)_2$ -Si-$(OSi)_2$	-95
Q^3	(RO) -Si-$(OSi)_3$	-105
Q^4	$Si-(OSi)_4$	-110

The SPE MAS (Single Pulse Excitation Magic Angle Spinning) mode in solid state ^{29}Si NMR allows a quantitative characterization of the sample. By spectra deconvolution using dmfit[14] it is possible to determine the proportion of each substructure and with the Equation II.1. Notably, it is possible to calculate the condensation degree (CD) of the silica network.

$CD\ (\%) = \sum_{n=4}^{4} \frac{nQ^n}{f}$ (Equation II.1) with n = number of siloxane bond ($0 \leq n \leq 4$) and f = functionality of the silicon atom (i. e. f = 4)

Figure II.6 displays the quantitative spectra of UV cross-linked PDMOS and PDEOS films. In each case, Q^3or Q^4 siloxane species are dominant, indicating that the photoinduced sol-gel process leads to well-condensed materials.

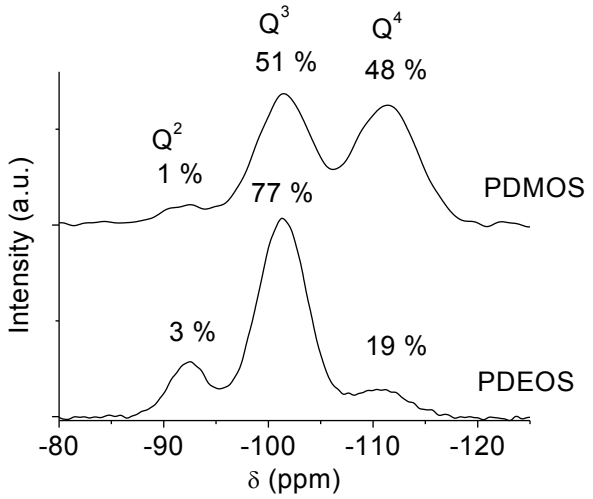

Figure II.6: Solid-state ^{29}Si SPE MAS NMR spectra of UV cross-linked PDEOS (A) and PDMOS (B) films. Irradiation conditions: UV conveyor, H lamp, 1.46 J/cm^2/pass, 5 passes.

Condensation degrees calculated for PDMOS and PDEOS were 87 % and 78 % respectively. Substitution of methoxy for ethoxy groups tends to lower the siloxane network condensation. Such result is in agreement with the tendency reported in the literature for classic sol-gel process.[12,13]

II.4. BY-PRODUCTS OF THE REACTION

II.4.1. RT-FTIR study

Another key point of our study is to determine and understand the by-products of the reaction and their eventual trapping in the film. According to scheme II.1, hydrolysis reaction consumes water and releases methanol whereas condensation reactions release water and methanol. It is also important to remind that in our photoinduced process, water is not initially added but continuously supplied by atmospheric water. The presence of water dissolved in PDMOS was evidenced by its bending mode at 1640 cm^{-1}, whose area was assessed continuously throughout the irradiation as represented in Figure II.7A. Despite the relative hydrophobicity of the methoxy

oligomeric precursor, water is already apparent in the IR spectrum of PDMOS before reaction (t = 0 s).The hydrolysis stage is marked by a progressive enrichment in water. This apparent contradiction may be explained by:

- An enhanced film hydrophilicity as a result of the replacement of alkoxide groups by hydroxyl groups, thereby increasing the water adsorption ability,[15]
- The water generated as a by-product of the condensation (occurring concomitantly with hydrolysis)
- Theentrapment of water molecules by virtue of hydrogen bonding with silanol groups and the formation of a solid oxo-polymer network.

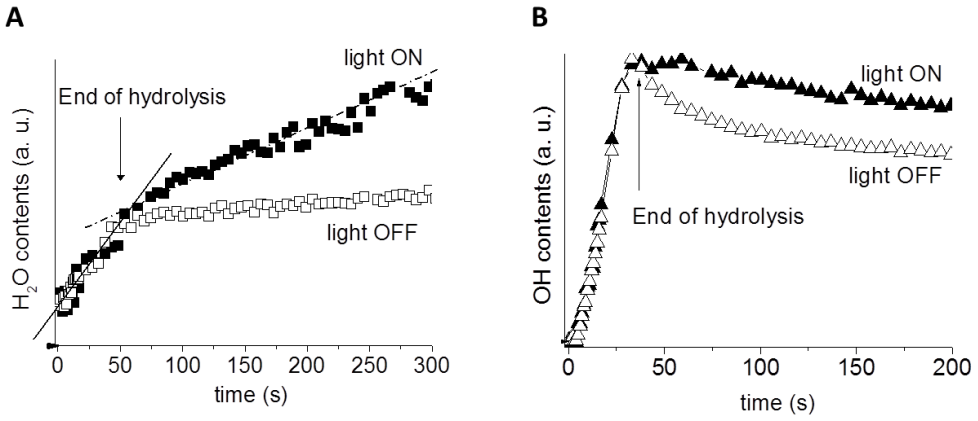

<u>Figure II.7:</u> Variation in H_2O content (A) and in OH functions (B) in a UV irradiated PDMOS film determined respectively from the integrated absorbance of the FTIR bands at 1640 cm^{-1} (δH_2O) and 3400 cm^{-1} (νOH). Full symbols indicate a continuous irradiation while open symbols correspond to a 50 s irradiation (a time corresponding to the end of hydrolysis).

A more detailed observation of the water content (Figure II.7A) actually reveals a two-step regime in water uptake: a fast linear increase with the irradiation time that declines substantially after the end of hydrolysis. This is consistent with a change in water vapour permeation after hydrolysis, which will be discussed in section III.1.

Unlike water, methanol by-product is not manifested by a distinctive vibrational band in the IR spectrum. The OH stretching vibration in the 3800 - 2800 cm^{-1} region actually includes the contribution of all hydroxyl-containing species, making the precise identification of alcohol tedious. However, evaporation of methanol could be evidenced indirectly by observing the downward evolution of OH stretching band at the end of hydrolysis (t > 50 s, Figure II.7B). Compared to a film under continuous irradiation, stopping the UV light after hydrolysis causes surprisingly a faster decrease in the OH band. Given that condensation is significantly slowed after the UV shutdown, it appears justified to relate this decrease to the progressive desorption of volatile methanol. Under continuous irradiation, methanol evaporation still takes place (as

well as further silanol condensation) but the loss of hydroxyl containing compounds is partially offset by a significantly enhanced formation of water, as displayed in Figure II.7A, leading to a slower decline of the OH band.

A limited methanol concentration in the film is particularly relevant in view of the secondary effects of alcohol in sol-gel chemistry. Alcohols are indeed not inert solvents as they are known to promote reesterification (reverse process of hydrolysis), and depolymerization reactions. According to Le Châtelier's principle, the system should respond to the elimination of methanol by increasing the forward reaction rates consuming the methoxysilyl groups. As a result of alcohol evaporation, the position of the hydrolysis "equilibrium" is thus shifted to the right, which may account for the fast hydrolysis rates found in this system.

II.4.2. Solid state ^{1}H NMR study

The residual presence of methanol and water by-product was also investigated in the final material through ^{1}H MAS NMR spectroscopy (Figure II.8). The high field region is characteristic of silanol groups with two signals at 1.1 and 2.3 ppm assigned respectively to vicinal (Q^3) and germinal (Q^2) Si-OH, whose relative intensity is consistent with the ^{29}Si NMR spectrum[16](Figure II.6). The existence of water is exemplified by at least two resonances: a large signal at 4.9 ppm (liquidlike physisorbed water) and a broad shoulder at 7 ppm (strongly hydrogen-bonded water).[17] Of interest is also the distinct double maximum signal around 3.5 ppm. An assignment to less hydrogen bonded water molecules can be tentatively considered at this chemical shift, but this multimodal resonance may also mirror the presence of methanol trapped in the oxo-polymer network. The maxima at 3.4 and 3.6 ppm are fully consistent with the methyl and hydroxyl groups of methanol respectively.

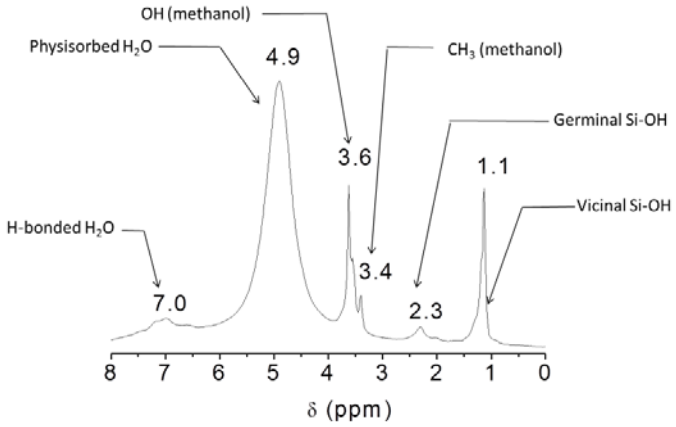

Figure II.8: 1H MAS NMR spectrum of UV cross-linked PDMOS film. Irradiation conditions: UV conveyor, H lamp, 1.46 J/cm2/pass, 5 passes.

II.5. ACTINIC WAVELENGTH EFFECT ON THE INORGANIC NETWORK

There is another question which begs to be answered in regard to the driving forces of the hydrolysis-condensation reactions. It has been well established that Brönsted photoacids can act as efficient photocatalysts of the sol-gel polymerization, with a mechanism presumably similar to that described in conventional acid-catalyzed sol-gel process.[18] In addition, we considered the possibility that the electronic excitation promoted by energetic UV photons might favor a densification of the inorganic network. In order to assess the relevance of this hypothesis, we focused on the condensation reactions occurring after the hydrolysis stage (t > 50 s). Upon using a UV lamp equipped with a 254 nm reflector instead of 365 nm reflector (used in all the previous experiments), a higher amount of photons below 300 nm can be produced by the same Hg-Xe lamp. The emission spectra with the two reflectors are presented in Figure II.9.As shown in Figure II.10A, this slight change caused a faster decrease of the band assigned to silanol (930 cm^{-1}) and OH groups (3400 cm^{-1}).

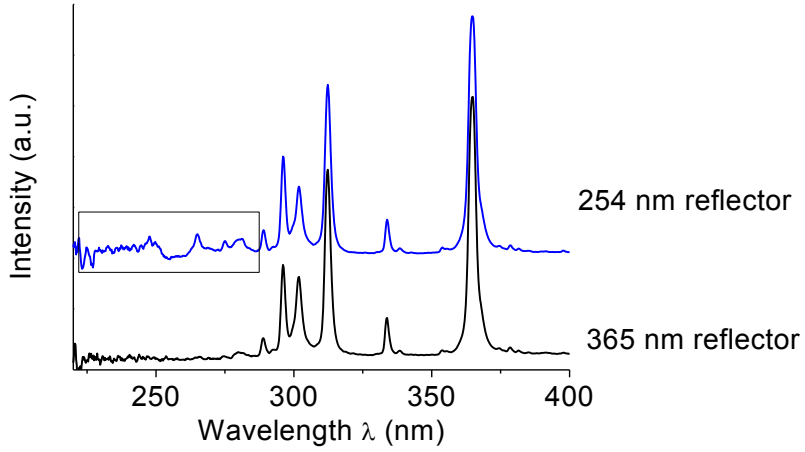

Figure II.9: Emission spectra of the Hg-Xe lamp with a reflector at 365 and 254 nm

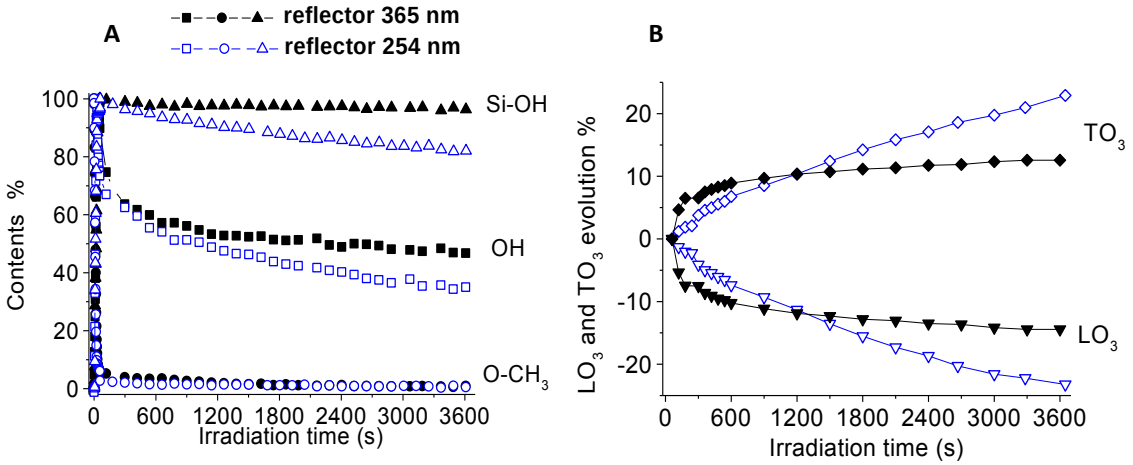

Figure II.10: Evolution of the O-CH$_3$ (●,○), OH (■,□) and Si-OH (▲,△) FTIR bands during the UV irradiation of a PDMOS film with a Hg-Xe lamp (200 mW/cm^2) (A). Variation of the TO$_3$ (◆,◇) and LO$_3$ (▼,▽) Si-O-Si antisymmetric stretching bands (B).

Accordingly, the evolution of the LO_3 and TO_3 components of the broad envelope in the 1000 - 1260 cm^{-1} was significantly enhanced using the 254 nm reflector as displayed in Figure II.10B. Both results agree for a substantial acceleration of the condensation process, making clear that energetic photon UV can directly induce a silica densification, in addition to a photoacid-catalyzed condensation. Note that irradiation raised the substrate temperature by less than 40 °C. Thus, the structural changes in silica films are assumed to be mainly ascribed to electronic processes stimulated by irradiation. The concept of UV photoinduced densification of sol-gel derived metal oxide films (SiO_2, TiO_2) has been already reported in the literature, mostly with energetic UV light source such as low pressure mercury lamps (254 nm),[19] excimer lamps (172 nm).[20,21] Imai *et al.*[22] suggested that energetic enough photons can stimulate the electronic excitation of silanol groups and Si-O-Si bonds, to induce silanol condensation and the structural rearrangement of the silica network. In our case, the ongoing condensation might occur by the presence of UVC (100–280 nm) enhanced by the 254 nm reflector that was sufficient to induce electronic excitation and consumption of Si-OH groups.

III. INFLUENCE OF VARIOUS PARAMETERS ON THE HYDROLYSIS KINETICS

In the first part of the chapter, we showed that well-condensed silica films can be achieved in a matter of minutes under ambient atmosphere despite conditions that might appear not optimal with a moisture-limited atmosphere (RH = 30 %) and the use of non-polar precursors converted into solid cross-linked films. In sol-gel photopolymerization, the overall reaction kinetics is expected to be controlled by two independent phenomena:

- the water vapor permeation into the film during the hydrolysis step

- the intrinsic chemical reaction rates

Their relative importance is discussed with respect to the effects of several processing parameters on the hydrolysis kinetics. First, we address the influence of variables affecting mainly the permeation of atmospheric water into the sol-gel matrix, such as the RH and the film thickness. On the other hand, the context of reaction control would suggest a higher sensitivity to other parameters such as the exitance, the photoacid structure and concentration that are investigated thoroughly. A systematic approach has been adopted to investigate the effects of various reaction primary parameters and infer the prevailing rate-controlling regime. As previously, results are discussed in detail for PDMOS and comparison is done with PDEOS.

Using the linear part of the hydrolysis conversion versus time plots ,it is possible to determine the maximal rates of hydrolysis (r_p, (L.mol^{-1}.s^{-1})). In our study, a relative rate of hydrolysis was determined (Equation II.2). This later was calculated, taking as the reference a system with a thickness of 0.9 µm (1.9 µm with PDEOS), a RH of 30 % and a PAG concentration of 2 % wt. and under maximum exitance (200 mW/cm^2).

$$r_p^{rel} = r_p([PAG], RH, thickness) \Big/ r_p(ref) \quad \text{Equation II.2.}$$

Table II.5 below is a summary of the different relative rates of hydrolysis calculated for PDMOS and PDEOS films.

Table II.5: Effect of various experimental parameters on hydrolysis degree and rate during the sol-gel photopolymerization of PDMOS and PDEOS.

		PDMOS		PDEOS	
		r_p^{rel}	**Hydrolysis (%)**	**r_p^{rel}**	**Hydrolysis (%)**
Liquid film thickness (um)	1.5	0.63	>95		
	2.3			0.71	>95
	0.9	1.00	>95		
	1.9			1.00	>95
	0.8	1.30	>95		
	1.4			1.12	>95
Relative Humidity (%)	21	0.58	>95	0.58	>95
	24	0.84	>95	0.65	>95
	30	1.00	>95	1.00	>95
	55	1.16	85	-	-
[PAG] (wt. %)	1	0.86	>95	0.64	>95
	2	1.00	>95	1.00	>95
	3	1.06	>95	1.14	>95
	4	1.03	>95	1.29	90
Exitance (mW/cm^2)	50	0.77	>95	0.33	>95
	100	1.00	>95	0.57	>95
	150	1.14	>95	0.78	>95
	200	1.00	>95	1.00	>95
Counter-ion	PF_6^-	1.00	>95		
	$CF_3SO_3^-$	0.68	>95		
	$CH_3\Phi SO_3^-$	0.1	>95		
	Cl^-	<0.005	10		

III.1. ATMOSPHERIC WATER PERMEATION

The dependency of film thickness and RH (RH = 20 to 55 %) on the hydrolysis kinetics of PDMOS and PDEOS films was illustrated in Figure II.11A, B, C and D.

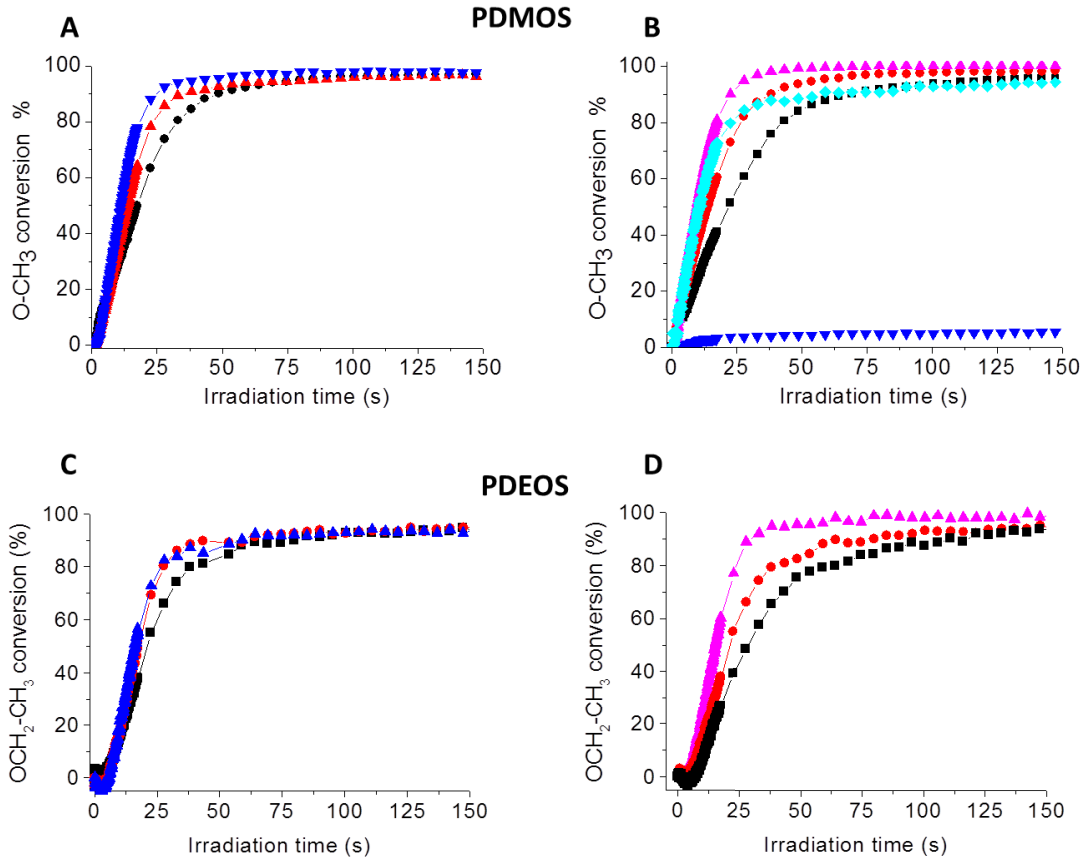

Figure II.11:Methoxy and Ethoxyconversion during the sol-gel photopolymerization of PDMOS and PDEOS respectively. Influence of film thickness (A and C): (A) 1.5 µm (●), 0.9 µm (▲) and 0.8 µm (▼); (C) 2.3 µm (●), 1.9 µm (▲) and 1.4 µm (▼).Effect of RH (B and D): 21 % (■), 24 % (●), 30 % (▲), 55 % (♦). The effect of laminated conditions that prevent the entry of atmospheric moisture was also assessed (▼).

Although a complete hydrolysis was achieved regardless of the thickness, FigureII.11A and C clearly showed a differentiation between the samples with a maximal hydrolysis rate decreasing with the film thickness. A diffusion limitation effect was evidenced with faster hydrolysis kinetics obtained with thinner films, promoting the permeation of water. Similarly, an increase of RH at constant temperature and air pressure (Figure II.11B and D) implies a higher water vapour pressure. As expected, such conditions were suitable to the entry of water vapour into the film, affording higher initial hydrolysis rates.

Nevertheless, a limiting conversion (90 %) was found for PDMOS film at the highest RH of 55 %. After the first seconds of irradiation, the hydrolysis rate witnessed a sharp decrease, whereas that of the others reactions conducted at lower RH remained relatively steady. This later result reflects a solvatation effect of the superacids by water molecules. In water excess, superacids are hydrolyzed leading to their replacement by H_3O^+ with a lower acidity and weaker catalytic

activity. The acidity of the superacids is limited indeed by the basicity of water initially present, leading to the formation of H_3O^+ hydronium ions.

The ambient atmosphere plays the determining role of water reservoir, as proved by a simple experiment in which the permeation of water was blocked by the presence of a UV and IR transparent BaF_2 pellet placed at the top of the PDMOS film (Figure II.11B). Under these conditions, hydrolysis was significantly inhibited: a slower reaction rate and a final conversion of less than 10 % were obtained. The film remained liquid after 5 minutes of irradiation and the water initially dissolved into the oligomeric precursor presumably accounts for the partial hydrolysis of the methoxysilyl functions. In laminated conditions, water consumed by the reaction cannot be replenished by the atmosphere but the depletion of water initially dissolved in PDMOS (by evaporation) is also impossible. Although there are two chemical reactions in a sol-gel process, with only hydrolysis step consuming water, the final degree of condensation will also depend on water vapour permeation.

At the beginning, a free chain motion is associated with the liquid alkoxy oligomer chains. Despite their hydrophobicity minimizing the solubility coefficient, siloxane chains are thought to participate in the diffusion process due to internal chain micromotions, enabling a larger amount of free volume in which diffusion may take place to ensure an efficient hydrolysis. As a result of sol-gel transition, the film becomes cross-linked and hydrophilic properties appear due to the replacement of alkoxide groups (OR) with hydroxyl groups (OH). Under these conditions, water permeation becomes controlled by the solubility characteristic, and less by diffusivity because of limited chain mobility in amorphous cross-linked silica. With the formation of hydrophilic silanol, the water vapour will have an enhanced solubility parameter, close to that of the film, offsetting the loss of diffusivity related to solidification.

A corollary of a diffusion-controlled regime is the possible formation of a composition gradient across the z axis. In other words, a gradual change in composition throughout the film thickness may possibly occur with the external layers being more condensed than the interior layers closer to the substrate. Owing to the submicrometric size scale of the film thickness, a non-uniform conversion is very difficult to evidence. Nevertheless, diffusion-controlled hydrolysis kinetics demonstrated previously does not necessarily imply composition gradient in the film. Combination of thin films and continued condensation due to the persistence of photoacids are likely to level the degree of condensation to a rather constant value despite apparent differences in hydrolysis kinetics.

III.2. CHEMICALS AND PHOTOCHEMICALS PARAMETERS

III.2.1. PAG concentration and exitance

With regard to chemical reaction parameters, the concentration in PAG has been varied from 1 to 4 % wt., and the exitance of the Hg-Xe lamp has been varied from 50 to 200 mW/cm^2.

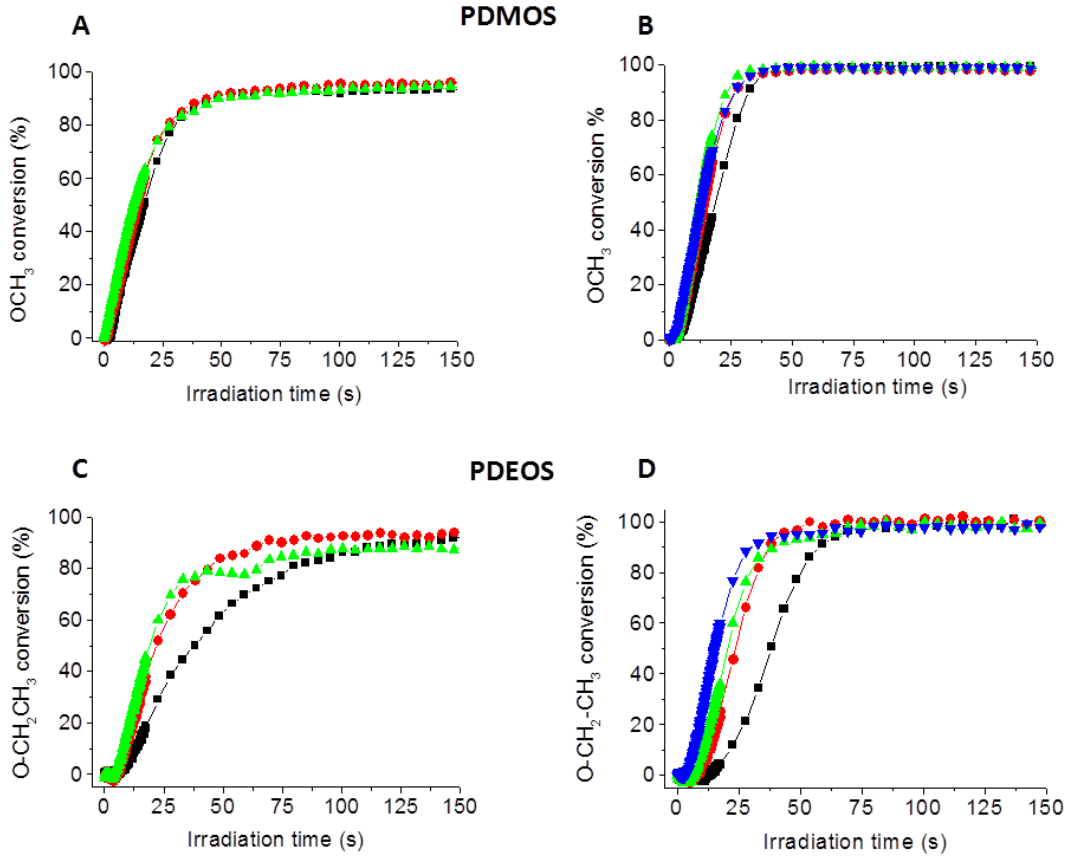

Figure II.12:Methoxy (top) and Ethoxy (bottom) conversion during the sol-gel photopolymerization of PDMOS and PDEOS respectively. Influence of PAG concentration(A and C): 1% (■), 3% (●) and 4% (▲).Effect of exitance(B and D): 50 mW/cm² (■), 100 mW/cm² (●), 150 mW/cm² (▲), 200 mW/cm² (▼).

For PDMOS (Figure II.12A and B) there is no significant variation in the rate and the extent of hydrolysis in the selected range of PAG concentrations. In contrast, traditional sol-gel polymerization in water solution is known to be strongly influenced by the concentration of the acid catalyst.[18,23,24] This result argues for a diffusion-controlled regime even at low PAG concentration (1 %) due to the high reactivity of the UV-generated photoacids. Similarly, a decrease of the exitance which affects the PAG photolysis rate shows small effects on the hydrolysis conversion curves. In the present conditions, the rate-determining step is clearly the water permeation in the film. Though a diffusional resistance is evidenced, such result must be

analyzed and be put into proper perspective since very fast hydrolysis reactions were obtained regardless of the experimental conditions chosen. In contrast, PDEOS (Figure II.12C and D) shows a higher dependency to PAG concentration and exitance variation, suggesting a combined rate limiting regime. As observed in sol-gel chemistry, increasing the steric hindrance of the alkoxy group is marked by lowered hydrolysis kinetics, which enhances the effect of chemical reaction parameters.[12,13]

III.2.2. Nature of the PAG

In this paragraph, we choose to keep the cationic part of the PAG intact and only change the counter-ion. Structures of the different PAG tested are presented in Table II.4.

Table II.4: Structures of the different PAG tested

Diphenyliodonium			
hexafluorophosphate (PF_6^-)	**triflate ($CF_3SO_3^-$)**	**toluene sulfonate ($CH_3\Phi SO_3^-$)**	**chloride (Cl^-)**
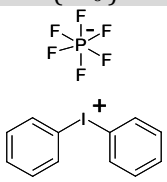	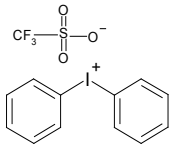	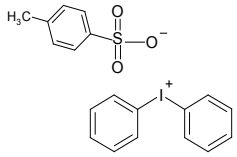	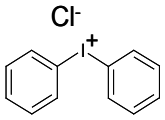

The structure is thus defined by the nature of the counter-ion, which is a weakly coordinating anion. We know that the nature and stability of the anion will influence the acid strength and will be determinant for the initiation efficiency of the reaction. The dependency of PAG structure on the hydrolysis kinetics of PDMOS films was illustrated in Figure II.13.

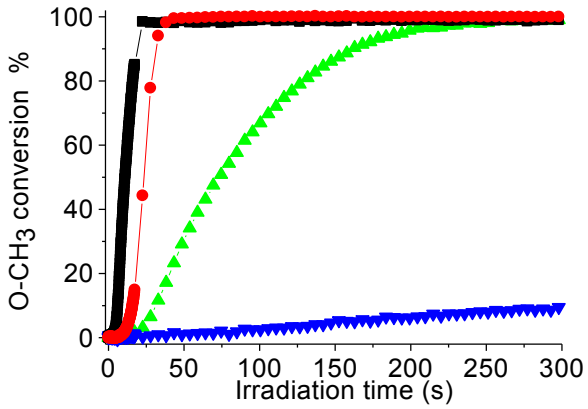

Figure II.13: Methoxy conversion during the sol-gel photopolymerization of a PDMOS film containing 2 % wt. of PAG with different counter-ion: hexafluorophosphate(PF_6^-, ■), triflate ($CF_3SO_3^-$,●), toluene sulfonate ($CH_3\Phi SO_3^-$,▲) and chloride (Cl^-,▼).

Important variations were observed in the hydrolysis conversion plots depending on the nature of the counter ion. Although a full consumption of the methoxysilyl groups was reported with hexafluorophosphate, triflate and toluene sulfonate as counter ions, a retarding effect of the lower acid catalyst is clearly evident. In the case of $H^+ Cl^-$, only 10 % conversion was obtained. This is not only the result of a decreased catalyst activity with the low nucleophilic chloride anion, evaporation of hydrochloric acid in thin film precursor possibly accounts for this result. Other photoacid possessing bulkier anions are less likely to evaporate. It should be noted finally that with a decrease of the photocatalyst reactivity, the system is likely to become reaction rate control.The nature of the photoacid exerts the greatest effects on the hydrolysis kinetics. Results obtained are completely in agreement with the literatureof cationic photopolymerization of epoxy or vinyl ether monomers, a greater charge delocalisation of the anion confers generally a stronger acidity and implies a higher catalytic efficiency[25]. The reactivity order observed is generally: hexafluorophosphate (PF_6^-) > triflate ($CF_3SO_3^-$) > toluene sulfonate ($CH_3\Phi SO_3^-$) >> chloride (Cl^-).

IV. APPLICATION TO HYBRID FILMS PDMOS/PDMS

The versatility of the PDMOS photopolymerization outlined above makes this methodology easily applicable to the synthesis of hybrid films. Organic-inorganic nanocomposite materials are characterized by molecular or nanoscale dispersion of the hybrid components enabling fine-tuned properties and novel applications.

Following the same process, a homogeneous film comprising a solvent- and water-free mixture of PDMOS and silanol functionalized PDMS mixture in presence of a PAG was prepared. The choice for PDMS as co-monomer was motivated by it structure close to the one of PDMOS precursor in a view to promote their co-condensation and improve the homogeneity of the resulting hybrid material. In addition, in the literature hybrid PDMS/TEOS or TMOS are well studied.[4,26,27] Various amounts of PDMS (25 up to 75 wt. %) were added to a solution to PDMOS and our goal was to understand how the addition and copolymerization of PDMS impacts the hydrolysis and condensation reactions (Figure II.14).

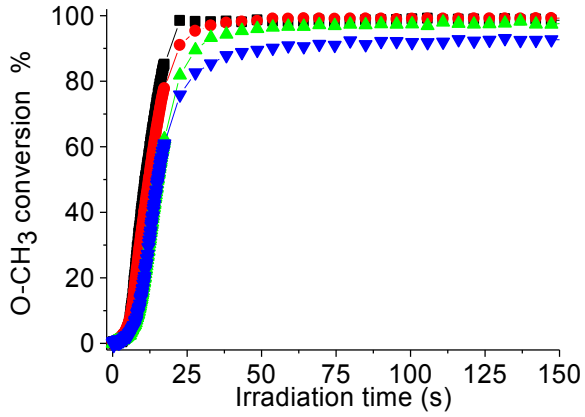

Figure II.14:Methoxy conversion during the sol-gel photopolymerization of a PDMOS film containing 0% wt., ■; 25 % wt.,●;50 % wt.,▲ and 75 % wt.,▼ of PDMS.

The hydrolysis kinetic profiles were almost unaffected by the addition of PDMS. The increase in hydrophobicity and viscosity resulting from the presence of PDMS was not mirrored by any retarding effect on hydrolysis. Only at the highest content in PDMS (75 % wt.), a limiting conversion of 90 % became visible whereas a full conversion was obtained for lower silicone concentrations. A question which arises from these kinetic results is whether co-condensation between PDMS and PDMOS actually occurs. In contrast to pure PDMOS samples, the strong envelope of IR absorption bands associated to stretching modes of Si-O-Si bonds is of limited utility to assess the condensation progress because of many overlapped signals. To provide answers, CP-MAS (Cross-polarization Magic Angle Spinning) ^{29}Si NMR spectra of two PDMS/PDMOS films were recorded (Figure II.15).Unlike SPE-MAS, CP-MAS is not quantitative, however under specific acquisition conditions (see Annex II.2) it is possible to obtain semi-quantitative spectra comparable to SPE-MAS spectra.

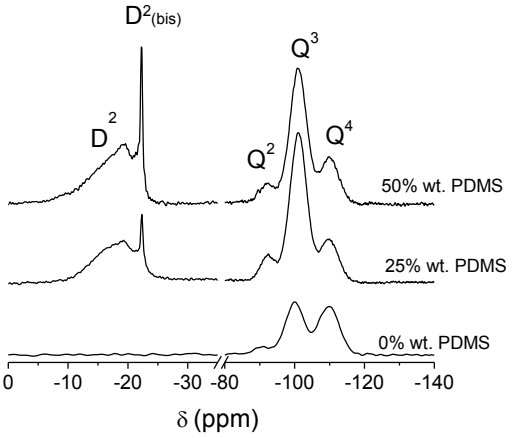

Figure II.15:Solid-state ^{29}Si CP MAS NMR spectra of UV cross-linked PDMOS film containing 0% wt., 25 % wt. and 50 % wt. of PDMS. Irradiation conditions: UV conveyor, H lamp, 1.46 J/cm^2/pass, 5 passes.

The confirmation of crosslinker condensation was given by the triplet of Q^2, Q^3 and Q^4 units around-100 ppm straightforwardly assigned to crosslinked PDMOS. In addition to the Q units assigned to PDMOS, D^2 signals from the PDMS appear around -20 ppm.[4,28,29] D units correspond to the formation of dimers (C_2SiO_2) and the subscript refers to the formation of two siloxane bonds.

In an attempt to shed light into the silicate speciation arising from the PDMS segments, a deconvolution of the D^2 massif was performed (Figure II. 16). Although it was not unique, our best deconvolution revealed five distinct peaks displaying an increasing linewidth as the chemical shifts increased.

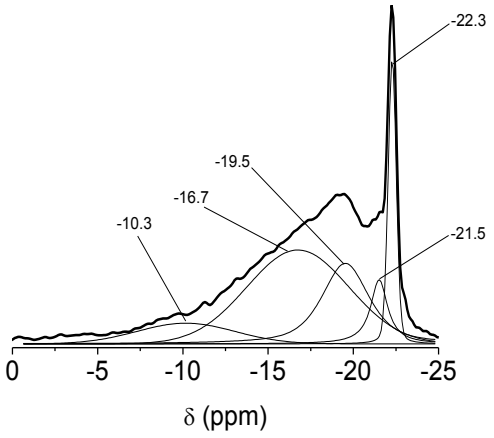

Figure II.16: Deconvolution of ^{29}Si CP-MAS NMR spectra of the PDMS/PDMOS (50/50 wt. %) films conditions. Irradiation conditions: UV conveyor, H lamp, 1.46 J/cm^2/pass, 5 passes.

Solid state NMR spectroscopy is also a very useful characterization technique to highlight the difference of mobility that takes place within the sample. Very sharp peaks are expected to arise from mobile environment whereas much broader peaks translate more rigid media. Following this line of thought, the major feature of this portion of the ^{29}Si spectrum could be understood in terms of a diminished mobility causing the D^2 resonance to shift toward more positive values and become broader. The two sharp components at -22.3 ppm and -21.5 ppm were thus attributed to D^2 silicon units in a mobile environment and presumably localized in the PDMS chain interior ($(D^2)_x$-D^2-$(D^2)_y$). According to Babonneau *et al.*,[4] their occurrence might appear as the indirect evidence of homopolymerization between PDMS chains affording longer linear chains. By contrast, the three broader D signals at -19.5 ppm, -16.7 ppm and -10.3 ppm reflected a more rigid environment arising for a closer proximity of cross-linked Q^n neighbours. Additionally, their breath is due to the overlap of a large number of single resonance lines produced as a result of the highly varied environments of the silicon nuclei. Depending on the proximity with Q species and their extent of condensation (Q^2-Q^4), both the environment and rigidity of the D^2 silicon sites change, resulting in very broad linewidths. The more downfielded signal at -10.3 ppm was thus tentatively assigned to D^2 units directly attached to Q units (Q^n-D^2-$(D^2)_x$) while the intermediate broad signals might correspond to D^2 more distant of the Q units (Q^n-D^2-D^2-$(D^2)_x$). Knowing the exact attribution of D^2 species was obviously not possible, but the presence of these broad features was apparently consistent with hetero-condensation reactions. It was not possible to reliably resolve the presence of uncondensed D^1 species at -11 ppm. However, the absence of narrow lines arising at this chemical shift from these very mobile silicon nuclei argued for an extended condensation of the terminal silanols. The PDMS concentration has a marked effect on this isolated signal: the increase from 25 to 50 % wt. in PDMS content caused a significant enhancement of the sharp feature, suggesting a decrease in the number of chemical linkages between PDMS and the siloxane network. Although the CP-MAS spectra are not quantitative, the general trend supports that the hybrid films consist of well condensed oxo-polymer network between D and Q units.

CONCLUSION

In this study, the photoacid-catalyzed sol-gel polymerization of films based on inorganic methoxy and ethoxysilane oligomeric precursors was studied. RT-FTIR represents a complete and comprehensive technique to study *in situ* the photoacid-catalyzed sol-gel polymerization. A full picture of this inorganic photopolymerization mechanism has been provided, from hydrolysis to condensation kinetics, as well as an insight into the fate of water and alcohol by-products. In particular, we detected two consecutives stages: in a first step, hydrolysis and

condensation occur simultaneously and concurrently and in a second step of slow post-condensation was observed. During these reactions, water and alcohol were formed and in large majority evaporate from the film whereas a minor part was trapped in the film due notably to hydrogen bonding with silanol species and increasing hydrophilicity of the film. Solid state ^{29}Si NMR confirmed the formation of highly crosslinked siloxane network. In addition, substitution of methoxy moieties by ethoxy showed a slowdown in the hydrolysis rate and less condensed inorganic networks were obtained as expected from the literature and steric hindrance. Concerning the driving forces of this reaction, it has been established that in addition to a catalytic effect by the photogenerated Brönsted acids, the energetic photons (UVC) are responsible for a direct densification through electronic excitation of silanol groups and siloxane bonds. Furthermore, the occurrence of a water permeation controlled-regime was demonstrated with the methoxy precursor (PDMOS), whereas its ethoxy analogue shows a combined regime dependent also on the intrinsic chemical reaction parameters (exitance, PAG nature and concentration).

Finally, we showed that photoinduced sol-gel process is a simple and easy to use pathway to prepare highly crosslinked and homogeneous hybrid PDMS/PDMOS films. We suggest that this pathway could be transposable for synthesis of various hybrid materials. Fast hydrolysis rates and the elimination of organic solvent (and even water) are major features of sol-gel photopolymerization compared with a conventional sol-gel methodology.

CHAPTER II REFERENCES

(1) Chemtob, A.; Versace, D.-L.; Belon, C.; Croutxe-Barghorn, C.; Rigolet, S. *Macromolecules* **2008**, 41, 7390.
(2) Belon, C.; Chemtob, A.; Croutxe-Barghorn, C.; Rigolet, S.; Le Houérou, V.; Gauthier, C. *J. Polym. Sci., Part*A**2010**, 48, 4150.
(3) Chemtob, A.; Belon, C.; Croutxe-Barghorn, C.; Brendle, J.; Soulard, M.; Rigolet, S.; Le Houerou, V.; Gauthier, C. *New J. Chem.***2010**, 34, 1068.
(4) Babonneau, F. *Polyhedron***1994**, 13, 1123.
(5) Galeener, F. L. *Phys. Rev. B***1979**, 19, 4292.
(6) Matos, M. C.; Ilharco, L. M.; Almeida, R. M. *J. Non-Cryst. Solids***1992**, 147-148, 232.
(7) Niznansky, D.; Rehspringer, J. L. *J. Non-Cryst. Solids***1995**, 180, 191.
(8) Rubio, F.; Rubio, J.; Oteo, J. L. *Spectrosc. Lett.***1998**, 31, 199.
(9) Fidalgo; A.; Ilharco; L., M. *J. Non-Cryst. Solids***2001**, 283, 144.
(10) Innocenzi, P. *J. Non-Cryst. Solids***2003**, 316, 309.
(11) Anderson, R.; Larson, G. L.; Smith, C. *Silicon Compounds: Registerand Review*; Hüls America, **1991**.
(12) Loy, D. A.; Baugher, B. M.; Baugher, C. R.; Schneider, D. A.; Rahimian, K. *Chem. Mater.***2000**, 12, 3624.
(13) Judeinstein, P.; Sanchez, C. *J. Mater. Chem.* **1996**, 6, 511.
(14) Massiot, D.; Fayon, F.; Capron, M.; King, I.; Le Calvé, S.; Alonso, B.; Durand, J.-O.; Bujoli, B.; Gan, Z.; Hoatson, G. *Magn. Reson. Chem.***2002**, 40, 70.

(15) Innocenzi, P.; Kidchob, T.; Bertolo, J. M.; Piccinini, M.; Guidi, M. C.; Marcelli, C. *J. Phys. Chem. B***2006**, 110, 10837.
(16) Vega, A. J.; Scherer, G. W. *J. Non-Cryst. Solids***1989**, 111, 153.
(17) Trzpit, M.; Rigolet, S.; Paillaud, J.-L.; Marichal, C.; Soulard, M.; Patarin, J. *J. Phys. Chem. B***2008**, 112, 7257.
(18) Brinker, C.; Scherer, G. *Sol-Gel Science: The Physics and Chemistry of Sol Gel Processing*; Academic Press Inc: San Diego, **1990**.
(19) Maekawa, S.; Ohishi, T. *J. Non-Cryst. Solids***1994**, 169, 207.
(20) Imai, H.; Awazu, K.; Yasumori, M.; Onuki, H.; Hirashima, H. *J. Sol-Gel Sci. Techn.***1997**, 8, 365.
(21) Tsuzuki, Y.; Oikubo, Y.; Matsuura, Y.; Itatani, K.; Koda, S. *J. Sol-Gel Sci. Techn.***2008**, 47, 131.
(22) Imai, H.; Yasumori, M.; Hirashima, H.; Awazu, K.; Onuki, H. *J. Appl. Phys.* **1996**, 79, 8304.
(23) Aelion, R.; Loebel, A.; Eirich, F. *J. Am. Chem. Soc.***1950**, 72, 5705.
(24) Pope, E. J. A.; Mackenzie, J. D. *J. Non-Cryst. Solids***1986**, 87, 185.
(25) Crivello, J. V. *J. Polym. Sci. Part A***1999**, 37, 4241.
(26) Glaser, R. H.; Wilkes, G. L. *Polym. Bull.***1988**, 19, 51.
(27) Wen, J.; Wilkes, G. L. *Chem. Mater.***1996**, 8, 1667.
(28) Tsuru, K.; Aburatani, Y.; Yabuta, T.; Hayakawa, S.; Ohtsuki, C.; Osaka, A. *J. Sol-Gel Sci. Technol.***2001**, 21, 89.
(29) Salinas, A. J.; Merino, J. M.; Babonneau, F.; Gil, F. J.; Vallet-Regí, M. *J. Biomed. Mater. Res. Part B*: **2007**, 81B, 274.

CHAPTER III: SOL-GEL PHOTOPOLYMERIZATION OF INORGANIC ALKOXYSILANE PRECURSOR IN PHOTOBASE CATALYSIS

A. Chemtob, H. De Paz-Simon, C. Dietlin, C. Croutxé-Barghorn, A.-C. Chany, L. Vidal, S. Rigolet *"A Highly Reactive Photobase Catalytic System for Sol-Gel Polymerization. Application in Metal- and Solvent-Free Silicone Cross-Linking"* submitted in *Thin solid films.*

A. Chemtob, H. De Paz-Simon, C. Croutxé-Barghorn, S. Rigolet *"UV-Activated Silicone Oligomer Cross-Linking Through Photoacid and Photobase Organocatalysts."* Accepted in *J. Appl. Polym. Sci.*

INTRODUCTION

Hydrolysis and condensation reactions rates are known to be strongly influenced by the type of catalysis (i. e. acid or basic).[1] Different mechanisms are involved that will further have an important impact on the film microstructure and final properties. Acid catalysis is known to preferentially form chain polymeric structures leading to dense films whereas basic catalysis mostly forms colloidal particles leading to porous films.

Among base catalysts, amines have already proved their catalytic utility[1] for alkoxysilane inorganic polymerization. For example, ammonia is known for decades as an efficient catalyst for hydrolysis and condensation of alkoxysilane functions in aqueous solutions. In addition, tertiary amines such as dimethylamino pyridine and *N*-methyl imidazole caused even quicker gelation than strong acids at similar concentration.[2] Furthermore, the effectiveness of the amine as a sol-gel catalyst appears to be less dependent on strong nucleophilicity and basicity. This context drove us to consider that some photogenerated tertiary amines of weak nucleophilicity could be suitable for use in high speed cross-linking of alkoxy monomers without the need for additional heating.

Compared to system catalyzed by photoacid, photobase catalyzed systems are much less studied in the literature and only few studies[3-6] report the use of such catalysts for initiating hydrolysis and condensation reactions. At the end of the 1990's, Harkness *et al.*[3,4] proposed a photobase catalyzed sol-gel process for application in photopatterning. The authors start with hydrogen silsesquioxane precursors and 2 types of photolatent bases: a 2-Nitrobenzyl Carbamates and N-Methylnifedipine releasing respectively free amine or an alkylammonium hydroxide base. Fast hydrolysis of sylil hydrid by residual water was observed; however heating under air atmosphere was necessary to complete the conversion to silica glass. Later on, Uraoka[6] proposed a system where photogenerated alkyl amines are used as catalysts for the condensation reaction but once again a subsequent heat treatment at 400°C was realized to promote cross-linking of Si-OH groups. Finally, photobase catalyzed sol-gel process has already been studied within our laboratory[5], starting from organically modified trialkoxysilane precursor in presence of an α-aminoketone photolatent base; we were able to simultaneously catalyze the anionic photopolymerization of epoxy functions and the hydrolysis/condensation of alkoxysilane moieties. Nevertheless, in order to obtain a fully cross-linked film a heating step was also necessary.

Starting from this knowledge, in the present chapter, we will investigate the photosol-gel reaction of PDMOS in basic conditions. The first part of the work consists in finding the best

conditions to have an efficient photobase-catalyzed sol-gel process where no subsequent heat treatment was necessary. An association of α-aminoketone PBG with a photosensitizer (benzophenone, (BP)) and an oxygen scavenger (triphenylphosphine, (TPP)) was required to afford a fast curing of methoxysiloxane precursors without the need for solvent or water and additional thermal step. Such a tricomponent photolatent catalytic system which generates *in situ N*-alkyl morpholine tertiary amines represents one of the most efficient photobase-catalyzed sol-gel process reported so far. Then in a second part, the particular characteristics reaction mechanism, kinetics, silicate microstructure of this efficient photobase-catalyzed sol-gel route are investigated for the first time through a combination of spectroscopic and electron microscopy techniques. To emphasize the impact of the catalyst on the polymer microstructure, we compare systematically our results with an equivalent photoacid-catalyzed sol-gel process involving a diaryliodonium PAG. As expected, photobase and photoacid conditions strongly impact the reaction mechanism, with direct effects on the silicate film's morphology and porosity. Finally, in a third part, the utility of this photoprocess in cross-linking with silicone such as PDMS is discussed. Hybrid organic-inorganic films of PDMOS/PDMS are prepared under basic conditions and co-condensation is studied.

I. EXPERIMENTAL CONDITIONS

In this work we used a Methyl-1[4-(methylthio)phenyl]-2-morpholinopropan-1-one (BASF) as PBG, BP as photosensitizer and TPP as oxygen scavenger. Structure of the photoreactive molecules and corresponding absorption spectra are given in Scheme III.1 below.

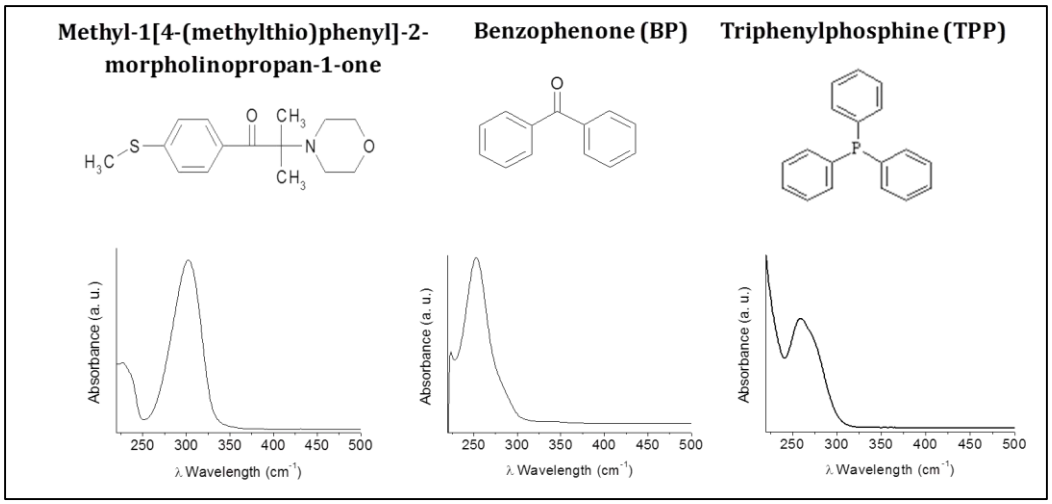

Scheme III.1: Structure of the photoreactive molecules and corresponding absorption spectra in dichloromethane (5.10^{-5}M)

In a typical procedure, PBG/BP/TPP photocatalytic mixture (2/2/2 wt. %) was dissolved in PDMOS to form a photolatent solution in the absence of UV light. The resultant solution was

homogeneous and stable in absence of UV light with a pot life exceeding 3 months. Casting was carried out onto the substrate (BaF_2 pellet, silicon wafer or borosilicate glass plate). A 2 µm thick film was then formed using a bar coater, and the film thickness was checked by profilometry measurements. In comparative experiments using photoacid catalysis, the PBG mixture was simply replaced by a PAG (diphenyliodonium hexafluorophosphate, 2 wt. %), keeping the described procedure unchanged.

For RT-FTIR experiments, IR transparent BaF_2 pellets were used as a substrate for PDMOS film deposition. In this specific case, the film was irradiated at room temperature by the polychromatic light of a mercury-xenon lamp fitted with a 365 nm reflector, at a light intensity of 200 mW/cm^2. The experiments were done in an environmental cell and the relative humidity (RH) was maintained between 27 and 33 % throughout the illumination. FTIR and UV irradiation were triggered concomitantly in a similar setup as the one describe in chapter II. Films studied by AFM, TEM and SEM were also prepared with this irradiation device and a silicon wafer was used as substrate.

For NMR study, the films were prepared onto borosilicate glass plate and irradiated at room temperature under a UV conveyor with a belt speed of 10 m/min using a microwave powered mercury vapor lamp (H bulb, Fusion). The samples were subjected to 10 successive passes under the conveyor to yield solid silicate films under acid or base conditions. During the UV irradiation, the room humidity was maintained between 27 and 33 %.

II. FUNDAMENTAL ASPECTS OF PHOTOBASE-CATALYZED SOL-GEL PROCESS

In this study, we choose to work with α-aminoketones because they are interesting photolatent base catalysts despite the limited pK_a jump marking the shift from latent form to active form. For the PBG implemented in this study, there is only a moderate increase from 8.5 to 9.1.[7] As depicted in Scheme III.2 the latent and the active structures contain a similar tertiary amine active group, but the higher reactivity of the active form relies on its steric deprotection *via* a photoinduced α-cleavage mechanism. The release of the bulky phenyl group significantly enhances the tertiary amine's accessibility and nucleophilicity. In addition, the effectiveness of the amine as a sol-gel catalyst appears to be less dependent on strong nucleophilicity and basicity.

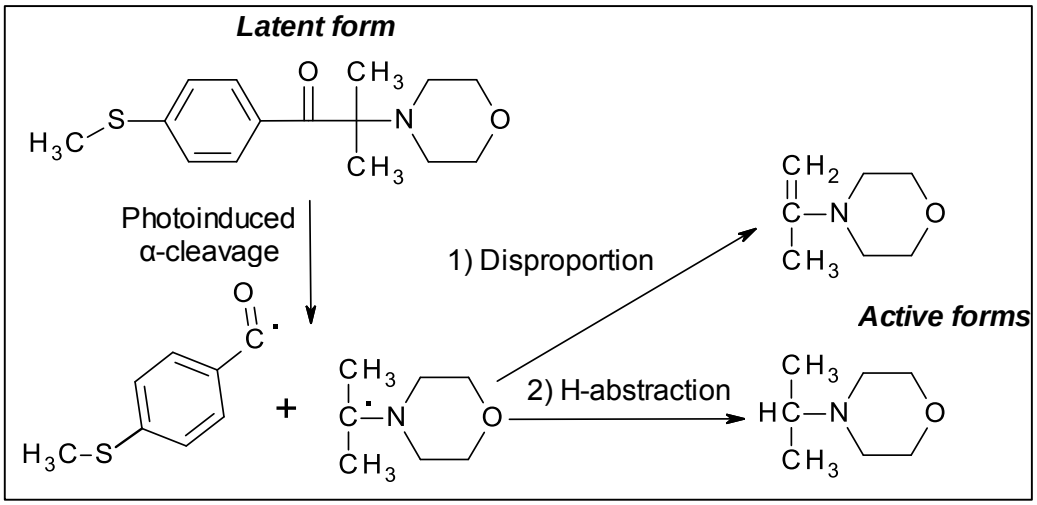

Scheme III.2: 2-step photolysis of the α-aminoacetophenone PBG

II.1. ROLE OF THE PHOTOSENSITIZER AND THE OXYGEN SCAVENGER

RT-FTIR was useful to shed light on the hydrolysis kinetics occurring in thin film. The relative evolution of the stretching band (ν_{sym} (CH_3)) at 2848 $cm^{-1}$was followed within the irradiation of PDMOS film.

As illustrated by a series of hydrolysis kinetics in Figure III.1, α-aminoketone/BP/TPP mixture proceeds through a synergetic effect.

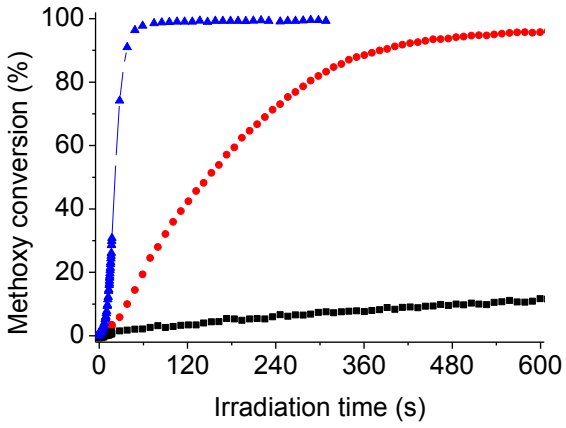

Figure III.1: Methoxysilyl or hydrolysis conversion ($\nu_{sym}(CH_3)$ at 2848 cm^{-1}) during the photobase-catalyzed sol-gel process of PDMOS films in presence of 2 wt. % PBG (■), 2/2 wt. % PBG/BP (●) and 2/2/2 wt. % PBG/BP/TPP (▲).

The α-aminoketone is obviously the nucleophilic photogenerator[7], and removing this component affords no reaction (not represented). Used alone (2 wt. %), sluggish kinetics are found with less than 10 % conversion after 10 minutes irradiation. Addition of BP (2 wt. %) as photosensitizer has a positive effect on reactivity. BP/α-aminoacetophenone is a well-known initiating pair in

radical photopolymerization[8]. In presence of BP, a full conversion is achieved after an irradiation time of 10 min. Finally, the simple addition of TPP (2 wt. %), an oxygen scavenger, to the previous mixture causes a significant surge in reactivity with a complete hydrolysis reaches this time in 60 s. This drastic effect of TPP must be interpreted in the light of the photochemical decomposition mechanism of the PBG depicted in Scheme III.2. Prior to the tertiary amine's photogeneration, aminoketone α-cleavage yields benzoyl and aminoalkyl radicals which are sensitive to oxygen inhibition. These radicals are prone to react with atmospheric oxygen diffusing readily within a system deposited as a thin film to produce peroxyl radicals (O_2 can also quench the BP photosensitizer molecule in its excited triplet state). Although the active species for the sol-gel process are clearly nucleophiles, the use of transient radical species is likely to make the process oxygen-sensitive.

Evidence for the inhibition effect of molecular oxygen is provided indirectly by examining the influence of film thickness on hydrolysis kinetics in Figure III.2. With a PBG/BP mixture, the absence of oxygen scavenger induces a strong dependency of the hydrolysis rates on sample thickness. As expected, thinner samples in which atmospheric oxygen diffuses more readily experience a dramatic decrease of the reaction rates, suggestive of an enhanced oxygen inhibition. Upon decreasing film thickness, a better diffusion of atmospheric moisture can be also promoted[9]. Two opposite effects are therefore in competition in regards to hydrolysis kinetics: an accelerating effect related to water and an inhibiting effect due to oxygen. Our results show a prevalent effect of O_2. By contrast, addition of TPP increases substantially the hydrolysis rates, and levels off the film thickness dependency.

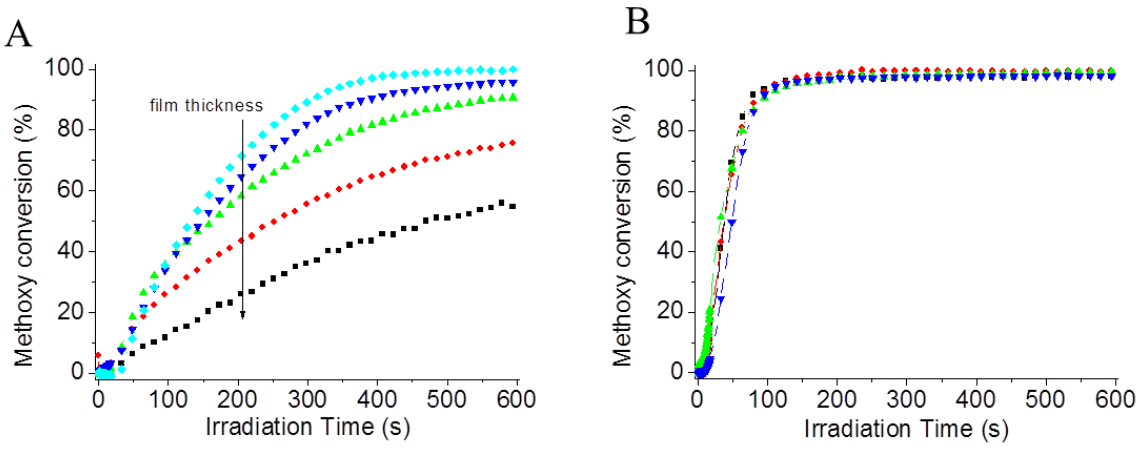

Figure III.2: Influence of film thickness on the hydrolysis conversion-time curves of PDMOS films. Thickness: (■) 0.8 µm, (●) 1.3 µm, (▲) 1.8 µm, (▼) 2.1 µm and (♦) 3.4 µm. Plot A is obtained with a 2/2 wt. % PBG/BP photocatalytic mixture while B is performed with the addition of an oxygen scavenger, 2/2/2 wt. % PBG/BP/TPP.

As shown in Scheme III.3, three different mechanisms can possibly account for the effect of TPP:

1/ TPP can scavenge the peroxyl radical resulting from the reaction of an aminoalkyl radical with oxygen.[10] 2-morpholino-2-propanol can form that may act as amine catalyst.

2/ The triplet state of BP formed after light excitation is able to sensitize the formation of singlet oxygen with a good quantum yield (0.39 in benzene).[11] After sensitization, singlet oxygen is scavenged by TPP to form triphenylphosphine oxide and diphenylphosphinate.[12]

3/ An electron transfer may occur between TPP and the BP triplet state, yielding the triphenylphosphonium cation. This latter is known to add efficiently on oxygen.[13]

While the first mechanism favors the formation of an alternative amine catalyst, the two latter mechanisms contribute to a full consumption of oxygen in the medium, thereby enabling the disproportion or hydrogen abstraction of the aminoalkyl radical to create subsequently the catalyst.

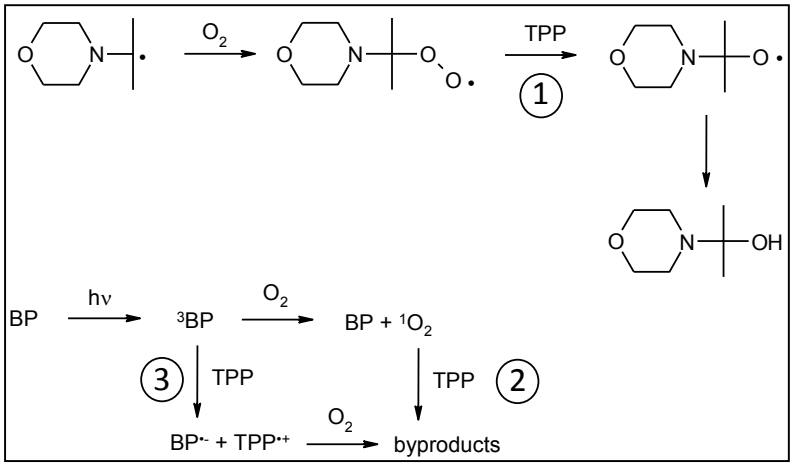

<u>Scheme III.3:</u> Three possible routes involving TPP during the photoirradiation of the α-aminoketone/BP/TPP mixture: 1. Peroxyl radicals scavenged by TPP; 2. Singlet oxygen scavenged by TPP; and 3. Electron transfer between TPP and BP.

II.2. <u>KINETICS, REACTION MECHANISM</u>

Like in chapter II, to give insight into the sol-gel process, the evolution of two characteristic IR bands is investigated temporally in Figure III.6, ν_{sym} (CH_3) at 2848 cm^{-1} representative of methoxysilyl functions ($SiOCH_3$) gives evidence of hydrolysis progress, while ν(Si-O-, Si-OH) at 930 cm^{-1} is a more qualitative marker of condensation.

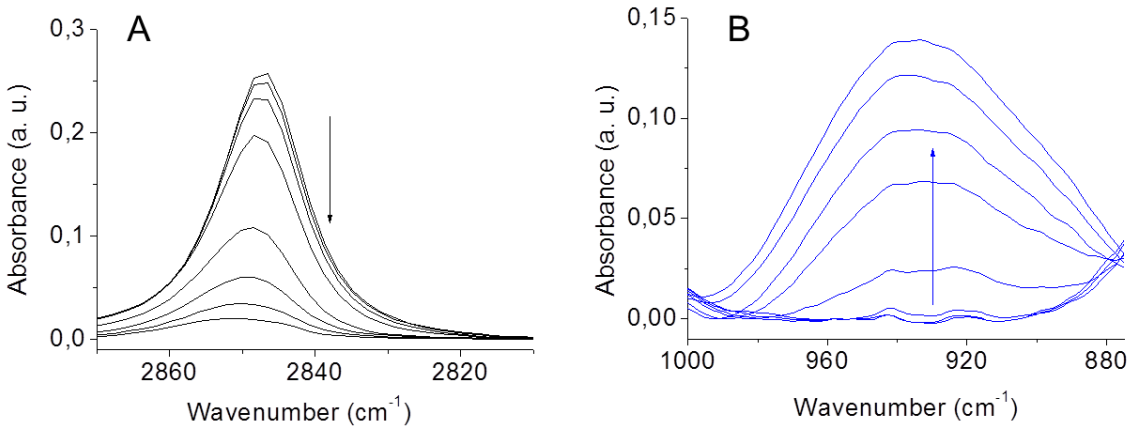

Figure III.3: Real-time FTIR experiments showing the evolution of two vibrational modes during the UV irradiation of a PDMOS film in presence of 2/2/2 wt. % PBG/BP/TPP. (A) ν_{sym} (CH_3) centred at 2848 cm^{-1}; and (B) ν(Si-O⁻, Si-OH) at 930 cm^{-1}.

In order to reveal the differences of mechanism between acid and base-catalyzed processes, the obtained results are systematically compared with an equivalent system containing a similar weight concentration in PAG. Figure III.4 is a plot showing the temporal evolution of these two characteristic IR bands throughout the irradiation.

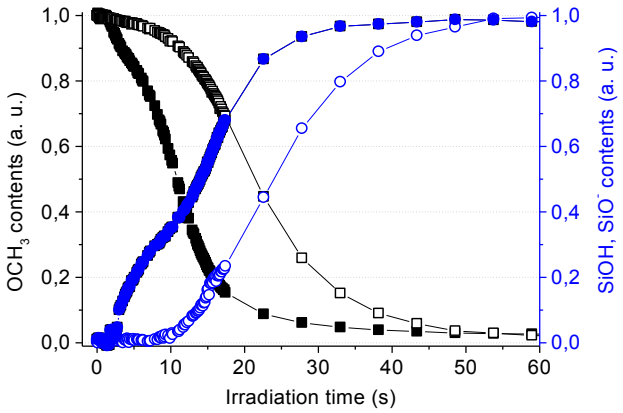

Figure III.4: Temporal evolution of two integrated IR band absorbances: $\nu_{sym}(CH_3)$ (■) and ν(SiO) (●) during the inorganic photopolymerization of a PDMOS film. Open symbols are for photobase conditions while full symbols are in photoacid catalysis.

Although the photoacid catalysis results in faster hydrolysis kinetics, we note the possibility to achieve high hydrolysis rates and full completion in 60 s with weak tertiary amine nucleophiles. In regards to hydrolysis mechanism, attack by nucleophilic hydroxyl anions generally reported in base conditions[14] is improbable here. Clearly, bulk conditions and weak tertiary amine bases do not favour water dissociation. In the presence of a tertiary amine such as N-alkyl morpholine, a "nucleophile activated substitution" is likely to proceed as described by Corriu *et al.*.[15] In this

proposed mechanism (Scheme III.4), the coordination of the amine to form a five coordinated intermediate lowers the activation barrier for the subsequent hydrolysis reaction.[16] Water then attacks the silicon atom to form a six coordinated intermediate. Displacement of an alkoxide anion and the nucleophile complete the hydrolysis process.

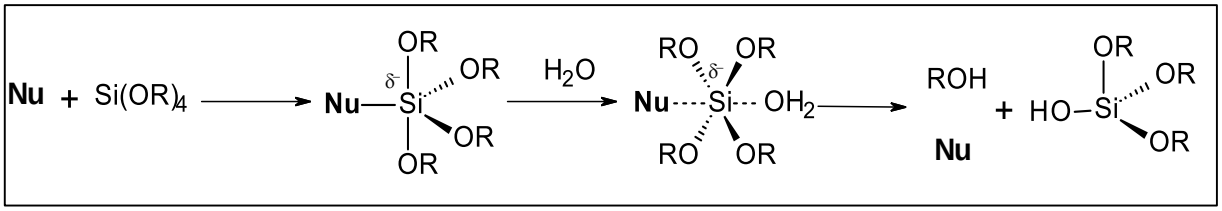

Scheme III.4: Hydrolysis reaction mechanism[15]

Absent from the initial formulation, the water for hydrolysis is provided instead by the atmosphere (RH ≈ 30 %) through diffusion in the micrometric film. As an indirect proof, blocking moisture diffusion with a hermetic BaF_2 pellet placed at the top of the PDMOS film is found to inhibit significantly the course of the hydrolysis. In addition, the progressive acceleration of the hydrolysis during the first 20 s is specific to photobase catalysis. This peculiarity is in agreement with the scheme that each successive hydrolysis reaction occurs more readily than the previous one. As the silicon acquires a formal negative charge in the intermediate (Scheme III.4), this mechanism is sensitive to inductive effects. Substitution of OCH_3 for more electron withdrawing substituents such as OH or OSi is thus expected to enhance the hydrolysis rate by stabilizing the negative charge on silicon.[1] Unlike photoacid catalysis, the growth of the SiOH (SiO^-) band in presence of PBG does not coincide precisely with the consumption of the methoxy groups, and begins only after 10 s when the hydrolysis is ca. 10 %. This suggests that condensation reactions proceed simultaneously with hydrolysis with a fast condensation of silanol groups just after their creation. Under base conditions, the nucleophilic addition is carried out preferentially through deprotonated silanol ($\equiv Si\text{-}O^-$) which are better nucleophiles than protonated silanols ($\equiv Si\text{-}OH_2^+$) active in acid catalysis. The pK_a values for the couple Si-OH/ SiO^- is estimated between 6-9 depending on siloxane cross-linking and H-bonding.[17] Silanol are thus more acidic than alcohol and are readily deprotonated under basic conditions to afford more nucleophilic silanolates. In our case, a typical base-catalyzed condensation is assumed to be the favored mechanism (Scheme III.5), involving the attack of a nucleophilic deprotonated silanol on a neutral silicate species as proposed by Iler.[18] After 50 s, the SiOH band hardly changes, thus suggesting very few new condensation reactions after this period.

$$\equiv SiO^- + Si(OH)_4 \rightarrow \equiv Si\text{-}O\text{-}Si\equiv + OH^-$$

Scheme III.5: Condensation reaction mechanism in basic conditions

II.3. SILICATE MICROSTRUCTURE

The difference in siloxane microstructure can be examined by ^{29}Si solid-state NMR. Figure III.5 displays the ^{29}Si SPE-MAS spectra of the photobase and photoacid-catalyzed silica films in which $Q^3(HOSi(OSi)_3$, -101 ppm) and Q^4 ($Si(OSi)_4$, -111 ppm) siloxane species are clearly dominant in both cases. This supports the ability of our photobase catalyst to generate well-condensed materials (81 %). The lower degree of condensation compared to the photoacid-catalyzed product (87 %) is apparently inconsistent with the picture of highly condensed clusters generated under basic conditions *versus* weakly branched structures with acid catalysts.[19] However, our solvent-free conditions permit a silica film formation without transition through a sol, which is clearly non-conventional in sol-gel synthesis. Slower kinetics are clearly observed with base catalysts, but it is plausible that the formation of highly branched clusters can cause in this case an earlier gelation, hindering the progress of the condensation reactions.

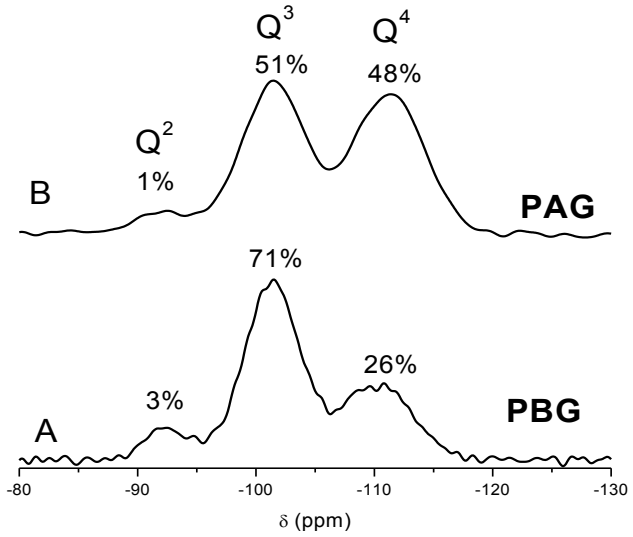

Figure III.5: SPE-MAS 29Si NMR spectra of the UV cross-linked PDMOS films including (A) 2/2/2 wt. % PBG/BP/TPP and (B) 2 wt. % PAG. Irradiation conditions: UV conveyor, H lamp, 1.46 J/cm²/pass, 10 passes.

II.4. FILMS MORPHOLOGIES AND OPTICAL PROPERTIES

In contrast to an organic cross-linking reaction proceeding usually in a single step, sol-gel polymerization is based on two concurrent hydrolysis and condensation reactions whose

respective rates are strongly dependent on the catalyst[14]. Consequently, the polymer microstructure at the gel point is predicted to be considerably different in acid and base catalysis. As shown in Figure III.6, the physical differences between films in photoacid or photobase conditions are clearly illustrated by comparison of the respective film morphologies using a combination of microscopic techniques: AFM, SEM and TEM.

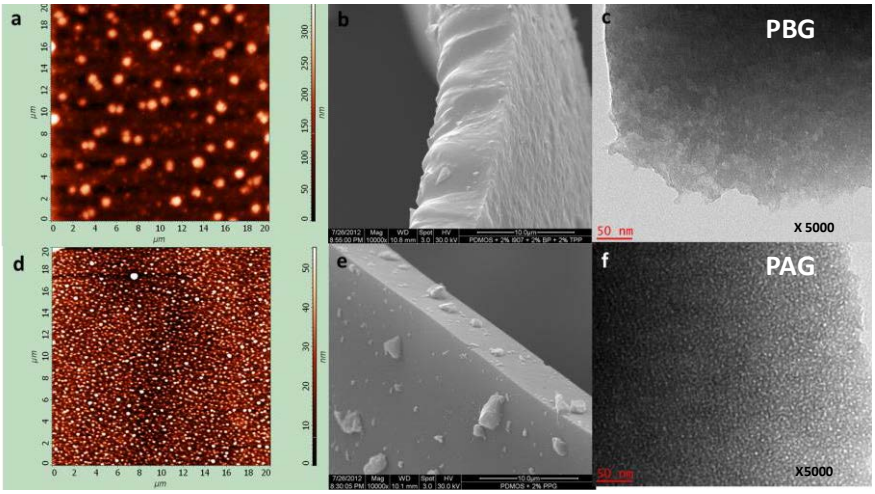

Figure III.6: AFM (a, d), SEM (b, e) and TEM (c, f) images of photopolymerized PDMOS films under photobase (first line) and photoacid (second line) conditions. Irradiation conditions: Hg-Xe lamp, 200 mW/cm²

AFM characterization shows a photobase-catalyzed film surface composed of large aggregated spherical particles (200-800 nm). These large diameters resulted in light scattering properties giving a turbid aspect to the film. Slight abrasion caused the formation of a fluffy powder suggesting that the particles are not well bonded together. As reported in the literature, basic catalysis promotes a "cluster-monomer" aggregation process to afford a particulate morphology, in a similar fashion as the Stöber silica particles are formed.[20] Because precursor species are less acidic than more highly branched species, further condensation occurs preferentially between clusters (SiO^-) and monomers (SiOH) rather than between monomers, thus giving birth to this particular morphology. In contrast to the Stöber process,[21] the bulk conditions prevent the formation of monodisperse particles and the aggregation is not ordered. In accordance with the formation of large particles, capillary pressure is low during the film drying resulting in surface roughness, as evidenced by SEM. However, the TEM image does not reveal any porosity.

The film produced under photoacid conditions still appears to be particulate (Figure III.4), but on a much finer scale, as revealed by AFM. Consistent with this morphology is the mechanism of acid-catalyzed condensation reactions occurring preferentially between neutral species and protonated silanols contained respectively in monomers and end chains (inductive effects make

these latter silanols the most basic). The result is highly entangled polymer chains with a poor tendency to form large clusters. Only nanoparticulate domains (< 100 nm) are visible at the surface. The roughness is generally less than 10 nm, and accordingly, the film surface appears smooth in the SEM micrograph. This results in a silicate film which is optically clear and relatively dense. Its high mechanical strength originates presumably from the strongly bonded network. When examined by TEM, the acid-catalyzed film exhibits a very fine microstructure and very small micropores that appear quite uniform throughout the material. This suggests that during the film gelation, the small nanoclusters are aggregated and compacted due to strong capillary pressure.

To gain further insight into the microstructural differences of the photobase-catalyzed film, UV-visible spectra are taken throughout UV irradiation. Figure III.7 is a graph of experimental apparent absorbance versus λ between 0 and 300 s. Before irradiation, the PBG-based film exhibits two maxima around 248 and 303 nm ascribed to $\pi\pi^*$ (BP) and $n\pi^*$ (α-aminoketone) absorption from the ketone groups. In only 20 s irradiation (ca. 40 % hydrolysis), photolysis induces a fast decline of these chromophore signatures and a fast rise of the absorbance. The appearance of an absorbance curve with λ^{-n} wavelength dependency is indicative of light scattering. Clearly, this change in optical properties and the formation of an optically thick UV-cured film are linked to the entrapment of submicrometric silica particles as proved by AFM and SEM investigations. The large scattering power of the films prepared with photobase is also largely conditioned by the relatively high refractive index of silica (n_{SiO2} = 1.45). With an equivalent photoacid system, the apparent absorbance values are much smaller due to the considerable decrease of the scattering coefficients with smaller grain size.

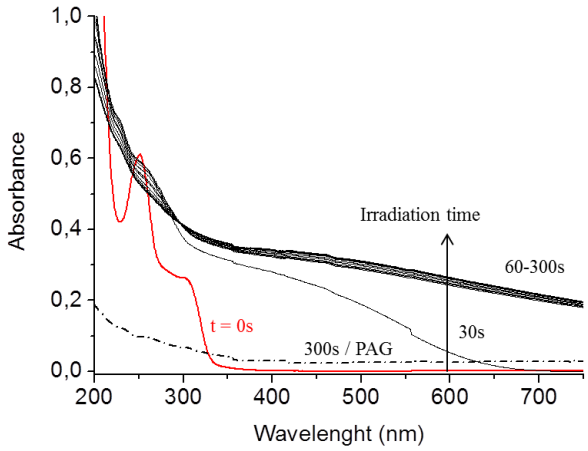

Figure III.7: UV-vis spectra of PDMOS-based films containing 2/2/2 wt. % PBG/BP/TPP at different irradiation times (0 - 300s). For comparison, the equivalent UV cured film prepared under photoacid conditions has been represented in the same plot with dotted lines.

III. APPLICATION TO HYBRID FILMS

Like in previous chapter, we wanted to extend the straightforward methodology of photobase-catalyzed sol-gel photopolymerization to prepare cross-linked PDMS in a fast single step. Following the same route, a homogeneous and photolatent film (5 µm) comprising a solvent- and water-free mixture of PDMOS and silanol-functionalized PDMS was irradiated in presence of a PBG/BP/TPP photocatalytic system. Figure III.8 displays the hydrolysis-time curves at several PDMS concentrations (0-75 wt. %). We observed that upon increasing the amount of silicone, kinetics of the photobase-catalyzed hydrolysis are only hardly affected. The conclusions emerging from this latter system are consistent with the results obtained under acid photocatalysis (Figure III.8B) showing accordingly a limited impact of PDMS on kinetics.

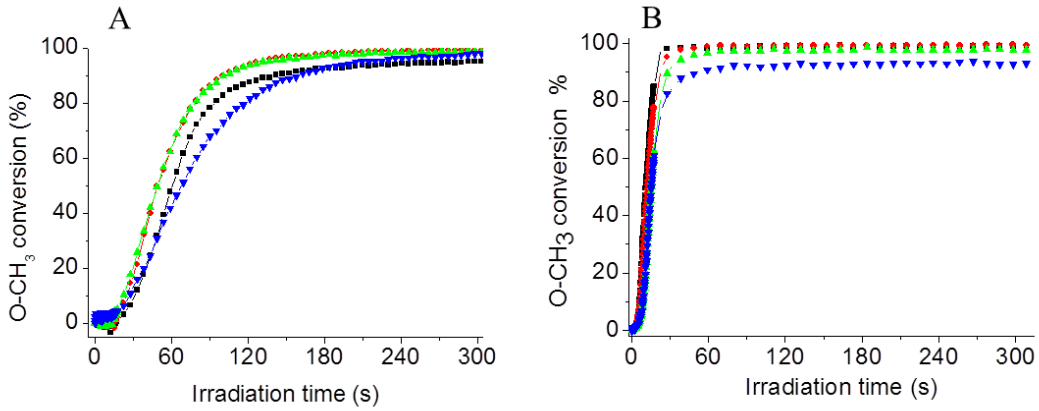

Figure III.8: Hydrolysis conversion of PDMOS-based hybrid films containing different concentrations in OH-terminated PDMS: (■, 0 wt. %), (●, 25 wt. %), (▲, 50 wt. %) and (▼, 75 wt. %). Plot A is obtained with a 2/2/2 wt. % PBG/BP/TPP mixture and curve B with 2 wt. % PAG.

^{29}Si solid-state NMR was used to obtain information on the hybrid microstructure determined by the ratio of homo- or hetero-condensation reactions between the OH-PDMS and the methoxysilane derivative. The polysiloxane structures which arise from the silane cross-linker and PDMS can be distinguished, and described respectively in terms of D and Q notations. Figure III.9 compares the ^{29}Si CP-MAS NMR spectra of two PDMS films containing 50 wt. % methoxysilane under photoacid and photobase conditions.

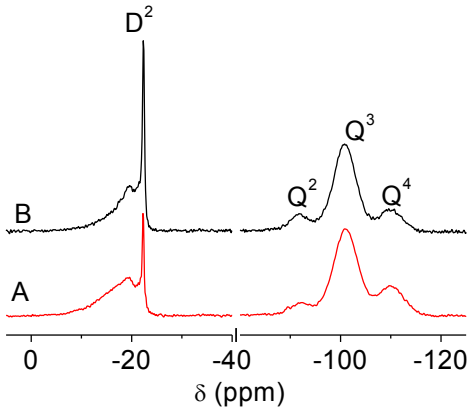

Figure III. 9: ^{29}Si CP-MAS NMR spectra of the PDMS/cross-linking agent (50/50 wt. %) films prepared under (A) photoacid and (B) photobase conditions. Irradiation conditions: UV conveyor, H lamp, 1.46 J/cm2/pass, 10 passes.

Confirmation of cross-linker condensation was given by the triplet of Q^2, Q^3 and Q^4 units straightforwardly assigned to crosslinked PDMOS. In addition, a broad D^2 signal at ca. -20 ppm indicated in both conditions the incorporation of PDMS.[22-24] The NMR spectra obtained for hybrid PDMS/PDMOS photoacid-catalyzed film has already been discussed in detail in chapter II (paragraph IV). We noticed two environments for the D^2 species synonymous of difference of mobility: two sharps lines corresponding to PDMS homopolymerization (mobile environment) and three broad linewidth significant of a more rigid environment due to close proximity with the tri-dimensional inorganic network from PDMOS. Clearly, our interpretation can be extended to the NMR spectrum of the photobase-catalyzed film (Figure III.10) displaying also five deconvoluted peaks in the D^2 region with only slight variations in their maxima position.

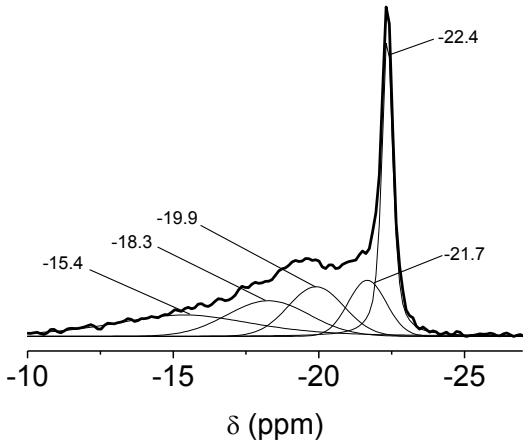

Figure III.10: Deconvolution of ^{29}Si CP-MAS NMR spectra of the PDMS/PDMOS (50/50 wt. %) films prepared under photobase conditions. Irradiation conditions: UV conveyor, H lamp, 1.46 J/cm^2/pass, 10 passes.

By comparing PAG and PBG systems, we found that the nature of the photocatalyst had also an effect on the shape of the D resonance. Thus, the proportion in sharp resonances (-22.3 and -22.0 ppm) was significantly enhanced in the photobase-catalyzed system, suggesting a decrease in the number of chemical linkages between PDMS and the Q polysiloxane network (Figure III.9). A faster homocondensation between SiOH terminated PDMS oligomers is presumably favoured under base conditions.

CONCLUSION

Inorganic cross-linking of a PDMOS was performed with a α-aminoketone molecule acting as a photolatent base catalyst. Our study disclosed an efficient photobase-catalyzed sol-gel reaction operating without thermal activation. In contrast to conventional sol-gel processing methods, silicate films were prepared in one-step without transition through a sol, and the need for water or organic solvent. Of interest is that sol-gel polymerization does not claim for highly basic catalyst to yield condensed silicate films at high rates. Hence, photogenerated tertiary amines exhibiting a moderate nucleophilicity (pK_a = 9.1) showed a high catalytic activity. A too high pK_a base is presumably not recommended because condensation requires the coexistence of both protonated and deprotonated silanols.

One of the guideline points of this chapter related to the comparison with a photoacid-catalyzed sol-gel process. Several spectroscopic and microscopic methods revealed significant differences in respect to morphology, density, surface roughness, and optical properties. Most results could

be reconciled with the effect of the catalyst on the reactivity of silicon alkoxides reported in conventional sol-gel film forming process. Photobase catalysis resulted in rough film surface, low optical transmission, coarse particular morphology, but a nonporous texture. By contrast, the photoacid-catalyzed samples were dense, smooth, transparent, further condensed. Finally, such tertiary amine photobase was also efficient to promote co-condensation with OH terminated silicone leading to interesting futures applications for hybrid films cross linking.

CHAPTER III REFERENCES

(1) Brinker, C.; Scherer, G. *Sol-Gel Science: The Physics and Chemistry of Sol Gel Processing*; Academic Press Inc: San Diego, **1990**.
(2) Corriu, R.; Guerin, C.; Henner, B.; Wang, Q. *Organometallics* **1991**, 10, 3200.
(3) Harkness, B.; Takeuchi, K.; Tachikawa, M. *Macromolecules* **1998**, 31, 4798.
(4) Harkness, B.; Takeuchi, K.; Tachikawa, M. *Polym. Advan. Technol.* **1999**, 10, 669.
(5) Chemtob, A.; Courtecuisse, F.; Croutxe-Barghorn, C.; Rigolet, S. *New J. Chem.* **2011**, 35, 1803.
(6) Uraoka, Y.; Tadanaga, K.; Tatsumisago, M. *Chem. Mater.* **2010**, 22, 6125.
(7) Kura, H.; Oka, H.; Birbaum, J.; Kikuchi, T. *Photopolym. Sci. Tech.* **2000**, 13, 145.
(8) Fouassier, J. P. *Photochemistry and UV Curing: New Trends*; Research Signpost: India, **2006.**
(9) De Paz, H.; Chemtob, A.; Croutxé-Barghorn, C.; Le Nouen, D.; Rigolet, S. *J. Phys. Chem. B* **2012**, 116, 5260.
(10) Belon, C.; Allonas, X.; Croutxe-Barghorn, C.; Lalevee, J. *J. Polym. Sci., Part A: Polym. Chem.* **2010**, 48, 2462.
(11) Chattopadhyay, S. K.; Kumar, C. V.; Das, P. K. *J. Photochem.* **1985**, 30, 81.
(12) Tsuji, S.; Kondo, M.; Ishiguro, K.; Sawaki, Y. *J. Org. Chem.* **1993**, 58, 5055.
(13) Alfassi, Z. B.; Neta, P.; Beaver, B. *J. Phys. Chem. A* **1997**, 101, 2153.
(14) Brinker, C. J. *J. Non-Cryst. Solids* **1988**, 100, 31.
(15) Chuit, C.; Corriu, R.; Reye, C.; Young, J. C. *Chem. Rev.* **1993**, 93, 1371.
(16) Ignatyev, I. S.; Montejo, M.; Gonzalez, J. J. *Chem. Phys.* **2009**, 11, 841.
(17) Loy, D. A.; Russick, E. M.; Yamanaka, S. A.; Baugher, B. M.; Shea, K. J. *Chem. Mater.* **1997**, 9, 2264.
(18) Iler, R. K. *The chemistry of Silica*; Wiley: New York, **1979**.
(19) Brinker, C. J.; Keefer, K. D.; Schaefer, D. W.; Assink, R. A.; Kay, B. D.; Ashley, C. S. *J. Non-Cryst. Solids* **1984**, 63, 45.
(20) Brinker, C. J.; Keefer, K. D.; Schaefer, D. W.; Ashley, C. S. *J. Non-Cryst. Solids* **1982**, 48, 47.
(21) Stöber, W.; Fink, A. *J. Colloid Interf. Sci.* **1968**, 26, 62.
(22) Babonneau, F. *Polyhedron* **1994**, 13, 1123.
(23) Tsuru, K.; Aburatani, Y.; Yabuta, T.; Hayakawa, S.; Ohtsuki, C.; Osaka, A. *J. Sol-Gel Sci. Techn.* **2001**, 21, 89.
(24) Salinas, A. J.; Merino, J. M.; Babonneau, F.; Gil, F. J.; Vallet-Regí, M. *J. Biomed. Mater. Res. B* **2007**, 81B, 274.

ABBREVIATIONS

C	Concentration
CD	Condensation degree
CMC	Critical micellar concentration
CP-MAS	Cross polarization magic angle spinning
CSA	Cooperative self-assembly
CSD	Chemical solution deposition
CTAB	Cetyltrimethylammonium bromide
CTAC	Cetyltrimethylammonium chloride
D_p	Pore diameter
EASA	Electrochemically-assisted self-assembly
EISA	Evaporation induced self-assembly
EO	Ethylene oxide
FSM	Folder sheets mesoporous
HETCOR	Heteronuclear correlation
HLB	Hydrophilic-lipophilic balance
I	Irradiance
LCT	Liquid crystal template
LISA	Light induced self-assembly
LO	Longitudinal optic
LPM	Low pressure mercury (lamp)
MCM	Mobil crystalline materials
NMR	Nuclear magnetic resonance
PAG	Photoacid generator
PDMOS	Polydimethoxysiloxane
PEO	Polyethylene oxide
PO	Propylene oxide
PPO	Polypropylene oxide
RH	Relative humidity
RT-FTIR	Real-time Fourier transform infrared
S_{BET}	BET surface
SPE-MAS	Single pulse excitation magic angle spinning
T	Temperature
TEM	Transmission electronic microscopy
TEOS	Tetraethoxysilane
TMOS	tetramethoxysilane
TO	Transversal optic
V_p	Pore volume
W_{thick}	Wall thickness
XRD	X-ray diffraction

CHAPTER IV: SURFACTANT-TEMPLATED MESOPOROUS SILICA: AN EMPHASIS ON FILM SYNTHESIS AND THE USE OF UV LIGHT

INTRODUCTION

In the second part of this manuscript, our goal is to propose a novel UV-mediated route for the preparation of mesoporous silica films. Before we can understand the added-values of such novel process, it is important to review in a progressive manner some decisive aspects of the surfactant-templated mesoporous silica approach. Our focus is clearly on silica framework although a variety of inorganic oxide[1-4] or hybrid mesostructures[5,6] with important technological applications have been highly investigated.

Thus, our first approach is general starting from the pioneering studies, and then describing some fundamental concepts about surfactants, self-assembly, and synthesis of surfactant/inorganic mesophases. The second point will bring us closer to our subject in reviewing the preparation and applications of mesoporous materials as thin films, with a special emphasis on the role of block copolymer template (non-ionic surfactant) which have been systematically employed in our study. The last point will reveal different cases in which UV light has been used related to mesoporous materials preparation or surfactant self-assembly.

I. PREPARATION OF MESOPOROUS SILICA BY A TEMPLATE-BASED APPROACH

I.1. PRINCIPLE AND INTEREST

The discovery of surfactant-templated silica mesophases in 1992 has led to a great deal of attention on the synthesis of ordered mesoporous inorganic oxides to extend existing applications of microporous zeolitic materials (with a typical pore size < 2 nm)[7]. According to IUPAC definition[8], ordered mesoporous materials contain pores with diameters in the size range of 2 to 50 nm, the upper limit marking the demarcation with macroporous materials. Mesoporous materials are also characterized by their high surface area comprised between 500 and 1000 m^2/g, their large and uniform pore size as well as perfectly controlled mesostructures[9,10].

A mesoporous material originates from a mesostructured hybrid material, which is formed by polymerization of inorganic precursors by a sol gel process around an organic mesophase working as template[7]. The porosity is ultimately created by template removal. The formation of such materials relies on two crucial aspects:

- Mesostructuration, i. e. the self-assembly of an organic surfactant in liquid crystal structures which drives the nanophase separation of hydrophobic and hydrophilic parts.

The synthesis of highly ordered mesostructured materials shows a direct correlation between the surfactant array size and shape and the final pore size and geometry.

- Sol-gel chemistry which is the mineral polymerization process converting the molecular inorganic precursor into a hydrophilic oxo-polymer network. In the case of alkoxysilane (molecular silica source), the versatility of the sol-gel process is particularly useful to work under conditions where the condensation rate of the hydrophilic silica precursors can be minimized. The underlying idea is not to disturb the self-assembly process by premature gelation that would favor amorphous kinetically-trapped products.

The success of the surfactant templating method is reflected today in the high number of publications (Figure IV.1) and its technological impact in catalysis, active control of mass transport, low k dielectrics or laser devices. Importantly for applications, the templating approach enables pore size, geometry and composition to be finally tuned by many experimental parameters (surfactant structure and concentration, aging conditions of the sol, auxiliary chemicals, choice of solvents, template removal method, etc.) or processing conditions (temperature, relative humidity (RH), deposition technique for films). Currently, a majority of works has concentrated on silica[11], transition metal oxide[1,2,12,13] and organic–inorganic hybrid mesostructures[5,6] with an emphasis on powder and monolith morphologies suitable to catalysis[14-16] and adsorption[17] applications.

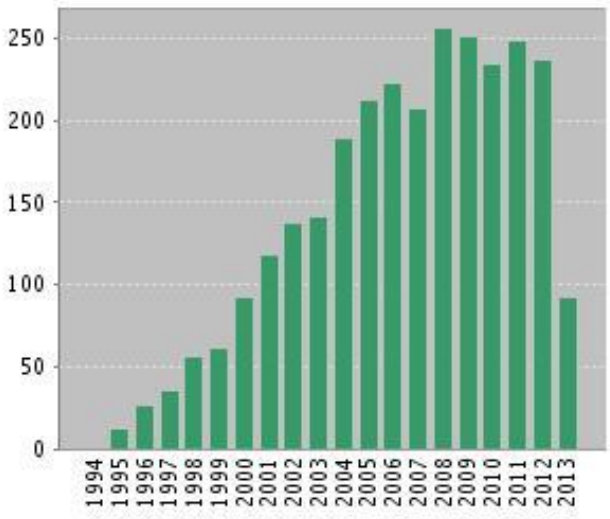

Figure IV.1: Evolution of the number of publications concerning the use of surfactant templating process for preparation of mesoporous material from 1994 until today. (Source: Web of knowledge, keywords "surfactant template mesoporous")

I.2. EARLY 1990S: THE FIRST INORGANIC MESOPHASES

The first work concerning mesoporous solids with a controlled porosity dates back from 1990. Yanagisawa *et al.*[18] reported the synthesis of folder sheets mesoporous material (FSM) by intercalation of quaternary ammonium (C_nTMA^+) between sheets of hydrated sodium silicate. Solid material with porous channel and hexagonal symmetry was obtained. Almost at the same time in 1992, a group of researchers from the Mobil Research and Development Corporation[19-22] released the synthesis of mesoporous material formed hydrothermally as powders, just like zeolites. Starting from tetraethoxysilane (TEOS) precursor as silica source and ionic surfactant consisting in a long-chain alkyltrimethylammonium halide, mesoporous silica exhibiting a hexagonal or cubic arrangement of pores (1.5 to 10 nm) with a maximal surface area above 700 m^2/g was achieved. The mesostructures were conclusively elucidated by transmission electron microscopy (TEM) and X-ray diffraction (XRD) analysis, thus paving the way to a systematic method to interpret the mesophase structure.

However, as early as 1969, a patent from Chiola *et al.*[23] reported a sol-gel process including tetra alkyl silicate precursors and a cationic surface active agent (quaternary ammonium halide, $[NR_4]^+X^-$). Nevertheless, at that time, the authors were not aware that the resultant powders possessed a hexagonal silica/surfactant mesostructure. It was only in 1997 that Di Renzo repeated the experimental procedure of the patent, and found that a well-ordered mesostructure was obtained[24]. However, the enthusiasm for mesoporous material has really started with the Mobil work on mesoporous silicas. Mobil Crystalline Materials, MCM-41 (hexagonal), MCM-48 (cubic) and MCM-50 (lamellar) are the three typical structures described in their studies. (Figure IV.2).

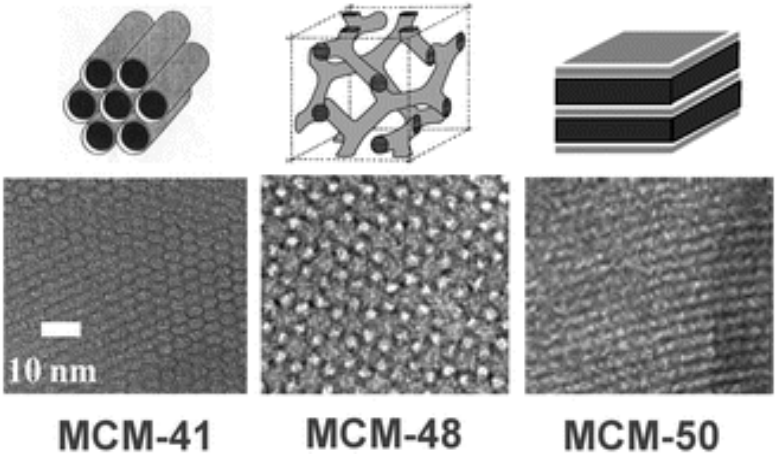

Figure IV.2:Structure of M41S family of mesoporous material (MCM-41, MCM-48, MCM-50)[19-22,25]

In addition to the novelty of the route, the strength of this study is to suggest brilliant perspectives such as application to non-siliceous precursors, access to organic-inorganic structures by post-functionalization and formation of the three mesophases. Furthermore, the authors sketched the complexity of the templating mechanism with the possible participation of inorganic species to the self-assembly process (Cooperative Self Assembly, CSA). Obviously, there is a "before" and an "after" 1992 in the field of mesoporous materials. It is remarkable to observe more than 20 years after how this study was inspiring and how surfactant template-based route has emerged as a new era of great technological and scientific interest[26,27].

I.3. THE SURFACTANT TEMPLATE

Before describing how mesoporous materials are formed, we must understand why and how surfactant makes up the mesophase.

I.3.1. Definition

A surfactant is generally described as a bifunctional molecule having a solvent-philic (lyophilic) component and a solvent-phobic (lyophobic) component to form an amphiphilic structure. Surfactants are usually classified depending on the charge of the hydrophilic moiety: ionic (cationic or anionic) or nonionic (i. e. block copolymer)[28]. When placed in solution, surfactant has the particularity to self-assemble into supramolecular arrays gathering a high number of entities with a final geometry depending on the nature, charge, shape and concentration of the individual molecule. Self-assembly is generally defined as the spontaneous, reversible organization of individual surfactant molecules by means of non-covalent interactions (i. e. Van der Waals, electrostatic interactions and hydrogen bonding). Their collective character involving a higher number of groups and molecules drives the formation of regular assemblies of separated hydrophilic and hydrophobic moieties.

I.3.2. Critical micelle concentration

An important point in the chemistry of surfactant is the critical micelle concentration (CMC) which corresponds to the concentration of surfactant at which micelle starts forming. When the surfactant concentration C < CMC, free molecules of surfactant tends to form a single layer at the interface air/liquid or solubilize as individual entities in solution. Just above the CMC, the micelles can be viewed as small spherical and isotropic aggregates of surfactant molecules; they represent the first example of supramolecular assembly generated at low concentration. In regular micelles, the hydrophilic groups form the outer surface while the hydrophobic tails point

toward the center in a way to minimize the unfavorable interactions with the solvent (water for example). The CMC is characteristic of each surfactant and also depends on various factors such as temperature, pressure, electrolyte and co-solvent[28]…The extent of micellization, the shape of the micelles, and the aggregation of micelles into liquid crystals depends mainly on the surfactant concentration. At higher concentration than the CMC, the micelle initially spherical generally elongates as the amount of solvent available between the micelle decreases. The shift from spherical micelles to cylindrical micelle is often referred to occur at a CMC2. Further increase in the surfactant concentration leads eventually to the formation of close-packed liquid crystal phase (or lyotropic phase, i.e. mesophase controlled by the solvent quality). Liquid crystals have the ordered molecular arrangement of solid crystals but the mobility of liquids. Depending on the concentration of surfactant and temperature, cubic bicontinuous, hexagonal and lamellar phase are formed (Figure IV.3).

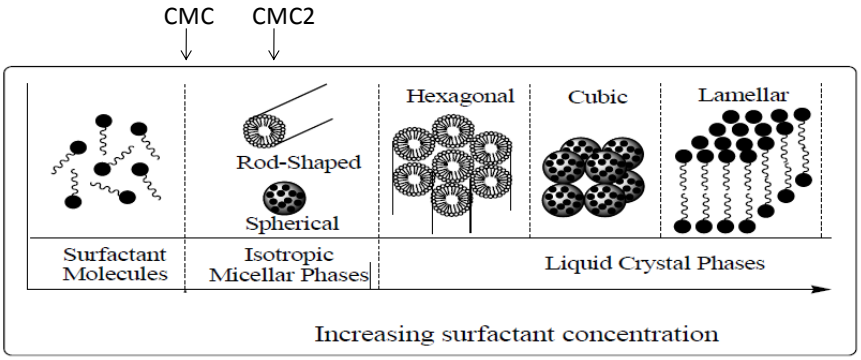

Figure IV.3: Evolution of surfactant from free molecules to liquid crystal phase[29]

The coexistence of the different phases depending on these conditions is generally represented as phase diagram and depends on each surfactant. Figure IV.4 presents the characteristic phase diagrams in water of two ionic and nonionic surfactant conventionally used in the preparation of mesoporous silica: cetyltrimethylammonium bromide ($CH_3(CH_2)_{15}N(CH_3)_3^+Br^-$ or $C_{16}TMABr$) and Pluronic® P123 ($(PEO)_{19}(PPO)_{69}(PEO)_{19}$, PEO = polyethylene oxide CH_2-CH_2-O, PPO = polypropylene oxide $CH(CH_3)$-CH_2-O, and the subunit is the number of monomeric motifs).

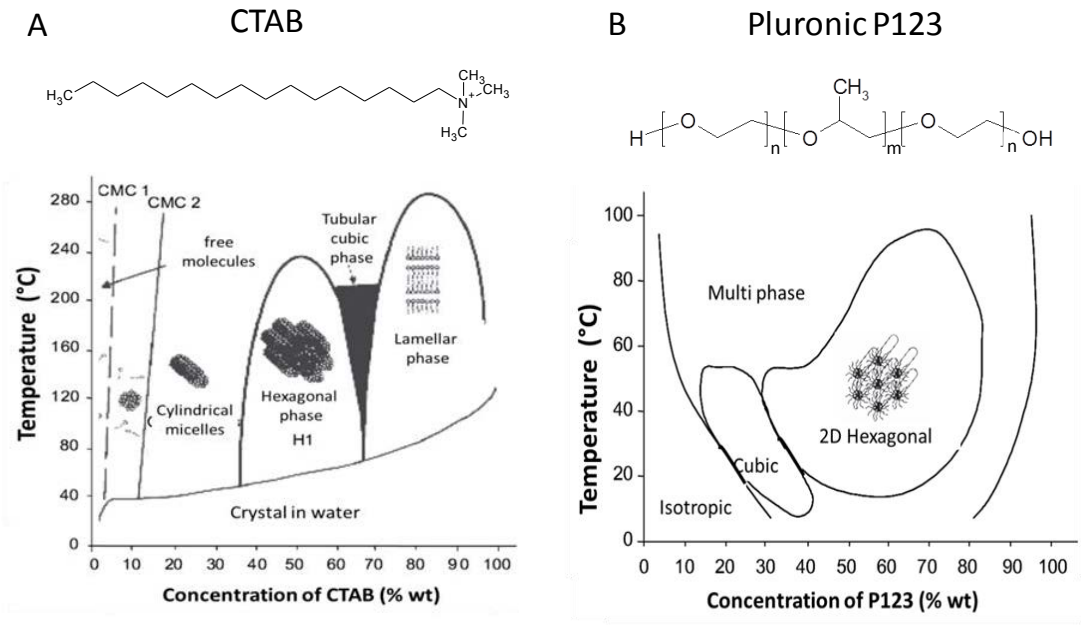

Figure IV.4: Phase diagram of CTAB cationic surfactant[30] (A) and Pluronic P123 block copolymer (n = 19, m = 69)[31] (B)

The aggregation of surfactant into micellar phase and then into liquid crystal phase at higher concentration is governed by various thermodynamic parameters including the interactions between hydrophilic and hydrophobic moieties. Among these variables, the Hydrophilic-Lipophilic Balance (HLB) and the critical packing parameter *g* are worth to be commented on.

The HLB of a surfactant defines the equilibrium between the hydrophilic and lipophilic part. This concept was first introduced by Griffin in 1946[32], and become more and more complex with time[33]. The HLB equation initially proposed by Griffin applied only to nonionic surfactant, and is expressed as:

$$HLB = 20 * \frac{M_H}{M}$$

Where M_H is the molar mass of the hydrophilic portion of the molecule, and M is the total molar mass. The Griffin HLB generally ranges from 0 to 20. Surfactants displaying a HLB < 10 are typically water-insoluble. By contrast, those having an HLB> 10 are soluble in water.

The packing parameter g was defined by Israelachvili, Mitchell and Ninham in 1976[34,35] and is frequently used to predict the geometry of the mesophase formed and the space occupied by the hydrophilic and hydrophobic groups of the surfactant molecule. g is defined as:

$$g = \frac{V_H}{a_0 l_c}$$

Where V_H is the volume of the hydrophobic portions of the amphiphilic part, a_0 is the area occupied by the hydrophilic part and l_c is the length of the hydrophobic chain. Of high

significance is that *g* is directly related to the curvature of the monolayer that a surfactant can form. Hence, *g* substantially differs depending on the morphology of the aggregate (Table IV.1 and Figure IV.5).

Table IV.1: Value of the packing parameter and the predicted form of the micelle

Value of *g*	Micelle morphology
g = 0 - 1/3	Spherical micelle
g = 1/3 - 1/2	Cylindrical micelle (precursor of the hexagonal phase)
g = 1/2 -1	Flexible bilayer, vesicles or disklike micelles
g = 1	Lamellae, planar bilayer
g > 1	Reverse structures

The value of *g* dictates the behavior of the surfactant in water and in the precursor solution: the larger the value, the less the curvature in the aggregate. For example spherical micelles with a large curvature have a low *g* value (< 1/3) while *g* of planar lamellae is close to 1. In general, any increase in surfactant concentration results in phase transition corresponding to a decrease in the surface curvature (higher *g*). Indeed, the decreased concentration in solvent resulting from the addition of more surfactant causes a reduction in the effective size of the hydrophilic head (a_0) that will increase the value of *g* and the aggregate morphology (sequence Cubic →Hex → Lam).

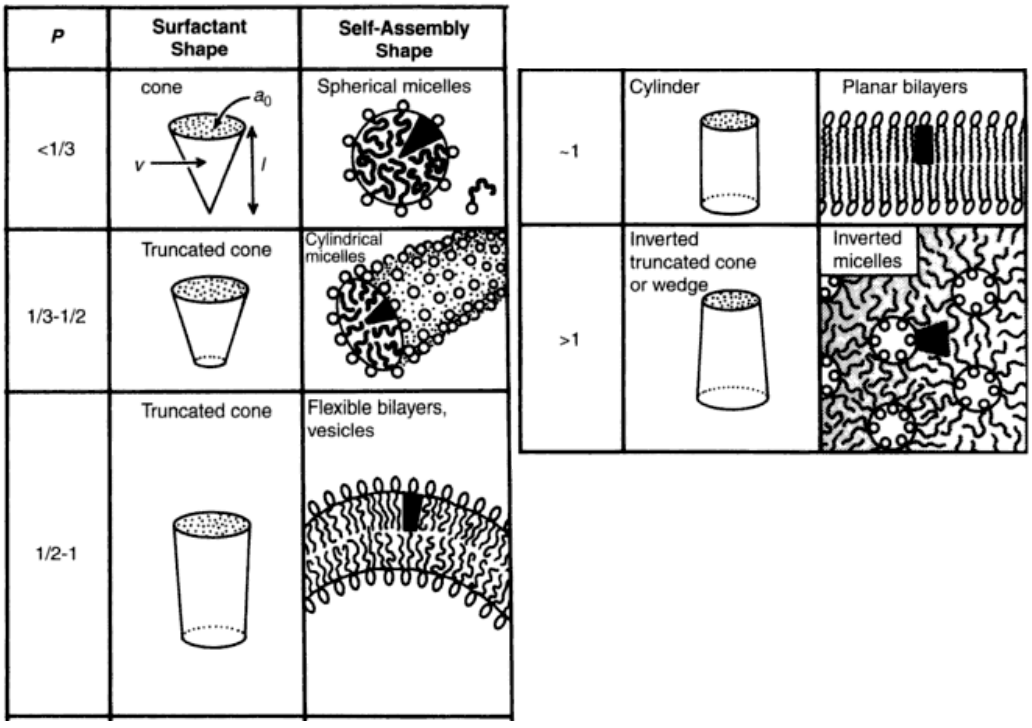

Figure IV.5: Schematic representation of the different micelle mophologies depending on the packing parameter value "g"[36]

In general, simple single-chain surfactants with a large head groups such as cationic surfactants (C_{16}TMABr) are chosen in mesoporous synthesis. They exhibit low values of g to avoid the formation of lamellar structures that tend to collapse when the template is removed.

I.3.3. The surfactant/silica mesophase

The principle for the formation of mesoporous material is in appearance simple, and relies on a sol-gel process in presence of surfactant mesophase template. The key is to transcribe the mesoscopic order of a surfactant liquid crystal phase into inorganic materials (Figure IV.6). The concept of hydrophilic components organizing around micellar arrays, and condensing to form oxides has many common points with biomineralization. Many biological structures emphasize the nucleation, growth and aggregation of inorganic species around organized assemblies of organic macromolecules[37]. For mesoporous silica, a typical synthesis includes at least four ingredients: surfactant, silica source, water and catalyst. The silica source dictates the reaction conditions.

- For nonmolecular silica sources including fumed silica or sodium silicate (water glass), a nonhomogeneous mixture including all the reagents is formed and treated hydrothermally at 75-180°C for several hours to several days to yield a solid precipitate[19]. The surfactant concentration is relatively high reaching 15-30 wt %. The organic-inorganic mesostructured product was filtered, washed with water and air-dried. The product was then calcined (500 °C) to eliminate the surfactant, and yield the mesoporous material.
- By contrast, when a molecular silica source is chosen such as alkoxysilane precursors (TMOS or TEOS), which corresponds to the majority of the published experiments, the starting solution includes only the precursor, water and catalyst to form a homogeneous solution. The surfactant is then added to this micellar solution. The mesostructure generally forms in seconds to minutes at moderate temperature. Lower concentrations in surfactant are generally used and a co-solvent is often added to the solution to ensure homogeneity and maximize product yield. During the synthesis, the inorganic network is condensed around the lyotropic phase formed by the structure directing agent in solution. Finally, after elimination of the organic part (liquid extraction, incineration at elevated temperature) a well-ordered and controlled porosity is generally obtained leading to organized mesoporous material[20,38].

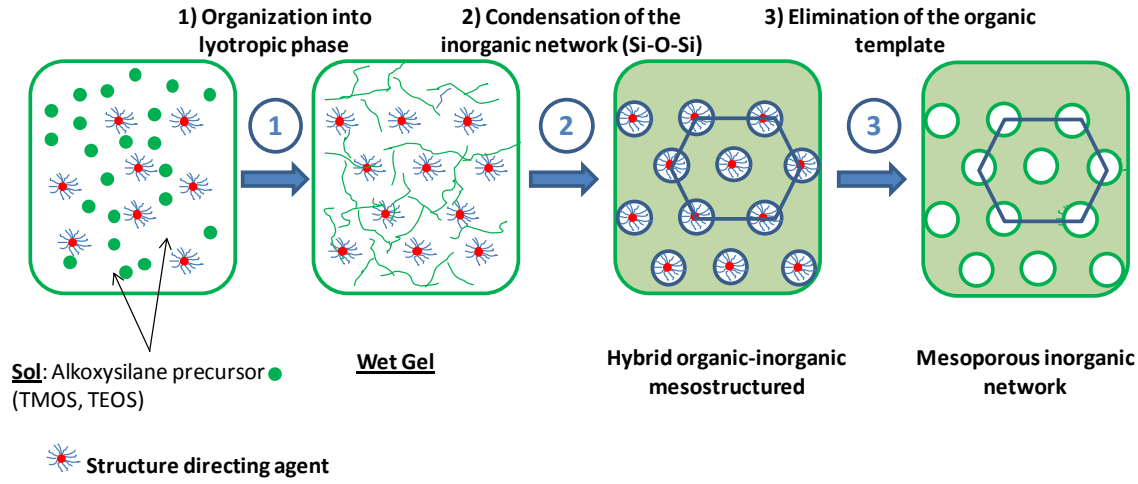

Figure IV.6: Simplified representation of the elaboration of mesoporous material

Of high importance in the mesophase synthesis is the nature of the surfactant-matrix interaction which is governed by the reagents and the experimental conditions[39]. Different templating approaches are generally reported (Figure IV.7): S^+I^-, S^-I^+, $S^+X^-I^+$, $S^-M^+I^-$, S-I and S^0I^0, where S is the surfactant, I is the inorganic phase, X is the mediating anion and M the mediating cation. In the conditions of this work implying block copolymer and acid conditions, the assembly is supposed to be driven by a double layer hydrogen bonding $(S^0H^+)X^-I^+$ because the EO moieties of block copolymers are readily protoned in strongly acidic media[10,40].

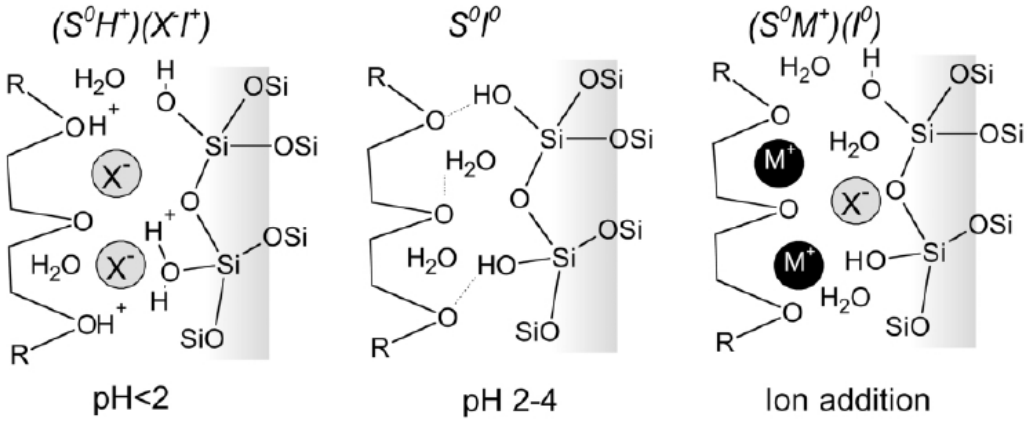

Figure IV.7: Representation of the different interactions possible existing between non ionic polymer (S) and the inorganic phase (I)[10].

All the mechanisms proposed are strongly inspired by the similarity between the lyotropic phase formed by the surfactant in water and the hybrid silica/surfactant mesophase. This led to the concept of Liquid Crystal Templating (LCT). Among the different pathways, two are particularly relevant and deserve to be mentioned. In the first one, the inorganic polymerization

occurs at accessible interfaces built by preorganized supramolecular templates. Herein, it is suggested that the lyotropic phase are completely formed and the inorganic network condenses around the stabilized liquid-crystal phase. This pathway can be active when high surfactant concentration (> 30 wt % in water) is employed or when robust mesophase are formed with special block copolymer[41,42]. Under these conditions, the surfactant arrays are relatively insensitive to the addition of inorganic precursor and appear to act as a cast or mold in which the precursors polymerize[41]. However this mechanism was judged too simple and restrictive and another complementary mechanism has been proposed. In this latter, the interactions of silicate species with the surfactant mediates the ordering. In this case, spherical then cylindrical micelles can be initially present but the final hexagonal structure arises from interactions between the silica precursor and the micellar phase. This implies that silica and surfactant cooperatively organize into an inorganic-organic liquid crystalline phase during the course of the reaction. This mechanism is generally called "Cooperative Self-Assembly" (CSA)[7]. Comparison between Liquid Crystal Template and Cooperative Self Assembly pathways is represented in Figure IV.8.

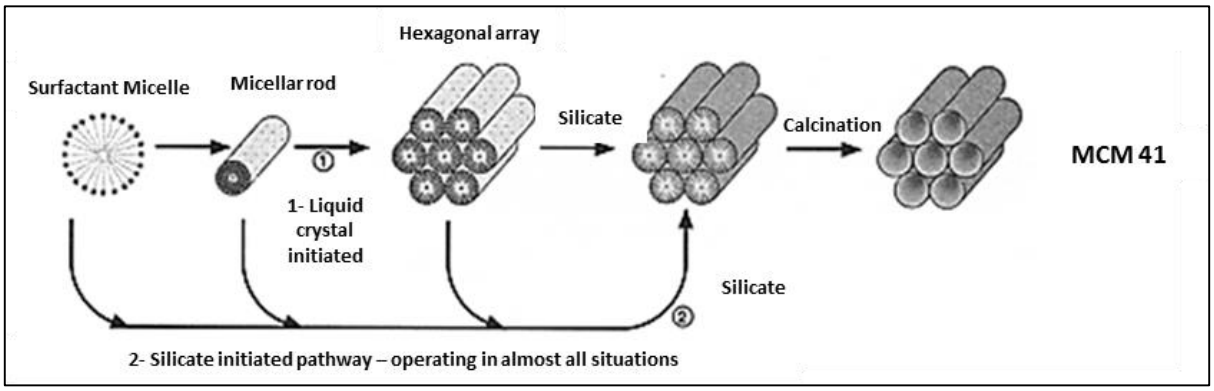

Figure IV.8: Schematic representation of the LCT (pathway 1) and CSA (pathway 2) mechanism[25]

II. SYNTHESIS OF MESOPOROUS SILICA THIN FILMS

The research on surfactant-templated silica materials has been largely focused on powdered materials using a hydrothermal route for use in catalysis notably[16]. Since 1996, alternative pathways have been designed to synthesize mesoporous materials shaped as thin films with a view to further widen their application spectrum[5,6]. The point of view of Jeffrey Brinker (Sandia National Laboratories) on this recent evolution is particularly evocative[43] "*When I first became aware of the Mobil work on mesoporous silica, I thought it would be an important thing to make these materials as films, because after calcination to remove the surfactant, they would be useful as membranes, sensors, and low dielectric constant insulators*". In this chapter, the preparation of

mesoporous silica thin films will be described. We will review the main preparation methods in particular the evaporation-induced self-assembly (EISA) method and the main applications domains.

II.1. A FOCUS ON EISA

First reported by the groups of Ozin[31,44] and Brinker[45], the solvent EISA process is the preferential method for the preparation of mesostructured thin films. By its versatility, the EISA process has rapidly gained in popularity and earned recognition as the reference methodology of preparing mesostructured films. This process has the advantage of allowing a fast mesophase formation. In addition, surface area, pore dimension and shape can be tailored through the adjustment of numerous chemical and processing parameters such as initial sol composition, pH, aging time, RH, evaporation rate, deposition technique, etc. In this method, film mesostructuration is governed by a delicate balance between kinetics and thermodynamic parameters.

Practically in EISA, a homogeneous solution (*i*) of a soluble silica precursor and surfactant prepared in a diluted mixed alcohol/water/catalyst solvent system undergoes preferential evaporation of alcohol during film deposition (*ii*), thus concentrating the depositing film. The progressively increasing surfactant concentration drives the organization of the surfactant into lyotropic liquid crystalline mesophases. The inorganic network is finally stabilized by post-treatments (*iii*), in particular thermally induced condensation reactions and template elimination to yield porosity. Figure IV.9 summarizes the whole concept of the EISA process.

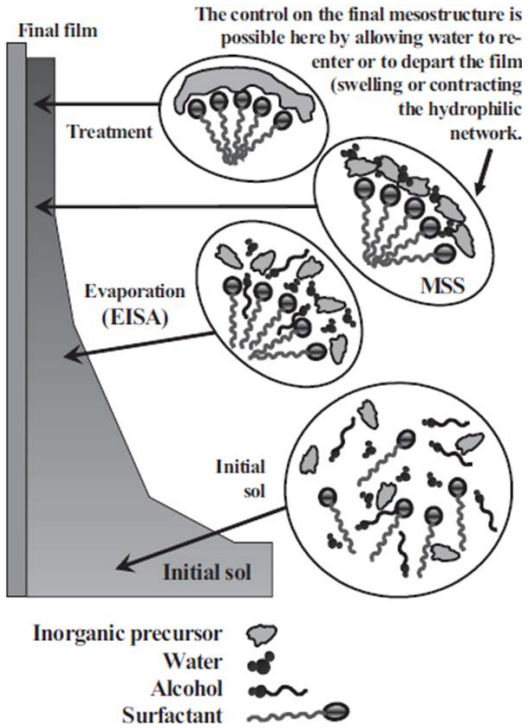

Figure IV.9: Schematic representation of the different step of the EISA process[46]

In this section, the three key consecutive steps of the EISA –sol preparation, film deposition and film post-treatment are reviewed thoroughly.

II.1.1. Initial sol preparation

In a first step, the surfactant is added in solution to a prehydrolyzed low-polymerized inorganic precursor (silica source) in presence of water and a large excess of a volatile solvent usually ethanol (Figure IV.10). In general the template volume ratio is taken between 20 to 80% in volume compared to the inorganic precursor. The initial surfactant concentration C_0 in solution is far below the CMC and the presence of a good solvent (ethanol) hinders any self-aggregation ability. For this, ethanol is suitable to provide a good miscibility with the inorganic precursor, an excellent wetability with the substrate and volatility. The suppression of inorganic condensation is also essential before the film deposition. The pH of the initial sol needs to be adjusted in order to favor fast hydrolysis of the inorganic precursor and slow condensation. For silica films, it is achieved by preparing the initial sol under highly acidic conditions at a pH < 3 below the isoelectric point of colloidal silica so as to favor fast hydrolysis and low condensation. HCl is well suited because its volatility ensures its departure from the film during casting, after having fulfilled its catalytic role in the solution. Aging time for the sol requires to be controlled as it will influence the condensation degree of the inorganic oligomers and thus the film

mesostructuration. Finally the ratio between surfactant and the inorganic precursor has to be carefully selected in agreement with the phase diagram of the surfactant in water.

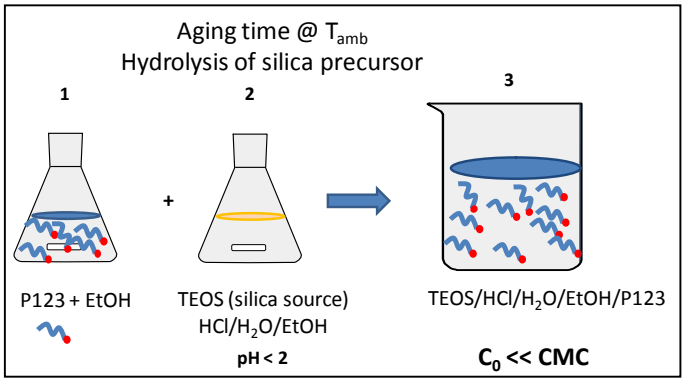

Figure IV.10: Typical preparation of the initial sol in the EISA process

II.1.2. Film deposition

In a second step, the latter isotropic solution is cast by spin or dip coating resulting in the evaporation of the volatile components and the increase of the surfactant concentration above the CMC. This step causes two major events forming the cornerstones of the EISA approach: the formation of self-assembled surfactant mesophases and the slow formation of the inorganic network through condensation reactions (Figure IV.11). Deposited films are generally optically transparent and completely featureless on the micrometer-length scale. Two important parameters have to be checked during the film deposition: the RH and the evaporation rate. Control of the RH will be essential in the film mesostructuration; low humidity in the chamber (20 %) favors water to leave the film and is detrimental to film mesostructuration whereas at higher humidity well organized mesophase can be formed. As suggested by Grosso *et al.*[46] the role of RH is difficult to interpret as it can act on various phenomena: the condensation kinetics, the viscosity, the thermodynamics of self-aggregation; all these parameters affecting eventually the mesostructuration. As shown in Figure IV.9, the authors introduced the concept of Modulable Steady State (MSS), as a crucial step where the inorganic network is not too highly condensed, sufficiently fluid and the film mesostructuration can be modulated through the RH.

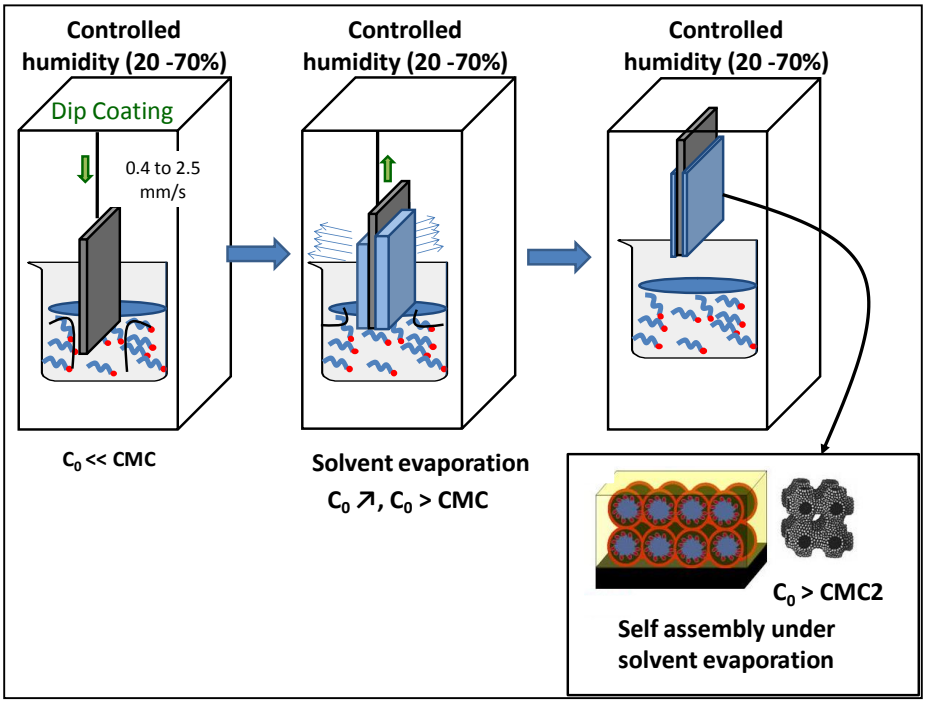

Figure IV.11: Typical film deposition in the EISA process

II.1.3. Film post-treatment

This step is essential for the stabilization and further condensation of the inorganic network as well as for the elimination of the organic template in order to liberate the porosity (Figure IV.12). It is crucial that the inorganic network is sufficiently rigid before template removal in order to prevent collapse of the mesostructure. Films with a high concentration of surfactant are more likely to collapse after elimination of the template[46]. In most cases, the elimination of the template is done by thermal decomposition. Such treatment is accompanied by a unidimensional contraction of the mesodomain also called "film shrinkage"[47]. However, this technique can cause important film damage and decrease mesoporosity of the film. In the literature, it is possible to find less damaging process for the organic template elimination. Extraction through washing with acidic aqueous solutions is preferred for ionic template and soxhlet extraction with ethanol is used to remove block copolymer template[6]. Finally, chemical treatment under NH_3 atmosphere is currently used with ionic template to post-condense the inorganic network and to prevent too high contraction of the film[48].

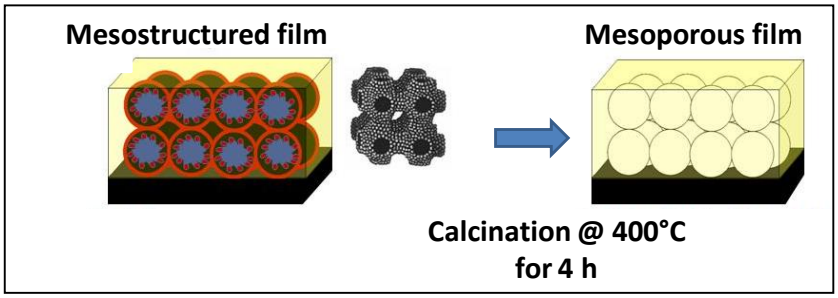

Figure IV.12: Post treatment of the mesostructured film prepared by an EISA process

II.2. ALTERNATIVE METHODS

II.2.1. Chemical solution deposition technique (CSD)

In the first alternatives methods proposed, the principle is based on EISA process and the only major difference comes from the chemical solution deposition technique. Initially, the EISA used dip-coating[49] in which the substrate is progressively withdrawed from the solution at a constant rate. Variant methods are employed:

- Spray-coating: Solution is pulverized onto the surface of the substrate by an aerosol generator or an atomizer[50].
- Spin coating: A droplet of solution is deposited at the center of the substrate and spread by centrifugation[51].
- Meniscus coating: A meniscus of solutions containing silicate, surfactant, alcohol, and water is formed. Then the solution from the bulk droplet spreads to the drying region, enriching the surfactant/silica concentration at the edge of the meniscus by the convective flux of solvent[52].

II.2.2. Vapor phase synthesis

Most of the works concerning vapor phase synthesis was proposed by the Japanese group of Nishiyama *et al.* (Osaka University)[53-56]. The approach consists in the preparation of a layer of pure surfactant placed in a saturated vapor phase of inorganic precursor in presence of a catalyst. The volatile inorganic precursor is adsorbed on the template and undergoes hydrolysis and condensation reactions inducing rearrangement or locking of the mesostructure. Vapor of TEOS was infiltrated into a surfactant film consisting of pluronic triblock copolymer. Nanophase transition from a lamellar structure to a two-dimensional cage structure of a silica–surfactant nanocomposite was found under vapor infiltration. The rearrangement into the cage structure implies high mobility of the silica–surfactant composites in solid phase[55]. The nanophase

transition under vapor infiltration contains two competitive processes: the penetration of silica precursor vapor into the film and the reaction of the silanol group[54].

Very recently in 2013, another Japanese group, Yamauchi *et al.* (Waseda University) proposed a chemical vapor approach to prepare direct replication of mesoporous silica films from block copolymer films[57]. They work with TEOS vapor and HCl/THF as acid catalysts and they used triblock copolymer with 50% hydrophilic sulfonic groups as surfactant. In opposition to previous works, the resulting mesostructure is truly a cast of the original mesostructure of the used polymer.

In addition to a simpler process, the vapor infiltration method presents various advantages within the conventional sol–gel techniques. The films prepared from vapor phase show superior characteristics, such as high structural stability up to 900 °C and high resistance to water adsorption. The densified silica wall hardly contracts under a calcination process[53]. This method is attractive for mass production of a variety of organic–inorganic composite materials and inorganic porous films. In addition, after a second vapor treatment with TMES, they were able to prepare mesoporous silica films with reduced dielectric constant ($k \approx 1.5–1.7$)[56].

II.2.3. Growth at interface

Another alternative method involves the growth of a film at air-water or oil-water interface. The various reactive (inorganic precursor + templating agent) are concentrated at interface in order to form a templated silica film[44,58,59]. A typical synthetic procedure is as follows: Films were grown on substrates in acidic solution containing TEOS, water, HCl, and hexadecyltrimethyl ammonium chloride ($C_{16}TAC$)[60]. Free-standing films were grown by the nucleation at the air-water interface at room temperature or at 80 °C under hydrothermal conditions. Despite a longer process than the classic EISA process, this method presents various advantages such as free standing and self-supporting films. In addition it also allows preparation of thicker crack-free mesoporous films[31].

II.2.4. Electrochemically assisted self-assembly (EASA)

Electro-assisted deposition is also a possible alternative and is often used for the preparation of mesoporous thin ceramic film on electrodes surfaces. This technique is principally developed by the group of Walcarius (Nancy University)[61-63]. EASA involves the application of a suitable cathodic potential to an electrode immersed in a hydrolyzed sol solution containing the surfactant, in order to generate OH^- species locally at the electrode/solution interface, thus

inducing polycondensation of the silane precursors and film deposition. Well-packed mesopore channels growing in a direction normal to the electrode were prepared by this electrochemically-driven cooperative self-assembly of surfactant micelles and silica. Such perpendicular orientation is expected to be of great interest for applications where the rate-determining step is mass transport, as for electrochemical sensing.[61,62] In a recent work of 2009, Walcarius *et al.*[63] report the preparation of vertically oriented hexagonally packed 1D mesoporous films from TEOS and CTAB precursors. Thanks to fast mass transport from the external solution through the film to the electrode surface, such film exhibits reveals sensitive responses to solution-phase redox probes. Electrochemistry is likely to induce self-assembly of surfactant-templated (organo) silica thin films on various conducting supports, homogeneously over wide areas. In addition, the EASA method allows growth of highly ordered mesoporous silica films perpendicular to the electrode surface, ensuring good accessibility. This method is compatible with electrochemically driven nanolithography for designing complex patterns of widely accessible mesostructured materials.[61]

All these alternatives techniques are schematically summarized in Figure IV.13.

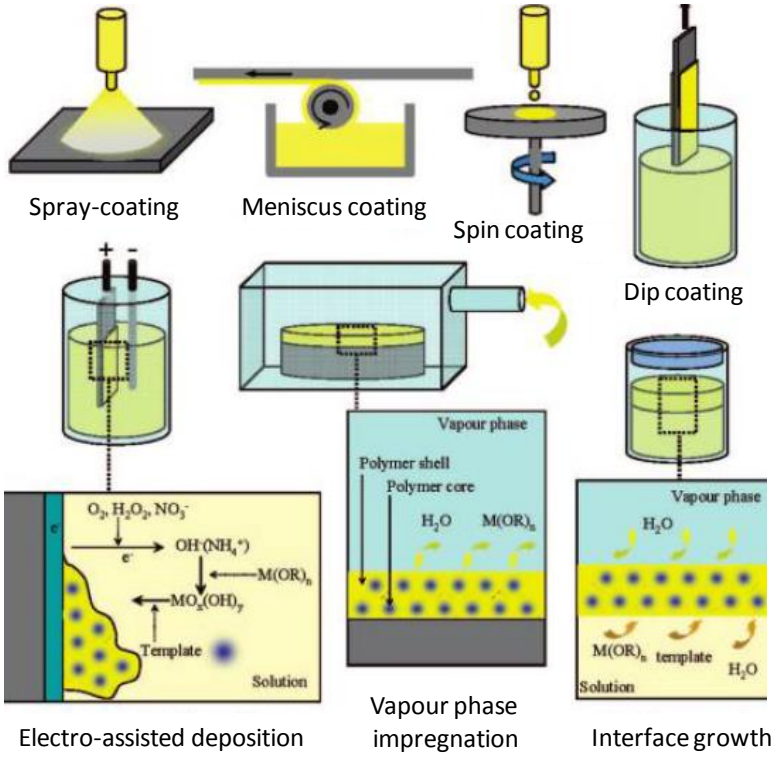

Figure IV.13: Various processing methods for the preparation of mesostructured thin films[6]

II.3. APPLICATIONS OF MESOPOROUS SILICA FILMS

The motivation for synthesis of mesoporous thin films originates from the appreciation of their technological potential as membrane, sensors, surfaces for heterogeneous catalysis, and insulating layers of low dielectric constant for microelectronics. For all the above applications, thin film morphology is recognized to be essential. In the literature, the large majority of the applications are dedicated to silica and titania films, however here we will only focus on pure or hybrid silica films. Mesoporous silica and hybrid films cover a large panel of applications and numerous reviews on the subject can be found in the literature.[5,6,64]. They highlighted that in most cases, optical, electrical and mechanical properties were strongly dependent on film thickness, porosity, pore size and pore structure. Herein, our goal is to underline some typical applications of mesoporous silica thin films: low-k dielectrics membrane, optical sensors and membrane separation.

II.3.1. Application as low-k dielectrics membranes

In the course for miniaturization, materials with very low *k*-dielectric constant (k < 2) are in increasing demand for application in integrated circuits[65,66]. One of the most promising applications of the mesoscopically-ordered silica films is their use as insulators in integrated circuit devices. Indeed due to ultralow dielectric constant, good mechanical strength and thermal stability silica films present a high potential for use as insulator in such device. In addition porosity, hydrophobicity and pore structure for such films can also be adjusted. In the literature a very large number of reviews concerning the use of mesoporous silica films for such application exist[67-71]. Different possible approaches for lowering the dielectric constant are reported: increase the porosity or increase the hydrophobicity in order to avoid interaction with highly polarizable molecule.

- Moleculary templated mesoporous silica films provide a rational and controlled porosity (45-75%), pore size (20-90 Å) and pore structure[72]. For the same mesostructure larger porosities generally give lower k values. However, a compromise must be found between porous volume, mechanical stability, hydrophobicity and dielectric constant[73].
- Increasing the surface hydrophobicity is also crucial to keep a low k value. Even after calcination, mesoporous silica films are silanol-rich. Decreasing polar hydroxyl groups is a key point in order to render the inner surface hydrophobic, hexamethyldisilazane (HMDS) or trimethylchlorosilane (TMCS) vapor treatments are very often performed[68]. To keep *k* low, it is essential to have low water absorption; Silica films are very sensitive

to humidity due to the strong trends of moisture absorption. In order to have a real reduction of water uptake during pronounced exposure to humidity, mix inorganic/organic walls and surface modification have also been performed to prepare very hydrophobic material with low *k*[72,74]. Figure IV.14 shows the process for preparation of such dielectric material and highlight the different film properties required.

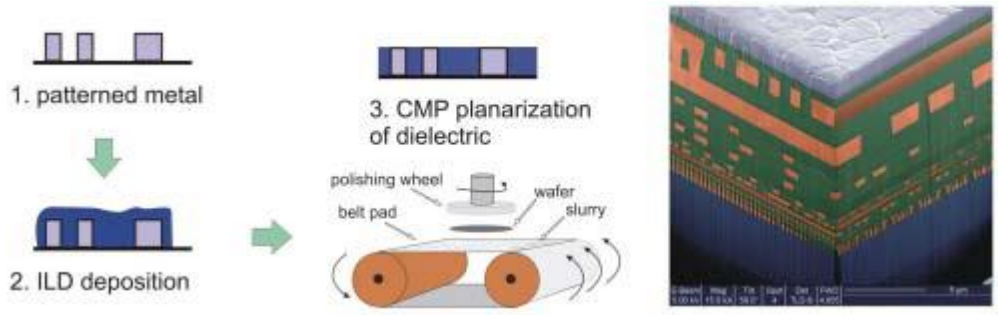

Table 1 Important properties for materials in low-*k* applications

Structural	Electrical	Mechanical	Chemical
Small, closed pores Thickness uniformity No channel continuity	Low *k* Low leakage current Low charge trapping Low dielectric loss High breakdown resistance	High Young's modulus High hardness Low residual stress High thickness threshold High adhesional strength	Low moisture absorption No metal corrosion No fluorine/chlorine loss Etch selectivity Good chemical/thermal stability

Figure IV.14: Process for the preparation of interlayer dielectric material and recap of the most important properties required for such material[66]

II.3.2. Application as sensors

Due to their large open porosity and high surface area allowing a good analyte diffusion and probe accessibility, mesoporous films are also interesting and adapted for application as sensors. Furthermore, mesoporous films are able to resist to huge capillary stresses and the sensing probe can be directly anchored to or within the framework avoiding leaching of the functionality. Different types of sensors: optical, electrochemical[62,75] and quartz crystal microbalance-based (QCM) sensors are reported in the literature depending on their detection mode. Here, we choose to present only example of optical sensor.

Optical sensors are frequently used for the detection of pH change[76], metallic cation pollutant (uranyl) or gas detection (oxygen, vapor of TNT or methanol…)[77]. For pH sensor, pH sensitive dyes (fluorescein dyes) are covalently linked with the mesoporous silica films in the framework or into the pore. The emission of the dye is recorded, when pH increases an increase of the

integrated emission is also obtained. This type of sensor is particularly efficient and present a fast response time due to high porosity and open pore.

II.3.3. Applications as permselective membranes

Finally, mesoporous silica films also present interesting properties as semi-permeable barriers (membranes) in order to prevent two phases from getting into contact. They must be permselective to allow only some components of one phase to diffuse into the other. In order to ensure good transport properties, pores microstructure, definition and size as well as their connectivity will be very important. An essential prerequisite is to prepare thin layer showing proper phase separation without decreasing the diffusion flow. For easy handling, separation layers are always deposited onto several macro- to meso-porous layers[5]. In this area of application, we will only present application for ultrafiltration of polymer solution.

Most works concerning preparation of mesoporous silica membranes for application in ultrafiltration have been proposed by Boissiere *et al.*[78-81] Highly ordered silica films are not suitable for membrane preparation due to parallel alignment of the porous network to the support. In order to overcome such problem, they propose the use of 3D wormlike mesoporous silica membrane (MSU-X) having low tortuosity. Membranes were prepared with PEO based surfactant and TEOS as silica source. They reported a two-step synthesis pathway that allowed simultaneously to control the kinetics and the final structure (pore diameter, pore size and morphology). They used a micellar templating process where in a first step, a stable sol of spherical silica-surfactant micelles (≈ 10 nm) was prepared then in a second step inorganic condensation was induced by addition of fluorine salt. This process presents various advantages such as kinetics control (the sol is stable for days and condensation can be triggered on demand by addition of catalyst), film thickness control, good reproducibility and localized condensation of silica area.

III. USE OF UV LIGHT IN MESOPOROUS FILM SYNTHESIS AND SURFACTANT SELF-ASSEMBLY

There have been very few papers addressing the use of UV irradiation in the preparation of mesostructured and mesoporous materials. In all of them, the role of UV light remains secondary in the sense that it is never involved directly in the mesostructuration or self-assembly process. We distinguish 3 major applications of UV light for preparation of mesostructured materials or copolymer self-assembly.

- Firstly, the spatial control enabled by UV irradiation was exploited to pattern mesoporous films. Obviously, specific patterning of mesoporous films produced via the EISA method is not compatible with dip-coating or spin-coating of the precursor solution onto a substrate without further processing[82].
- Second, UV light was employed as a less aggressive way to eliminate the organic template from the silica/surfactant mesostructured film. Compared to calcinations process conducted at high temperature, this photochemical method is suitable to temperature-sensitive substrates (plastic, metal) and diminishes the risk of film cracking and mesostructure damages.
- The third approach reports the use of light as a trigger of copolymer self-assembly (micellization) in solution, at low concentration. Although no application in mesoporous systems has been reported, it is worthwhile mentioning the principle of a light-induced self-assembly that forms the basis of the photochemical method devised in this manuscript.

III.1. UV PATTERNING OF MESOPOROUS SILICA FILMS

The possibility to pattern mesoporous silica films under UV exposure was first demonstrated by Brinker *et al*. in 2000[83,84]. Subsequently, they used a range of other patterning techniques: dip-pen nanolithography, ink-jet printing and selective dewetting[85] to create spatially-controlled silica mesoporous patterns. However, their first choice was clearly a simple UV patterning technique. Their procedure differs from the EISA protocol only by the addition of a photoacid generator (PAG0. To facilitate its incorporation in the initial precursor solution (TEOS/EtOH/water/ HCl/$C_{16}H_{33}(OCH_2CH_3)_{10}OH$: 1/20/3.1/0.0065/0.063 to 0.127 moles ratio), an amphiphilic PAG (diaryliodonium salt bearing a long hydrocarbon chain) was employed (0.0156 moles ratio). As expected from the EISA route, the film deposition enables the formation of poorly condensed but well-ordered hexagonal hybrid silica-surfactant mesophases. The resultant mesostructured film was then exposed to UV light through a mask. The spatially-controlled irradiation causes the local decomposition of the PAG in the exposed areas, which promotes the selective siloxane condensation resulting in patterned regions of more or less highly condensed silica. As illustrated in the different schemes of Figure IV.16, three types of patterns were generated. In scheme 1, the non-exposed areas are much less condensed and can be readily etched with an aqueous base solution to remove totally the hybrid film. The result is a hierarchically structured film in which organization resides on multiple length scales: porosity at typically 2-10 nm, film thickness (50-500 nm), and pattern size (0.5-2 μm). A second aspect of the approach revealed in Scheme 2 is the optical definition of film mesostructure. For this, the

patterned surfactant-silica hybrid film was heated to create adjoining regions of different refractive index ($\Delta n = n_{irradiated} - n_{unirradiated} > 0$). Remarkably, Δn is controlled by the UV dose which determines the siloxane condensation of the exposed parts. The ability to pattern the refractive index was exploited to create optical diffraction gratings. In a third application at higher surfactant concentration displayed in Scheme 3, it was possible to induce a mesophase transformation from hexagonal to tetragonal structure related to silica-surfactant reorganization due to an increase of siloxane condensation.

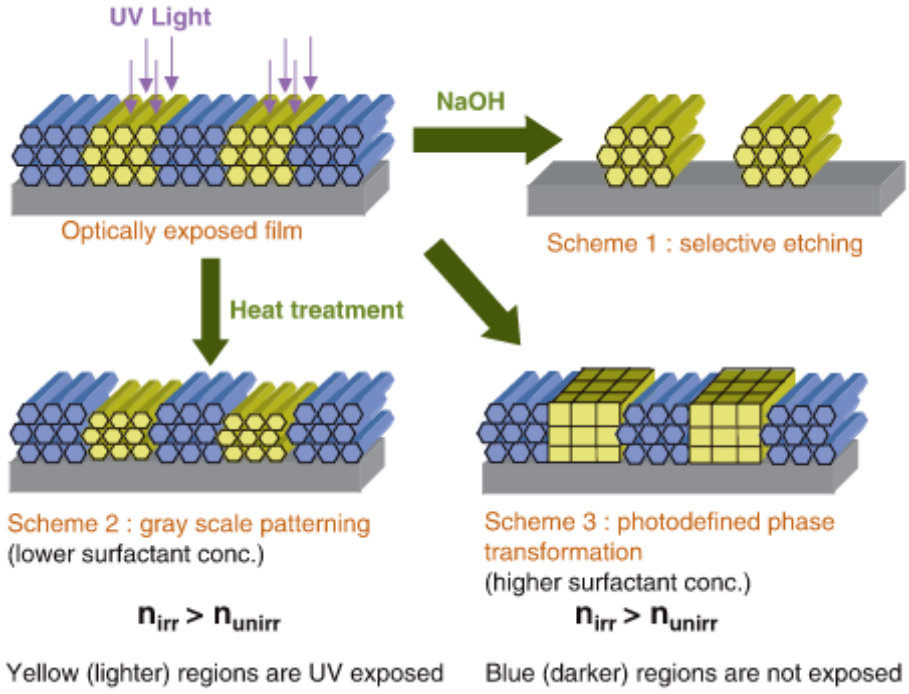

Figure IV.16: Summary of the different possible use of UV light and PAG proposed by Doshi et al.[83]

This idea of UV patterning was taken up and elaborated on some years later by Watkins *et al.* (Cornell University)[86-88]. For these authors, the main issue was the contradiction between the diffusivity of the photoacid species in a mobile poorly condensed film just after deposition and the spatial restriction imposed by the lithographic approaches for pattern generation. The mobility of the photoacids to unexposed areas to catalyze condensation was a major hurdle to increase the mesostructure definition. Hence, the authors proposed to decorrelate the mesophase formation from the inorganic precursor condensation and reported an alternative method to the EISA. For this, the surfactant template is first prepared from bulk amphiphilic block copolymer. Then TEOS is infused into this template using supercritical CO_2 as delivery medium without disturbing the mesophase order. In a first study[86], they developed this method with block copolymer including a PAG to fabricate directly patterned mesoporous silicate films.

Before performing domain selective precursor condensation, the templates were exposed to UV radiation through a photomask that has device scale features. Photolithographic exposure triggers generation of acid in the illuminated regions, which in turn leads to formation of a patterned silicate network upon infusion of Si alkoxides. Because the acid generated in UV-exposed field segregate further into hydrophilic domains of the block copolymer, precursor condensation is controlled at the device level via the mask and domain level by the block copolymer morphology. Removal of the template by calcination (400 °C) yields a patterned mesoporous silica film directly. Figure IV.17 shows a process schematic and the results for patterning of Pluronic F108 ($(PEO)_{135}(PPO)_{52}(PEO)_{135}$).

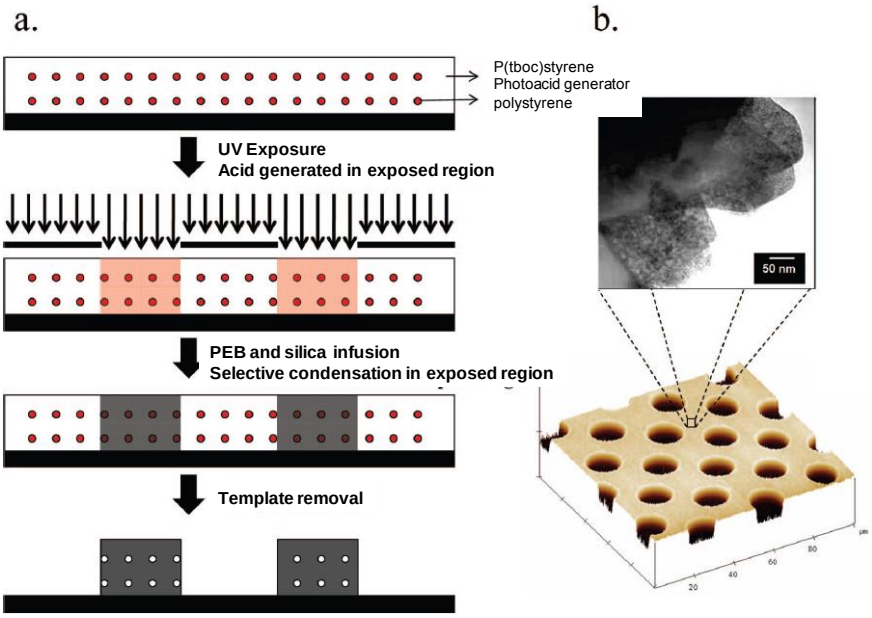

Figure IV.17: (a) Schematic of direct patterning process utilizing photolithography and supercritical CO_2 infusion process to produce patterned mesoporous silica without an etching step. (b) AFM and TEM images of patterned mesoporous silica synthesized through the direct patterning approach with a PS-b-PtbocSt block copolymer as template. The AFM image shows the device level patterning, while the TEM image shows domain level porosity arising from the block copolymer template.[86]

However, facilitated diffusion of photoacids in this latter system led to modest pattern resolution with poorly defined boundaries. To overcome this problem, they used chemically amplifiable block copolymer template such as poly(styrene-*b*-tert-butoxycarbonyyloxy styrene) (PS-*b*-PtbocSt). In addition to condensing TEOS, photoacids change the PtbocSt block in a more hydrophilic poly(4-hydroxystyrene) block. This establishes a higher polarity and T_g gap between the exposed and non-exposed areas, which restricts the diffusion of photogenerated acids in non-exposed areas, thereby providing sharper boundaries. Well-defined patterned domains were obtained but the mesostructured structures were not ordered due to low phase separation between the two blocks of the copolymer. More recently, they proposed in another example,

directly patterned mesoporous silicate films using positive and negative tone strategies using poly-(styrene-b-tert-butyl acrlyate) (PS-b-PtbA) templates[87]. Template exposure through the mask triggers area selective generation of acid from the PAG, which in turn both deprotects the poly(tert-butyl acrlyate) block to yield poly(acrylic acid) block and provides a catalyst for silica.

Another paper from Song *et al.*[89] in 2008 also reported the use of PAG and UV light for preparation of nanoporous material on multiple length scale. The idea relies on: i) the self assembly of amphiphilic molecules for mesopores formation, (< 10 nm) ii) the polymer-polymer phase separation for macropores formation (50 -200 nm) and iii) photopatterning to reach device level structure (1 -100 um) as represented in Figure IV.18. Such materials with different length scale of pore size present interesting sensing applications thanks to enhanced surface area, improved transport of material and improved electrochemical response. Process is quite similar as the one described by Watkins and the inorganic network formation is governed by the location and mobility of the PAG.

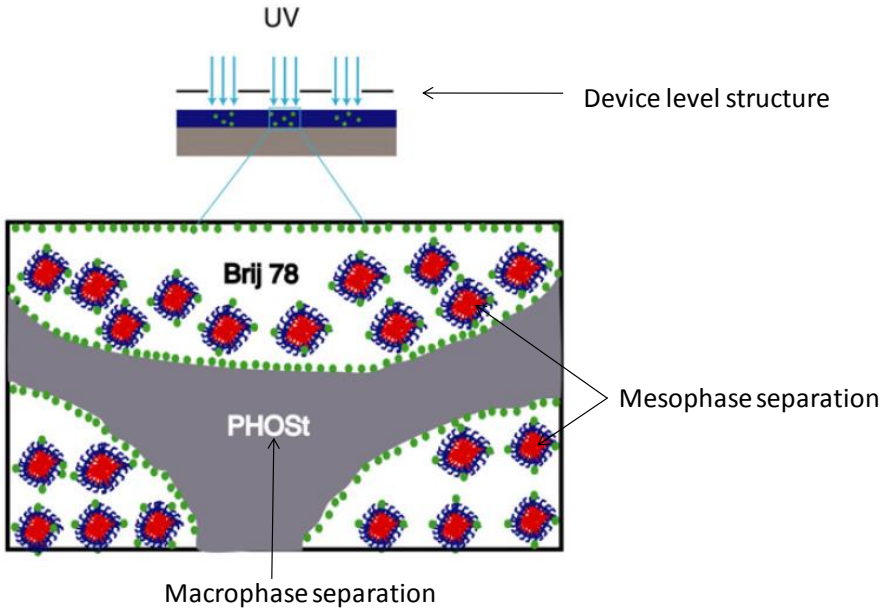

Figure IV.18: Multiple length scale formation of nanoporous silica material[89]

III.2. ORGANIC TEMPLATE REMOVAL VIA UV PHOTODEGRADATION

Another topic in which UV light and mesoporous materials clearly overlap is the elimination of the organic template. In the literature, such approach was reported independently in 2000 by two groups of researchers: Hozumi *et al.* (Nagoya University, Japan) and Parikh et *al.* (University of California, USA). Their motivation is the selective removal of the organic template while preserving not only the integrity of the silica mesostructure (size, geometry) but also that of the

substrate which can be solvent or thermally sensitive. Indeed, calcination is known to cause film distorsion or mesostructure collapse owing to the considerable amount of internal stress generated by film shrinkage during the heating at high temperature. UV ablation is anticipated to bring up substantial advantages to thermally unstable silica/surfactant mesostructured materials which tend to collapse owing to an excessive thermal instability. As a first difference, the group of Hozumi *et al*. focused on the photoablation of ionic surfactant (CTAC) versus block copolymer template (Brij, Pluronic) for the Parikh's group. The second difference resides in the type of UV irradiation device. Hozumi et al.[90,91] employed very energetic photons (deep UV) arising from a monochromatic excimer UV light (λ = 172 nm, 10 mW/cm^2) requiring a harmful and expensive vacuum chamber. By contrast, Parikh et al. implemented a more affordable low-pressure mercury lamp (LPM lamp)[92-94]. Preferred applications of the UV low pressure lamps normally include disinfection of water, air and surfaces in the food and beverage industry and in water works. Even if 85 % of the emission occurs near 254 nm, the LPM lamp has also lower levels of radiation at wavelengths about 185 nm.

Although a complete destruction of the template was reported in both cases, the mechanism is not completely elucidated. Short wavelengths (185 nm, 172 nm) can facilitate the dissociation of oxygen from the ambient atmosphere to produce *in situ* ozone and atomic oxygen. For the longer wavelengths of the LPM lamp (254 nm emission line), a direct cleavage of C-C and C-H bonds can occur to destroy the surfactant molecules into ions, free radicals and excited polymer fragments. Finally, the activated organic species can be further decomposed via a complex set of oxidation processes involving oxygen and ozone to form simpler volatile products such CO_2, H_2O and N_2 escaping from the film sample. According to Hozumi, the elimination rate of the organic species is dependent on O_2 concentration and may vary with the pressure of the chamber[91]. The same authors found that photocalcination causes much less damage in the film distortion and stress as well as the conservation of most silanol moieties. This later point is very interesting for pores modification as silanol moieties can act as anchoring point for silane coupling reagents. Parikh et al. used FTIR spectroscopy to assess the progressive elimination of the copolymer surfactant (Figure IV.19A). They showed an efficient and complete removal of the template (60 – 120 min) and concomitantly a densification of the silica skeleton[94]. Finally, both groups employed the selective UV removal of surfactant to form micropatterned silica films with alternating mesostructured and mesoporous regions. A spatial control of patterning was reported by Hozumi[95,96]. Similarly, Parikh *et al.* were also able to prepare patterned mesoporous region by use of a mask and exposure to UV[97].

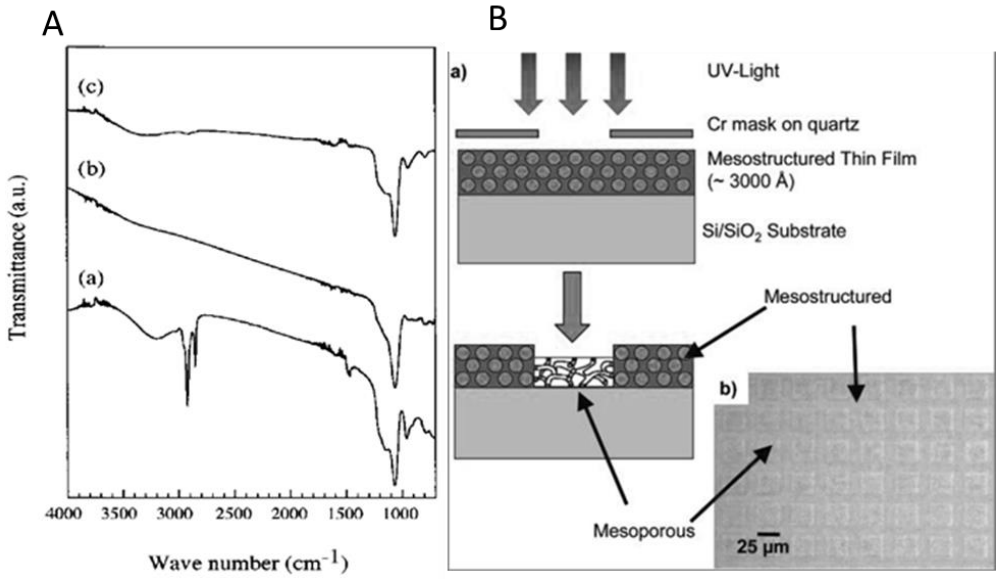

Figure IV.19: A) IR spectra of mesoporous silica films (a) as synthesized, (b) thermocalcined at 573K for 1h and (c) photocalcined for 3h[90] B) Preparation for patterned mesostructured/mesoporous silica thin films[97]

III.3. UV INDUCED MICELLIZATION

Recently, UV light has been demonstrated to foster micellization of light-responsive block copolymer in organic solution[22]. The first studies of Yoshida *et al.* in 2007 investigated photo-induced micellization through photodecomposition of a hydrophobic PBSt blocks into an insoluble hydrophilic poly(vinyl phenol) blocks using PAG[98]. This concept of light-induced copolymer self-assembly may appear out of the scope, but the reader will see how it can be reconciled with the mechanism of copolymer self-aggregation under UV light. The main difference is that previous studies focused on the photoinduced modification of a specific block to change its affinity for the solvent. By contrast, our process relies on the modification of the solvation properties (the change from hydrophobic alkoxy precursor to hydrophilic silanol species) to trigger the micellization, without altering the copolymer structure. In this paragraph we will only review micellization induced through photolysis[21] but recent studies revealed also micellization induced by photoelectron transfer[89] and photoClaisen rearrangement[16].

By using dynamic light scattering (DLS), Yoshida *et al.* showed how UV light stimulus allowed to form micelle in dichloromethane starting from a soluble poly(4-tert-butoxystyrene)-*b*-polystyrene (PBSt-b-PSt) dissolved. The addition of bis(alkylphenyl)iodonium hexafluorophosphate acting as PAG to the block copolymer was necessary. Under UV irradiation with a high-pressure mercury lamp, they observed rapid micellization, as confirmed by TEM picture showing the presence of spherical particles. The micellization was attributed to the

hydrolysis of tertbutoxy moieties due to photoacidcatalysis (Figure IV.20). The^{1}H NMR spectroscopy confirmed the elimination of the tertbutoxy groups and the formation of poly(4-vinylphenol)block. Micellization was dependent on the degree of the vinylphenol moieties formation and the efficiency and concentration of PAG.

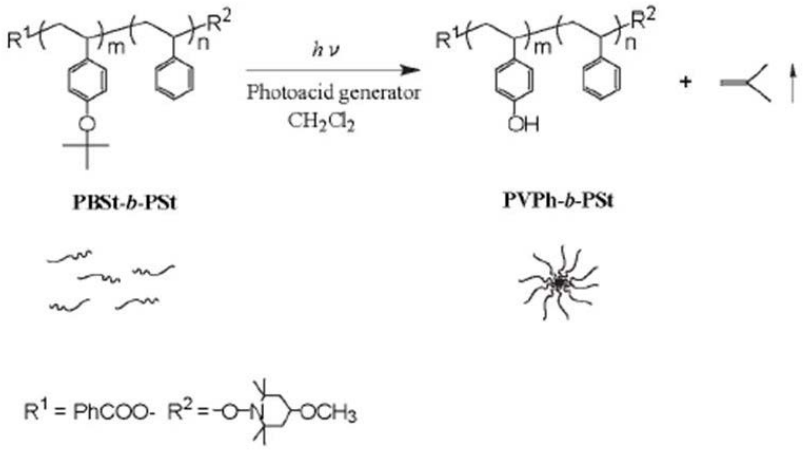

Figure IV.20: Micellization induced by photolyisis of PBSt-b-PSt[22]

Very recently, Rieger *et al.*[99] reported a photoinduced pathway to prepare hybrid organic/inorganic nanoparticles. As described by Yoshida *et al.*, their procedure used similarly the photoacid-induced micellization of a PBSt-b-PStblock copolymer. The main difference lies on the addition of siloxane crosslinker soluble (Figure IV.21) in the core of the micelle made up the poly(4-vinylphenol)block. Core crosslinking of micelle represents a straightforward approach to yield highly rigid cross-linked organic-inorganic structure. A complete encapsulation of the PAG during micelle formation was necessary to ensure well-defined nanoparticles and avoid intermicellar crosslinking reactions.

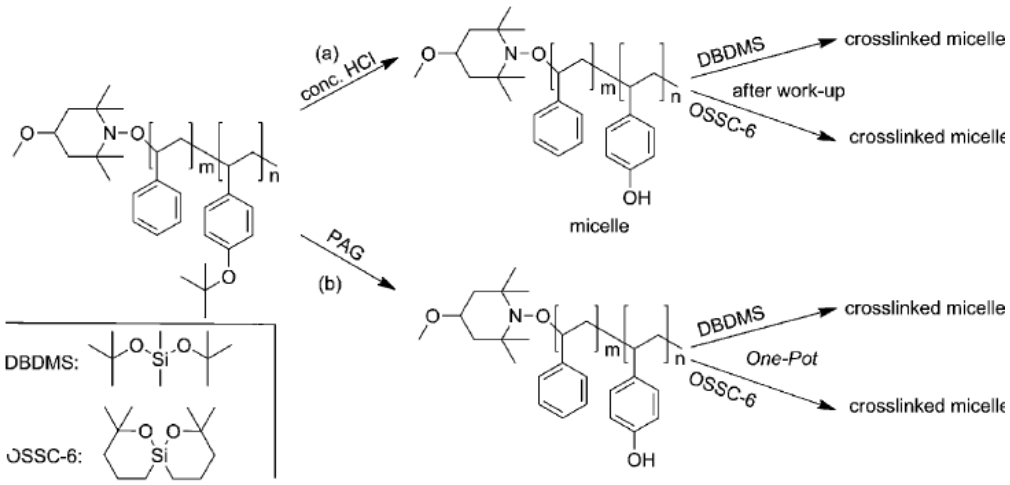

Figure IV.21: Micelle formation and sucessive alkoxysilane cross linking by (a) conventional sol-gel or (b) photoacid catalyzed pathway[99]

In 2011, Bertrand *et al.* reported the synthesis and self-assembly of a photocleavable block copolymers (poly(dimethoxynitrobenzyl acrylate)-block-polystyrene (PDMNBA-b-PS)[100]. The block copolymer is first dissolved in a good solvent. Then upon light illumination, the cleavage of the side chromophores occurred, unmasking the acrylic acid (AA) functions. As a result, the PDMNBA block is turned into a fully hydrophilic PAA block which is insoluble in the used solvent (chloroform). Self-assembly thus occurs, forming micelles made of a PAA core and a PS corona (Figure IV.22). In a second time, hydrophilic molecules are trapped into the core of the micelle. Light induced micellization is very promising for encapsulation. The successful photocleavage of these block copolymers was followed and demonstrated by UV-vis spectroscopy while the formation of micelles during the irradiation was evidenced by DLS and TEM experiments. In addition, the ability of the system to act as a trapping agent was demonstrated by the encapsulation of coumarin 343 into the micellar core produced during the irradiation of the block copolymers in solution.

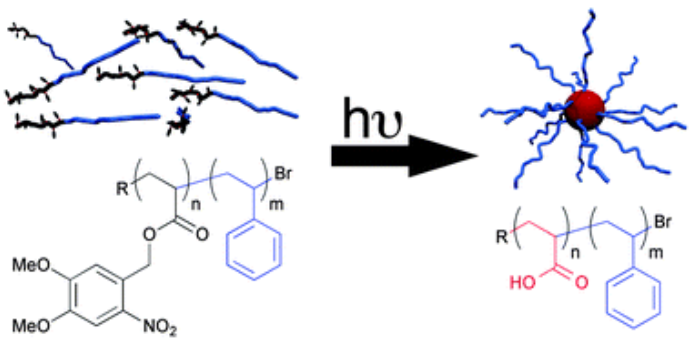

Figure IV.22: Photoinduced micellization of block copolymers bearing 4,5-dimethoxy-2-nitrobenzyl side groups[100]

In the recent review of Gohy *et al.*[101], the authors highlight the particular advantages of light for micelles formation (and disruption). "*Among the available stimuli, light has attracted much attention since it can be localized in time and space, and it can also be triggered from outside of the system. […] Moreover, a lot of parameters such as the intensity and the wavelength of light can be adjusted during the reaction time that enables good control over the reaction.* Indeed, light is efficient for various reactions such as photocleavage, photoisomerization and photocycloaddition reactions.

CONCLUSION

In this chapter, our goal was to remind the lector with some basics of mesoporous material. We first review the first step of the preparation of surfactant templated mesoporous silica with the work of Mobil Oil Company. The year 1992 was a corner in the development of such material and until today it still arouses an important interest. For the understanding of mesoporous material preparation it was necessary to remind some definition of basis notion. We first get back to the definition of a surfactant, the notion of CMC and packing parameter and we highlighted the importance of phase diagram. We also emphasized the interaction between the template and the inorganic network and the formation of surfactant/silica mesophase with the importance of sol-gel process.

Then, we have focus on preparation of mesoporous material tailored as thin films, the EISA method was describe in detail including sol preparation, deposition phase and the post treatment step. Other alternatives methods were also proposed. In order to illustrate interest for mesoporous silica films we presented some of the most well-known applications of such material.

Finally in the third and last part of this chapter, a state of the art of previous works concerning utilization of UV light for the preparation of mesoporous films or for triggering self-assembly of surfactant was realized.

In the next chapters (chapter V to VII), we focus on a new synthesis process where UV light is directly used to induce simultaneously self-assembly of surfactant and formation of the inorganic network. Chapter V is dedicated to the study of the viability of the process as well as analysis of various parameters influencing the mesostructuration. In chapter VI thanks to 2 original characterization techniques (RT-FTIR and solid state NMR), phase separation occurring in mesostructured material is highlighted. And finally, chapter VII remains on process

optimization in order to prepare mesoporous films with long range order and implementation of a 100% UV system.

CHAPTER V REFERENCES

(1) Crepaldi, E. L.; Soler-Illia, G. J. d. A. A.; Grosso, D.; Cagnol, F.; Ribot, F.; Sanchez, C. *J. Am. Chem. Soc.* **2003**, 125, 9770.
(2) Pan, J. H.; Zhao, X. S.; Lee, W. I. *Chem. Eng. J.*, In Press, Corrected Proof.
(3) Lee, U.; Hwang, Y. K.; Kwon, Y.-U. *Stud. Surf. Sci. Catal.* **2003**, 146, 77.
(4) Pan, J. H.; Zhao, X.; Lee, W. I. *Chem. Eng. J.* **2011**, 170, 363.
(5) Nicole, L.; Boissiere, C.; Grosso, D.; Quach, A.; Sanchez, C. *J. Mater. Chem.* **2005**, 15, 3598.
(6) Sanchez, C.; Boissière, C.; Grosso, D.; Laberty, C.; Nicole, L. *Chem. Mater.* **2008**, 20, 682.
(7) Xu, R.; Pang, W.; Yu, J.; Huo, Q.; Chen, J. *In Chemistry of Zeolites and Related Porous Materials: Synthesis and Structure*; John Wiley & Sons ed. **2007**, p 467.
(8) McCusker, L. B. *Rev. Mineral. Geochem.* **2005**, 57, 1.
(9) Soler-Illia, G. J. d. A. A.; Sanchez, C.; Lebeau, B.; Patarin, J. *Chem. Rev.* **2002**, 102, 4093.
(10) Soler-Illia, G. J. d. A. A.; Crepaldi, E. L.; Grosso, D.; Sanchez, C. *Curr. Opin. Colloid In.* **2003**, 8, 109.
(11) Wan, Y.; Zhao *Chem. Rev.* **2007**, 107, 2821.
(12) Wang, J.; Zhou, J.; Li, Z.; He, Y.; Lin, S.; Liu, Q.; Zhang, M.; Jiang, Z. *J. Solid State Chem.*, 183, 2511.
(13) Reddy, K. M.; Moudrakovski, I.; Sayari, A. *J. Chem. Soc,. Chem. Comm.* 1994, 1059.
(14) Corma, A. *Chem. Rev*. **1997**, 97, 2373.
(15) Galarneau, A.; Desplantier-Giscard, D.; Di Renzo, F.; Fajula, F. Catal. Today 2001, 68, 191.
(16) Taguchi, A.; Schüth, F. *Micropor. Mesopor. Mat.* **2005**, 77, 1.
(17) Liu, A.; Hidajat, K.; Kawi, S.; Zhao, D. *Chem. Commun.* **2000**, 1145.
(18) Yanagisawa, T.; Shimizu, T.; Kuroda, K.; Kato, C. *Bull. Chem. Soc. Jpn* **1990**, 63, 988.
(19) Beck, J. S.; Vartuli, J. C.; Roth, W. J.; Leonowicz, M. E.; Kresge, C. T.; Schmitt, K. D.; Chu, C. T. W.; Olson, D. H.; Sheppard, E. W. *J. Am. Chem. Soc.* **1992**, 114, 10834.
(20) Kresge, C. T.; Leonowicz, M. E.; Roth, W. J.; Vartuli, J. C.; Beck, J. S. *Nature* **1992**, 359, 710.
(21) Yoshida, E.; Kuwayama, S. *Colloid Polym. Sci.* **2008**, 286, 1621.
(22) Yoshida, E.; Kuwayama, S. *Polymers* **2010**, 2, 623.
(23) Chiola, V.; US 3556725A **1971.**
(24) Cauvel, A.; Brunel, D.; Di Renzo, F.; Garrone, E.; Fubini, B. *Langmuir* **1997**, 13, 2773.
(25) Schmidt, H. *J. Non-Cryst. Solids* **1985**, 73, 681.
(26) Kresge, C. T.; Roth, W. J. *Chem. Soc. Rev.* **2013**, 42, 3663.
(27) Lebeau, B.; Galarneau, A.; Linden, M. *Chem. Soc. Rev.* **2013**, 42, 3661.
(28) Rosen, M. J. *Surfactants and Interfacial Phenomena*; Wiley, **2004**.
(29) Wen, J.; Wilkes, G. L. *Chem. Mater.* **1996**, 8, 1667.
(30) Schmidt, H.; Jonschker, G.; Goedicke, S.; Mennig, M. J. *Sol-Gel Sci. Techn.* **2000**, 19, 39.
(31) Nace, V. *Nonionic Surfactants: Polyoxyalkylene Block Copolymers*; Marcel Dekker Incorporated, **1996**.
(32) Griffin, W. C. *J Soc Cosmetic Chemists* **1946**, 1, 311.
(33) Davies, J. In Proceedings *of the 2nd International Congress on Surface Activity*; Butterworths London: **1957**, p 426.
(34) Israelachvili, J. N.; Mitchell, D. J.; Ninham, B. W. *J. Chem. Soc., Faraday Trans.* **1976**, 72, 1525.
(35) Israelachvili, J. N. I*ntermolecular and surface forces*: revised third edition; Academic press, **2011**.
(36) Zana, R. *Dynamics of Surfactant Self-Assemblies: Micelles, Microemulsions, Vesicles and Lyotropic Phases*; Taylor & Francis, **2005**.
(37) Tanev, P. T.; Pinnavaia, T. J. *Science* **1996**, 271, 1267.
(38) Göltner, C. G.; Henke, S.; Weissenberger, M. C.; Antonietti, M. *Angew. Chem. Int. Ed.* **1998**, 37, 613.
(39) Tanev, P. T.; Pinnavaia, T. J. *Science* **1995**, 267, 865.
(40) Wan, Y.; Shi, Y.; Zhao, D. *Chem. Commun.* **2007**, 0, 897.
(41) Attard, G. S.; Glyde, J. C.; Goltner, C. G. *Nature* **1995**, 378, 366.
(42) Thomas, A.; Schlaad, H.; Smarsly, B.; Antonietti, M. *Langmuir 200*3, 19, 4455.

(43) Brinker, C. J. *MRS Bulletin* **2004**, 29, 631.
(44) Yang, H.; Kuperman, A.; Coombs, N.; Mamiche-Afara, S.; Ozin, G. A. *Nature* **1996**, 379, 703.
(45) Brinker, C. J.; Lu, Y.; Sellinger, A.; Fan, H. *Adv. Mater.* **1999**, 11, 579.
(46) Grosso, D.; Cagnol, F.; Soler-Illia, G. J. d. A. A.; Crepaldi, E. L.; Amenitsch, H.; Brunet-Bruneau, A.; Bourgeois, A.; Sanchez, C. *Adv. Funct. Mater*. **2004**, 14, 309.
(47) Grosso, D.; Balkenende, A. R.; Albouy, P. A.; Ayral, A.; Amenitsch, H.; Babonneau, F. *Chem. Mater.* **2001**, 13, 1848.
(48) Grosso, D.; Balkenende, A. R.; Albouy, P. A.; Lavergne, M.; Mazerolles, L.; Babonneau, F. *J. Mater. Chem*. **2000**, 10, 2085.
(49) Lu, Y.; Ganguli, R.; Drewien, C. A.; Anderson, M. T.; Brinker, C. J.; Gong, W.; Guo, Y.; Soyez, H.; Dunn, B.; Huang, M. H.; Zink, J. I. *Nature* **1997**, 389, 364.
(50) *Sol Gel technology for thin films, fibers, preforms, electronic and specialty shapes*; L.C. Klein ed.; Noyes Pub., **1988**.
(51) Aelion, R.; Loebel, A.; Eirich, F. *J. Am. Chem. Soc.* **1950**, 72, 5705.
(52) Yuan, Z.; Burckel, D. B.; Atanassov, P.; Fan, H. *J. Mater. Chem.* **2006**, 16, 4637.
(53) Nishiyama, N.; Tanaka, S.; Egashira, Y.; Oku, Y.; Ueyama, K. *Chem. Mater.* **2002**, 14, 4229.
(54) Nishiyama, N.; Tanaka, S.; Egashira, Y.; Oku, Y.; Ueyama, K. *Chem. Mater.* **2003**, 15, 1006.
(55) Tanaka, S.; Nishiyama, N.; Oku, Y.; Egashira, Y.; Ueyama, K. *J. Am. Chem. Soc.* **2004**, 126, 4854.
(56) Maruo, T.; Tanaka, S.; Hillhouse, H. W.; Nishiyama, N.; Egashira, Y.; Ueyama, K. *Thin Solid Films* **2008**, 516, 4771.
(57) Torad, N. L.; Suzuki, N.; Matsuura, M.; Maekawa, K.; Tanabe, H.; Wu, K. C. W.; Yamauchi, Y. *Chem. Eur. J.* **2013**
(58) Yang, H.; Coombs, N.; Sokolov, I.; Ozin, G. A. *Nature* **1996**, 381, 589.
(59) Yang, H.; Coombs, N.; Dag, O.; Sokolov, I.; Ozin, G. A. *J. Mater. Chem.* **1997**, 7, 1755.
(60) Yang, H.; Coombs, N.; A. Ozin, G. *J. Mater. Chem.* **1998**, 8, 1205.
(61) Walcarius, A.; Sibottier, E.; Etienne, M.; Ghanbaja, J. *Nat. Mater.* **2007**, 6, 602.
(62) Walcarius, A.; Kuhn, A. *TrAC Trend. Anal. Chem.* **2008**, 27, 593.
(63) Goux, A.; Etienne, M.; Aubert, E.; Lecomte, C.; Ghanbaja, J.; Walcarius, A. *Chem. Mater.* **2009**, 21, 731.
(64) Nagarajan, S.; Bosworth, J. K.; Ober, C. K.; Russell, T. P.; Watkins, J. J. *Chem. Mater.* **2007**, 20, 604.
(65) Maex, K.; Baklanov, M.; Shamiryan, D.; Brongersma, S.; Yanovitskaya, Z. *J. Applied Physics* **2003**, 93, 8793.
(66) Hatton, B. D.; Landskron, K.; Hunks, W. J.; Bennett, M. R.; Shukaris, D.; Perovic, D. D.; Ozin, G. A. *Mater. Today* **2006**, 9, 22.
(67) Bruinsma, P.; Hess, N.; Bontha, J.; Liu, J.; Baskaran, S. In *MRS Proceedings*; Cambridge Univ Press: **1996**; Vol. 443.
(68) Baskaran, S.; Liu, J.; Domansky, K.; Kohler, N.; Li, X.; Coyle, C.; Fryxell, G. E.; Thevuthasan, S.; Williford, R. E. *Adv. Mater.* **2000**, 12, 291.
(69) Wirnsberger, G.; Yang, P.; Scott, B. J.; Chmelka, B. F.; Stucky, G. D. *Spectrochim. Acta A* **2001**, 57, 2049.
(70) Fan, H.; Bentley, H. R.; Kathan, K. R.; Clem, P.; Lu, Y.; Brinker, C. J. J. *Non-Cryst. Solids* **2001**, 285, 79.
(71) Hatton, B. D.; Landskron, K.; Whitnall, W.; Perovic, D. D.; Ozin, G. A. *Adv. Funct. Mater.* **2005**, 15, 823.
(72) Yang, C. M.; Cho, A. T.; Pan, F. M.; Tsai, T. G.; Chao, K. J. *Adv. Mater.* **2001**, 13, 1099.
(73) Treichel, H.; Ruhl, G.; Ansmann, P.; Würl, R.; Müller, C.; Dietlmeier, M. *Micro. Engn*. **1998**, 40, 1.
(74) Melde, B. J.; Holland, B. T.; Blanford, C. F.; Stein, A. *Chem. Mater*. **1999**, 11, 3302.
(75) Bearzotti, A.; Bertolo, J. M.; Innocenzi, P.; Falcaro, P.; Traversa, E. *J. Eur. Ceram. Soc. **2004**, 24, 1969.*
(76) Wirnsberger, G.; Scott, B.; Stucky, G. D. *Chem. Commun.* **2001**, 119.
(77) Qi, Z.-m.; Honma, I.; Zhou, H. *Anal. Chem.* **2006**, 78, 1034.
(78) Boissière, C.; Larbot, A.; Prouzet, E. *Stud. Surf. Sci. Catal.* **2001**, 135, 179.
(79) Boissière, C.; Martines, M. A.; Kooyman, P. J.; de Kruijff, T. R.; Larbot, A.; Prouzet, E. *Chem. Mater.* **2003**, 15, 460.
(80) Boissière, C.; Martines, M. U.; Larbot, A.; Prouzet, E. *J. Membrane Sci.* **2005**, 251, 17.
(81) Prouzet, É.; Boissière, C. *C. R. Chimie* **2005**, 8, 579.
(82) Falcaro, P.; Costacurta, S.; Malfatti, L.; Takahashi, M.; Kidchob, T.; Casula, M. F.; Piccinini, M.; Marcelli, A.; Marmiroli, B.; Amenitsch, H.; Schiavuta, P.; Innocenzi, P. *Adv. Mater.* **2008**, 20, 1864.

(83) Doshi D. A.; Huesing N. K.; Lu M.; Fan H.; Lu Y.; Simmons-Potter K.; Potter B. G.; Hurd A. J.; Brinker, C. J. *Science* **2000**, 290, 107.
(84) Doshi, D.; Fan, H.; Huesing, N.; Hurd, A.; Brinker, C. J.; US20020127498, **2004**.
(85) Fan, H.; Lu, Y.; Stump, A.; Reed, S. T.; Baer, T.; Schunk, R.; Perez-Luna, V.; Lopez, G. P.; Brinker, C. J. *Nature* **2000**, 405, 56.
(86) Nagarajan, S.; Bosworth, J. K.; Ober, C. K.; Russell, T. P.; Watkins, J. J. *Chem. Mater.* **2007**, 20, 604.
(87) Nagarajan, S.; Russell, T. P.; Watkins, J. J. *Adv. Funct. Mater.* **2009**, 19, 2728.
(88) Chen, H.-T.; Crosby, T. A.; Park, M.-H.; Nagarajan, S.; Rotello, V. M.; Watkins, J. J. *J. Mater. Chem.* **200**9, 19, 70.
(89) Song, L.; Wu, Q.; Vogt, B. D. J. Colloid Interf. Sci. **2008**, 328, 374.
(90) Hozumi, A.; Yokogawa, Y.; Kameyama, T.; Hiraku, K.; Sugimura, H.; Takai, O.; Okido, M. Adv. Mater. **2000**, 12, 985.
(91) Hozumi, A.; Sugimura, H.; Hiraku, K.; Kameyama, T.; Takai, O. *Chem. Mater.* **2000**, 12, 3842.
(92) Clark, T.; Ruiz, J. D.; Fan, H.; Brinker, C. J.; Swanson, B. I.; Parikh, A. N. *Chem. Mater.* **2000**, 12, 3879.
(93) Parikh, A. N.; Navrotsky, A.; Li, Q.; Yee, C. K.; Amweg, M. L.; Corma, A. *Micropor. Mesopor. Mat.* **2004**, 76, 17.
(94) Dattelbaum, A. M.; Amweg, M. L.; Ruiz, J. D.; Ecke, L. E.; Shreve, A. P.; Parikh, A. N. *J. Phys. Chem.* B **2005**, 109, 14551.
(95) Hozumi, A.; Sugimura, H.; Hiraku, K.; Kameyama, T.; Takai, O. *Nano Letters* **2001**, 1, 395.
(96) Hozumi, A.; Kizuki, T.; Inagaki, M.; Shirahata, N. *J. Vac. Sci. Technol. A* **2006**, 24, 1494.
(97) Dattelbaum, A. M.; Amweg, M. L.; Ecke, L. E.; Yee, C. K.; Shreve, A. P.; Parikh, A. N. *Nano Letters **2003**, 3, 719.*
(98) Yoshida, E.; Kuwayama, S. *Colloid Polym. Sci.* **2007**, 285, 1287.
(99) Anger, C.; Deubel, F.; Salzinger, S.; Stohrer, J.; Halbach, T.; Jordan, R.; Veinot, J. G. C.; Rieger, B. *ACS Macro Letters* **2013**, 2, 121.
(100) Bertrand, O.; Schumers, J.-M.; Kuppan, C.; Marchand-Brynaert, J.; Fustin, C.-A.; Gohy, J.-F. *Soft Matter* **2011**, 7, 6891.
(101) Gohy, J.-F.; Zhao, Y. *Chem. Soc. Rev*. **2013**.

CHAPTER V: PREPARATION OF MESOPOROUS SILICA FILM VIA A PHOTOINDUCED SOL-GEL PROCESS

De Paz, H.; Chemtob, A.; Croutxé-Barghorn, C.; Rigolet, S.; Lebeau, B. *Micropor. Mesopor. Mat.***2012**, 151, 88.

De Paz-Simon, H.; Chemtob, A.; Crest, F.; Croutxe-Barghorn, C.; Michelin, L.; Vidal, L.; Rigolet, S.; Lebeau, B. *RSC Advances* **2012**, 2, 11944.

INTRODUCTION

Herein we report an innovative and simple approach towards mesoporous silica films based on a fast photoinduced sol-gel process employing photoacid generators and investigated thoroughly in the previous chapters. The principle relies on the photogeneration of acid species able of catalyzing hydrolysis and condensation reactions. In contrast to EISA, our procedure begins with non-hydrolyzed alkoxy silicate precursors in absence of solvent and water. The corollary is that self–assembly is now photochemically induced and thus no longer dependent on film deposition conditions, solvent evaporation and the complex chemistry associated with a silica sol.

As described in chapter IV, a photochemical approach has already been used by Brinker *et al*. to pattern mesoporous films[1] but requires the preparation of a silica sol (HCl catalysis). UV irradiation served solely after the mesostructuration to increase silica condensation and enable subsequent etching of the unexposed areas. As far as we know, there is only one other group which reported the use of a photoacid-catalyzed sol-gel process for mesoporous silica film synthesis[2,3]; Watkins *et al.* described a vapor phase process with preorganized copolymer template. Under UV irradiation through a mask, photoacids were locally generated leading to photopatterned mesoporous silica films. However in both cases, mesostructuration was not directly induced by UV irradiation.

In chapter V, we investigate in a first point the viability of a solvent and water free photochemical approach. A photoinduced sol-gel process was proposed and systematically compared with a solvent-based system including water and ethanol. According to the results obtained (and others works presented in chapter VI) we tried to give an insight into the mechanism of self-assembly triggered by UV light. Then in a second point, in an attempt to shed some light on the film formation mechanism, we have assessed the impact of different parameters. Among them, the surfactant/PDMOS (polydimethoxysiloxane) wt. ratio (x), the PAG concentration and the copolymer surfactant structure. For each parameter, different characterization techniques were used: ^{29}Si solid-state NMR, XRD, TEM and N_2 sorption. By this way, the chemical, structural and textural properties of the resultant hybrid and inorganic films have been exhaustively determined.Finally in a third point, we tried to identify why despite variation of different parameters that are supposed to enhance organization within the film, only wormlike films were prepared.

I. EXPERIMENTAL CONDITIONS

The inorganic precursor chosen was the PDMOS which was studied in detail in the first part of the manuscript. Choice of such basic inorganic precursor was evident for us as we wanted to study the feasibility of the system. In the literature, TEOS and TMOS are the most frequently used inorganic precursors for the elaboration of pure mesoporous silica films.

The template used was a triblock copolymer: Pluronic P123 (Scheme V.1). It is composed of two hydrophilic blocks of polyethylene oxide (PEO) and in the center an hydrophobic block of polypropylene oxide (PPO) of the form: $(PEO)_n(PPO)_m(PEO)_n$, with n = 19 and m = 69. Such neutral template was selected rather than ionic surfactant to ensure a good miscibility in the inorganic precursor without addition of solvent. The solubilization of various concentrations of P123 into PDMOS was realized at room temperature and homogeneous formulations were obtained. For high amount of template (x > 0.50), a slight heating (≈ 50°C) can help faster the solubilization.

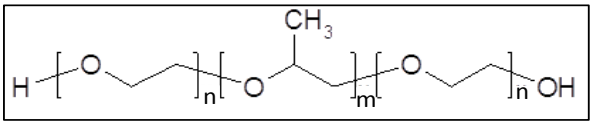

Scheme V.1: Structure of the triblock copolymer (P123) used with n = 19 and m = 69

The PAG was a diphenyliodonium hexafluorophosphate salt (Φ_2I^+ PF_6^-). It was chosen for the same reasons already explained in chapter II (i.e. good solubility in the inorganic precursor and high efficiency).

In a typical synthesis performed at room temperature, a variable amount (25 to 75 wt. %) of copolymer template (P123) was dissolved in PDMOS prior the addition of a 2% wt. of PAG (Φ_2I^+ PF_6^-). The homogeneous resultant was found to be stable in the absence of UV light. The P123/PDMOS wt. ratio is defined as x and varies between 0.25 up to 0.75.

The homogeneous solution was deposited onto a glass substrate using an automatic film applicator equipped with a wire wound bar to form a non-volatile liquid film with an initial thickness of 10 µm. The UV insulation was carried out at room temperature under a UV conveyor using a microwave powered mercury vapour lamp (H bulb, Fusion). The belt speed of the conveyor was set at 10 m/min and the lamp intensity at 100 %. In these conditions, for each pass, the UV exposure time is 0.23 sec and the emitted light dose is 1.46 J/cm^2. Samples were subjected to 10 successive passes under the conveyor to yield transparent hybrid solid films. During UV irradiation, the RH was carefully monitored to be comprised in the range 27-33 %.

The setup is represented in Scheme V.2. Dry film is then scratched in order to collect powder. Calcination was performed without preliminary hydrothermal treatment at 480 °C for 4 h in air.

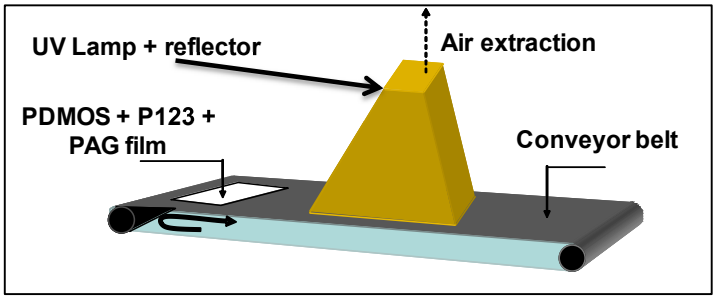

Scheme V.2: Schematic representation of the UV conveyor irradiation system used to produce mesostructured silica films.

II. TOWARD A PHOTOINDUCED PATHWAY TO MESOPOROUS SILICA FILMS

II.1. VIABILITY OF A SOLVENT AND WATER-FREE APPROACH

Our goal was to use water and solvent free conditions compatible with the photosol-gel process. In contrast, water and solvent are essential in the EISA process and their evaporation trigger the self-assembly. Here, we wanted to investigate the possibility to form mesoporous films starting from solvent and water free formulation; the typical wt. ratio used isPDMOS/PAG/P123 = 1/0.02/0.50. For comparison a solvent-based system containing water and ethanol was also studied, similar ratio as used in EISA was tested: PDMOS/PAG/P123/EtOH/H_2O = 1/0.02/0.50/2.8/0.4 (wt. ratio).

The first point concerned the sol-gel process and the crosslinking of the inorganic network despite the presence of surfactant. After ten passes under the UV conveyor, dry films were obtained for both formulations. Evidence for the efficiency of the sol-gel photopolymerization was first provided by ^{29}Si solid-state NMR (SPE-MAS sequence) of the as-synthesized x = 0.50 film with and without solvent (not represented). They exhibit three signals attributed to Q^2 ($(RO)_2Si(OSi)_2$,), Q^3 ($ROSi(OSi)_3$,) and Q^4 substructures ($Si(OSi)_4$). Well condensed structures were achieved by UV irradiation despite high content in surfactant, thus obviating the need of post-synthesis treatments to further stabilize the network. Condensation degree (CD) of film with and without solvent was respectively 80 and 81 %. Similar results were obtained, reflecting almost no effect of the solvent presence on the film final condensation.

The second point investigated concerns the mesostructuration of the film and the access to mesostructured/mesoporous films by the photosol-gel process with and without water and

solvent. Figure V.1.shows the XRD pattern and corresponding TEM images of calcined samples for films prepared at x = 0.50 P123/PDMOS ratio with and without solvent.

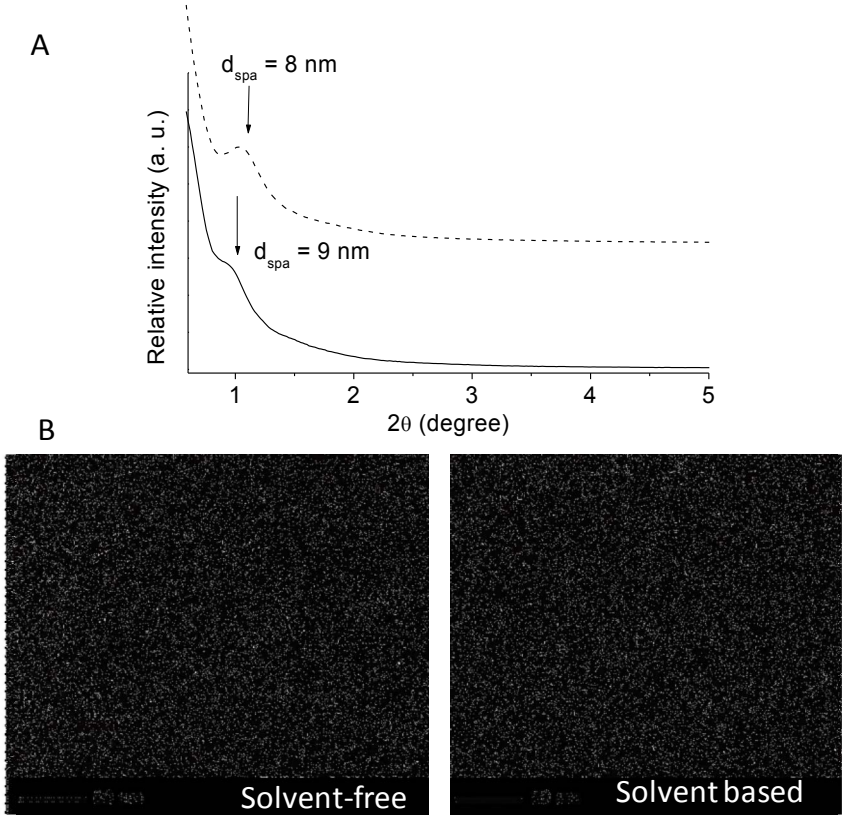

Figure V.1: (A)XRD patterns of calcined (480 °C) films with an x = 0.50P123/PDMOS ratios. (—) and (------) curves are respectively for methods with and without solvent. (B) Corresponding TEM images of films prepared with solvent free and solvent based method.

Regardless of the route, XRD patterns show a single broad diffraction peak at low 2θ angle. The absence of higher angle reflections rules out a long-range symmetry, suggesting rather a disordered mesoporous structure with a uniform repeating pore motif[4]. Such XRD patterns are consistent with the wormlike pore structure of the earlier studies on MSU-X[5,6] or HMS[7,8] powders in the mid-nineties. The structure was also confirmed by representative TEM images. As displayed in Figure V.1B, the disordered wormlike channels are devoid of any long-range symmetry, the d-spacing arising from XRD reflections are consequently related to the pore–pore distance rather than to a pore arrangement. The d-spacing value can be regarded as a measurement of the average distance between wormlike channels centers. According to XRD patterns and comparison of peaks widths and intensities, the solvent-free method seems to afford a more uniform pore repartition, indeed, more resolved and finer peak were obtained (Figure V.1A). The pore-pore distance seems to be affected by the presence of solvent. Indeed,

higher d-spacing values (9 nm) were obtained in presence of ethanol/water compared to the solvent-free route (8 nm).

Nitrogen sorption measurement was also performed in order to evaluate the specific surface (S_{BET}), the pore volume (V_p) and the pore diameter (D_p) of the mesoporous films. Isotherms and pore size distributions obtained for calcined samples prepared by the solvent based and the solvent free process are displayed in Figure V.2.

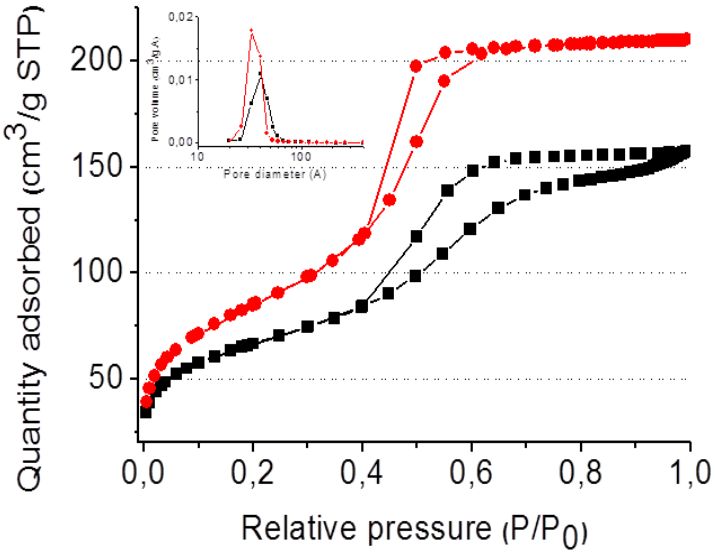

Figure V.2: Isotherms and pore size distribution obtained for the solvent-free (●) and the solvent-based (■) method.

According to IUPAC classification[9], type IV isotherms typical of mesoporous systems were obtained whatever the method implemented confirming the mesoporosity of the samples. The sharp pore size distribution highlights the uniformity of the mesopores present in the film formed. Almost similar pore diameters (4.1 nm) were obtained for solvent free and solvent based process. Nevertheless larger pore volume were obtained for the solvent free method (V_p = 0.33 cm^3/g) compared to solvent based method (V_p = 0.24 cm^3/g) leading to larger specific surface reached for the solvent free methodrespectively308 m^2/g *versus* 237 m^2/g. As larger *d* spacing value and similar pore diameter were obtained for the solvent based process by consequence larger wall thickness was also found for this pathway.

In summary, we showed that it was possible to form highly condensed wormlike mesoporous silica films via a photoinduced pathway in presence or not of water and solvent. In addition, the shift to a solvent-free method, a more "green" approach was accompanied by an increase of

$V_p$and S_{BET}.In the following paragraphs, the solvent free method was chosen as the reference process.

II.2. A FIRST INSIGHT ON SELF-ASSEMBLY MECHANISM

Based on the preliminary study and results, we tried to understand the driving force for the mesostructuration of the block copolymer in the photosol gel process. We suggest that our quite simple procedure relies on three essential components (Scheme V.3step 1):

- PDMOS a fully alkoxylated oligomeric precursor, serving both as non-volatile silica source and solvent of the template.
- Simple diphenyliodonium salt (Φ_2I^+ PF_6^-) acting as a PAG. This later is introduced in the initial formulation in its non-active form affording photolatency to the initial formulation. After UV absorption, it affords a set of homolytic and heterolytic cleavages yielding protonic Brönsted superacids of the structure H^+PF6^- able of catalysing hydrolysis and condensation reactions.
- The template, a block copolymer (P123, $(PEO)_n$-$(PPO)_m$-$(PEO)_n$) added as structure directing agent to form a homogeneous solution.

The initial formulation is homogeneous and stable in absence of light. XRD pattern of the initial formulation deposited as thin film showed no diffraction peak confirming the absence of mesophase formed before UV irradiation (Figure V.3).

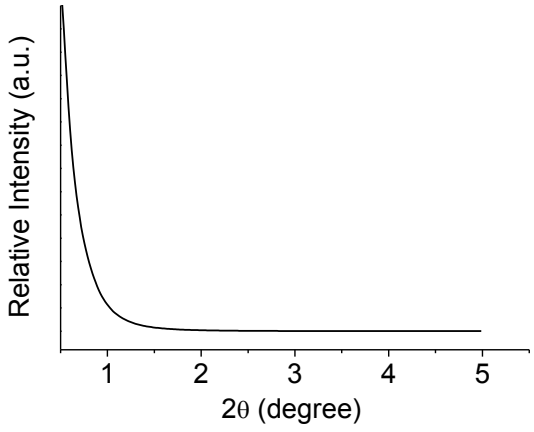

Figure V.3:XRD pattern of a P123/PDMOS x = 0.50 film before UV irradiation .Absence of diffraction peak at low 2θ angle, confirming the absence of mesostructure formed.

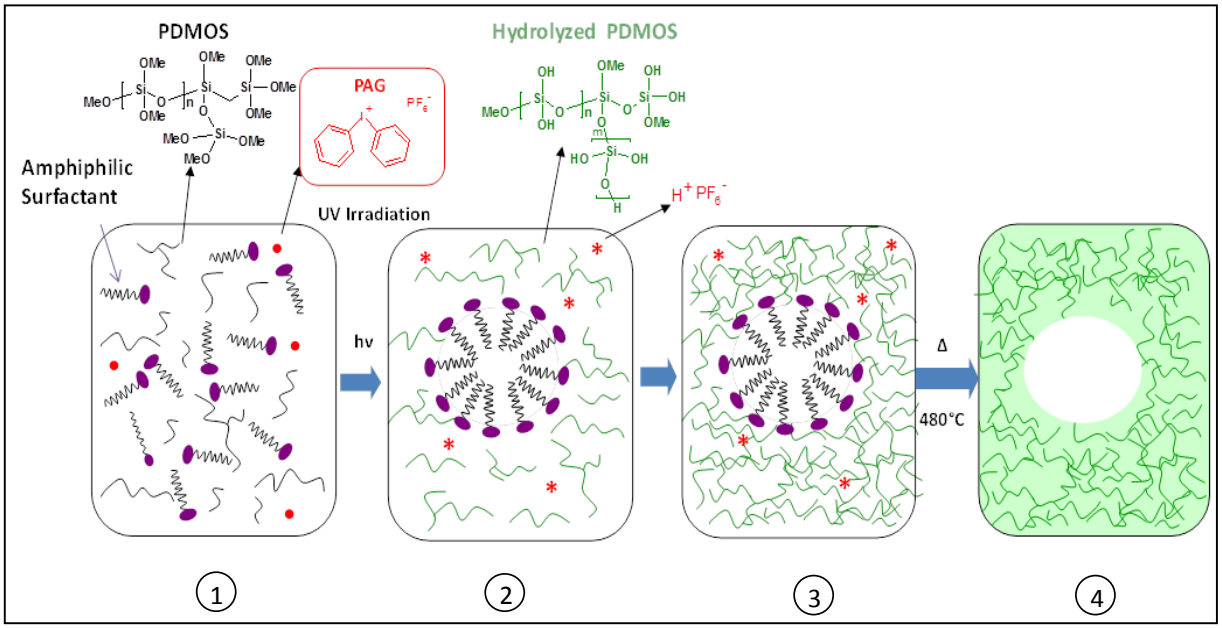

Scheme V.3: Schematic pathway for the preparation of mesoporous silica films via light induced self-assembly (LISA) process.

Under UV irradiation (Scheme V.3 step 2), the PAG photolysis involves the generation of a series of photoproducts (cations, radicals, radical cationic species) resulting from the homolytic and heterolytic Φ-I bond cleavage. The resulting cationic species interact with hydrogen donors (i. e. from precursor molecules or impurities) to create Brönsted acid of the structure $H^+PF_6^-$. These protonic superacids are thought to play a prominent role in the catalysis of the sol-gel process. Hydrolysis of PDMOS induces a polarity change in the media from a hydrophobic to a hydrophilic environment and triggers self-assembly of the copolymer where PEO blocks are in contact with silica and PPO blocks are in the core of the micelles.

The third step (Scheme V.3 step 3) implies the condensation and densification of the inorganic network around the mesophases; the system rigidifies and locks the mesostructure.

Finally the last step (Scheme V.3step 4) permits the liberation of the porosity by elimination of the template. In our case, we used calcination under air at 480°C for 4 hours. However, different techniques exist such as solvent etching or UV irradiation.

III. EFFECT OF VARIOUS PARAMETERS ON SILICA MESOSTRUCTURED FILM

The initial formulation (step 1 of the process) can be adjusted in order to prepare mesoporous silica films. In this paragraph, our goal is to understand how change of various parameters influences the mesostructuration of the film. Parameters investigated are the P123/PDMOS ratio (x), the PAG concentration and the copolymer structure. For each parameter, four

characterization techniques are used: ^{29}Si solid-state NMR in order to evidence the inorganic network condensation and to determine the condensation degree, XRD andTEM for the determination of the type of mesostructure as well as the evaluation of *d*-spacing and N_2 sorption for the valuation of specific area (S_{BET}), pore volume (Vp) and pore diameter (Dp).

III.1.P123/PDMOS RATIO

The P123/PDMOS ratio is an important factor in the initial formulation; indeed it will determine the final mesostructure of the film. It is also supposed to influence structural and textural properties of films.

Dry films and well condensed inorganic networks were obtained in all case. Increasing the P123 concentration seems to afford more condensed Si-O-Si network. Condensation degree from 76% up to 85% were obtained for ratio ranging respectively from x =0.25 up to 0.75 (Table V.1).This result was quite surprising as we expect that the presence of surfactant would have hindered the silica network condensation and thus lowered the condensation degree. This trend will be discussed in detail later in the manuscript (chapter VI).

Film's mesostructure was investigated by XRD at low 2θ angle and confirmed by TEM .Figure V.4 displays the typical diffraction patterns of the calcined samples for x = 0.25 to 0.75, together with the corresponding TEM images.

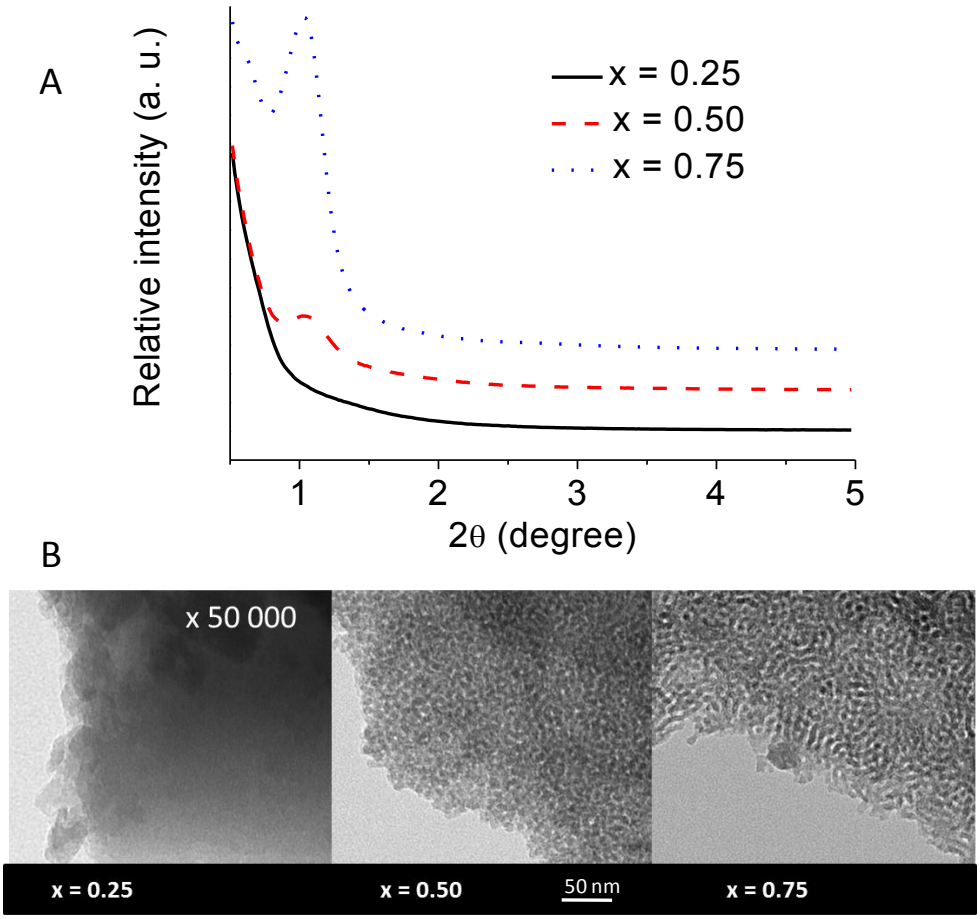

Figure V.4:(A) XRD patterns obtained for calcined samples at various P123/PDMOS wt. ratios: x = 0.25 (—), x = 0.50 (—) and x = 0.75 (—). (B)TEM images of the corresponding calcined films.

As represented in Figure V.4, the combined characterization of the samples by XRD and TEM reveal a strong dependency between the level of mesostructuration and the concentration in surfactant. At x = 0.50, the XRD pattern shows clearly a single broad diffraction peak at low 2θ angle with a *d*-spacing of 8.2 nm. As confirmed by TEM, such pattern is typical of a wormlike mesostructure devoid of long-range crystallographic order[7,10,11]. Further increase in P123 content (x = 0.75) produces a film with similar *d*-spacing but a more intense and narrow XRD peak, indicative of an increased phase segregation and degree of mesostructuration, also visible in the TEM picture. By contrast, the sample possessing lowest contents in P123 (x = 0.25) lacks of any discernible mesoscopic feature, reflecting an amorphous hybrid sample. In conclusion, we find that the copolymer concentration dramatically influences mesostructure development and a sufficient concentration in template (x ≥ 0.50) is required. Surprisingly, similar d-spacing of 8.2 nm were obtained for x =0.50 and x = 0.75 suggesting that the P123/PDMOS ratio influences the uniformity and phase segregation rather than the pore-pore distance.

Nitrogen sorption measurement was also performed, leading to a series of isotherms presented in Figure V.5, obtained at different ratios. Type I isotherms typical of microporous system have been obtained for x = 0.25 ratio whereas others samples exhibited type IV isotherms confirming the mesoporosity. Textural parameters such as the specific surface (S_{BET}), the pore volume (V_p) and the pore diameter (D_p) were extracted from these isotherms and gathered in Table V.1.

Table V.1: Physicochemical properties of mesoporous silica films prepared by sol-gel photopolymerization

x =	0.25	0.50	0.75
d-spacing (nm)	-	8.2	8.2
S_{BET}(m^2/g)		308	374
V_p (cm^3/g)	0.13	0.33	0.61
D_p (nm)	<1.7	4.2	6.5
W_{thick} (nm)	-	4.0	1.7
CD (%)	76	81	85

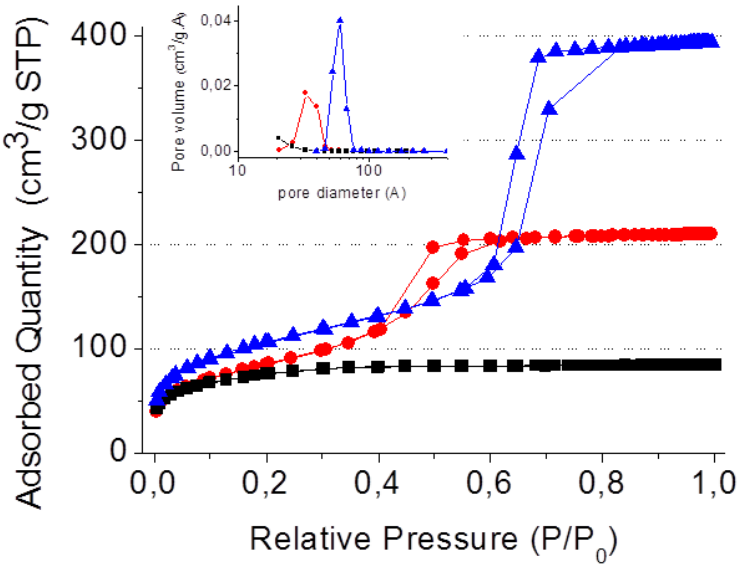

Figure V.5: Isotherms and pore size distribution obtained for the solvent-free with several P123/PDMOS wt. ratios x: (0.25,■), (0.50,●) and (0.75,▲).

An increased surfactant concentration generates a higher number of pores which are also larger in size and in volume. D_p from less than 1.7 nm up to 6.5 nm were obtain when increasing the ratio from 0.25 to 0.75. Alongside, V_p and S_{BET} increases were also noticed. According to XRD and sorption results, a higher concentration in P123 affords larger and more regular pores. However as the *d*-spacing data remains steady while pore diameter increases thinner walls are also calculated with a ratio extent. Very thin walls (1.7 nm) were even obtained with x = 0.75 leading to a specific surface area of 374 m^2/g, versus 308 m^2/g at x = 0.50.

For mesoporous silica precipitated in presence of Pluronic triblock copolymers, hydrophobic PPO chains are generally located inside pores while a majority of hydrophilic PEO chains are interpenetrated with the silica network[12]. However, the colocalization of the PEO chains with the silica phase strongly depends on their hydrophilic character, which is very sensitive to the environment. The decrease of PDMOS fraction is likely to reduce the amount of PEO chains interpenetrated in silica, thereby affording thinner wall thickness. An increased fraction of PEO chains is thus displaced into the pores causing an increase of their diameter. Such reasoning might explain why the pore-pore distance may be constant with variable pore size and wall thickness.

III.2. PAG CONCENTRATION

An increase in PAG concentration was also considered both as a means to yield further condensed mesostructures able to withstand surfactant extraction and to favor even faster sol-gel kinetics in line with process intensification and optimization. The XRD patterns at high [PAG] are depicted in Figure V.6.

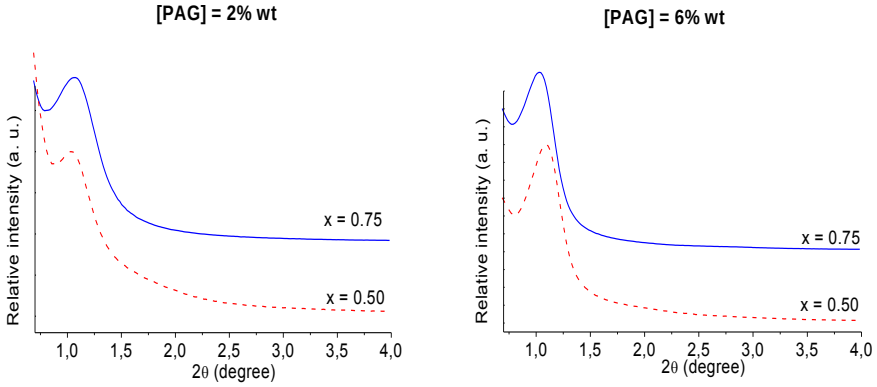

Figure V.6: XRD patterns of calcined (480 °C) films with different P123/PDMOS wt. ratios: x = 0.50 (- - -) and x = 0.75(—) and two PAG concentrations: 2 and 6 % wt.

A single and broad diffraction peak was obtain in all case corresponding to wormlike structure. Increasing the PAG concentration from 2 to 6 wt. % affordsthinner and more resolved XRD peaks in line with a better crystallinity and uniform porosity. In addition, at higher PAG concentration, lower *d*-spacing were measured suggesting more condensed inorganic network. *d*-spacing values are reported in Table V.2.

Table V.2: Physico-chemical properties of mesoporous silica film prepared by sol-gel photopolymerization at different [PAG].

x =	0.50		0.75	
[PAG] % wt.	2	6	2	6
d-spacing (nm)	8.2	8.0	8.2	7.8
S_{BET}(m^2/g)	308	380	374	620
V_p (cm^3/g)	0.33	0.43	0.61	0.93
D_p (nm)	4.2	4.5	6.5	6.0
W_{thick} (nm)	4.0	3.5	1.7	1.8
CD (%)	81	-	85	-

Nitrogen sorption measurement was also performed, leading to a series of isotherms presented in Figure V.7. Textural parameters such as the specific surface (S_{BET}), the pore volume (V_p) and the pore diameter (D_p) were extracted from these isotherms and gathered in Table V.2.

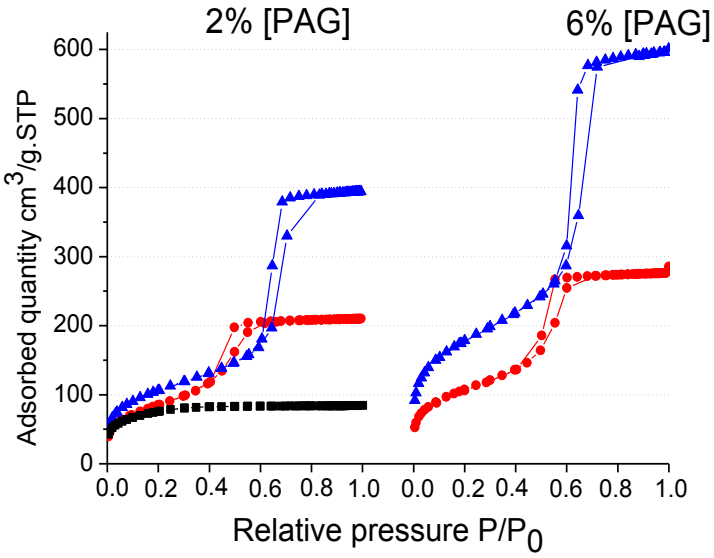

Figure V.7: Isotherms and pore size distribution obtained with several P123/PDMOS wt. ratios x: (0.25,■), (0.50,●) and (0.75,▲) and two PAG concentrations: 2 and 6 % wt.

Upon increasing PAG concentration, only low variation of pore diameter was recorded whereas an important increase of S_{BET} up to 620 m^2/g and pore volume (0.93 cm^3/g) was noticed, particularly for x = 0.75. This result suggests that the increase in PAG concentration prevented the partial structure collapse of the mesoporous framework on calcination. Hence, mesostructures with better defined pores and larger specific surface areas were achieved under these conditions.

III.3. COPOLYMER STRUCTURE

Our approach requires the solubilization of the surfactant in PDMOS. Table V.4 compares systematically the solubility of various commercially available copolymers $(PEO)_n(PPO)_m(PEO)_n$ in PDMOS and in water, differing from the degree of polymerization of their hydrophilic (*n*) and hydrophobic (*m*) blocks.

Table V.3: Solubility of various amphiphilic triblock copolymers in PDMOS and water.

Pluronic	HLB	Molecular weight	$(PEO)_n(PPO)_m(PEO)_n$	wt % PPO	Solubility/ PDMOS	Solubility/ Water
L81	2	2750	$PEO_3PPO_{39}PEO_3$	90	Yes	No
L121	2	4400	$PEO_5PPO_{70}PEO_5$	90	Yes	No
L62	4	2500	$PEO_6PPO_{30}PEO_6$	80	Yes	No
L43	6	1850	$PEO_6PPO_{21}PEO_6$	70	Yes	Yes
P103	6	4950	$PEO_{17}PPO_{60}PEO_{17}$	70	Yes	Yes
P123	6	5750	$PEO_{19}PPO_{69}PEO_{19}$	70	Yes	Yes
P84	8	4200	$PEO_{19}PPO_{43}PEO_{19}$	60	Yes	Yes
P65	10	3400	$PEO_{20}PPO_{30}PEO_{20}$	50	Yes	Yes
P85	10	4600	$PEO_{26}PPO_{40}PEO_{26}$	50	Yes	Yes
P105	10	6500	$PEO_{37}PPO_{56}PEO_{37}$	50	Yes	Yes
F127	14	12500	$PEO_{99}PPO_{65}PEO_{99}$	30	No	Yes
F108	16	14600	$PEO_{132}PPO_{50}PEO_{132}$	20	No	Yes

With low Hydrophilic-Lipophilic Balance (HLB) surfactants, PDMOS demonstrates an extended solubilisation domain[13] in comparison with water. As expected, the most hydrophobic surfactants such as L81, L121 and L62 (HLB < 6) featuring short PEO chains and scarcely used in EISA show an appreciable solubility in PDMOS. Note that these ethylene oxide derivatives do not show inverse temperature effect on solubility (which is actually the case with water), and may become soluble in PDMOS on moderate heating. However, the most hydrophilic surfactants such as F127 and F108 (HLB ≥ 14) faced solubility problems in PDMOS while their dissolution in water proved to be easy.

For the rest of the study, we selected three representative amphiphilic copolymer surfactants: L121, P123 and P105 with a HLB spanning from 2 to 10 and comprising a wt. ratio in hydrophobic PPO block of 90, 70 and 50 % respectively.

The achievement of solid films after photopolymerization appears as a first evidence for an effective condensation of silicate species. The samples showed high condensation degrees ranging from 76 % up to 88 %, without further treatment.

Figure V.8 displays the typical diffraction patterns of the calcined samples for surfactant/PDMOS wt. ratios (x) ranging from 0.25 to 0.75, together with the corresponding TEM images.

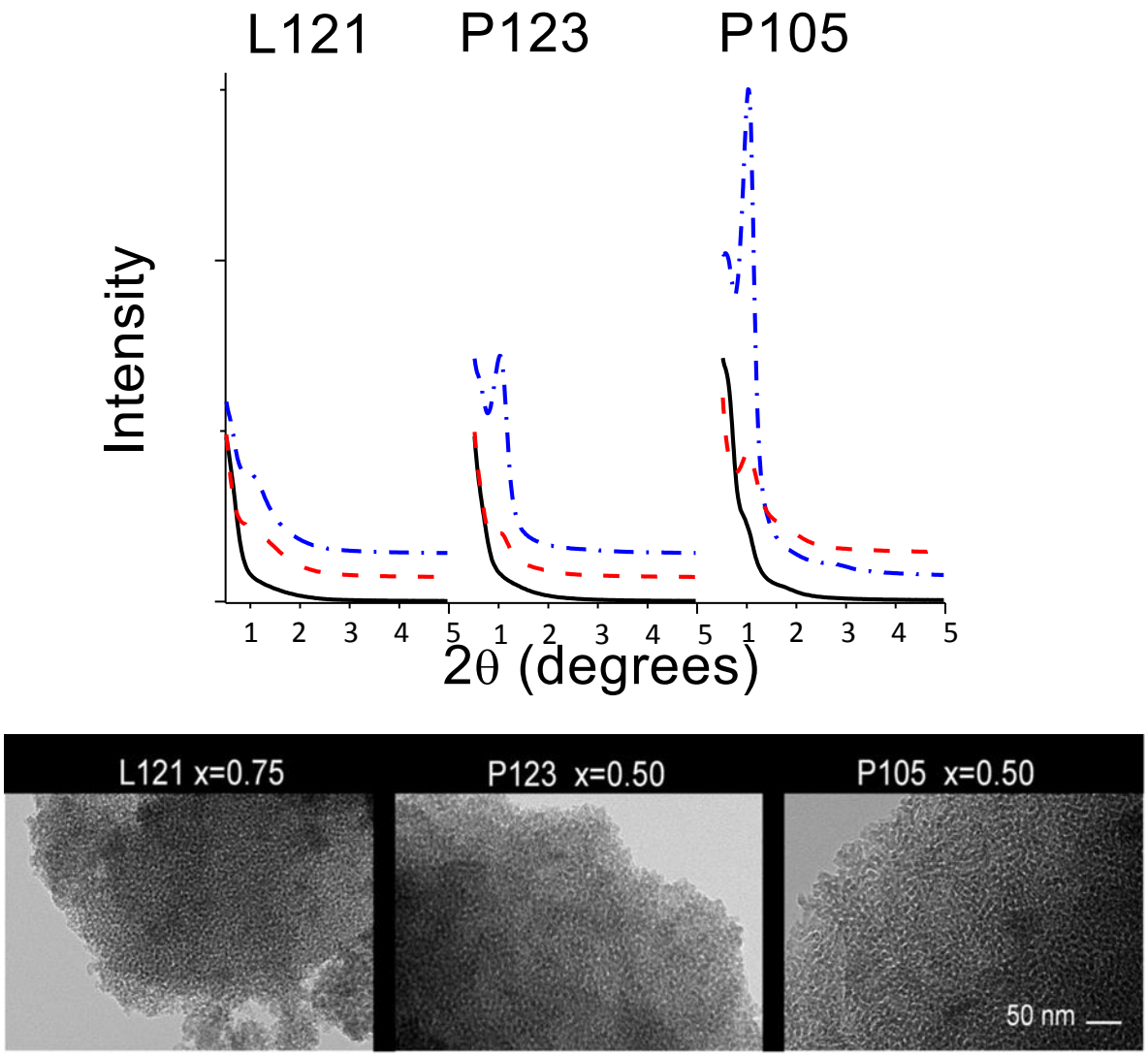

Figure V.8:(A) XRD patterns obtained for calcined samples of L121, P123 and P105 at various copolymer/PDMOS wt. ratios: (—) x = 0.25, (- - -) x = 0.50 and (-·-·-·-) x = 0.75. (B) TEM images of the as-calcined films: L121-PDMOS (x = 0.75), P123-PDMOS (x = 0.50), and P105-PDMOS (x = 0.50)

For all three systems (P123, L121 and P105), we find that the copolymer concentration dramatically influences mesostructure development. The definitive structural assignment was furnished by the TEM pictures confirming for the three selected surfactants the formation of an interconnected (bicontinuous) vermicular structure with relatively well-defined pore size but apparently devoid of long-range order. Nitrogen sorption measurements were also performed, leading to a series of isotherms shown in Figure V.9, obtained for each surfactant at different template/PDMOS ratios.

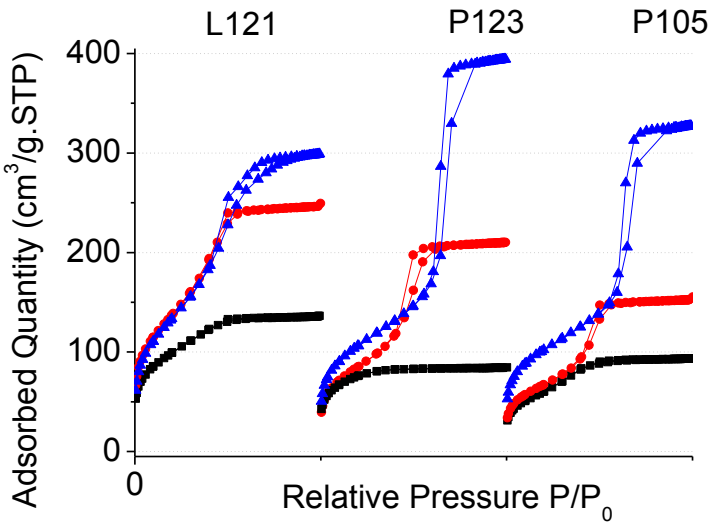

Figure V.9: N_2 adsorption/desorption isotherms of calcined films obtained with various surfactants (P123, L121, P105) at three surfactant/PDMOS wt. ratios: x = 0.25 (■), x = 0.50 (●) and x = 0.75 (▲)

Table V.4: Summary of the physico-chemical properties of mesoporous silica films prepared by sol-gel photopolymerization with different amphiphilic block copolymer templates (L121, P123 and P105).

Copolymer/PDMOS wt. ratio (x)	L121			P123			P105		
	0.25	0.50	0.75	0.25	0.50	0.75	0.25	0.50	0.75
***d*-spacing (nm)**	-	6.6	7.9	-	8.2	8.2	8.4	8.3	8.3
S_{BET}(m^2/g)	346	500	489	269	308	374	219	241	356
V_p (cm^3/g)	0.21	0.38	0.46	0.03	0.33	0.61	0.14	0.24	0.51
D_p (nm)	2.4	3.1	3.8	2.2	4.2	6.5	2.6	4.0	5.7
W_{thick} (nm)	-	3.5	4.1	-	4.0	1.7	5.8	4.3	2.6
CD (%)	-	-	88	76	81	85	-	85	-

Type I isotherms typical of microporous system have been obtained with the three surfactants for x = 0.25 ratio whereas others samples exhibited type IV isotherms confirming the mesoporosity. Textural parameters such as the specific surface (S_{BET}), the pore volume (V_p) and the pore diameter (D_p) were extracted from these isotherms and gathered in Table V.4. Whatever the surfactant, an increased surfactant concentration generates a higher number of pores which are also larger in size, resulting in thinner walls.

For non-ionic amphiphilic copolymer, pore size is not only controlled by the hydrophobic PPO block length (m) but also by its hydrophilic PEO block (n) as only a portion of the PEO chain interacts with the silica network forming the future walls[14-17]. Very short PEO block (n = 5) of L121 generates the smallest pores (≈ 2 nm) as the main contribution for the hydrophobic internal zone results only from the PPO block (m = 70) in this case. As expected, larger pores (4-6.5 nm) were obtained with P123 endowed with a comparable PPO block (m = 69) but a longer

PEO block (n = 19). Compared with P105 (n = 56, m = 37), the longer PPO block of P123 is likely to reinforce the hydrophobicity of the PEO chains even if these latter are shorter, accounting presumably for the pore diameter expansion with P123[18].

IV. WHY DISORDERED MESOSTRUCTURE?

In this paragraph, the aim is to understand why despite variation of different parameters, only disordered mesoporous silica films were obtained. Indeed, it is surprising that parameters such as the PEO/PPO block ratio and the copolymer/PDMOS ratio, which are known to be determinant in the phase behavior of poloxamer block copolymers[19], remain ineffective to generate more ordered mesophases. In the literature, Grosso *et al.*[20] proposed that wormlike structures often results from too highly condensed sols or insufficient surfactant concentration: some conditions which do not apply to the present system.

Rather, we believe that the limited water concentration in the film may be responsible for the systematic formation of disordered mesostructures. Prior to irradiation, the initial formulation does not include water or polar solvent. As previously demonstrated by Alexandridis *et al.*[21], the interfacial curvature (micellar interface) which is initially set by the macromolecular architecture can be further influenced by the ability of the copolymer blocks to swell to different extents with selective solvents. As neat "solvent", hydrolyzed silica species are probably not sufficiently selective for the PEO block to ensure the formation of ordered mesostructures. Although they presumably occupy the polar domains of the microstructure and promote a self-assembly, they do not contribute to the swelling of the PEO blocks. In this sense, the resultant $(SiO)_{4-x}Si(OH)_x$ species should behave similarly as a non-aqueous polar solvent in which amphiphilic copolymers are known to form micelles at considerably higher surfactant concentrations than those formed in water[22,23]. However, the addition of a more PEO-resembling solvent, such as water which is a key feature in the access of ordered mesostructured films via EISA[24,25] swells the PEO block and enhances the block segregation, thereby inducing the formation of structures with higher interfacial curvature[26](hexagonal, cubic). While the permeation of the atmospheric water into the sample proves to be sufficient to enable the hydrolysis, the water uptake is presumably not enough to induce the ordering of the mesophases.

The essence of this reasoning can be captured by the evolution of several textural parameters:

- the fact that the mesostructure only arises at high template concentrations (x = 0.50).

- the size of the mesopores remains low (< 6 nm) compared to other mesoporous systems based on block copolymer[27](d = 7 - 10 nm with P123), showing that a contracted final mesostructure is preferentially built up.
- the intensity of XRD peaks as a probe for order, we clearly identify that P105 having the longest PEO block improves substantially the nano-segregation without being able to induce an organization.

In addition to its thermodynamical effect, Grosso*et al.*[20] suggested an additional role for water: retained in the film, the residual water could confer to the medium fluidity essential to the transition from disordered to ordered micelles. In our water-poor system, the lack of mobility combined with a fast UV-induced gelation is obviously not favorable to the effective conduct of this transition, thus inhibiting the organization of the template in a liquid crystal phase. Consequently, the ability of the block copolymers to exhibit much richer structural polymorphism and to form a great variety of lyotropic phases would require a higher hydration of the silica phase. A high RH is known to promote a higher water concentration inside the film, while a low RH encourages water to evaporate. Further studies using a variety of experimental parameters (RH, light intensity, nature of the surfactant…) are now underway to create the conditions for progressing toward periodically ordered mesostructures.

CONCLUSION

In this chapter, we described an alternative and simple approach to mesostructured and mesoporous silica films based on a self-assembly process induced by UV light and no longer by solvent evaporation. The light controllable self-assembly relies on the *in situ* photogeneration of hydrophilic silica species by the release of photoacids, thus driving the partial solubility and self-assembly of $(PEO)_n(PPO)_m(PEO)_n$amphiphilic copolymers. This approach has significant comparative advantages pertaining to photolatency, removal of solvent and water and achievement of highly condensed mesostructures. The corollary is that self–assembly will no longer be dependent on film deposition conditions, solvent evaporation and the complex chemistry associated with a silica sol. In addition, one indirect advantage of using a non-diluted medium is the formation of micrometer thick films whereas mesoporous films of only several hundred nanometers are generally reported in the literature[28]. Additionally, photoacids are liberated *in situ* under UV giving a temporal control and stable initial formulation. Then, the catalytic efficiency of the photogenerated acids implies much faster reaction kinetics and well-condensed films with no further need for thermal or chemical post treatment[19].

CHAPTER V REFERENCES

(1) Doshi D. A.; Huesing N. K.; Lu M.; Fan H.; Lu Y.; Simmons-Potter K.; Potter B. G.; Hurd A. J.; Brinker, C. J. *Science***2000**, 290, 107.
(2) Nagarajan, S.; Bosworth, J. K.; Ober, C. K.; Russell, T. P.; Watkins, J. J. *Chem. Mater.***2007**, 20, 604.
(3) Nagarajan, S.; Russell, T. P.; Watkins, J. J. *Adv. Funct. Mater.***2009**, 19, 2728.
(4) Park, I.; Pinnavaia, T. J. *Micropor. Mesopor. Mat.***2009**, 118, 239.
(5) Kim, S.-S.; Pauly, T. R.; Pinnavaia, T. J. *Chem. Commun* .**2000**, 835.
(6) Bagshaw, S. A.; Prouzet, E.; Pinnavaia, T. J. *Science***1995**, 269, 1242.
(7) Tanev, P. T.; Pinnavaia, T. J. *Science***1995**, 267, 865.
(8) Tanev, P. T.; Pinnavaia, T. J. *Science***1996**, 271, 1267.
(9) Sing, K. S. W.; Everett, D. H.; Haul, R. A. W.; Moscou, L.; Pierotti, R. A.; Rouquérol, J.; Siemieniewska, T. *Pure Appl. Chem.* **1985**, 57, 603.
(10) Prouzet, E.; Boissiere, C. *C.R. Chim.***2005**, 8, 579.
(11) Bagshaw, A.; Prouzet, E.; Pinnavaia, T. J. *Science* **1995**, 269, 1242.
(12) Ruthstein, S.; Schmidt, J.; Kesselman, E.; Talmon, Y.; Goldfarb, D. *J. Am. Chem. Soc.***2006**, 128, 3366.
(13) Malucelli, G.; Bongiovanni, R.; Sangermano, M.; Ronchetti, S.; Priola, A. *Polymer***2007**, 48, 7000.
(14) Zhao, D.; Yang, P.; Melosh, N.; Feng, J.; Chmelka, B. F.; Stucky, G. D. *Adv. Mater.***1998**, 10, 1380.
(15) Flodström, K.; Alfredsson, V. *Micropor. Mesopor. Mat.***2003**, 59, 167.
(16) Zhao, D.; Huo, Q.; Feng, J.; Chmelka, B. F.; Stucky, G. D. *J. Am. Chem. Soc.***1998**, 120, 6024.
(17) Kipkemboi, P.; Fogden, A.; Alfredsson, V.; Flodström, K. *Langmuir***2001**, 17, 5398.
(18) Prouzet, E.; Boissiere, C. *C.R. Chim.***2005**, 8, 579.
(19) Wan, Y.; Zhao *Chem. Rev.***2007**, 107, 2821.
(20) Grosso, D.; Cagnol, F.; Soler-Illia, G. J. d. A. A.; Crepaldi, E. L.; Amenitsch, H.; Brunet-Bruneau, A.; Bourgeois, A.; Sanchez, C. *Adv. Funct. Mater.***2004**, 14, 309.
(21) Alexandridis, P.; Lindman, B. *Amphiphilic Block Copolymers: Self-Assembly and Applications*; Elsevier Science, **2000**.
(22) Penfold, J.; Staples, E.; Tucker, I.; Cummins, P. *J. Colloid Interf. Sci.***1997**, 185, 424.
(23) Ivanova, R.; Lindman, B.; Alexandridis, P. *Langmuir***2000**, 16, 3660.
(24) Soler-Illia, G. J. A. A.; Crepaldi, E. L.; Grosso, D.; Durand, D.; Sanchez, C. *Chem. Commun*. **2002**, 0, 2298.
(25) Crepaldi, E. L.; Soler-Illia, G. J. d. A. A.; Grosso, D.; Cagnol, F.; Ribot, F.; Sanchez, C. *J. Am. Chem. Soc.***2003**, 125, 9770.
(26) Svensson, B.; Olsson, U.; Alexandridis, P. *Langmuir***2000**, 16, 6839.
(27) El-Safty, S. A.; Evans, J. *J. Mater. Chem.***2002**, 12.
(28) Soler-Illia, G. J. d. A. A.; Sanchez, C.; Lebeau, B.; Patarin, J. *Chem. Rev.***2002**, *102*, 4093.

CHAPTER VI: NOVEL ANALYTIC METHODS TO STUDY KINETICS AND SELF-ASSEMBLY IN UV INDUCED MESOSTRUCTURED SILICA FILMS

De Paz-Simon, H.; Chemtob, A.; Crest, F.; Croutxe-Barghorn, C.; Michelin, L.; Vidal, L.; Rigolet, S.; Lebeau, B. *RSC Advances* **2012**, 2, 11944.

De Paz-Simon, H.; Chemtob, A.; Croutxé-Barghorn, C.; Rigolet, S.; Michelin, L.; Vidal, L.; Lebeau, B. *Langmuir* **2013**, 29, 1963.

INTRODUCTION

The present chapter highlights two powerful techniques, scarcely reported in mesoporous materials literature: RT-FTIR spectroscopy and solid-state NMR. The combination of these *in situ* and *ex situ* techniques respectively aims to provide an original picture of the self-assembly taking place during the formation of surfactant templated silica films.

RT-FTIR has been already implemented as *in situ* characterization technique in mesostructured silica films[1-5], but its potential has been limited so far by the processing conditions. In EISA approach, self-association takes place concomitantly with evaporation (≈ 1 min), which makes its investigation particularly tricky. For such evaporating systems, RT-FTIR has been mainly used to monitor silica network condensation[1-3], solvent evaporation[4] and dynamic water concentration[5] providing limited insight into surfactant micellization and ordering. In the previous chapter, we have introduced an alternative light induced self-assembly (LISA) route circumventing the addition of volatile compounds in the starting formulation. Under these new conditions, the use of RT-FTIR is both simplified and its interest greatly enhanced. Without the interference of solvent prone to saturate the IR signal, this technique provides a new perspective on the course of the sol-gel process in mesostructured films.

In a first point, RT-FTIR is conventionally used to translate the temporal change in chemical composition of PDMOS at microscopic level. Indeed, we suspect that the surfactant concentration as well as it self-organization ability are two important factors impacting the sol-gel kinetics. Then in a second time, in addition to assessing the change of composition, rapid-scan FTIR can be also sensitive to local polarity and hydration states[6], and their variations have been successfully used as indicators of self-assembly. As a result, it becomes possible to correlate compositional information (hydrolysis) with mesostructure formation. Finally in a last point, a second technique addressed in this feature is solid-state NMR spectroscopy in a view to characterize ex-situ the level of mesostructuration of the as-synthesized silica-copolymer hybrids. Several solid-state NMR experiments were already conducted previously to establish, in particular, the spatial separation of the two blocks in copolymer-silica self-assembled systems[7,8] using proton spin diffusion[9], proton relaxation and 2D ^{1}H-^{13}C HETCOR (Heteronuclear correlation) technique[10]. Here, we have focused on the acquisition and analysis of simple 1D high-resolution ^{1}H to assess the level of mesostructuration. Through its marked sensitivity to local environment, we show that these spin-1/2 nuclei can be used to probe the difference of nanophase segregation depending on the concentration in copolymer.

I. EXPERIMENTAL CONDITIONS

In a typical synthesis performed at room temperature, a variable amount of copolymer template P123, (25 to 75 wt. %), was dissolved in PDMOS prior the addition of a PAG ($\Phi_2I^+ PF_6^-$, 4 wt. %). For specific time-resolved FTIR experiments, the formulations were deposited onto a BaF_2 substrate using a bar coater to produce films of 10 µm thick. The *in situ* IR analysis was performed, simultaneously with the UV irradiation triggering the polymerization process. In this case, films were irradiated at a light intensity of 200 mW/cm^2 by the polychromatic light of a mercury-xenon lamp fitted with a 365 nm reflector and coupled with a flexible light-guide. During this series of experiments, the RH was also carefully maintained between 27 and 33 %.

For NMR study as an important amount of sample is needed, the initial formulation (alkoxide/PAG/copolymer) was deposited onto a glass substrate using an automatic film applicator equipped with a wire wound bar to form a nonvolatile liquid film with an initial thickness of 10 µm. The UV irradiation was carried out at room temperature under a UV conveyor using a microwave powered mercury vapor lamp (H bulb, Fusion). Samples were subjected to 10 successive passes under the conveyor to yield transparent hybrid solid films. During UV irradiation, the relative humidity (RH) was carefully monitored to be comprised in the range 27-33 %.

II. RT-FTIR AS A TOOL TO INVESTIGATE SOL-GEL KINETICS

II.1. EVOLUTION OF THE SPECTRA WITHIN THE IRRADIATION TIME

In situ RT-FTIR experiments were performed to shed light onto the complex and concomitant processes triggered by UV irradiation. In our RT-FTIR setup, UV irradiation controlling the sol-gel process and indirectly the mesostructuration is triggered simultaneously with the analyzing IR beam. Therefore, RT-FTIR's interest is substantially enhanced since a complete dynamic survey of the sol-gel polymerization becomes accessible. For the first time, hydrolysis as well as other processes such as silica network condensation and film water content were assessed kinetically. Figure VI.1 plots a selection of tridimensional FTIR absorption spectra acquired *in situ* during irradiation of a 50 wt % P123-PDMOS sample, with wavenumber, irradiation time and absorbance as x, y and z axis.

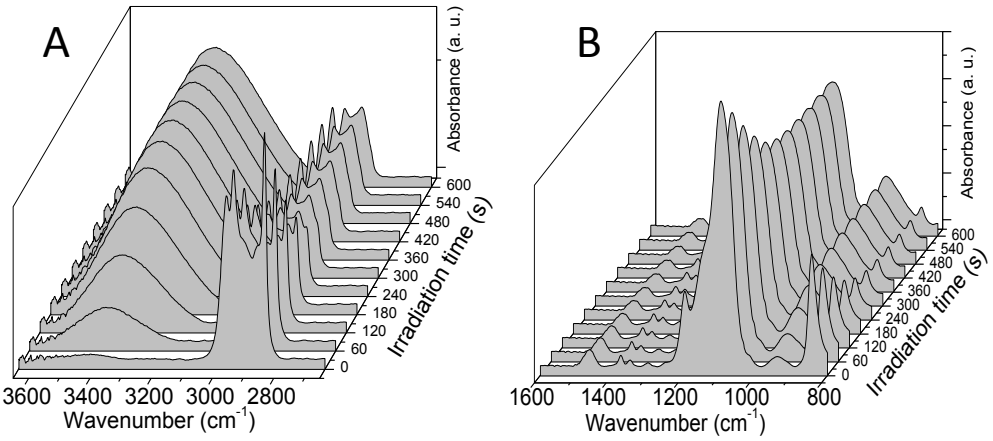

Figure VI.1: In situ time-resolved FTIR spectra on a timescale of 600 s of a PDMOS film containing 50 wt % of P123 under UV irradiation in the range of 2700-3650 cm^{-1} (A) and 800-1600 cm^{-1} (B)

Our present discussion emphasizes three distinct regions that will be commented on separately.

II.2. CH_2-CH_3 STRETCHING MODE AND OH BAND (2800 - 3400 CM^{-1})

Prior to irradiation, a broad massif of C-H stretching bands is visible in the region spanning 2800 - 3000 cm^{-1}, and containing the overlapping symmetric (ν_{sym}) and asymmetric (ν_{asym}) stretching modes of CH_2 and CH_3 groups. In contrast to methylene moieties which are only part of the copolymer, the methyl can originate both from the PPO block and from the methoxy groups of PDMOS. Of high interest is the possibility to distinguish the $\nu_{sym}(CH_3)$ and $\nu_{asym}(CH_3)$ from the template and from the silicate precursor. In methoxysilyl, the proximity of the oxygen has been shown to cause the red shift of the $\nu_{asym}(CH_3)$ (from 2970 to 2950 cm^{-1}) and the $\nu_{sym}(CH_3)$ bands (from 2900 to 2848 cm^{-1}). We note that this latter spectral feature is sufficiently resolved and separated from the other vibration modes to be taken as a marker of the methoxysilyl functions' hydrolysis. In addition this band has already been used in chapter II to follow *in situ* the hydrolysis of the PDMOS in absence of template. As expected, the UV exposure causes a progressive decrease of the methoxy stretching bands at 2848 cm^{-1} supporting our attribution and the occurrence of an effective photoacid-catalyzed hydrolysis. Concomitantly, a broad envelope centered at ~ 3400 cm^{-1} is expanding. This band is straightforwardly assigned to the OH-O bonds, reflecting the gradual conversion of the methoxy moieties into silanol groups and the possible adsorption of sol-gel by products (H_2O, methanol). After 600 s of UV irradiation, the sharp peak at 2848 cm^{-1} has completely vanished, suggesting a complete hydrolysis. Systematic integration of the $\nu_{sym}(O\text{-}CH_3)$ band gives a unique insight into the hydrolysis kinetics and the influence of the template concentration for P123 films, as displayed in Figure VI.2. We observe that the presence of surfactant affects dramatically the hydrolysis rate.

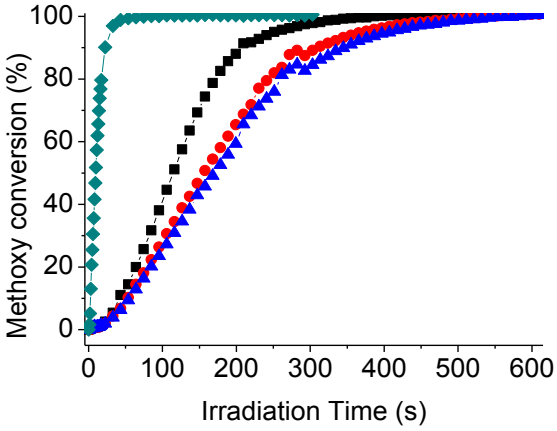

Figure VI.2: Methoxy hydrolysis degree during the sol-gel photopolymerization of films containing various ratios (x) in P123, x = 0 (♦, pure PDMOS), x = 0.25 (■), x = 0.50 (●) and x = 0.75 (▲).

The addition of 25 % in template in the formulation initially devoid of P123 implied a brutal slow-down in the hydrolysis kinetics. A straightforward explanation rests on the significant viscosity rise caused by the copolymer dissolution into PDMOS. For the P123 system, we note a 4, 9 and 16-fold increase in viscosity with x = 0.25, 0.50 and 0.75 respectively, compared with a pure alkoxide-based film (x = 0). Many experimental results[11,12] proved that a higher viscosity can affect substantially the water vapor permeation, which is the main mechanism responsible for hydrolysis.

Additionally, we observed in the precedent chapter that no mesostructuration occurs for x = 0.25 whereas mesostructured films are formed for x ≥ 0.50. The differing kinetic profiles between the amorphous sample (x = 0.25) and the two mesostructured films (x ≥ 0.50), strengthens the argument that the *in situ* self-assembly may also impact the hydrolysis progress. Both hydrolysis and surfactant self-assembly need water to be effective; therefore a competition between these two processes is likely to take place. In comparison to amorphous random system, the structuration means a swelling of the PEO block and presumably a nanosegregation of water in the vicinity of the hydrophilic blocks. This confined geometry may impose water limitation for a polar methoxysilyl functions, causing a slow-down of the hydrolysis kinetics.

II.3. Si-O-Si stretching mode (1000 – 1250 cm^{-1})

Before irradiation, this region represents the contribution of different vibration bands: the Si-O-Si stretching modes from the oligomeric precursor as well as the C-O stretching associated with the methoxysilyl functions of PDMOS and the PEO or PPO block of the template. The high overlapping of these vibrational modes coupled with the consumption of the methoxysilyl functions during the hydrolysis stage (< 300 s) makes the observation of the siloxane

condensation particularly tricky. However, after the completion of hydrolysis, a qualitative evaluation of the siloxane condensation becomes feasible (Figure VI.3). Evidence of progressive polycondensation reactions is reflected by the increase in absorbance of the envelopes of absorption bands assigned to longitudinal optical (LO) and transverse optical (TO) asymmetric stretching modes of siloxane bonds at 1163 cm^{-1} and 1078 cm^{-1} respectively.

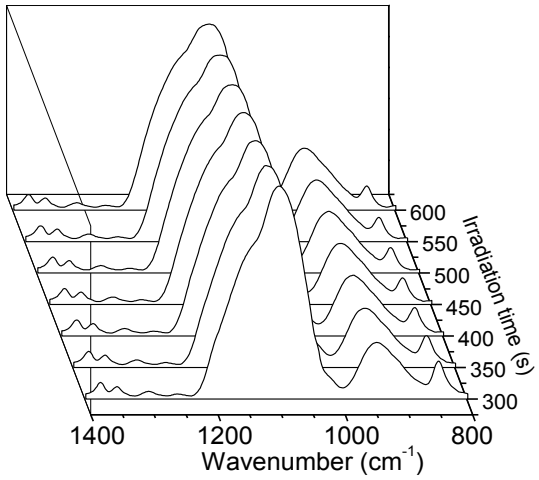

Figure VI.3: Infrared absorption spectra of the P123-PDMOS film (x = 0.50) in the range 800-1500 cm^{-1}, recorded at different irradiation times after the hydrolysis completion

II.4. H_2O BENDING MODE (1640 CM^{-1})

The presence of molecularly adsorbed water can be evidenced by a distinctive band at 1640 cm^{-1} attributed to scissor bending vibration[5]. Interestingly, this water band has been shown to be good discriminatory, non-destructive, indicator of water content within the film. Its interest lies on its higher selectivity compared to the molecular stretch vibrations (with maximum at 3400 cm^{-1}) assigned to OH stretching, and including therefore the contribution of all the hydroxyl-containing compounds such as silanol and methanol groups. Figure VI.4 plots the temporal evolution of the integrated absorbance of the 1640 cm^{-1} band throughout the irradiation for different contents in amphiphilic copolymer (P123). Whether a surfactant is present or not, an equivalent concentration in water is dissolved within the film prior irradiation (although no water was added to the initial formulation). Apparently, the amphiphilic copolymer with hydrophilic PEO chains is unable to confer additional hydrophilicity to the initial film.

In contrast to water stretching modes whose position is very sensitive to increased strength of hydrogen bonding, there is no clear shift of the bending mode following the change from apolar PDMOS environment to hydration sphere within the siloxane network. However, we note an increased intensity of this band during the irradiation process.

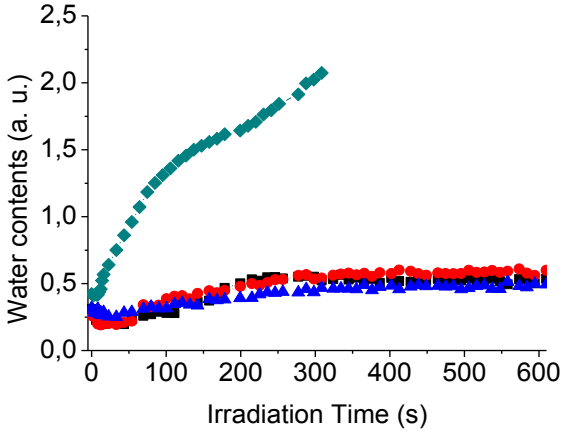

Figure VI.4: Water contents evolution during the sol-gel photo-polymerization of P123-PDMOS films containing various ratios in copolymer: x = 0 (♦), x = 0.25 (■), x = 0.50 (●) and x = 0.75 (▲).

In all concentrations of P123, we observe a gradual enrichment in water. Such a trend is consistent with the *in situ* generation of hydrophilic silica species resulting from hydrolysis, favoring presumably the absorption of atmospheric water. Additionally, water can be released within the film as by product of condensation reactions. However, we note that this increase is much more moderate in samples prepared with surfactant. Such a low concentration in water observed in copolymer-based films can be correlated with the slow-down of the hydrolysis kinetics compared to pure PDMOS samples. Water migration in polymer membranes is governed by the interplay of two physical processes: water solubility and diffusion. In P123, the presence of a dominant hydrophobic part (70 wt. %) in the copolymer presumably affects the solubility coefficient in comparison with a pure hydrophilic silica network. In addition, a macromolecular surfactant may be seen as an obstacle to water mobility, altering this time the diffusion process.

III. RT-FTIR AS A TOOL TO INVESTIGATE COPOLYMER SELF-ASSEMBLY

In this paragraph, RT-FTIR is used to provide insight into the self-assembly pathway, by exploiting its marked sensitivity to local environment and inter- or intramolecular interactions. The key feature is the hydration state change of the amphiphilic copolymer during the structuration process.

P123 has hydrophilic ethylene oxide (EO) groups, which can accommodate water molecules and silica by forming hydrogen bonds (O-H•••O), and hydrophobic propylene oxide (PO) moieties. P123 is initially dissolved in unhydrolyzed PDMOS, which represents an isotropic apolar environment for both blocks. After irradiation, two possible fates must be considered with regards to the hydration state of the PPO block:

- An effective self-assembly should drive a phase separation preventing their hydration process, since the hydrophobic PPO environment (micellar core) becomes isolated from the water-rich PEO/silica phase.
- In contrast, the formation of an amorphous silica-copolymer structure implies a molecular colocalization of the PPO block and silica phase, leading to a substantial hydration of apolar sites with the formation of H-bonds between alkyl groups and water (C-H•••O-H)[13].

Several studies already demonstrated that alkyl groups' hydrophobic hydration could induce a blue-shift of the C-H stretching bands. The band shift was found to be large enough ($\Delta\upsilon \approx 20$ cm^{-1}) to study thermal-induced phase transition of alkyl-based polymers (poly(vinyl methyl ether)[6,14] poly (N-alkyl acrylamide)[15]) or quantify critical micellar temperature[16] and concentration[17] of amphiphilic copolymers in water. These early developments suggest that specific IR bands sensitive to water-alkyl interactions may represent a powerful diagnostic marker for investigating the phase separation behavior in more complex systems such as copolymer surfactant templated silica mesophases.

Instead of the C-H stretching vibrations (2800 – 3050 cm^{-1}) which are the most reported in the literature, we rather focused on the CH_3 symmetric deformation mode ($\delta(CH_3) \approx 1374$ cm^{-1}) uniquely representative of the PPO hydrophobic block (not overlapped by the IR modes of the Si-OCH_3). FTIR spectra profiles of non-mesostructured (x = 0.25) and mesostructured (x = 0.75) films in the region 1355-1400 cm^{-1} at different irradiation times are reported in Figure VI.5.

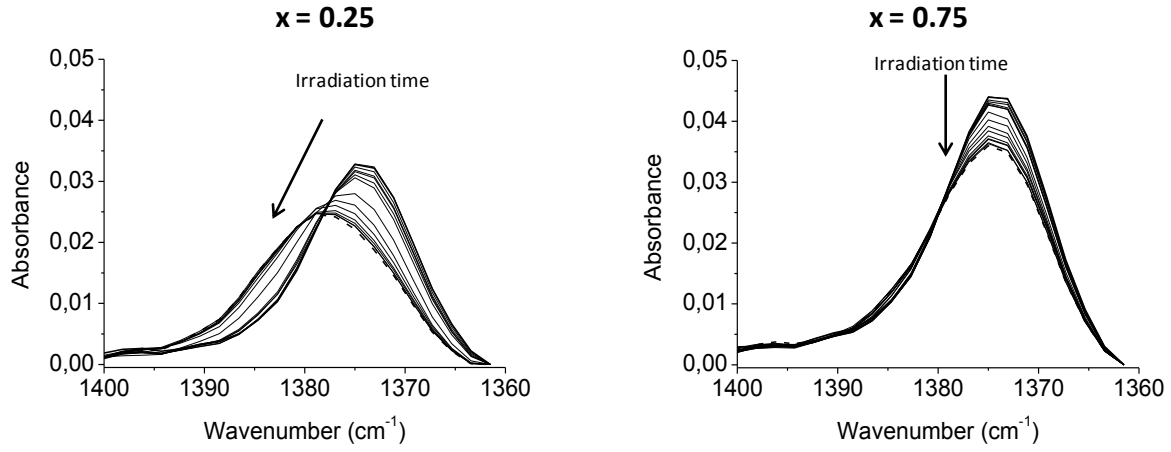

Figure VI.5: FTIR spectra evolution for P123-templated silica film as a function of irradiation time in the region 1360-1400 cm^{-1}: amorphous film (x = 0.25) and mesostructured film (x = 0.75).

In both cases, prior to the UV irradiation the band is centred at 1374 cm^{-1}, indicating an apolar environment consistent[18] with the close contact between the PPO block and the non-reacted PDMOS precursor. Accordingly, we note an exact match in terms of band position with pure PPO

homopolymer and bulk P123 (not represented). Depending on template concentration, we observe upon UV irradiation noticeably different band shift. For the non-mesostructured film, a gradual broadening and shift from the initial 1374 to 1379 cm^{-1} is visible, while this red-shift is almost not apparent for the mesostructured sample ($\Delta\bar{\upsilon} \approx 1$ cm^{-1}). First, these shifts can be reconciled with a medium becoming more hydrophilic, which is consistent with the replacement of methoxysilyl by silanol functions and the uptake of water into the silica network. Above all, the difference of scenario must be understood in terms of the greater hydration of the PPO segments with H-bonding interactions (C-H•••O-H) in the non-segregated samples.

Additional evidence for the interest of the methyl deformation band to act as a signature for the PPO hydration states and indirectly to monitor the copolymer self-association is provided by its deconvolution for three different concentrations in surfactant (x = 0.25, 0.50 and 0.75), as sketched in Figure VI.6.

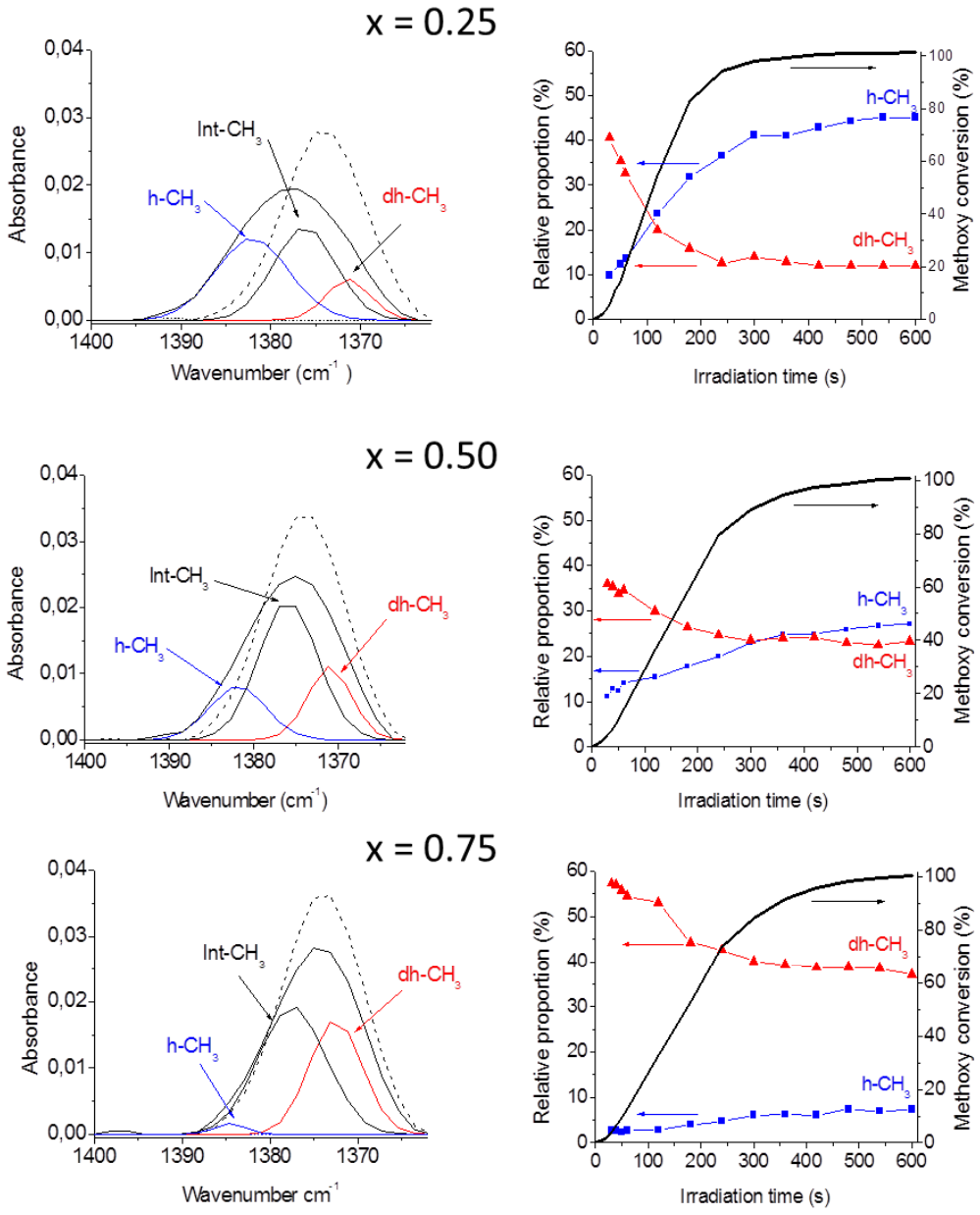

<u>Figure VI.6:</u> (Left) Evolution of the CH_3 symmetric deformation mode ($\delta(CH_3)$ 1360-1400 cm^{-1}) before (dashed line) and after (solid line) UV irradiation at various concentrations in copolymer. Deconvolution of the FTIR absorption spectrum for the as-irradiated sample is also shown. (Right) Relative evolution of the integrated absorbance of two components of the $\delta(CH_3)$ band: δ(h-CH_3) (■, hydrated CH_3, 1382 cm^{-1}) and δ(dh-CH_3) (▲, dehydrated CH_3, 1371 cm^{-1}) at three different concentrations in copolymer.

In all cases, three distinct spectral features appear at 1382, 1376 and 1371 cm^{-1}, which can be related to distinct PPO environments. Following the assignment of Liu et al.[17], the most red-shifted band at 1382 cm^{-1} is ascribed to hydrated methyls (hydrophobic hydration, δ(h-CH_3)), the second at 1371 cm^{-1} to dehydrated methyls (hydrophobic interactions, δ(dh-CH_3)) and the intermediate at 1376 cm^{-1} to interfacial methyls in a mixed environment δ(int-CH_3). Scheme VI.1 depicts the local and mesoscopic structure of the copolymer-silica hybrid system with a

multiplicity of PPO environments consistent with these FTIR data. A majority of the PPO chains are localized in a dehydrated segregated micellar core (dh-PPO), whereas a minor part of the PPO is concentrated in interfacial regions separating the silica matrix and the hydrophobic core (Int-PPO). The non-phase separated copolymer chains in close proximity with the silica network (in minority in mesostructured films whereas in majority in amorphous blends) are assumed to be highly hydrated (h-PPO).

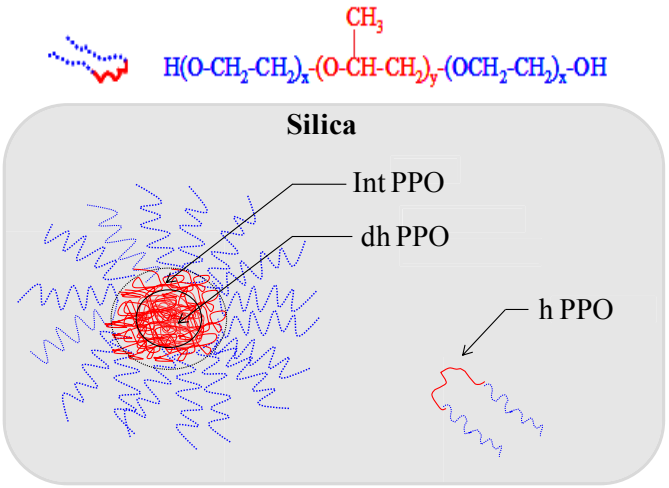

Scheme VI.1: Silica-block copolymer microenvironment in a worm-like mesostructure showing the local separation of the PEO and PPO blocks.

Furthermore, we quantitatively analyze the evolution of δ(h-CH_3) and δ(dh-CH_3), by plotting the evolution of their integrated absorbance during the irradiation time. Of high significance is the possibility to have in the same graphic the temporal evolution of hydrolysis.

At low P123 concentration (x = 0.25), the beginning of hydrolysis is accompanied by an intensification of the band at 1382 cm^{-1} (h-CH_3) together with the opposite dynamic behavior for the band at 1371 cm^{-1} (dh-CH_3). Such a scheme is fully consistent with the low level of mesoscopic organization reported with this sample with XRD and TEM data (chapter V). As the sol-gel reaction occurs, the δ(dh-CH_3) decreases reflecting the gradual change of environment from methoxy silicate $-(SiO)_x(OMe)_y$ to hydrophilic silicate species $-(SiO)_x(OH)_y$. Due to the incapacity of P123 to segregate (self-assemble) from the silica domain, the PPO block cannot avoid hydration, as exemplified by the growth of the δ(h-CH_3) mode. These data confirms the colocalization of the two blocks of the template with silica and also that the change of medium polarity for the PPO block occurs progressively to yield at the end of the UV process only a minor contribution of dehydrated methyl (1371 cm^{-1}) representing only 10 % of the band. By contrast, at higher concentrations in surfactant ($x \geq 0.50$), the δ(h-CH_3) band at 1382 cm^{-1} remains weak upon UV irradiation. Upon increasing the P123 ratio from 0.50 to 0.75 the δ(h-CH_3) component

decreases from 25 % to 75 %, which is in full agreement with a more resolved and sharp peak observed in XRD and suggestive of more uniform mesopores. In this second scenario, the hydrophobic interactions dominate and the PPO blocks are able to remain in an apolar environment despite the advent of the silica phase. This is consistent with the mesostructuration ability demonstrated in XRD and TEM by these copolymer-rich samples. Despite the change in medium polarity initiated by hydrolysis, the PPO blocks segregate: micelles with an isolated PPO core and a corona of hydrated PEO are formed. Although the methyl deformations hardly shift here, there is clearly a change in the environment of the PPO blocks because of the self-assembly, but they remain in a hydrophobic medium throughout the reaction. In conclusion, this study outlines the interest of the $\delta(h\text{-}CH_3)$ band as a probe to evaluate the extent of PPO segregation.

IV. SOLID STATE NMR AS A TOOL TO INVESTIGATE COPOLYMER SELF-ASSEMBLY

As depicted in Scheme VI.1, self-assembled amphiphilic block copolymers are characterized by a spatial separation at the nanometer scale of the hydrophilic and hydrophobic domains. Such a mesoscopic segregation has important consequences as regards to the mobility and the hydration state of the blocks. Interestingly, simple mono-dimensional (1D) spectra of spin-1/2 nuclei (^{1}H and ^{13}C) can be used to assess this dual concept of chain dynamics (i) and local environment (ii).

(i) It is well-established that resonance width is strongly dependent on the strength of the dipolar coupling among the nuclei involved (^{1}H, ^{13}C). Interestingly, the extent of homonuclear or heteronuclear coupling is very sensitive to motional processes within the material, which allows the use of line width as an efficient marker of the polymer chains' dynamics[19]. In segregated mesostructures, the interfacial surface between the antagonist blocks is significantly reduced, resulting in a greater mobility[20]. Consequently, effective block segregation should be manifested by a substantial sharpening of the resonances since the dipolar coupling is averaged out by faster molecular motions. In contrast, an amorphous hybrid microstructure in which the rigid silica network is intimately and randomly mixed with the copolymer is expected to increase the dipolar interactions, yielding a broader proton or carbon line width.

(ii) The second feature concerns the dual sensitivity of chemical shift to the chemical nature of adjacent atoms and to physical interactions with environmental molecules. For example, liquid-state ^{1}H NMR experiments with PEO-PPO-PEO copolymer solution demonstrated that the transfer from a hydrated medium to an apolar environment was accompanied by a slight upfield shift ($\Delta\delta \approx 0.05$ ppm) of the PPO protons[21,22]. The question arises whether such dependency can be extended to solid copolymer-silica materials to distinguish different hydration state of the

PPO block depending on the level of mesostructuration. The main challenge anticipated with solid-state ^{1}H spectra are the small chemical shift range and, above all, the strength of the dipolar interactions between the protons and the chemical shift anisotropy (only partially averaged by MAS)[23] which causes a significant broadening of the spectra, making the detection of such a weak δ shift tricky.

IV.1. MOBILITY OF PEO AND PPO BLOCKS

Figure VI.7 shows the ^{13}C CP/MAS spectra of the composite films comprising different contents in P123 (A) and the deconvoluted spectrum of the x = 0.50 (B). The isolated narrow feature at ~ 18 ppm was easily assigned to the PPO methyl. The carbons from CH_2 (PPO, PEO) and CH (PPO) arise as an envelope located at 65-80 ppm, which can be deconvoluted into a triplet resonance with a broad resonance centered at 70.6 ppm associated with the PEO methylenes, whereas the two sharp resonances at 75.7 and 73.6 ppm result from the CH_2 and CH of the PPO block, respectively. As expected from the mesostructured character of this sample, we note that all the ^{13}C linewidths associated to the occluded PPO blocks are significantly sharper than those from the PEO block in close contact with the rigid silica skeleton.

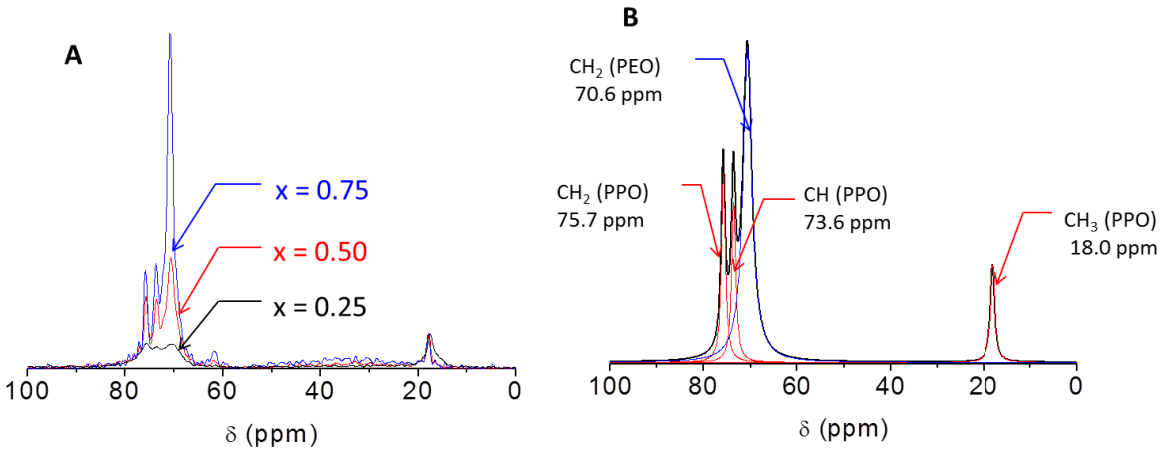

Figure VI.7: (A) Effect of the concentration of P123 on the ^{13}C CP-MAS NMR spectra (x = 0.25, 0.50 and 0.75). (B) Deconvoluted ^{13}C CP-MAS NMR spectrum of a P123/silica nanocomposite (x = 0.50)

As can be seen in Figure VI.7A, upon increasing the copolymer ratio from 0.25 to 0.75, the carbon linewidths measured for both the PEO and PPO blocks becomes narrower, which is consistent with an increased phase separation affecting positively the chain mobility. From an amorphous blend (x = 0.25) to a mesostructured composite (x = 0.50), we note in particular the dramatic change from a very broad spectrum to a more resolved spectrum allowing the speciation of the PEO and PPO components. Extended interface between the different PEO, PPO and silica domains contribute to enhance the dipolar interactions between protons, leading to an

extremely broad spectrum for the amorphous sample. The same reasoning can be applied to the ^{1}H MAS spectra shown in a similar way in Figure VI.8.

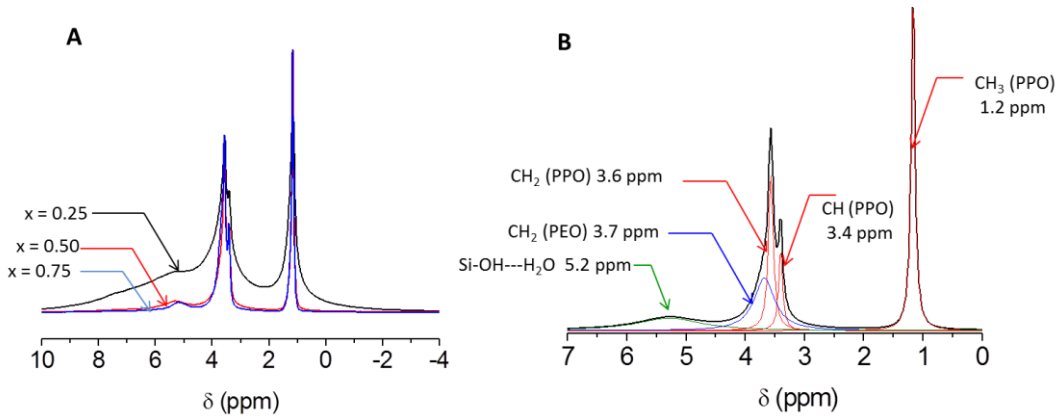

Figure VI.8: Effect of the concentration in P123 on the 1H MAS NMR spectra (x = 0.25, 0.50 and 0.75)(A). Deconvoluted ^{1}H MAS NMR spectrum of ax = 0.50 P123/silica nanocomposite (B).

Speciation in this spectrum is less trivial and contradictory interpretations were given in the literature for self-assembled PEO-b-PPO-b-PEO copolymer systems[9,10]. Our ^{1}H spectra of the as-synthesized hybrid films were recorded at fast MAS (25 kHz) to display enough resolution. The narrow feature at 1 ppm is straightforwardly attributed to the PPO methyl group, but the difficulties arise for the massif spanning 2-4 ppm including the unresolved contributions from the CH and CH_2 protons. In this region, valuable information can be extracted from $^{13}C(^{1}H)$ HETCOR experiments with x = 0.50 film (Figure VI.9), based on cross polarization through dipolar coupling. Clearly, the ^{13}C resonances located at 73.6 ppm (CH-PPO), 75.7 ppm (CH_2-PPO) and 70.6 ppm (CH_2-PEO) can be correlated to three distinct 1H resonances located at 3.4, 3.6 and 3.7 ppm, thus allowing their attribution. These results show that 2D HETCOR experiments can be used for the characterization of unresolved array of ^{1}H resonances. Note that this assignment is in full accordance with the area ratios 1/2/2 (CHPPO/CH_2PPO/ CH_2PEO), which can be exploited as the MAS spectrum is quantitative. Finally, the broad downfield resonance at ~ 5 ppm was assigned to residual silanol protons involved in a variety of H-bonds (water, PEO, PPO).

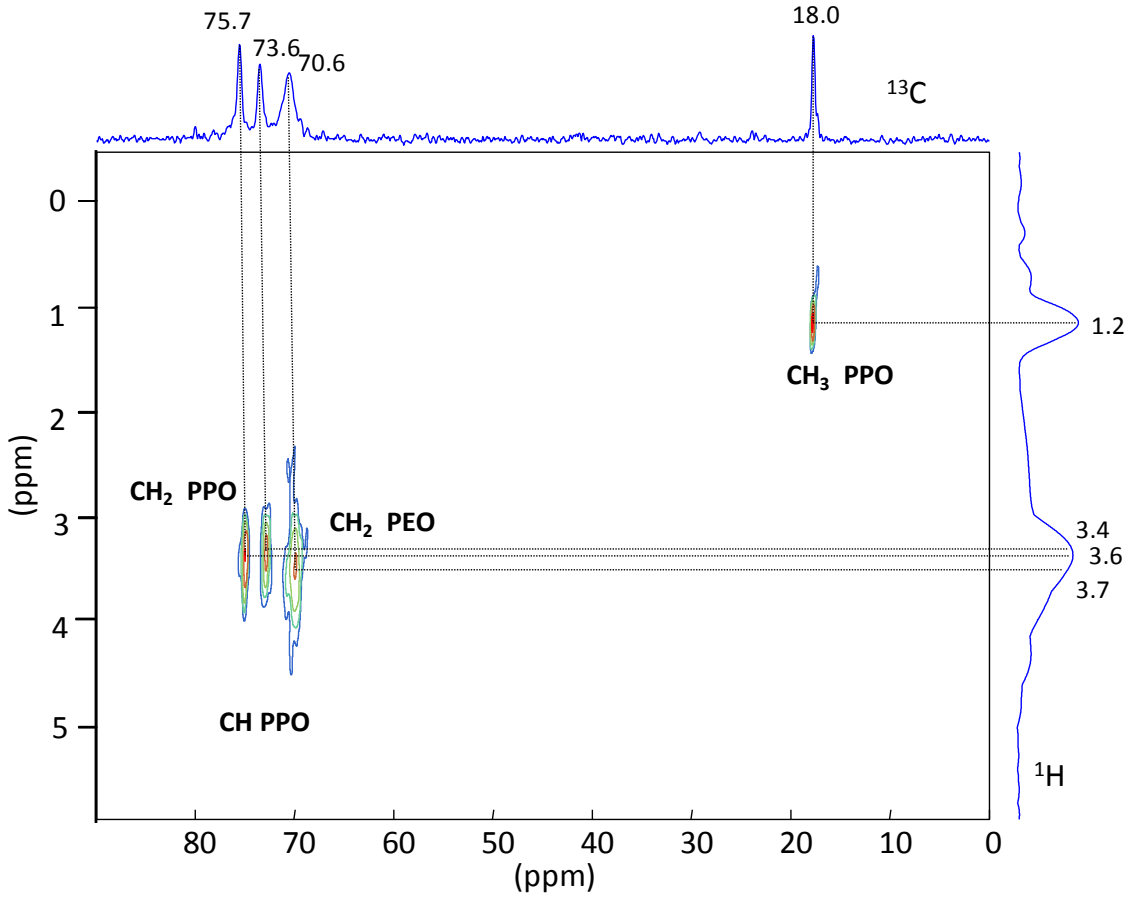

Figure VI.9: 2D ^{13}C-^{1}H HETCOR NMR spectrum of the 50 wt. % P123/silica hybrid film. ^{13}C and ^{1}H spectra are plotted along their respective axes.

As shown in Figure VI.8, the three proton linewidths related to the PPO segregated phases are substantially narrower than the single CH_2 component at 3.7 ppm assigned to the PEO methylenes. As raised previously, the resonance narrowing with the increase of P123 content applies both to the PEO and PPO blocks. Quantitative estimates of the evolution of the proton linewidth as a function of the P123 concentration are summarized in Table VI.1.

Table VI.1: Summary of data obtained from ^{1}H solid state NMR spectra (chemical shift, linewidth) of P123/silica films including different copolymer/PDMOS ratios (x = 0.25, 0.50 and 0.75).

	x = 0.25 (^{1}H)		**x = 0.50** (^{1}H)		**x = 0.75** (^{1}H)	
δ (ppm)	^{1}H MAS linewidth (Hz)	Relative Proportion (%)	^{1}H MAS linewidth (Hz)	Relative Proportion (%)	^{1}H MAS linewidth (Hz)	Relative Proportion (%)
CH_3(PPO) 1.2	78	35	34	38	31	37
CH (PPO) 3.4	34	3	34	10	34	10
CH_2 (PPO) 3.6	52	10	40	22	36	20
CH_2 (PEO) 3.7	319	52	168	30	110	33

The results are in accord with the transition from a homogeneous P123-silica blend to a progressive phase separation of the blocks. For example at x = 0.75, the linewidths of the

methylene protons of PPO and PEO are substantially narrower (36 and 110 Hz, respectively) than those obtained at x = 0.50 (40 and 168 Hz, respectively). The higher degree of condensation of the silicate network found at higher copolymer concentration (see chapter V) is finally consistent with all these experimental results. A greater block mobility and microphase separation in mesostructured samples imply that the cross-linking of the siloxane matrix is less perturbed by the presence of the copolymer.

IV.2. PPO LOCAL ENVIRONMENT AND HYDRATION STATE

The dependence of the isotropic chemical shift on the microenvironment of the nuclei is also exploitable to evidence the extent of mesostructuration. The spectral feature at ~ 1.2 ppm can be decomposed into 3 distinct resonances at 1.32 ppm (hydrated PPO, h-CH_3), 1.22 ppm (interfacial PPO, int-CH_3) and 1.16 ppm (dehydrated PPO, dh-CH_3). Their respective area is summarized in Table VI.2. As depicted in a series of ^{1}H MAS spectra (Figure VI.10), we note a small upfield shift (0.08 ppm) of the CH_3 protons from the PPO block with an increase of the template concentration from x = 0.25 up to 0.75.

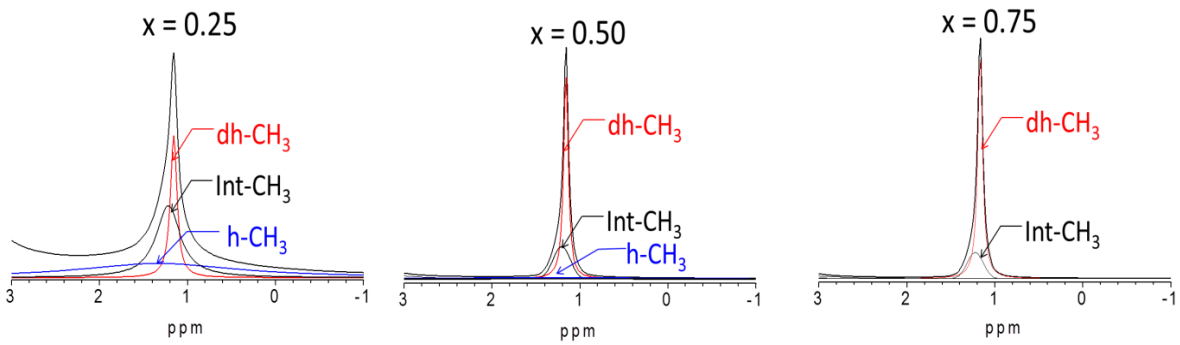

Figure VI.10. Effect of the P123 concentration (x = 0.25, 0.50 and 0.75) on the shape/chemical shift of the proton resonance of the PPO methyls (^{1}H MAS spectrum).

We assume that the progressive dehydration of the segregating PPO block accounts for the observed shift. A meticulous deconvolution reveals a triplet resonance, reflecting three different environments for the PPO methyls, in a similar fashion to what was observed in IR (Figure VI.10). The upfield and downfield spectral features at 1.16 and 1.32 ppm were assigned respectively to dehydrated and hydrated CH_3, while the interfacial methyls contribute to an intermediate resonance at 1.22 ppm. A comparison of their relative area at different concentrations in P123 is summarized in Table VI.2. The hydrated peak is always very broad and dominant at x = 0.25 (46 %) as expected from the PPO/silica intimate contact in non-mesostructured films. However, its contribution decreases drastically as the surfactant experiences self-association at concentration x= 0.50 (17 %), and completely vanishes at x =

0.75. In contrast, the dehydrated peak undergoes an opposite evolution, from 18 % in the blend its contribution rises to 79 % in the 75 wt % P123 mesostructured sample.

Table VI.2: Summary of data obtained from 1H solid state NMR spectra (chemical shift, linewidth) of P123/silica films including different copolymer/PDMOS ratios (x = 0.25, 0.50 and 0.75).

		x = 0.25		x = 0.50		x = 0.75	
δ (ppm)		^{1}H MAS linewidth (Hz)	Relative Proportion (%)	^{1}H MAS linewidth (Hz)	Relative Proportion (%)	^{1}H MAS linewidth (Hz)	Relative Proportion (%)
dh-CH_3	1.16	36	18	25	59	26	79
Int-CH_3	1.22	132	36	92	24	84	21
h-CH_3	1.32	881	46	1237	17	0	0

Figure VI.11 compares the IR and NMR data, which showed similarly the coexistence of three different environments of the PPO CH_3. Although the evolution of the h-, int- and dh-CH_3 components are clearly similar with both techniques, there is not exact match due to the uncertainties arising from the deconvolution treatment.IR data are based on the integrated absorbance of the δ(CH_3) band while those from NMR are determined from the integrated PPO CH_3 resonance at ≈ 1.2 ppm. Similarly, both IR band and proton signal can be decomposed in 3 components associated to these PPO local environments.

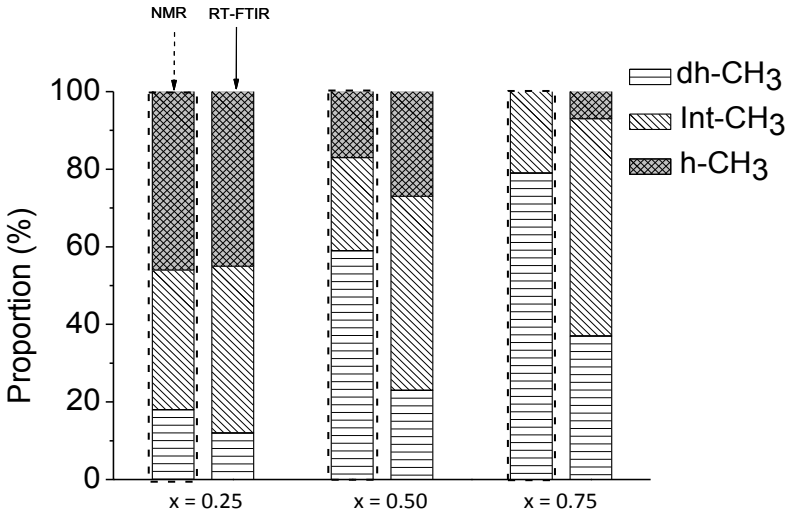

Figure VI.11: Comparison between the IR and ^{1}H MAS NMR results giving the proportion in hydrated (h), dehydrated (dh) and interfacial (int) PPO CH_3 depending on the P123/PDMOS ratio: x = 0.25, 0.50 and 0.75.

CONCLUSION

In the previous chapter, we proposed an alternative and simple approach to prepare silica/surfactant mesostructured films. The self-assembly process is now induced by UV light instead of solvent evaporation. We showed that the level of mesostructuration in the hybrid films was strongly dependent upon the concentration in copolymer surfactant; a threshold concentration of 50 wt % in copolymer was necessary to obtain films with amorphous to worm-like mesostructures.

In this chapter, we highlight how our procedure (devoid of solvent, and in which the sol-gel process is fully implemented after deposition) has significantly enhanced the interest of *in situ* FTIR spectroscopy. Contrary to the EISA conditions, a comprehensive study of the sol-gel process taking place, in particular during hydrolysis kinetics was now possible. We observe that the presence of surfactant affects dramatically the hydrolysis rate due to an increase of viscosity which decreases the vapor permeation and the self-assembly process that also require water. RT-FTIR permitted to structurally and compositionally investigate the self-assembly process. Photoacid-catalyzed hydrolysis was kinetically followed, while the self-assembly was studied by the gradual shift of spectral features sensitive to hydration state change in the course of the structuration process. In particular, the deformation mode of the PPO methyl provided a powerful diagnostic marker in assessing the gradual mesoscopic structuration. In addition, ^{1}H and ^{13}C MAS NMR were instrumental in evaluating the higher mobility of the PEO and PPO blocks in mesostructured films due to greater block segregation. The dependency of ^{1}H chemical shift to local environment enabled the distinction of various hydration degrees of the PPO block, which could be correlated to the extent of mesostructuration. Of particular interest is that FTIR and solid-state NMR data converged and demonstrated three distinct PPO domains: hydrated, interfacial and dehydrated, whose relative proportions reveal the extent of self-assembly.

CHAPTER VI REFERENCES

(1) Doshi, D., A.; Gibaud, A.; Goletto, V.; Mengcheng, L. U.; Gerung, H.; Ocko, B.; Han, S., M.; Brinker, C. J. *J. Am. Chem. Soc. 200*3, 125, 11646.

(2) Innocenzi, P.; Falcaro, P.; Grosso, D.; Babonneau, F. J. *Phys. Chem. B* **2003**, 107, 4711.

(3) Innocenzi, P.; Malfatti, L.; Kidchob, T.; Falcaro, P.; Guidi, M. C.; Piccinini, M.; Marcelli, A. *Chem. Commun.* **200**5, 2384.

(4) Innocenzi, P.; Kidchob, T.; Bertolo, J. M.; Piccinini, M.; Guidi, M. C.; Marcelli, C. *J. Phys. Chem. B* **2006**, 110, 10837.

(5) Falcaro, P.; Costacurta, S.; Mattei, G.; Amenitsch, H.; Marcelli, A.; Guidi, M. C.; Piccinini, M.; Nucara, A.; Malfatti, L.; Kidchob, T.; Innocenzi, P. *J. Am. Chem. Soc.* **2005**, 127, 3838.

(6) Maeda, Y. *Langmuir* **2001**, 17, 1737.
(7) Alonso, B.; Mineva, T.; Innocenzi, P.; Trimmel, G.; Stubenrauch, K.; Melnyk, I.; Zub, Y.; Fayon, F.; Florian, P.; Massiot, D. *C. R. Chimie* **2010**, 13, 431.
(8) Epping, J. D.; Chmelka, B. F. *Curr. Opin. Colloid. In.* **2006**, 11, 81.
(9) Alonso, B.; Fayon, F.; Massiot, D.; Amenitsch, H.; Malfatti, L.; Kidchob, T.; Costacurta, S.; Innocenzi, P. *J. Phys. Chem. C* **2010**, 114, 11730.
(10) Melosh, N. A.; Lipic, P.; Bates, F. S.; Wudl, F.; Stucky, G. D.; Fredrickson, G. H.; Chmelka, B. F. *Macromolecules* **1999**, 32, 4332.
(11) De Paz, H.; Chemtob, A.; Croutxé-Barghorn, C.; Le Nouen, D.; Rigolet, S. *J. Phys. Chem. B* **2012**, 116, 5260.
(12) Babonneau, F. *New J. Chem.* **1994**, 18.
(13) Hobza, P.; Havlas, Z. *Chem. Rev.* **2000**, 100, 4253.
(14) Sun, B.; Lai, H.; Wu, P. J. *Phys. Chem. B* **2011**, 115, 1335.
(15) Geukens, B.; Meersman, F.; Nies, E. *J. Phys. Chem. B* **2008**, 112, 4474.
(16) Su, Y.-l.; Wang, J.; Liu, H. *J. Phys. Chem. B* **2002**, 106, 11823.
(17) Su, Y.-l.; Wang, J.; Liu, H. *Langmuir* **2002**, 18, 5370.
(18) Su, Y.-l.; Wang, J.; Liu, H. *Macromolecules* **2002**, 35, 6426.
(19) Jiang, X.; Lavender, C. A.; Woodcock, J. W.; Zhao, B. *Macromolecules* **2008**, 41, 2632.
(20) Jiang, X.; Luo, S.; Armes, S. P.; Shi, W.; Liu, S. *Macromolecules* **2006**, 39, 5987.
(21) Ma, J.; Guo, C.; Tang, Y.; Wang, J.; Zheng, L.; Liang, X.; Chen, S.; Liu, H. J. *Colloid Interf. Sci.* **2006**, 299, 953.
(22) Ma, J.; Guo, C.; Tang, Y.; Liu, H. *Langmuir* **2007**, 23, 9596.
(23) Geppi, M.; Borsacchi, S.; Mollica, G.; Veracini, C. A. *Appl. Spectrosc. Rev.* **2009**, 44, 1.

CHAPTER VII: PERIODIC MESOSTRUCTURED SILICA FILMS MADE SIMPLER USING UV LIGHT

H. De Paz-Simon, A. Chemtob, C. Croutxé-Barghorn, S. Rigolet, L. Michelin, L. Vidal, B. Lebeau, "*Periodic Mesostructured Silica Films Made Simple Using UV Light",* under submission

INTRODUCTION

In the two previous chapters, we showed the feasibility of a photoinduced sol-gel polymerization for the synthesis of mesoporous silica films. In contrast to literature studies, UV irradiation was not exploited for organic template destruction[1-3] or film consolidation[3,4], but served instead to polymerize the inorganic precursors and trigger the self-assembly process through the efficient catalysis of photoacid generator. Disordered (wormlike) mesoporous silica films were achieved from a homogeneous and stable mixture including only nonvolatile constituents: PAG, alkoxysilane precursor and an amphiphilic PEO-PPO-PEO block copolymer[5-7].

In this chapter, we have found that controlling the relative humidity (RH) and exitance provide a rational basis to transform our initially disordered mesostructures into well-ordered silica-surfactant mesostructures. The first part of this work is dedicated to the design of a new photo irradiation set-up where these two parameters can be controlled. To conduct this study, we worked in the environmental cell under a controlled humidity atmosphere (RH = 20 – 60 %) and we switch for the Hg-Xe lamp set-up enabling the initial alkoxysilane/PAG/template film to be irradiated at variable exitance (35 – 200 mW/cm^2). As film properties are strongly related to pores structure and accessibility,[8] the precise design of pore architecture is therefore a very important objective. The second step consists in the examination of the effect of RH and irradiance on the resulting mesostructured films. It provides a wealth of information about the kinetic and thermodynamic rules regulating the self-assembly in silica-surfactant system. Indeed, by determining the water content inside the film, the RH can impact the hydrophilic/hydrophobic contrast, which is one of the main thermodynamic forces driving a nanophase segregation and the formation of ordered micellar arrays[9,10]. In addition, the transition from a short-range order phase to organized crystalline mesophases relies on gelation kinetics[11]. By contrast to a conventional process, control over polymerization kinetics is made easier with a UV-mediated method through a PAG decomposition rate dependent on light intensity. The special irradiation set-up and the influence of different experimental parameters gave insight into film mesostructuring which is described in a third part. Finally in a last point, we proposed a 100% UV process to prepare mesoporous silica film in one step. The idea relies on a double use of UV. With the same irradiation set-up, we were able firstly to form mesostructured films, wormlike or well organized depending on the template/silica ratio and on the processing conditions. Then in a second time, the organic template is in the continuity progressively and gently eliminated while the inorganic network condensation is extended leading to mesoporous silica films prepared in one step.

I. EXPERIMENTAL CONDITIONS

I.1. FILM PREPARATION

The photosensitive solution was prepared by mixing the PDMOS, PAG and P123 in the typical wt. ratio: 1/0.02/0.5. Although the resultant mixture is stable over months without exposure to UV, the solution can be immediately deposited after preparation (without aging) onto polished silicon wafer using a barcoater to form a nonvolatile liquid film with an initial thickness of 2-3 µm. This liquid film thickness was controlled by profilometry measurements.

I.2. PHOTO IRRADIATION SET-UP

As illustrated schematically in Scheme VII.1, all the irradiation procedures were performed in a controlled-environment chamber where the temperature (T) and relative humidity (RH) were adjusted. Experiments were carried out at 25 °C and a saturated NaCl solution was used to produce various equilibrium RHs. In a typical system, the air to be humidified was provided by a simple diaphragm pump. The air flows through the salt solution contained in a first jar and the humidified gas then passes through a tube into the controlled environment chamber containing the sample, and finally exits through a second tube in a jar containing a hygrometer. Changing the gas flow rate through the chamber was found to be an easy and reliable way to control precisely the equilibrium atmosphere (20 – 60 %). Once the desired RH condition was reached, it was maintained constant throughout the whole process. The chamber includes at the top a UV transparent BaF_2 window exactly in the same axis of the film position, which enables the irradiation of the sample. Illumination was performed through the focused light of a conventional medium-pressure mercury lamp fitted with a flexible light guide. Films were irradiated by the polychromatic light of a mercury-xenon lamp (Hamamatsu, L8251, 200 W) fitted with a 365 nm reflector and coupled with a flexible light-guide. The end of the optical guide was placed at a distance of 3 cm from the film and directed at an incident angle of 90° onto the sample. The irradiation device enables a precise control of the exitance (35 – 200 mW/cm^2) and is also equipped with a calorific filter that prevents heating of the sample. In the dynamic study (part III), films were characterized at different irradiation times. For this, samples were left in the environmental cell during ten minutes after the UV irradiation was stopped, then XRD measurements were performed immediately.

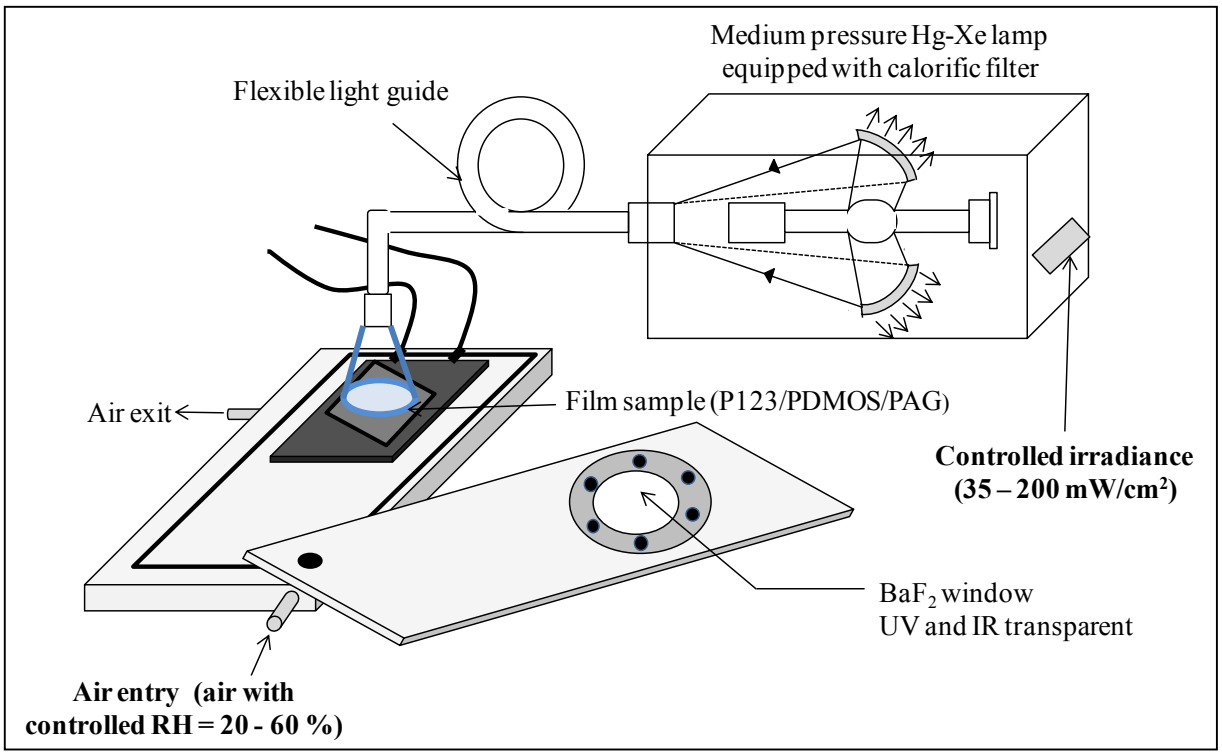

Scheme VII.1: Controlled environmental chamber used to irradiate films at different UV exitances and relative humidities.

II. SYNTHESIS OF PERIODICALLY MESOSTRUCTURED SILICA FILMS USING UV LIGHT

II.1. EFFECT OF RH – THERMODYNAMIC CONTROL

Water is absent of the film composition and the procedure begins with a homogeneous mixture of alkoxysilane precursor, surfactant and PAG cast as a photoreactive film (PDMOS/PAG/P123: 1/0.02/0.5 wt ratio). Hence, the relative humidity is the only way to control water concentration within the film. A high RH implies a water-saturated film with a preferential location of water molecules in the hydrophilic parts (PEO and silica network through H-bondings), while a low RH favors conditions of water depletion. The role of water is thus threefold: to enhance hydrolysis reactions, and to increase the inorganic/surfactant volume ratio and the micelle curvature. Because these two latter points can impact the mesophase structure and its level ordering[12,13], we expect an increased humidity to be an effective driver of self-assembly. Figure VII.1 shows the XRD patterns of films obtained at constant irradiance with a RH ranging from 20 to 60 %.

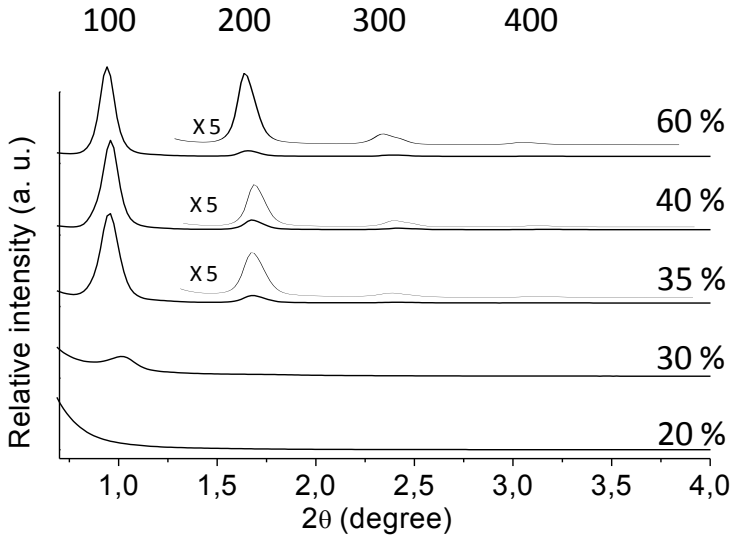

Figure VII.1: Effect of the relative humidity on the XRD patterns of "as synthesized" x = 0.50 P123/PDMOS films irradiated at I = 200 mW/cm² during 600 s.

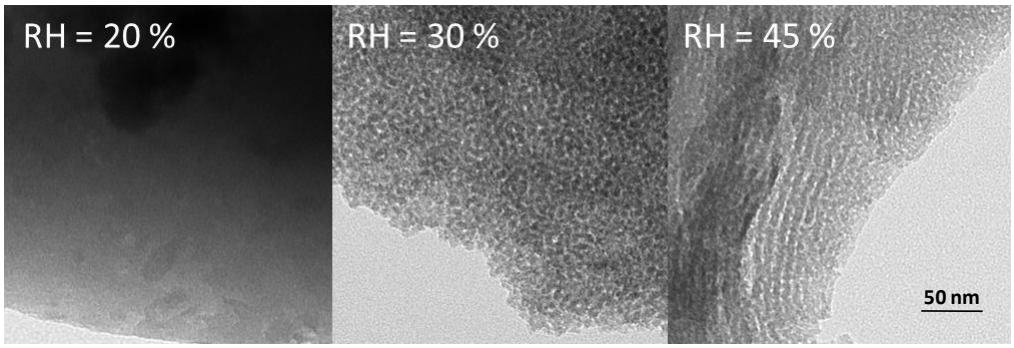

Figure VII.2: TEM images of "as synthesized" x = 0.50 P123/PDMOS films prepared under variable RH (20 %, 30 % and 45 %), t = 600 s, I = 200 mW/cm².

At a low RH value of 20%, the as-synthesized film exhibits a featureless XRD pattern consistent with an amorphous blend of copolymer chains and silica phase. Upon increasing the RH to 30 %, a single diffraction peak at low 2θ angle (0.75° – 1.25°) appears. This latter is attributed to randomly distributed wormlike mesostructures devoid of long-range order but with a constant correlation distance.[14-16] As expected, a further humidity increase has the dramatic effect of causing a "disorder-to-order" transition. Indeed, four peaks are thus observed above a threshold RH of 35 %, indexed as the (100), (200), (300) and (400) reflections of a lamellar symmetry lattice. The *d*-spacing deduced from this pattern is 9.4 ± 0.2 nm, which is in agreement with the typical lattice parameter values encountered with P123 surfactant mesophase (d_{spa} = 10 nm).[17] The samples prepared at greater RH (45 %, 55 % and 60 %) display the same reflection peaks with only small variations in their intensities. The three TEM images displayed in Figure VII.2 conclusively support the same trends deduced from the XRD data. Upon increasing the RH from 20 % to 30 %, then 45 %, the progressive change from amorphous samples to wormlike

mesostructures and finally well-ordered lamellar mesostructures is evident. To confirm their lamellar character, we mainly rely on the disappearance of the main XRD signals when these samples are calcined (not represented). Such collapse caused by the removal of surfactant provides a strong indication that the stripes are the signature of a layered structure forming a stack of lamellae. Unlike powders, mesostructured films can present an anisotropic orientation induced by the substrate. Thus, 2D hexagonal structures with an orientation of the mesochannels parallel to the substrate can give rise to similar morphology. However, this latter mesostructure is able to withstand the calcinations process.[17]

The first striking observation is the strong dependence of the mesostructuration on RH. The second major effect related to water is to drive the regular assembly of the copolymer chains in a lamellar mesophase. Under dry conditions (RH = 20 %), the hydrolyzed silica phase is not sufficiently selective for the PEO blocks to induce a block segregation of the hydrophobic PPO block. Self-assembly is thus hampered by inappropriate solvation conditions or dehydration conditions, leading to amorphous structures. Raising the RH up to 30 % creates a water enrichment of the silica phase, which becomes more selective for the hydrophilic block since water is nonsolvent of the PPO block. As a result, the phase segregation affords, first, wormlike mesochannels devoid of periodicity. At higher RH, a "disorder-to-order" becomes even possible. In agreement, several studies in dilute solutions demonstrated that block copolymer self-assembly was strongly dependent on the ability for the solvent to swell selectively certain blocks and segregate others.[18] On the other hand, some authors have interpreted the effect of a higher RH (higher water concentration) on non-thermodynamic grounds.[10] They postulated that a greater dilution of the silica and surfactant species might result in a more fluid environment suitable to mesophase rearrangement, and the subsequent formation of well-ordered mesostructures.[19] Clearly, mesostructuring then ordering are successively promoted by an increase of humidity.

II.2. EFFECT OF THE IRRADIANCE – KINETIC CONTROL

Although RH can affect hydrolysis and condensation rates, its impact on mesophase ordering can be essentially reconciled with a thermodynamically-driven self-assembly. To gain a complete picture of this photoinduced system, we have investigated whether a kinetic parameter such as the irradiance can induce, in a similar way, an ordering effect. One advantage of our process is that sol-gel kinetics are controlled photochemically.[6,7] Thus, any change of irradiance may slow down, or in contrast, accelerate the PAG photolysis rate with a direct effect on catalyst concentration and condensation rates.[20] Figure VII.3 shows the XRD patterns of as-irradiated

films obtained at various irradiances (35 to 200 mW/cm²) while maintaining the RH value constant at 30 %.

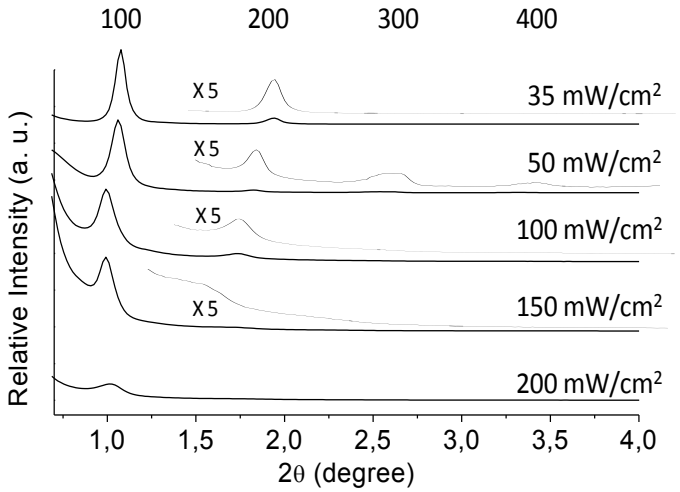

Figure VII.3: XRD patterns of "as synthesized" x = 0.50 P123/PDMOS films prepared under different irradiances, t = 600 s, RH = 30%.

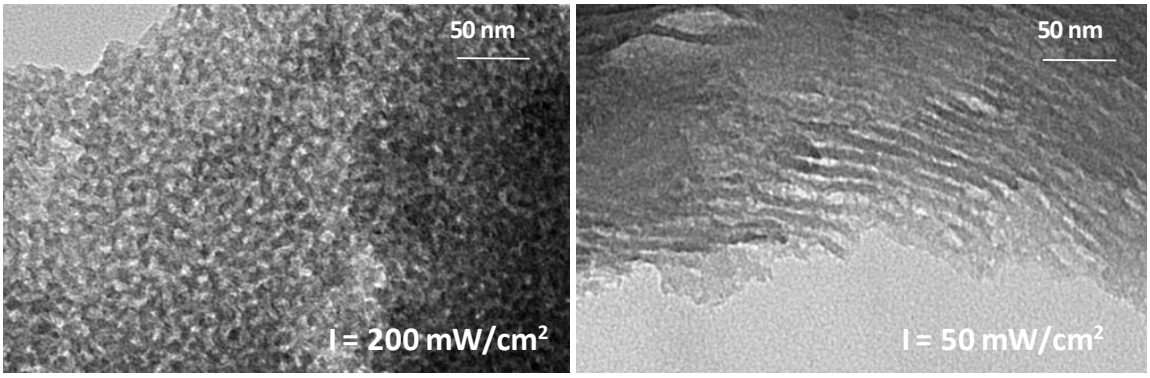

Figure VII.4: TEM images of "as synthesized" x = 0.50 P123/PDMOS films prepared under two different irradiances: 200 and 50 mW/cm², t = 600 s, RH = 30 %.

In agreement with the previous experiments, a wormlike disordered mesostructures is created at a high irradiance of 200 mW/cm², as exemplified by a small and broad peak at 2θ = 1.05°. Signs showing the onset of ordered mesophases appear upon decreasing the light intensity. At I = 150 mW/cm², the XRD pattern exhibits two (100) and (200) reflections indicating that a periodic lamellar mesostructure is now forming confirmed by TEM pictures (figure VII.4). For I ≤ 100 mW/cm², an additional (300) order of reflection becomes visible translating a more uniform lamellar packing. In addition, the formation of a highly ordered mesostructure is accompanied by a slight decrease of the *d*-spacing: 8.9 ± 0.1 nm at I ≥ 150 mW/cm² to 8.1 ± 0.2 nm at I ≤ 100 mW/cm². The higher mobility resulting from a better organization allows the inorganic network to be more condensed, thus causing a slight contraction of the interlayer distance.[7]

The role of the irradiance on mesophase ordering can be understood on the basis of the coexistence of two competitive processes: template ordering kinetics (k_{ord}) and kinetics of silica condensation (k_{cond}). A decreased irradiance causes a slower gelation process ($k_{ord} < k_{cond}$), leaving more time for the block copolymer to self-assemble into higher organized mesostructures. In contrast, we believe that a too fast condensation at high irradiance ($k_{cond} > k_{ord}$) can disturb self-assembly, and quench the system within an intermediate system.[21] The relative randomness and high stability of the siloxane network formed is likely precluding any extended signs of organization. Such results are in agreement with earlier conclusions drawn with the EISA method. One of the major aspects of this process, in terms of sol-gel chemistry, is to work under acid conditions where the condensation rate of the silanol species is known to be minimized. The goal is not to frustrate the self-assembly by gelation that would kinetically trap the system in a transient non-ordered state.[22] Also noteworthy is that the described kinetically-controlled mechanism is not systematic, but essentially valid at moderate RH (30 %). At a higher RH of 50 % for example, the mesostructuration becomes thermodynamically-driven since a long-range organization is achieved regardless of the irradiance as represented in Figure VII.5.

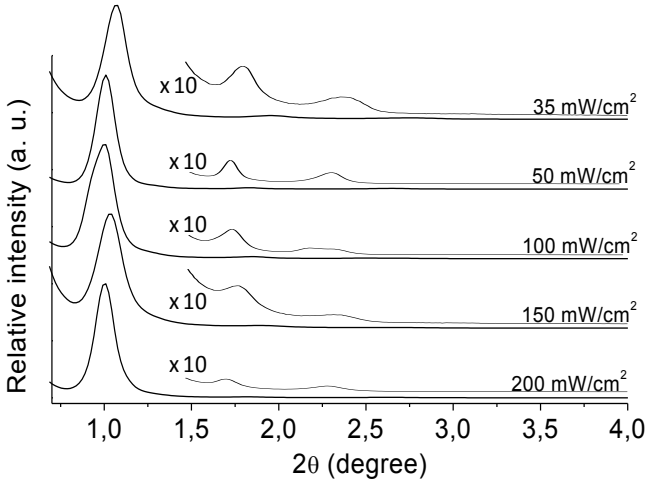

Figure VII.5: XRD patterns of "as synthesized" x = 0.50 P123/PDMOS films prepared under various irradiances 35 up to 200 mW/cm², t = 600 s, RH = 50 %.

II.3. REVEALING THE P123 POLYMESOMORPHISM

In principle, three mesophases are encountered with the binary P123-silica hybrid system: lamellar, 2D hexagonal and cubic.[17] Template/silica volume ratio is known as a straightforward variable to control thermodynamically the film mesostructure. Low concentration in P123 generally yields *Im3m* cubic mesostructure with high curvature. By contrast, medium content in template generates preferentially 2D hexagonal (*p6mm)* structure while lamellae are formed at higher concentration. To foster this polymorphism, three silica/surfactant hybrid films including

various copolymer/silica wt. ratios (x = 0.25, 0.35 and 0.50) have been prepared and analyzed by XRD (Figure VII.6). In order to promote self-assembly and mesophase ordering, these experiments were performed under optimized conditions as regards to irradiance (I = 35 mW/cm^2) and RH (50 %).

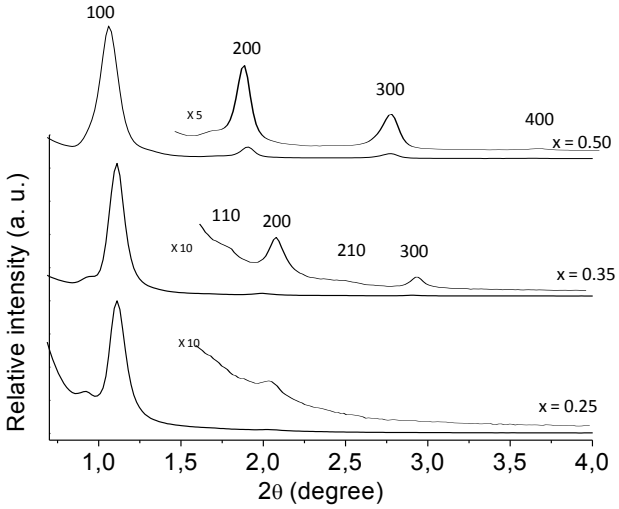

Figure VII.6: Influence of the P123/PDMOS ratio (x) on the XRD patterns of the as-synthesized silica films, t = 600 s, RH = 50%, I = 35 mW/cm^2.

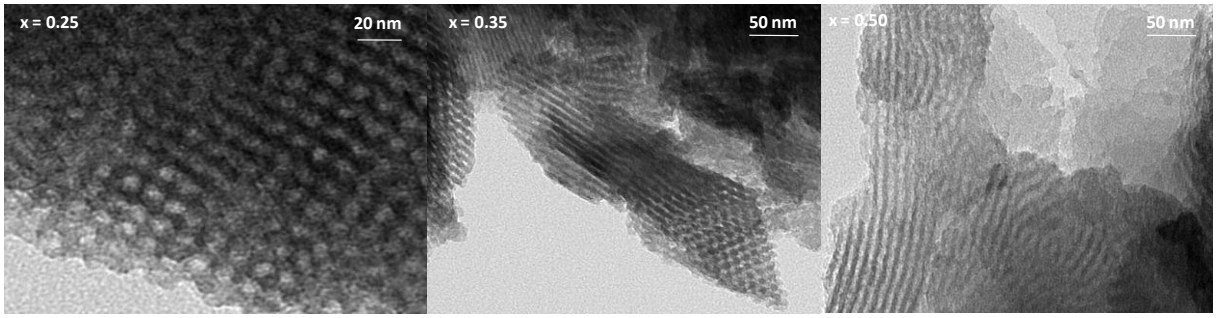

Figure VII.7: TEM images of the "as synthesized" silica films containing various P123/PDMOS wt. ratios (x = 0.25, 0.35 and 0.50). t = 600 s, RH=50%, I = 35 mW/cm^2.

The XRD pattern of the x = 0.50 sample exhibits a sequence of very sharp low-angle diffraction peaks suggestive of a lamellar mesostructure. The first intense peak (100) at 2θ = 1.06° corresponds to the interlayer distance, which was evaluated to be 8.3 nm. At higher angles, the other peaks are attributed to second (200), third (300) and fourth (400) order diffractions. Our attribution was confirmed by TEM (Figure VII.7) showing stacks of sheets well indicative of a lamellar phase disappearing after the surfactant removal by calcination. For the x = 0.35 sample, five peaks are observed which could be indexed as the (100), (110), (200), (210) and (300) reflections of a 2D hexagonal structure. In contrast to the (110) peak, the (100), (200) and (300) diffractions are highly intense suggesting an orientation of the channels parallel to the substrate. Accordingly, the TEM image of this film shows a mixed arrangement of hexagonally packed

mesostructures and, a high density of stripes suggesting the alignment of mesochannels parallel to the substrate. To support this interpretation, the influence of calcination on the film structure was examined. Accordingly, the XRD analysis (not represented) demonstrated the persistence of the mesostructure after calcinations, providing the direct evidence that a non-lamellar structure is formed. With a lower P123 concentration finally (x = 0.25), it seems that a cubic mesostructural ordering preferentially takes place. Our interpretation is based first on the TEM observation, and secondly on the XRD pattern of the as-irradiated films showing only a single intense peak in the 2θ range of 1°- 1.2° indexed as the (200) reflections of the *Im3m* cubic space group. Interestingly, the phase sequence lamellar → 2D hexagonal → cubic is fully consistent with the thermodynamics of amphiphilic aggregation of P123 in solution.

III. INSIGHT INTO THE MESOSTRUCTURATION MECHANISM

Like the EISA method, our photoinduced process presumably gives a prominent role to template self-organization to segregate the silica species into ordered hydrophilic mesodomains. However, the absence of silica sol, water and solvent in the initial formulation suggests a substantially different mechanism. In a view to shed light on the mesostructuring process, we have investigated the temporal evolution of the XRD patterns throughout the irradiation, as shown in Figure VII.8. For clarity reasons, experimental conditions (x = 0.50, RH = 50 % and I = 35 mW/cm²) have been chosen to promote the formation of model lamellar mesostructures.

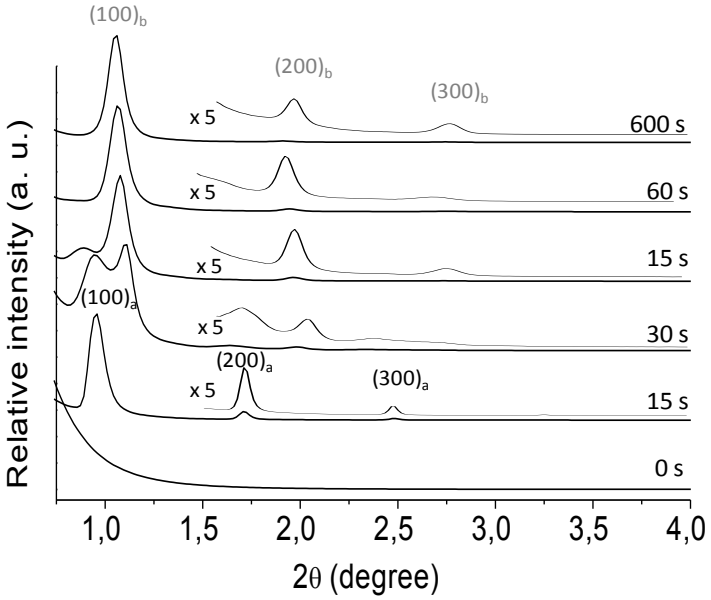

Figure VII.8: XRD patterns of as-synthesized x = 0.50 P123/PDMOS films exposed to various irradiation times ranging from 0 to 600 s, RH = 50 %, I = 35 mW/cm².

Prior to irradiation (t = 0 s), the precursor film does not exhibit any diffraction peak, which indicates that the PDMOS/P123/PAG mixture is isotropic and does not contain any preformed surfactant mesophase. PDMOS in its non-hydrolyzed form must be regarded as a good solvent of both PEO and PPO blocks inhibiting the block copolymer self-assembly. This result clearly evidences UV light as the unique stimulus of mesostructuration and polymerization. After only 15 s irradiation, the appearance of three (100), (200) and (300) reflection peaks marks the amorphous-to-order transition and the onset of a periodic P123/silica lamellar mesophase displaying a *d*-spacing of 9.2 nm. The intense and narrow (100) peak indicates that highly ordered mesostructures have been already generated at this early stage. A hydrolysis degree reaching 70 % is revealed by FTIR analysis (not represented), which illustrates that the silanol species participate actively to the self-assembly process. A complete hydrolysis of the methoxysilyl functions is achieved by continuing the irradiation (t = 30 s) and the corresponding XRD pattern shows this time a two-maximum peak in the 1° - 1.5° 2θ range. The deconvolution of this broad signal makes clearer the formation of a second lamellar mesophase with a decreased interlayer of 8.2 nm compared to the first lamellar mesophase. At t = 45 s, the progressive disappearance of the low angle peak (2θ = 0.9°) and the concomitant intensification of the second peak at larger angle (2θ = 1.1°) signifies the transformation (contraction) of the incipient lamellar structure. At t = 60 s, the proto-lamellar phase disappears and the XRD pattern shows a single lamellar phase with a stable interlayer distance of 8.2 nm.

From these XRD data, it is apparent that the onset of mesostructuration must lag behind the photogeneration of hydrolyzed species. Exposition to UV light liberates Brönsted superacids catalyzing hydrolysis reactions. The polarity increase resulting from the conversion of hydrophobic alkoxy precursors to hydrophilic silanol species drives the surfactant self-assembly. It seems that the reaction proceeds via a rapid preliminary hydrolysis of PDMOS to form poorly condensed transient silanol species. This creates suitable solvation conditions for the formation of a proto-lamellar structure (see the XRD pattern at t = 15 s). Additionally, the emergence of two distinct lamellar phases at t = 30 s and 45 s reveals significant insight into the self-assembly. Their evolution is consistent with a two-step mechanistic sequence decoupling hydrolysis and condensation reactions. First, transient mesostructures surrounded by poorly condensed hydrophilic silica species are generated, which can subsequently undergo Si-O-Si condensation in a manner which is compliant with a preorganized template. Such mechanism is apparent from the disappearance of the proto-lamellar mesophase ($d_{spa} \approx 9.2$ nm) and the formation of a more cross-linked and contracted mesostructures ($d_{spa} \approx 8.2$ nm). The estimated Δd_{spa} of ca. 1 nm between the two mesophases is totally in agreement with a shrinkage of the silica network due to more extended condensation reactions.[23] Furthermore, the condensation

of the silica network can be evidenced from the bands in the 1000-1250 cm^{-1} IR region mainly assigned to Si-O-Si antisymmetric stretching modes (Figure VII.9). Their gradual intensification is the sign that condensation occurs between the Si-OH groups of the trimethoxy head groups. In contrast to hydrolysis which is complete after 30 s, the condensation is active over a longer irradiation time. Thus, the FTIR data agrees with a two-step sequence hydrolysis and condensation.

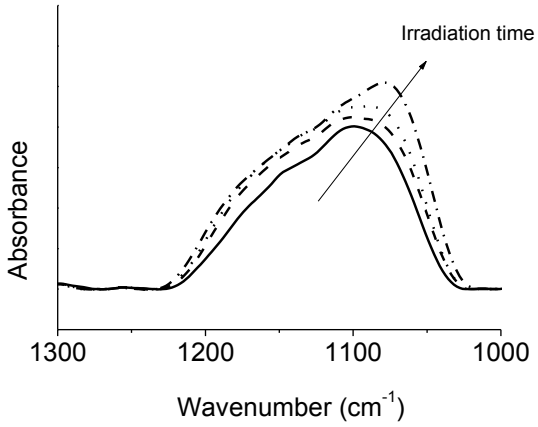

Figure VII.9: Temporal evolution of the IR spectra in the range 1000 - 1300 cm^{-1} of x = 0.50 P123/PDMOS films at various irradiation times: (—) 30 s, (- - -) 45 s, (… .) 60 s, and (- .-) 600 s, RH = 50 %, I = 35 mW/cm^2.

IV. TOWARD A 100% UV PROCESS

IV.1. PRINCIPLE AND IRRADIATION DEVICE

In surfactant templated mesoporous materials, the removal of surfactant appears generally as an unavoidable step to achieving porosity. Although a number of specific template-free routes have been reported,[24,25] most mesoporous materials are based on a templating approach that implies necessarily this final elimination step by solvent extraction and thermal calcination. As an alternative, deep or vacuum UV light (λ < 200 nm) has been utilized for the degradation of organic template at room temperature so as to obtain mesoporous silica[1,3,26,27] and non silica[28] films (see chapter IV page 118 for a state-of-the-art review). For the more energetic wavelenghts λ < 185 nm, the ablation method probably rests upon oxygen dissociation to produce ozone and atomic oxygen promoting the oxidation of the organic compounds. For the less energetic wavelengths λ > 254 nm, the degradation may proceed by direct cleavage of C-C and C-H bonds helped by the oxygenated reactives species. Compared to thermal calcination, this photocalcination method is carried out at ambient temperature and enables the use of temperature-sensitive substrates and a spatial control to produce patterned surfaces[2]. In

addition, it has been noted that a UV irradiation can strengthen the silica network due to post condensation of the silanol species. Finally, as template elimination is realized at room temperature film shrinkage, distorsion and damage are limited[29,30].

Here, we describe for the first time the synthesis of mesoporous silica films through an entire photoinduced process performing in one step self-assembly, condensation and surfactant degradation. Our procedure relies on a conventional medium-pressure mercury lamp equipped with a 254 nm reflector to enhance the emission of energetic photons < 300 nm. Such wavelength range permits the PAG photolysis, film mesostructuration and polymerization and the removal of surfactant. The key feature is to promote a slow enough degradation of the surfactant so that this latter can continue playing its structuring role before significant UV-induced cleavage alters its self-assembling properties. Uniquely, the same lamp can thus be used for the full process, obviating the need of excimer and low pressure mercury lamp commonly used for photocalcination and which are more harmful. Figure VII.9. represents in the same plot the UV absorption spectrum of the PAG together with the emission spectrum of this Hg-Xe lamp equipped with the 254 nm reflector.

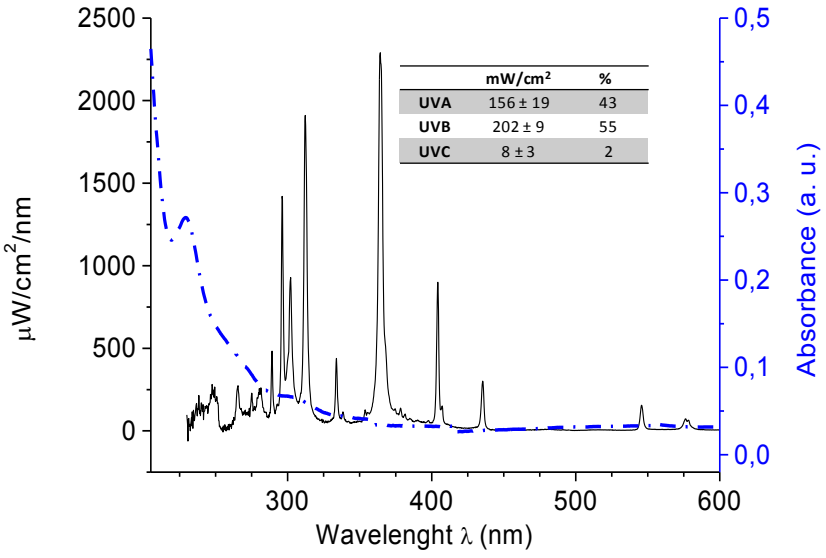

Figure VII.10: Overlapping of the PAG absorption spectrum (dash dotted line) in dichloromethane (5. 10^{-5} M) and the Hg-Xe lamp emission spectrum equipped with a 254 nm reflector (plain line) Insert: UVA, B and C proportion. (See chapter II, figure II.1 for similar figure with the lamp equipped with a 365 nm reflector)

IV.2. PREPARATION OF WORMLIKE MESOPOROUS FILMS BY A ONE-STEP UV PROCESS

IV.2.1. Kinetic study by RT-FTIR

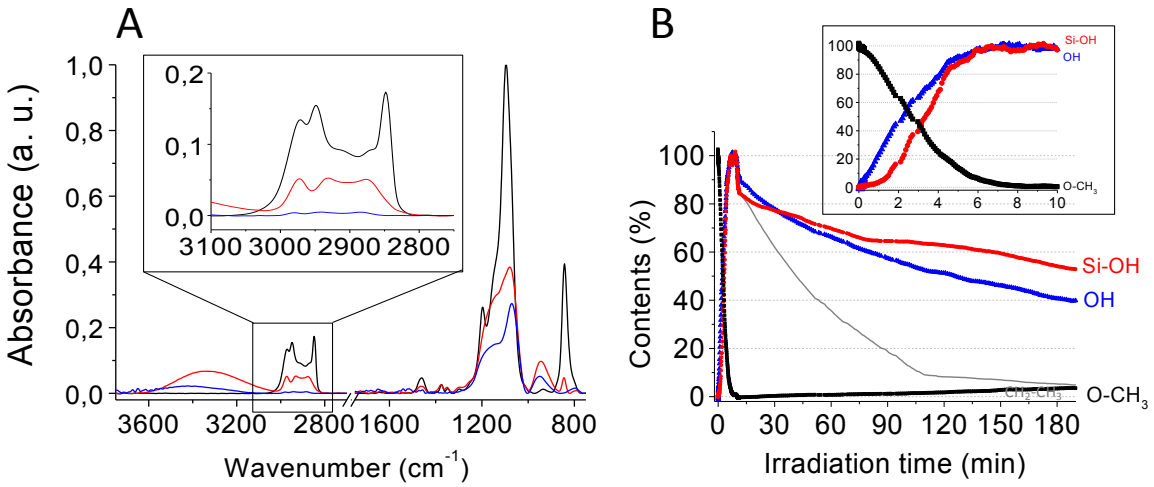

Figure VII.11: FTIR spectra of x = 0.50 P123/PDMOS film (__) before UV irradiation, (__) after 10 minutes of irradiation and (__) after 180 minutes of irradiation (A). Evolution of (■) ν sym O-CH_3, (●) ν Si-OH, (▲) ν OH (free) and (__) ν CH_2 and CH_3 of P123 within the irradiation time. RH = 30% and E = 400 mW/cm2 (B).

The possibility of a single-step synthesis was first examined with model wormlike mesostructured films. Films containing a wt. ratio P123/PDMOS of 0.5 were irradiated at I = 400 mW/cm^2. The structural changes during the UV irradiation were assessed by FTIR analysis (Figure VII. 11A). Before UV irradiation, we notice the presence of non-hydrolyzed PDMOS as shown by the sharp band at 2848 cm^{-1} corresponding to ν_{sym} O-CH_3. In addition, the CH_2 and CH_3 stretching bands of PEO and PPO in the 2800-3000 cm^{-1} range illustrates the presence of the amphiphilic block copolymer. Noteworthy is that no OH or silanol bands were present before irradiation. After 10 minutes UV irradiation, a mesostructured silica film is produced (*vide supra*). Accordingly, the UV spectrum shows a complete disappearance of the methoxy moieties (full hydrolysis), as well as the emergence of the SiOH (ν Si-OH) at 930 cm^{-1} and OH bands at ca. 3400 cm^{-1} . In addition, the presence of a broad OH band and the silanol band are representative of uncondensed silica species. In contrast, the CH_2 and CH_3 stretching and bending bands of the P123 are slightly affected at t =10 min, thus suggesting that the photodegradation of the template has hardly started. Indeed, we suppose that during the hydrolysis and the self-organization process, the template does not undergo a major decomposition. This is essential as the integrity of the template is required to guarantee a mesostructuration of the film. The evolution of the integrated absorbance of the bands ν_{sym} O-CH_3, ν Si-OH, ν OH and ν CH_2 and ν CH_3 of P123 within the irradiation time are summarized in Figure VII.11B.

After the first 10 min enabling the synthesis of the silica/surfactant mesotructured film, the sample was continuously exposed to UV light for additional 3 h in the same conditions. As shown in Figure VII.11A, there is almost no absorption in the 2800-3000 cm^{-1} at the end of the process (3h10min) indicating a complete degradation of the organic template. Most of the P123 decomposition (> 90 %) occurs within the first 120 minutes. The evolution of the ν CH_2 and ν CH_3 absorbance area in Figure VII.11B is used as a signature to estimate the gradual surfactant degradation. Concomitantly, a decrease in intensity of the OH and SiOH bands is observed as a proof of a progressive condensation of the inorganic network. In addition, after 3h UV treatment a more pronounced shoulder around 1200 cm^{-1} is present representative of Si-O-Si antisymmetric stretching band and provides evidence for the post-condensation of silica species[3,26]. Nevertheless, an important fraction of residual silanol (50%) remains in the film after template elimination, which are thus available for post-functionalization[29].

IV.2.2. Structural and textural characterization

XRD and TEM data of films irradiated 10 min and 3 h 10 min are provided in Figure VII.11. After 10 min, the film is hybrid as proved by FTIR analysis. Its XRD pattern displays a single broad diffraction peak assigned to a wormlike mesostructure. After 3h10min irradiation, the surfactant was removed, and the first strinking point is the preservation of the mesostructure. The only difference is the slight film shrinkage (~ 12%) because of further film condensation during the photocalcination process.

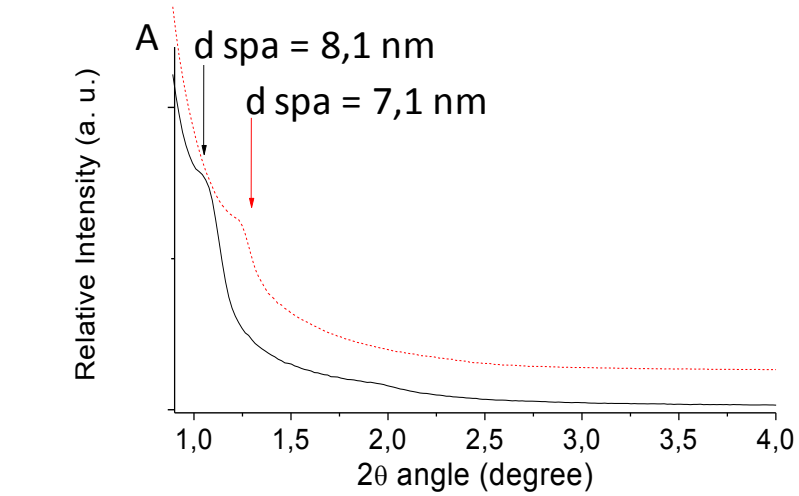

B

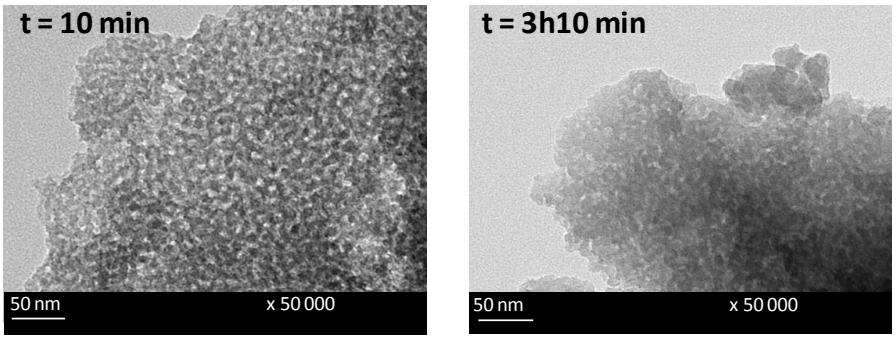

Figure VII.12: XRD patterns of x = 0.50 P123/PDMOS films (—) after 10 minutes and (-----) after 3h10 of irradiation (A). Corresponding TEM images (B). RH = 30% and E = 400mW/cm².

IV.2.3. Comparison with a two-step process: UV mesostructuration and thermocalcination

We have compared the latter single-step process with a conventional two-step process involving a synthesis of a silica/P123 mesostructured film by UV photopolymerization followed a thermal calcination. For this the UV irradiation time was obviously reduced to 10 min (x = 0.50, RH = 30%, E = 400 mW/cm²) instead of 3 h. Subsequently, the film was heated (2°/min) to 250°C for 3 h. To check the conservation of the mesostructure, TEM images before and after thermocalcination were represented in Figure VII.12. Like the photocalcined sample, the mesostructuration is preserved after elimination of the organic template, but a lower resolution is found.

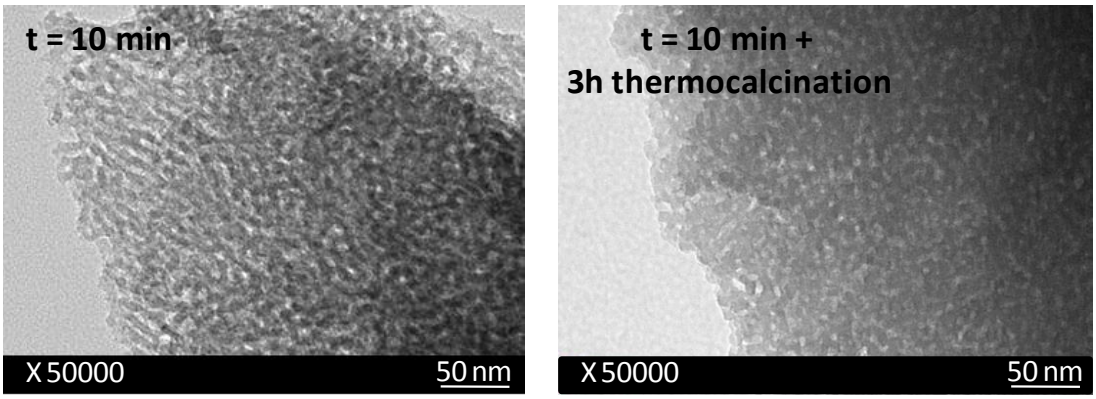

Figure VII.13: TEM images of x = 0.50 P123/PDMOS films after 10 minutes of irradiation and after 10 min irradiation (RH = 30% and E = 400mW/cm²) and thermocalcination (2°C/min up to 250°C + 1h @ 250°C).

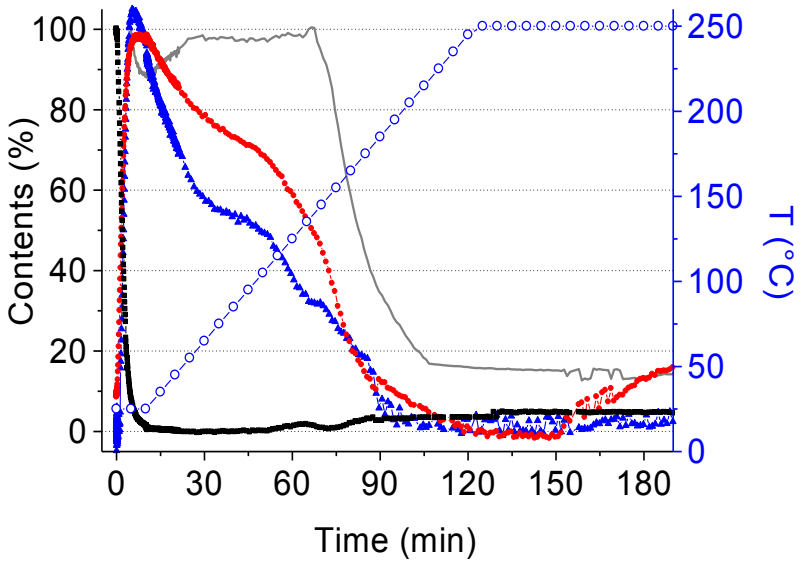

Figure VII.14: Evolution of (■) ν sym O-CH_3, (●) ν Si-OH, (▲) ν OH (free) and (—) ν CH_2 and CH_3 of P123 within the irradiation time (B). RH = 30%, E = 400 mW/cm² and t = 10 min then thermocalcination for 3 hours (2°C/min up to 250°C + 1h @ 250°C)

The evolution of FTIR spectra during the thermal calcination only are represented in Figure VII.14. Like the previous method, a complete disappearance of CH_2 and CH_3 stretching bands in the 2800- 3000 cm^{-1} region is observed suggesting a complete elimination of the organic template. Nevertheless, important differences can be noticed between the thermal and photochemical calcination processes. OH and SiOH bands are no longer present after thermal decomposition of the surfactant; this might be related to the increase of temperature which favors an extensive condensation of the inorganic network. In addition, the elimination actually occurs above a threshold temperature of 180°C. The elimination of P123 is then fast and brutal whereas the photoinduced elimination is slow and progressive. Photocalcination process proves

to be a softer approach for template elimination, taking place at room temperature, with the benefit of conserving most silanol species.

IV.3. A ONE STEP UV PROCESS TO PERIODIC ORGANIZED MESOPOROUS SILICA FIMS

In a last experiment, our one step procedure was tentatively applied to prepare an ordered mesoporous silica film. Exploiting the results obtained at the beginning of this chapter, a P123/PAG/PDMOS film (0.35/0.02/1 wt ratio) was first irradiated for 40 min at 60 mW/cm² at RH = 50% to afford an hexagonally packed hybrid mesostructure. Irradiation for 180 additional min at 400 mW/cm² at RH = 30% was performed subsequently to photocalcine the P123 surfactant. Using RT-FTIR, we probed the temporal evolution of O-CH_3 (2848 cm^{-1}), Si-OH (930 cm^{-1}) and OH bands (3400 cm^{-1}) as well as CH_2 and CH_3 bands of P123 template as shown in Figure VII.15

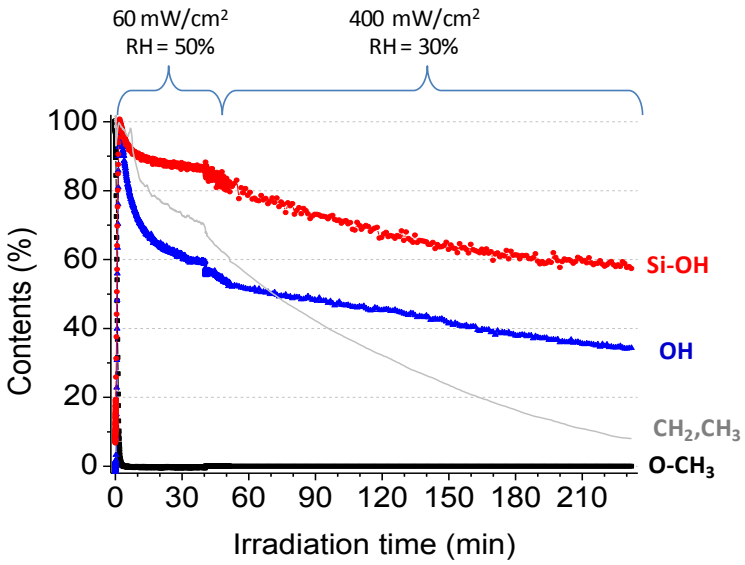

Figure VII.15. Evolution of (■) ν sym O-CH_3, (●) ν Si-OH, (▲) ν OH (free) and (—) ν CH_2 and CH_3 of P123 within the irradiation time. RH = 50% and E = 60 mW/cm², t = 40 min then RH ≈ 30%, E = 400 mW/cm² and t = 3 h.

Like the wormlike system, photocalcination demonstrates to be efficient with long range ordered systems since most P123 (> 90%) was eliminated at the end of the process. We suppose that the ≈ 10% remaining are not directly P123 but rather residue from the chain break that are trapped in the film. The degradation is soft, leaving an important fraction of residual silanol (≈ 60%) and OH species (≈ 40%) conserved. However, we observed that a slower disappearance of P123 in comparison with the disordered system. We suggest that this result might be related to organized system favoring higher condensation degree. XRD pattern (Figure VII.16) and TEM data (Figure VII.17) are consistent with 2D-hexagonal structure that seems to be conserved after

the photocalcination process. Thus, the intense (100) (200) and (300) peaks indicative of hexagonal channels aligned with the substrate are clearly present after the synthesis step (t= 40 min). At t = 210 min, the film is devoid of surfactant but the mesostructure is still maintained. The latter three peaks are still present as well as an additional (110) peak is visible.

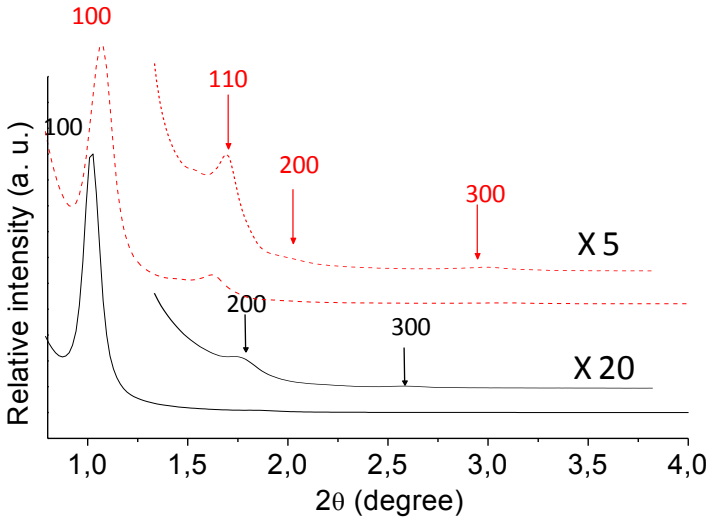

Figure VII.16: **XRD patterns of x = 0.35 P123/PDMOS films (——) RH = 50% and E = 60 mW/cm², t = 40 min and (-----) RH = 50% and E = 60 mW/cm², t = 40 min then RH ≈ 30% E = 400 mW/cm² and t = 3 h.**

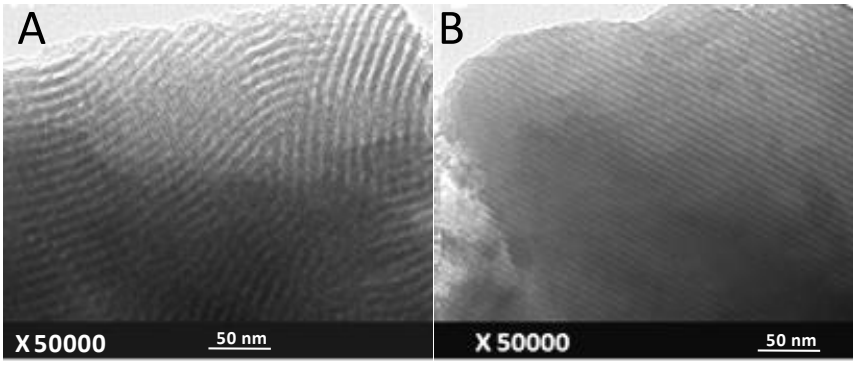

Figure VII.17: **TEM images of x = 0.35 P123/PDMOS films "as prepared" (A) and photocalcined (B). RH = 50% and E = 60 mW/cm².**

CONCLUSION

We have developed and optimized a UV-mediated pathway to surfactant templated periodic mesostructured films. As in a conventional evaporation induced self-assembly method, the processing conditions are critical to successfully self-assemble the amphiphilic copolymer and to order the resulting mesophases over large surface area (long-range order). The irradiation of the

films in an environmental chamber enabled to evidence the effect of several experimental parameters on mesostructuration. The keys to forming well-ordered films are to control the relative humidity and the exitance. In this regard, it is believed that the PEO and PPO domains in a mesostructured samples should be in separate domains, especially in higher humidity conditions since water is a nonsolvent for PPO but a good solvent for PEO. Clearly, humidity inside the sample plays two significant roles: it enhances the copolymer self-assembly ability and it promotes the formation of long-range ordered mesostructure. The disorder-to-order phase transformation is also sensitive to condensation kinetics. Decreasing the exitance slowdowns the formation rate of photoacids in a way to permit the reorganization of the organic surfactant species into highly ordered mesophases. XRD combined with FTIR were employed to study the light-induced self-assembly. In particular, we must emphasize the role of the *in situ* photogenerated silanol species in promoting self-assembly. In absence of solvent, these species apparently serve as nonvolatile hydrophilic fluids that replace water to induce the mesostructuration. By studying model lamellar silica/surfactant films, a two-step mechanistic sequence was evidenced implying the generation of transient mesostructures containing hydrolyzed species subsequently fixed by further condensation reactions. Finally, in a last point we displayed that it was possible to prepare mesoporous silica films by a new and original single step UV process. With the same light source, UV is used in a first time to induce film mesostructuration and in a second time deeper UV (UVC) are employed to eliminate the organic surfactant. We showed that the process is adapted for wormlike and ordered films as well.

CHAPTER VII REFERENCES

(1) Hozumi, A.; Yokogawa, Y.; Kameyama, T.; Hiraku, K.; Sugimura, H.; Takai, O.; Okido, M. *Adv. Mater.* **2000**, 12, 985.

(2) Dattelbaum, A. M.; Amweg, M. L.; Ecke, L. E.; Yee, C. K.; Shreve, A. P.; Parikh, A. N. *Nano Letters* **2003**, 3, 719.

(3) Dattelbaum, A. M.; Amweg, M. L.; Ruiz, J. D.; Ecke, L. E.; Shreve, A. P.; Parikh, A. N. *J. Phys. Chem. B* **2005**, 109, 14551.

(4) Dhaval A. Doshi; Nicola K. Huesing; Mengcheng Lu; Hongyou Fan; Yunfeng Lu; Kelly Simmons-Potter; B. G. Potter, J.; Alan J. Hurd; Brinker, a. C. J. *Science* **2000**, 290, 107.

(5) De Paz, H.; Chemtob, A.; Croutxé-Barghorn, C.; Rigolet, S.; Lebeau, B. *Micropor. Mesopor. Mat.* **2012**, 151, 88.

(6) De Paz-Simon, H.; Chemtob, A.; Crest, F.; Croutxe-Barghorn, C.; Michelin, L.; Vidal, L.; Rigolet, S.; Lebeau, B. *RSC Advances* **2012**, 2, 11944.

(7) De Paz-Simon, H.; Chemtob, A.; Croutxé-Barghorn, C.; Rigolet, S.; Michelin, L.; Vidal, L.; Lebeau, B. *Langmuir* **2013,** 29, 1963.

(8) Nagarajan, S.; Bosworth, J. K.; Ober, C. K.; Russell, T. P.; Watkins, J. J. *Chem. Mater.* **2007**, 20, 604.

(9) Cagnol, F.; Grosso, D.; Soler-Illia, G. J. d. A. A.; Crepaldi, E. L.; Babonneau, F.; Amenitsch, H.; Sanchez, C. *J. Mater. Chem.* **2003**, 13, 61.

(10) Grosso, D.; Cagnol, F.; Soler-Illia, G. J. d. A. A.; Crepaldi, E. L.; Amenitsch, H.; Brunet-Bruneau, A.; Bourgeois, A.; Sanchez, C. *Adv. Funct. Mater.* **2004**, 14, 309.

(11) Soler-Illia, G. J. d. A. A.; Crepaldi, E. L.; Grosso, D.; Sanchez, C. *Curr. Opin. Colloid In.* **2003**, 8, 109.
(12) Nicole, L.; Boissiere, C.; Grosso, D.; Quach, A.; Sanchez, C. *J. Mater. Chem.* **2005**, 15, 3598.
(13) Sanchez, C.; Boissière, C.; Grosso, D.; Laberty, C.; Nicole, L. *Chem. Mater*. **2008**, 20, 682.
(14) Bagshaw, S. A.; Prouzet, E.; Pinnavaia, T. J. *Science* **1995**, 269, 1242.
(15) Kim, S.-S.; Pauly, T. R.; Pinnavaia, T. J. *Chem. Commun.* **2000**, 835.
(16) Tanev, P. T.; Pinnavaia, T. J. *Science* **1995**, 267, 865.
(17) Alberius, P. C. A.; Frindell, K. L.; Hayward, R. C.; Kramer, E. J.; Stucky, G. D.; Chmelka, B. F. *Chem. Mater.* **2002**, 14, 3284.
(18) Alexandridis, P.; Lindman, B. *Amphiphilic Block Copolymers: Self-Assembly and Applications*; Elsevier Science, **2000**.
(19) Crepaldi, E. L.; Soler-Illia, G. J. d. A. A.; Grosso, D.; Cagnol, F.; Ribot, F.; Sanchez, C. *J. Am. Chem. Soc.* **2003**, 125, 9770.
(20) De Paz, H.; Chemtob, A.; Croutxé-Barghorn, C.; Le Nouen, D.; Rigolet, S. *J. Phys. Chem. B* **2012**, 116, 5260.
(21) Huo, Q.; Margolese, D. I.; Ciesla, U.; Demuth, D. G.; Feng, P.; Gier, T. E.; Sieger, P.; Firouzi, A.; Chmelka, B. F. *Chem. Mater.* **1994**, 6, 1176.
(22) Zhao, D.; Feng, J.; Huo, Q.; Melosh, N.; Fredrickson, G. H.; Chmelka, B. F.; Stucky, G. D. *Science* **1998**, 279, 548.
(23) Grosso, D.; Balkenende, A. R.; Albouy, P. A.; Ayral, A.; Amenitsch, H.; Babonneau, F. *Chem. Mater.* **2001**, 13, 1848.
(24) Yu, J.; Su, Y.; Cheng, B. *Adv. Funct. Mater.* **2007**, 17, 1984.
(25) Chi, B.; Zhao, L.; Jin, T. *J. Phys. Chem. C* **2007**, 111, 6189.
(26) Clark, T.; Ruiz, J. D.; Fan, H.; Brinker, C. J.; Swanson, B. I.; Parikh, A. N. *Chem. Mater*. **2000**, 12, 3879.
(27) Eslava, S.; Iacopi, F.; Baklanov, M. R.; Kirschhock, C. E. A.; Maex, K.; Martens, J. A. *J. Am. Chem. Soc.* **2007**, 129, 9288.
(28) Parikh, A. N.; Navrotsky, A.; Li, Q.; Yee, C. K.; Amweg, M. L.; Corma, A. *Micropor. Mesopor. Mat.* **2004**, 76, 17.
(29) Hozumi, A.; Sugimura, H.; Hiraku, K.; Kameyama, T.; Takai, O. *Chem. Mater*. **2000**, 12, 3842.
(30) Hozumi, A.; Sugimura, H.; Hiraku, K.; Kameyama, T.; Takai, O. *Nano Letters* **2001**, 1, 395.

GENERAL CONCLUSION

In this PhD manuscript, we have attempted to establish the main principles and concepts governing the photoinduced sol-gel polymerization under photoacid or photobase catalysis. The knowledge gained has served subsequently to design a novel UV-driven synthesis procedure to mesoporous silica films.

RT-FTIR was an essential tool to monitor hydrolysis and condensation reactions, to study the change in structural composition, and to identify the released by-products. Uniquely, hydrolysis depends on atmospheric water permeation through the film, as a result there is no direct addition of water in the film composition. Hydrolysis kinetics were strongly sensitive to film thickness and RH in the case of methoxysilane precursors. Substitution with more hindered ethoxysilane made the process both dependent on water permeation and intrinsic kinetics parameters like the PAG concentration and irradiance. For the first time, a complete picture of this inorganic photopolymerization has been provided. Not only photogenerated acids but also direct interaction with UVC wavelengths were proved to be responsible for a densification of the inorganic network during a photoacid-catalyzed sol-gel process of alkoxysilane inorganic films. Furthermore, it was possible to use α-aminoketone photobase as alternative photocatalyst of alkoxysilane sol-gel reactions. The type of catalyst had a significant effect on film properties. In acid catalysis, smooth, dense and optically transparent films were obtained while rough, particulate and opalescent films were prepared in basic conditions. Photopolymerization was also successfully applied for the cross-linking of silicone oligomers with either photacid or photobase catalysts. In addition, a range of original photobase-catalyzed organic cross-linking reactions could be contemplated. α-aminoketone photobase was efficient for epoxy-thiol, thiol-isocyanate and anionic photopolymerization. In addition, very promising results were obtained with hydridosilane precursors in which SiH is successively converted in SiOH then Si-O-Si. These latter results suggest interesting perspectives for the future of photocatalysts in hybrid materials science. In future works, other photoreleased tertiary amines could be studied.

A second focus has been the preparation of mesoporous silica films using an innovative UV pathway. Starting with an initial formulation without solvent and water, wormlike mesostructured films with a specific surface up to 650 $m^2.g^{-1}$ were achieved. However, in our first investigations using a UV conveyor, it was not possible to prepare films endowed with a long range order, presumably because of the lack of control over humidity, temperature and irradiance. The type of surfactant was found to play a significant role in the final material porosity. PEO-*b*-PPO-*b*-PEO soluble with the PDMOS oligomeric precursor was found to be a suitable template. RT-FTIR was useful to characterize completely hydrolysis and condensation kinetics. For the first time, this

technique was also employed to shed light on mesophase segregation occurring within the film during the mesostructuration. Indeed, CH_3 symmetric deformation mode of the PPO block (δCH_3 ≈ 1374 cm^{-1}) is sensitive to the local microenvironment and was used as a marker for self-assembly. Additionally, solid-state NMR highlighted difference of mobility and hydration of the PPO block between non structured and mesostructured sample. In a new irradiation set-up enabling the RH and light intensity to be precisely controlled, periodically ordered mesoporous films were eventually achieved. Under these conditions, the variation of the template/PDMOS ratio gave birth to a range of mesostructures (lamellar, 2D hexagonal, cubic). However, the irradiation performed in an environmental cell led to limited surface area sample (≈ 1 cm^2). Further works aim to scale-up the process using affordable and easily scalable UV fluorescent lamps. Finally, a fully UV-driven process was implemented in which surfactant self-assembly and subsequent degradation of surfactant were performed by UV activation in one-step lasting approximately 3 hours. To our knowledge, it is the first single-step process to mesoporous silica materials based on template route. Optimization of this innovative route is currently carried out.

As a final word of outlook, the LISA process developed during this PhD is simple, innovative and may be adaptable to a broad range of surfactants. Indeed, a first perspective would be the use of other templates based on ionic liquid or siloxane block copolymers. Indeed, in contrast to conventional ionic surfactants, ionic liquids are susceptible to exhibit a good solubility in PDMOS precursor due to the liquid state of the surfactant. Siloxane block copolymers could also be very promising; they could ensure the solubility with the inorganic precursor and form preformed mesophase before irradiation. Mesoporous films could therefore be prepared by direct nanocasting. Furthermore, this project creates new opportunities for novel applications. For example, the well-defined wormlike mesoporous films exhibiting high specific area would be a suitable candidate as permselective membrane. In addition, periodically ordered mesoporous films could be applied as low k dielectric films after optimization of the process and hydrophobic treatment. In general, a broad application scope could be considered, if one foresees all the achievements already accomplished by films prepared with the EISA method. Last but not least, we showed in the first part of the manuscript that it was easy to prepare hybrid films by incorporation of organosilane and direct co-condensation with inorganic network. Elaboration of mesoporous material having organic-inorganic hybrid walls by a photosol-gel process is very encouraging. A particularly promising research field for this photoinduced pathway would be the development of photopatterned mesoporous inorganic and hybrid films owing to unique capabilities related to spatial and temporal control of the photopolymerization.

CONCLUSION

Dans ce manuscrit de thèse, nous avons tenté d'établir les principaux concepts qui gouvernent la polymérisation sol-gel photoinduite catalysée par des photoacides ou des photobases. Les connaissances acquises ont par la suite servi pour concevoir une nouvelle voie de synthèse UV pour la préparation de films mésoporeux.

La RT-FTIR a été un outil essentiel pour suivre les réactions d'hydrolyse et de condensation, étudier les changements structuraux et identifier les sous-produits de la réaction.. L'hydrolyse dépend principalement de la pérméation de l'eau atmosphérique dans le film, conséquence directe de l'absence d'eau dans la formulation initiale. Les cinétiques d'hydrolyse sont très sensibles à l'épaisseur du film et au taux d'humidité relative dans le cas du précurseur PDMOS. La substitution des groupements méthoxy par des groupements plus encombrés éthoxy rend le procédé dépendant à la fois de la pérméation de l'eau et de paramètres cinétiques intrinsèques tels que la concentration en PGA et l'intensité lumineuse. Pour la première fois, une représentation complète de la photopolymérisation inorganique a été fournie. Lors du procédé sol-gel catalysé par des photoacides, à la fois les acides photogénérés et les longueurs d'onde UVC sont responsables de la densification du réseau inorganique. De plus, il a été possible d'utiliser une photobase de type α-aminocétone pour catalyser des réactions sol-gel à partir de précurseurs alkoxysilane. Le choix du type de catalyseur a un effet significatif sur les propriétés du film. En catalyse acide, des films lisses, denses et optiquement transparents ont été obtenus alors que la catalyse basique favorise la formation de films rugueux, particulaires et opalescents. La photopolymérisation a aussi été appliquée avec succès à la réticulation d'oligomères siliconés grâce à des catalyseurs photoacides et photobases. Une série de réactions organiques originales a pu ainsi être envisagée. La photobase α-aminocétone s'est montrée efficace pour la catalyse de réactions de type epoxy-thiol, thiol-isocyanate et photopolymérisation anionique. De plus, des résultats très prometteurs ont été obtenus avec des précurseurs hydridosilane, les groupements SiH sont successivement convertis en SiOH puis en Si-O-Si. Ces résultats offrent des perspectives intéressantes pour de futurs photocatalyseurs pour les matériaux hybrides. En perspective, d'autres amines tertiaires photogénérées pourront être étudiées.

Un second point d'intérêt a été la préparation de films de silice mésoporeuse en passant par un procédé innovant basé sur l'UV. Partant d'une solution initiale sans eau ni solvant, des films mésoporeux vermiculaires ont été obtenus avec une surface spécifique allant jusqu'à 650 $m^2\ g^{-1}$. Néanmoins, avec les synthèses réalisées sous le convoyeur UV, il n'a pas été possible de préparer des films avec un ordre à grande échelle. Nous avons suggéré que ceci était dû à un manque de contrôle du taux d'humidité, de la température et de l'intensité lumineuse. Le type de tensioactif

joue aussi un rôle prédominant dans la porosité du matériau final. Le copolymère tribloc PEO-*b*-PPO-*b*-PEO soluble dans le PDMOS est un bon agent structurant. La RT-FTIR a été particulièrement utile pour caractériser les cinétiques d'hydrolyse et de condensation. Pour la première fois, cette technique a aussi été utilisée pour mettre en avant la ségrégation de phase lors de la mesostructuration du film. En effet, la bande de déformation symétrique du CH_3 du PPO ($\delta CH_3 \approx 1374$ cm^{-1}) est sensible au microenvironnement local et a été utilisée comme marqueur de la séparation de phase. De plus, la RMN solide a souligné les différences de mobilité et d'hydratation des blocs PPO entre les systèmes amorphes et mésostructurés. Par la suite, grâce à un nouveau système d'irradiation qui permet un contrôle précis du taux d'humidité et de l'intensité lumineuse, des films mésoporeux avec une organisation périodique ont été élaborés. La variation du ratio tensioactif/PDMOS a permis d'atteindre différentes mésostructures (lamellaire, 2D hexagonale, cubique). Cependant l'irradiation étant réalisée dans une cellule environnementale, la surface irradiée est limitée à ≈ 1 cm^2. D'autres travaux ont été réalisés dans le but d'augmenter l'échelle du procédé, notamment grâce à des lampes UV fluorescentes. Au final, un procédé complètement basé sur l'UV a été développé ; l'assemblage du tensioactif puis sa photodégradation sont réalisés par l'activation UV en une seule étape durant approximativement 3 heures. A notre connaissance, c'est le premier procédé en une seule étape proposé pour la préparation de silice mésoporeuse. L'optimisation de cette voie de synthèse innovante est actuellement en cours.

D'un point de vue final, le procédé LISA (Light Induced Self-Assembly) développé au cours de cette thèse est simple, innovant et peut s'adapter à un large panel de tensioactifs. En effet, une des perspectives serait l'utilisation d'autres agents structurants basés sur des liquides ioniques ou des copolymères à bloc siloxane. En effet, contrairement aux tensioactifs ioniques conventionnels, les liquides ioniques sont susceptibles d'avoir une bonne solubilité dans le PDMOS grâce à l'état liquide du tensioactif. Les copolymères à bloc siloxane sont aussi très prometteurs ; la partie siloxane va assurer la miscibilité avec le précurseur inorganique ainsi des mésophases pourront être préformées avant l'irradiation. Des films mésoporeux pourront donc être préparés par « nanocasting » direct. En outre, ce projet crée de nouvelles opportunités pour de nouvelles applications. Par exemple, les films vermiculaires ayant une surface spécifique élevée seraient de très bons candidats comme membranes permsélectives. Les films organisés après optimisation du procédé et traitement hydrophobe peuvent être utilisés comme membrane à constante diélectrique très faible. De manière générale, un large champ d'applications peut être envisagé ; Finalement, nous avons montré dans la première partie du manuscrit qu'il était possible de préparer par voie photosol-gel des matériaux hybrides par incorporation d'organosilane et direct co-condensation avec le réseau inorganique. La préparation de films mésoporeux avec des parois

hybrides organique-inorganique par ce procédé photoinduit est très encourageante. Un champ de recherche particulièrement prometteur serait le développement de films inorganiques et hybrides photopatternés. Ceci est possible uniquement grave à la capacité de contrôle spatio-temporel de la photopolymérisation.

APPENDIX

APPENDIX I: DETAILS OF THE INORGANIC PRECURSORS

I. FTIR SPECTRA

Figures A1.1 and A1.2 represent FTIR spectra of liquid PDMOS and PDEOS precursors before UV irradiation. Assignment for major vibrations bands is also given on the figure. Liquid films were deposited with a bar coater onto a BaF_2 pellet. Liquid film thickness is respectively 0.9 and 2.1 µm for PDMOS and PDEOS.

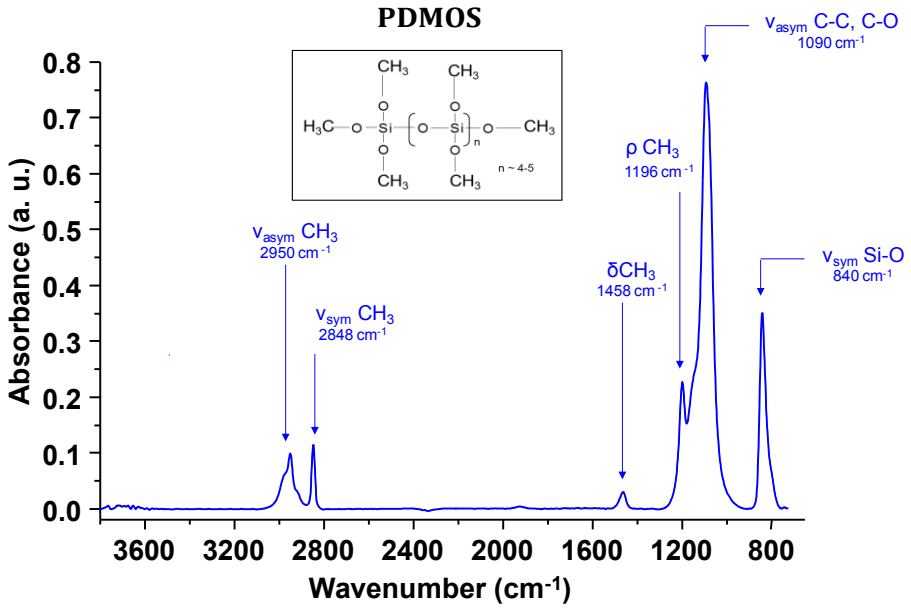

Figure A1.1: FTIR spectrum of PDMOS before UV irradiation

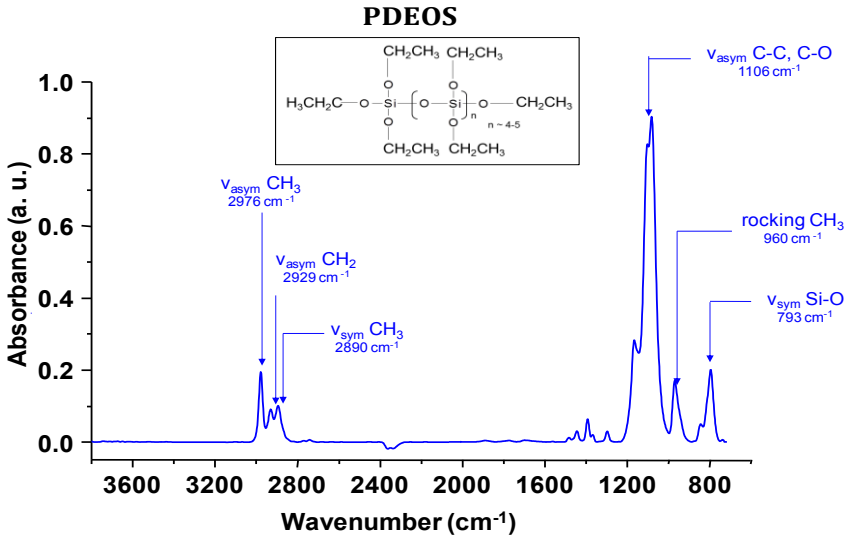

Figure A1.2: FTIR spectrum of PDEOS before UV irradiation

II. LIQUID STATE NMR STUDY:

In order to have more information on these precursors, liquid state NMR was performed. Spectra were obtained using a Bruker Avance spectrometer equipped with a Bruker broad-band BBI 5 mm probe. They were acquired at 79.49 MHz for ^{29}Si nuclei in $CDCl_3$ solution (30 vol %) without proton decoupling. Tetrametylsilane (TMS) was used as internal reference. A recycled delay of 20 s is sufficient for full spin relaxation, and the spectra were acquired for 12 h at room temperature using a π/3 pulse with a pulse time of 15 μs.

Although the ^{29}Si liquid-state NMR spectra are quite complex (Figure A1.3 and A1.4), they were useful for the speciation of the oligomeric silicate condensates, and the absence of hydrolysis products has simplified somehow the interpretation. Note that the multiplicity of resonances originates not only from the variety of possible silicate oligomers, but also from acquisition conditions performed without proton decoupling.

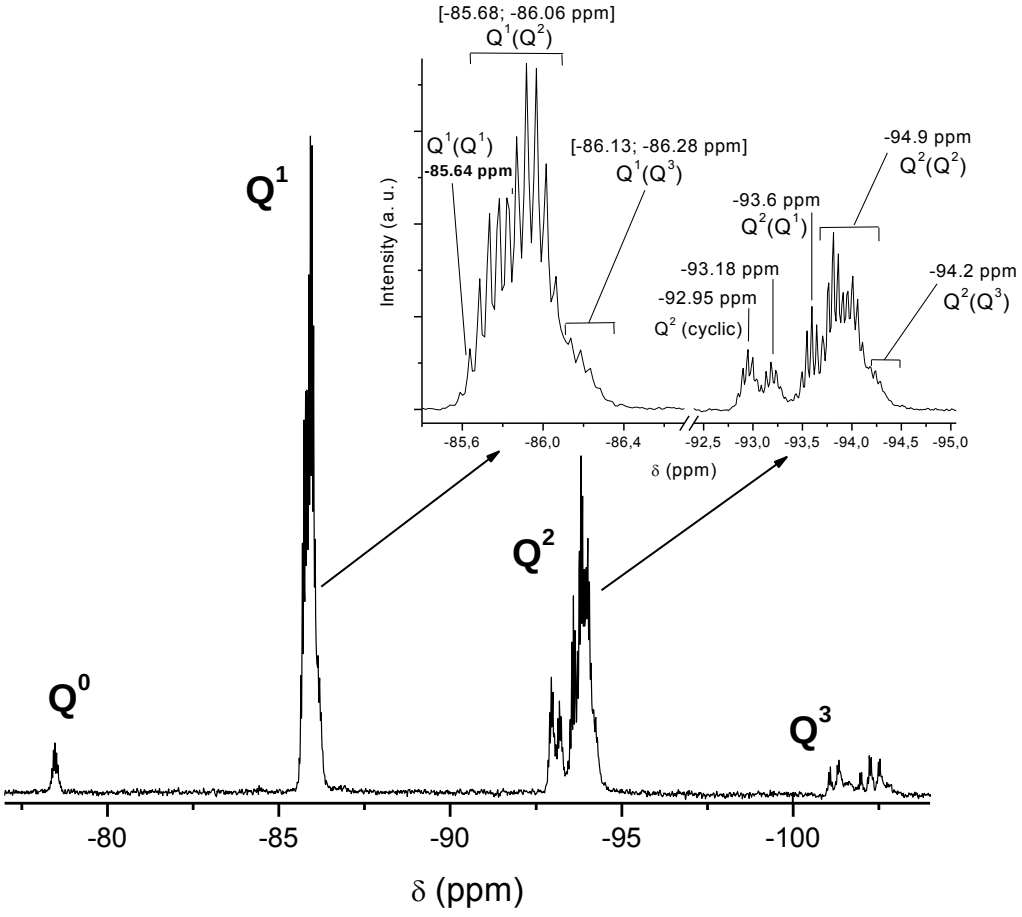

Figure A1.3: ^{29}Si liquid state NMR spectrum of PDMOS

The PDMOS spectrum contains four signals Q^0, Q^1, Q^2 and Q^3, the subscript referring to the number of siloxane bonds of the silicon atom. The Q^0 signal (δ = -78.47 ppm) represents less

than 2 % of the silicon atoms and was readily attributed to traces of TMOS monomers. The restricted range of chemical shifts (-78.42 - -78.52 ppm) confirms that the Q^0 species are fully methoxylated. The Q^1 range in which the silicon of interest is bonded to a single other OSi displayed a number of resolved signals. The precise assignment of all these signals is obviously not possible, giving the multitude of possible structures. However, families of Q^1 siloxane subspecies can be identified on the basis of the literature results[1-3]. We note the minority contribution from the Q^1 dimers (Q^1-Q^1) at -85.64 ppm. A progressive intensity increase is observed for the downfield signals which are attributed to Q^1 end groups connected to Q^2. The resolved differences in Q^1 silicon resonances correspond to terminal Q^1 in trimer (Q^1-Q^2-Q^1), tetramer ($Q^1Q^2Q^2Q^1$), pentamer ($Q^1Q^2Q^2Q^2Q^1$) linear oligomers and possibly longer oligomers. The upfield shoulder at -86.18 ppm was assigned to a smaller fraction of Q^1 attached to Q^3 branched species (for example $Q^1Q^3Q^1Q^1$). The observation of the Q^2 resonances showed the contribution from cyclic species in two complex upfield signals at -92.95 and -93.18 ppm. For example, Brunet et al. attributed these signals to tri- or tetra-siloxane species[4]. Linear and branched structures are known to cause the silicon resonance to shift towards more negative values. This accounts for the formation of the wide signal dominating the Q^2 range. The breadth of the Q^2 resonances is due to the overlap of a larger number of single resonance lines produced as a result of the highly varied environment of the silicon nuclei of condensed oligomeric species. The group of upfield signals around -93.6 ppm was tentatively attributed to Q^2 attached to Q^1 species. The dominant group of resonance lines at -94.9 ppm might correspond to Q^2 attached to other Q^2, which are the more abundant and translate the presence of longer chains. Similarly to Q^1, the shoulder at -94.2 ppm hints the distinctive presence of Q^2 connected to Q^3. Only weal signals (~ 4%) assigned to Q^3 environments were finally observed in the region -100 and -103 ppm.

Compared to PDMOS, the ethoxy silicate derivative is characterized by a higher proportion in Q^0 (7.9 % at -81.98 ppm) and Q^3 species (16.4 % between -101 and -105 ppm)). The shape of the Q^1 and Q^2 signals are relatively similar to the previous description and a similar reasoning applies in this case. We note also the importance of cyclic siloxane species (Q^2_C) around -95.5 ppm, which are more prominent in PDEOS than in PDMOS. As suggested by Kelts *et al.* [2], cyclisation of silicate condensates strongly depends on steric considerations.

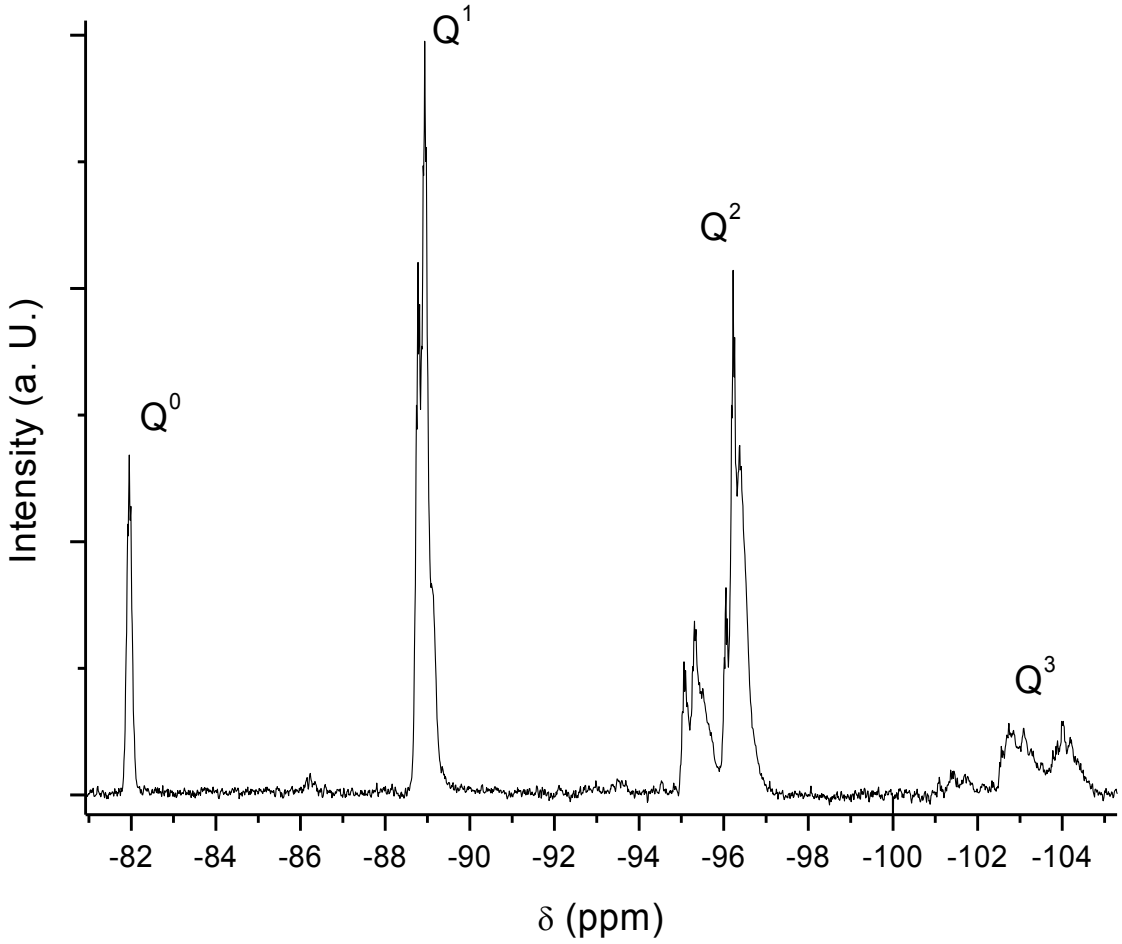

Figure A1.4: **^{29}Si liquid state NMR spectrum of PDEOS**

REFERENCES

(1) Depla, A.; Verheyen, E.; Veyfeyken, A.; Van Houteghem, M.; Houthoofd, K.; Van Speybroeck, V.; Waroquier, M.; Kirschhock, C. E. A.; Martens, J. A. *J. Phys. Chem. C*, **2011**, 115, 11077-11088.
(2) Kelts, L. W.; Effinger, N. J.; Melpolder, S. M. *J. Non-Cryst. Solids* **1986**, 83, 353-374.
(3) Lippert, J. L.; Melpolder, S. B.; Kelts, L. M. *J. Non-Cryst. Solids* **1988**, 104, 139-147.
(4) Brunet, F.; Cabane, B. *J.Non-Cryst. Solids* **1993**, 163, 211-225.

APPENDIX II: MAINS CHARACTERIZATION TECHNIQUES

I. FTIR (FOURIER TRANSFORM INFRARED SPECTROSCOPY)

I.1. PRINCIPE

FTIR spectroscopy is a quantitative and powerful tool exploiting the fact that molecules absorb specific frequencies characteristic of their structure. It allows analysis of molecular structure by determination of the presence (or not) of functional moieties. By coupling the spectrometer with a MCT (Mercury-Cadmium-Tellure) detector cooled with liquid nitrogen it is possible to considerably decrease spectra acquisition time as developed by Decker *et al.* in the 1990s[1]. RT-FTIR is particularly adapted to follow photopolymerization reaction. This technique is thus called "real-time" or time resolved Fourier transform infrared spectroscopy (RT-FTIR).

When photosensitive initial formulations are exposed to UV light, intensity of IR bands corresponding to functional moieties decreases (or increases) due to their degradation (or formation). The degree of conversion is directly related to the decrease in IR absorbance of the relevant band, and can be calculated as follows:

$$\text{Conversion } (\%) = \frac{(A)_0 - (A)_t}{(A)_0} \text{ x } 100$$

Where $(A)_0$ and $(A)_t$ are the area of the absorption bands before exposure (t = 0) and at irradiation time t respectively.

I.2. EXPERIMENTAL CONDITIONS

Irradiation was performed at room temperature under a UV irradiation device implemented for RT-FTIR, in which formulations were simultaneously exposed to UV light and to an IR analytical beam. Infrared spectra obtained by RT-FTIR were recorded in transmission mode with a Bruker Optics Vertex 70 spectrophotometer equipped with a liquid-nitrogen-cooled mercury-cadmium telluride (MCT) detector. The resolution of the infrared spectra was 4 cm^{-1}. All spectra were baseline corrected prior to integration with the software OPUS 6.5.

II. ^{29}Si solid state NMR (Nuclear Magnetic Resonance)

II.1. Principe

^{29}Si solid state NMR spectroscopy was a powerful tool to bring important information on the siloxane network crosslinking and the extent of condensation for the different system used in this thesis. This technique is based on the study of atoms nuclear spin when they are placed in a magnetic field. Resulting interactions are susceptible to give structural information on the material. Typically, chemical shift (compared to a reference) allows characterization of a nucleus local environment.

However compared to liquid NMR, solid state NMR generally displays larger peaks. Here we discuss two ways to minimize this effect:

- Magic Angle Spinning (MAS)[2,3]: this technique consists in spinning the sample (usually at a frequency of 1 to 70 kHz) at the magic angle θ_m (ca. 54.74°, where $\cos^2\theta_m=1/3$) with respect to the direction of the magnetic field, the normally broad lines become narrower, increasing the resolution for better identification and analysis of the spectrum. (Figure A2.1). A high resolution spectrum is thus obtained and despite a quite long acquisition time, data are quantitative.

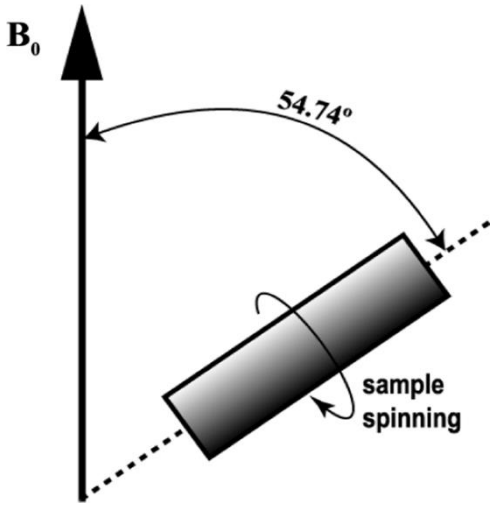

Figure A2.1: Schematic representation of a MAS probe

- Cross-Polarization Magic Angle Spinning (CP-MAS): this technique involves transferring polarization from the “abundant, high sensitivity nuclei" (^{1}H) to the “dilute” nuclei (like ^{13}C, ^{15}N, ^{29}Si …). The signal to noise ratio is thus improved. By changing the contact time, it is possible to selectively observe H-Si or H-C spatially close. This technique is not quantitative; however when acquired in similar conditions CP-MAS spectra can be compared and afford semi-quantitative information.

II.2. EXPERIMENTAL CONDITIONS

To obtain quantitatively reliable ^{29}Si solid state NMR spectra of the UV-cured films, single pulse magic angle spinning (SPE-MAS) experiments were performed on a Bruker Avance II 300 spectrometer operating at B_0 = 7.2 T (Larmor frequency: υ_0 (Si) = 59.6 MHz) with a Bruker double channel 7 mm probe. Spectra were recorded using a pulse angle of $\pi/6$, a recycling delay of 80 s, a spinning frequency of 4 kHz and high-power proton decoupling during the acquisition. These recording conditions ensured the quantitative determination of the proportions of the different Q^n siloxane species.

^1H (I = 1/2) MAS NMR experiments were performed with a double channel 2.5 mm Bruker MAS probe, a spinning frequency of 30 kHz and a $\pi/2$ pulse duration of 3.3 μs. ^1H spin lattice relaxation times (t_1) were measured with the inversion-recovery pulse sequence for each samples and a recycling delay of 8 s ensured the quantitative determination of the proportions of the different type of protons species.

^{29}Si solid state NMR spectra were obtained by performing Cross Polarization Magic Angle Spinning (CP-MAS) experiments at room temperature on a Bruker Avance II 400 spectrometer operating at 79.49 MHz with a Bruker double channel 7 mm probe. Spectra were recorded using a recycling delay of 5 or 10 s -depending of ^1H spin lattice relaxation times (t_1) estimated with the inversion-recovery pulse sequence-, a spinning frequency of 4 kHz and a contact time of 4 ms.

All NMR experiments were performed at room temperature and chemical shifts reported thereafter are relative to tetramethylsilane. Deconvolution of the spectrum was performed using Dmfit software.[4]

III. XRD (X-RAY DIFFRACTION)

III.1. PRINCIPE

XRD is a non destructive characterization technique used to determine crystalline structures or characterize amorphous solids with a local micro or meso order. XRD is based on diffraction of an X-ray beam by reticular plans of an ordered solid.

During acquisition, a X ray monochromatic source is fixed and the sample rotates around a vertical axis in order to avoid preferential orientation. The detector moves by rotation of a 2θ angle around the sample, (θ being the incident angle). When the studied solid has local order, one or several diffraction peaks are reemitted (Figure A2.2). From Bragg's law it is possible to evaluate the distance (d-spacing) between reticular planes. This later is related to the incidence angle (θ) by the following equation (Bragg's law):

$$2d \sin\theta = n\lambda$$

with d = spacing between diffracting planes, θ = incident angle, n = diffraction order and λ = wavelength of the beam.

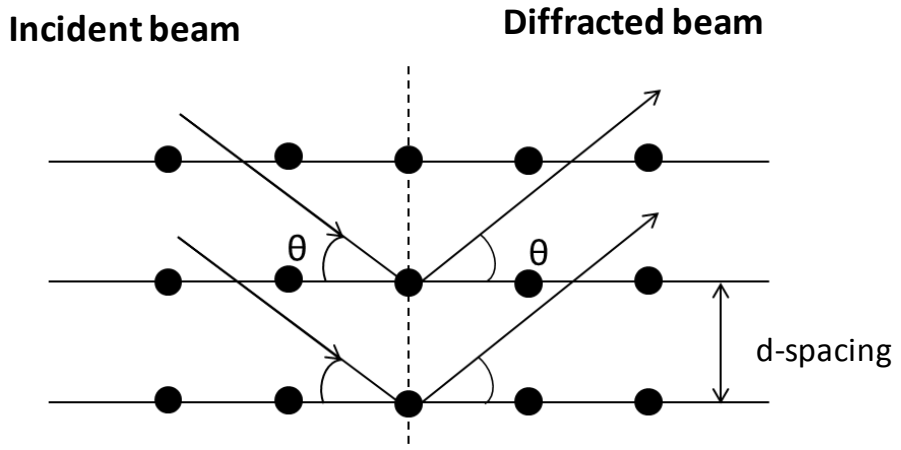

Figure A2.2: Incident X-ray diffracted by the layers of atoms in a crystalline material

III.2. CASE OF MESOPOROUS SILICA

Low angle XRD is a powerful tool to investigate mesostructure or mesoporosity in amorphous silica. XRD peaks are only present at low angle (2θ < 8°) due to absence of crystallinity. By this technique it is thus possible to determine the degree of organization of the sample. In addition, peaks intensities and widths are representative of the homogeneity of the sample. 3 types of patterns are generally reported:

- Absence of diffraction peak: silica is completely amorphous and does not have mesoporosity
- Single broad diffraction peak: mesoporous or mesostructured silica is obtained but no long range order is observed (wormlike or vermicular structure). In this case, the d-spacing is rather related to a pore-pore distance.
- Several diffraction peaks: they are representative of a given structure. The three most reported structures for mesoporous silica are lamellar, hexagonal and cubic.

Lamellar mesostructure generally shows well defined (100), (200), (300) diffraction peaks corresponding to the different layers of the materials and d-spacing corresponds to the interlayer distance. In the 2D hexagonal patterns, five peaks are generally observed which could be indexed as the (100), (110), (200), (210) and (300). But in the case of mesostructured/mesoporous thin films, patterns are usually quite different compared to bulk system, (100) and (200) peaks are presents whereas (110) is not represented because of preferential phase orientation on the substrate suggesting that channels are parallel to the substrate.

III.3. EXPERIMENTAL CONDITIONS

XRD patterns were acquired on a Philips X'pert Pro (PANalytical) diffractometer using Cu K_α radiation (λ = 0.15418 nm; 0.5 < 2θ< 10°; 0.02°/s). Depending on the experiments, samples as prepared or calcined were studied. In chapter V, samples were removed from the substrate, carefully grinded, deposited as a thin layer at the surface of a rough glass and fixed on a support prior to analysis. In chapter VII, samples were directly analysed on the substrate (silicon wafer) fixed on a support. Mesostructure was determined in function of the peak number and position. d-spacing was determined from the first most intense peaks (100).

IV. TEM (TRANSMISSION ELECTRON MICROSCOPE)

IV.1. PRINCIPE

Transmission electron microscopy (TEM) was used to investigate the film mesostructure. The principle is quite similar to a classic optical microscope except that electron beam is used instead of photons. An electron beam accelerated by a high tension is focalized with magnetic lens on a very thin sample; interactions between electrons and the sample allow the acquisition of a contrasted image depending on film thickness, density and chemical nature. In opposition to classic optical microscope, the resolution is not limited by the electron wavelength but rather by magnetic lens aberration giving a much larger resolution. However, due to low contrast and extensive sample preparation it is often difficult to obtain details on the sample. Most of the time, TEM images need to be regarded in parallel with XRD patterns.

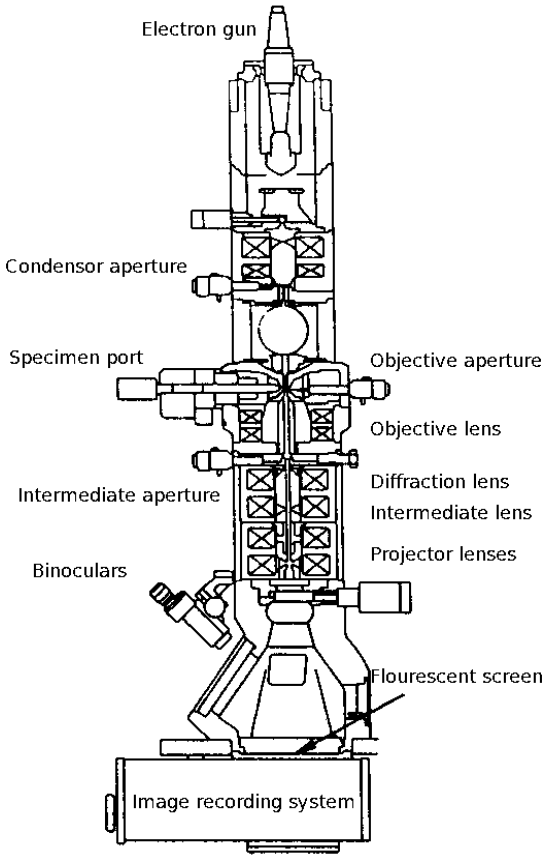

Figure A2.3: Schematic representation of a basic TEM system

IV.2. EXPERIMENTAL CONDITIONS

TEM micrographs of the calcined films were taken with a Philips CM200 microscope working at 200 kV. Prior to the observation, the scratched and powdered film was dispersed into water with ultrasounds and a few drops of the suspension were deposited at the surface of a copper observation grid. Depending on the experiments, samples as prepared or calcined were studied.

V. N_2 SORPTION

Nitrogen sorption measurement was performed to evaluate the specific surface (S_{BET}), the pore volume (V_p) and the pore diameter (D_p) of the mesoporous films. N_2 sorption is a widespread characterization technique for porous material.

V.1. PRINCIPE

The gas adsorption technique is performed by the addition of a known volume of gas (adsorbate), typically nitrogen, to a solid material in a sample vessel at cryogenic temperatures. At cryogenic temperatures, weak molecular attractive forces will cause the gas molecules to adsorb onto a solid material. An adsorbate (gas) is added to the sample in a series of controlled

doses, the pressure in the sample vessel is measured after each dosing. There is a direct relationship between the pressure and the volume of gas in the sample vessel. By measuring the reduced pressure due to adsorption, the ideal gas law can then be used to determine the volume of gas adsorbed by the sample. The resulting relationship of volume of gas adsorbed *vs.* relative pressure at constant temperature is known as an adsorption Isotherm. From the analysis, and the cross-sectional area of the adsorbate gas molecule, the surface area and pore size distribution of the sample can be derived. Isotherms represent the adsorbed gas volume for 1g of the sample (cm^3/g.STP) in function of the relative pressure (P/P_0). Depending on the appearance of the isotherms and the shape of the hysteresis, it is possible to qualitatively determine the textural properties of the analyzed sample. In addition, exploitation of isotherms with mathematics algorithms allows the determination of specific surface, porous volume and pore diameter characteristic of the analyzed sample.

V.2. EXPERIMENTAL CONDITIONS

N_2 adsorption/desorption isotherms were obtained on a Tristar 3000 (Micromeritics). Prior to measurement films were scratched, powdered and calcined. Then, samples were degassed at 150°C for 4 hours. Surface areas (S_{BET}) were determined by the BET method[5], average pore diameters (D_P) were estimated by the Gurvich method (d = 4V/S). Pore wall thicknesses (W_{thick}) were evaluated from the difference between d-spacing and pore diameter.

REFERENCES

(1) Decker, C. ; *Techniques de l'ingénieur* **2000**, base documentaire : TIB139DUO.
(2) Andrew, E. R.; Bradbury, A.; Eades, R. G. *Nature* **1958**, 182, 1659.
(3) Lowe, I. J. *Phys. Rev. Lett.* **1959,** 2, 285.
(4) Massiot, D.; Fayon, F.; Capron, M.; King, I.; Le Calvé, S.; Alonso, B.; Durand, J.-O.; Bujoli, B.; Gan, Z.; Hoatson, G. M *Magn. Reson. Chem.* **2002**, 40, 70.
(5) Brunauer, S.; Emmett, P. H.; Teller, E. A *J. Am. Chem. Soc.* **1938**, 60, 309.